NASA CR-72863

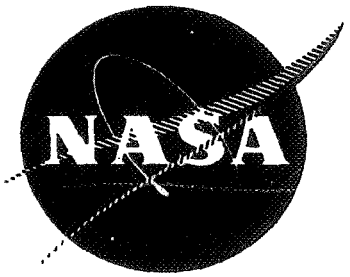

IMPROVED ALUMINIDE COATINGS for NICKEL-BASE ALLOYS

by

M.A. Levinstein and J.R. Stanley

GENERAL ELECTRIC COMPANY

prepared for

NATIONAL AERONAUTICS AND SPACE ADMINISTRATION

NASA-Lewis Research Center
Contract NAS 3-11160
R. Oldgieve, Project Manager
F. Harf, Project Manager
J.P. Merutka, Project Manager
S.J. Grisaffe, Research Advisor

Requests for copies of this report should be referred to:

National Aeronautics and Space Administration
Office of Scientific and Technical Information
Attention: AFSS-A
Washington, D.C. 20546

NASA CR-72863

Final Report

IMPROVED ALUMINIDE COATINGS for NICKEL-BASE ALLOYS

by

M.A. Levinstein and J.R. Stanley

GENERAL ELECTRIC COMPANY
Aircraft Engine Group
Cincinnati, Ohio 45215

prepared for

NATIONAL AERONAUTICS AND SPACE ADMINISTRATION

March 12, 1971

CONTRACT NAS 3-11160

NASA-Lewis Research Center
Cleveland, Ohio 44135
R. Oldgieve, Project Manager
F. Harf, Project Manager
J.P. Merutka, Project Manager
S.J. Grisaffe, Research Advisor
Aeronautics Procurement Section

ABSTRACT

Improved aluminide coatings for the NASA VIA nickel-base superalloy, developed for high-temperature jet engine components, were investigated. Coatings involved modifications of a base system representative of three approaches to improve coating stability: 1) oxide particle embedment, 2) chromium enrichment, and 3) aluminum enrichment. Both single-step and duplex coating processes were used. Coatings were tested at 2000°F (1366°K) in dynamic oxidation using both high- and low-velocity cycle burner rigs and ballistic impact. Coating systems identified exceeded 660 hours life at Mach 0.5 and 2000 hours at low velocity. Tensile and stress-rupture properties of NASA VIA were not affected by the coatings.

TABLE OF CONTENTS

TABLE OF CONTENTS (Concluded)

LIST OF TABLES

LIST OF TABLE (CONCLUDED)

LIST OF ILLUSTRATIONS

LIST OF ILLUSTRATIONS (CONTINUED)

LIST OF ILLUSTRATIONS (CONTINUED)

LIST OF ILLUSTRATIONS (CONTINUED)

LIST OF ILLUSTRATIONS (CONTINUED)

LIST OF ILLUSTRATIONS (CONTINUED)

LIST OF ILLUSTRATIONS (CONCLUDED)

SECTION 1.0

SUMMARY

The objective of this program was to identify an improved aluminide coating or coatings for the NASA VIA nickel-base alloy with a 2000°F (1366°K) 800-hour life in a Mach 0.5 burner rig. Improvement in the oxidation life of aluminide coatings had been achieved with in-house-developed coatings by embedding Al_2O_3 and TiO_2 particles (CODEP C-2). This basic approach was extended to coating modifications involving (1) other inert oxide particles, (2) higher chromium levels, and (3) higher aluminum levels. Fifteen coating modifications together with a baseline and reference coating were screened in low-velocity cyclic burner rigs at 2000°F (1366°K) with selected coatings tested in a Mach 0.5 burner rig. The coatings were applied to paddle-wheel-shaped specimens, a number of which had EDM-drilled holes to simulate cooling holes in turbine hardware.

In the first of two scheduled 800-hour Mach 0.5 tests, four inert oxide particle systems, a chromium-enriched Al_2O_3/TiO_2 particle system, and an aluminum-enriched Al_2O_3 particle system were evaluated along with a baseline and a reference coating (CODEP C-2/NASA VIA and CODEP C-2/IN100, respectively). Of these, only the chromium and aluminum-enriched systems, NC4-Cr and NC11-A, met the weight loss criterion of $\leqq 3$ mg/cm^2 to qualify for the second test. Initial testing in the Mach 0.5 burner rig was complicated by localized over-temperaturing of the specimens causing premature failures. Corrective action was only partially successful in the second test which was terminated after 662 hours for the same cause. However, the coatings were intact in areas where the 2000°F (1366°K) test temperature was monitored. A parallel test in a low-velocity burner rig completed 1568 hours at 2000°F (1366°K) before the failure criterion was exceeded. Based on metallographic examination of coating attack, the high-velocity test was judged to be $1\frac{1}{2}$ - 2 times as severe as the low-velocity test. Coating attack was observed to be less severe in areas of heavy Al_2O_3 particle concentration. X-ray diffraction indicated conversion of the original predominant NiAl phase to Ni_3Al, $NiAl_2O_4$, and Al_2O_3.

Processing parameter studies, to increase coating thickness and volume fraction of embedded particles, followed. Screening of fifteen processing variations in accelerated low-velocity burner rig testing resulted in the selection of the aluminum-enriched Al_2O_3-embedded coating, either single-cycle NC11-A-S1, or double-cycle NC11-A-D1 as the best. These coatings successfully completed 2000 hours of testing at 2000°F (1366°K) in two low-velocity burner rig tests.

Detailed analysis by metallography, microprobe, and X-ray diffraction provided evidence of the beneficial effects derived from the embedded Al_2O_3 particles in the coating in (1) promoting the formation of the stable α

Al_2O_3, (2) promoting the adherence of the oxide, (3) retarding the outward diffusion of aluminum from the coating, and (4) retarding the outward diffusion of nickel from the substrate.

Ballistic impact tests were conducted at room temperature and at 1800°F (1255°K) on flat panel specimens which were subsequently exposed at 2000°F (1366°K). Little coating degradation was noted on the compression side of the impact site; but, on the tension side, oxidation occurred where cracks in the coating penetrated to the substrate.

Selected coatings applied to tensile and stress-rupture bars produced no significant loss in mechanical properties. Oxidation/erosion wedges were coated for testing in the NASA-Lewis Mach 1 burner rig.

SECTION 2.0

INTRODUCTION

Evolutionary improvements in aircraft gas turbine technology have resulted in continually increasing turbine inlet temperatures and, consequently, more arduous demands on materials for such components as turbine blades and vanes. Formerly, these demands were met by simply using new stronger superalloys at these higher temperatures. This was possible because the stronger alloys were still operating at temperature levels and in environments where corrosion resistance was not a limiting factor. This is no longer the case. Today, operating temperatures have risen up to and above limits of superalloy resistance to long-time oxidation and sulfidation exposure. Therefore, protective coatings for high-temperature jet engine parts have become necessities in today's production and advanced engines. Although these coatings may suffice for today's application and alloys, better coatings will be required to reach the plateau of operating conditions for the next generation of engines.

The strongest current nickel-base alloy, VI-A, developed by TRW[1] under NASA sponsorship, falls into this category. In addition to its outstanding high-temperature mechanical properties, it has exceptional high-temperature oxidation resistance for substantial exposure times. However, for the more extended operating times required for advanced jet engines and certain adverse environmental conditions, protective coatings are a necessity. For use as a coated turbine airfoil, a long-range goal of 3000-hour life at 1900°F (1311°K) metal temperature has been established. As a more immediate objective, the purpose of this program was to identify a coating with at least a 2000°F (1366°K)/800-hour life under cyclic conditions in a high-velocity burner rig with a gas velocity of Mach 0.5.

Most metallic diffusion coatings currently used for jet engine components are based on depositing and diffusing aluminum into the base metal. The resulting coating consists mainly of nickel aluminide, NiAℓ, and small concentrations of the elemental constituents of the base metal. In some cases, additional alloying elements are introduced during the coating process to impart desired beneficial effects. It has been General Electric's experience, with its in-house-developed coatings, that the entrapment of oxide particles ($Aℓ_2O_3$ and TiO_2 - CODEP C-2) impart improved oxidation resistance to the coatings. Oxide particles are also found embedded in other commercial coatings, namely HOWMET Corporation's MDC1. In extended testing of the CODEP C-2 coating on Inconel 100 in a high-velocity burner rig (Mach 0.85) at Solar Division of International Harvester Corporation[2], coating life exceeded 2000 hours at 1870°F (1294°K), 1350 hours at 1950°F (1339°K), and 1100 hours at 2050°F (1394°K).

It has been observed with the CODEP C-2 coating that the embedded particles produce a fine-grain structure in the outer coating layer; whereas,

without these particles, the outer layer is a nominal one or two grains thick. The mechanism of oxidation improvement afforded by the particles is not clearly understood, but several possibilities have been considered.

1) It is well known that oxidation proceeds more rapidly along grain boundaries than transgranularly. With a fine-grain structure, the oxidation path is lengthened considerably, thereby increasing the length of time of coating penetration. Moreover, the embedded particles are partly retained in the grain boundaries, inhibiting oxidation attack.

2) The oxide particles have a pinning effect on the protective oxide layer that is formed, thus promoting scale adherence under cyclic conditions.

3) The particles act as mechanical barriers to the outward cation flux.

4) The particles interact chemically with coating constituents, forming complex oxides (spinels, perovskites, etc,) and reducing the cation participation in the surface oxidation reaction.

The basic approach of this program evolved around the concept of embedded particles and modifications thereof to achieve an improved aluminide coating and to gain an understanding of the oxidation improvement mechanism afforded by these and other oxides, ThO_2, Y_2O_3, La_2O_3, and MnO. The only reported oxidation studies in metals containing uniformly-dispersed oxide particles have involved the behavior of TD nickel[3,4], Cobalt-2% ThO_2[5], and a few cobalt base alloys containing 2% ThO_2[6]. These studies demonstrated that thoria particles decrease the oxidation rate of nickel and cobalt. Wasielewski[7] showed that minor additions of lanthanum and manganese to Hastelloy-X markedly improved oxide scale adherence and resistance to dynamic environments. The lanthanum increased the activity of Mn and Cr to form a stable $MnCr_2O_4$ spinel which minimized scale volatilization. Yttrium, on the other hand, is a major factor contributing to the outstanding oxidation resistance of the FeCrAlY[8] alloy. It has also proven beneficial to nickel-base alloys such as Rene' 100[9]. Coating modifications incorporating these oxide particles were categorized as the "Inert Oxide Particle Embedment" group.

The role of aluminum in imparting oxidation resistance to nickel base alloys is well known[10], in particular, the superiority of NiAl over Ni_3Al. Most coatings currently used for jet engine components are based on depositing and diffusing aluminum into the base metal. When these coatings degrade on exposure, the predominant failure mechanism is oxidation/erosion in which the aluminum content of the outer coating layer is depleted, leading to the formation of less-oxidation-resistance nickel-aluminum compositions (Ni_3Al and gamma). The higher the aluminum level within the NiAl compositional range, the longer it takes to deplete the aluminum level to the lesser

oxidation-resistant compositions. Thus, increasing the aluminum content of the coating along with the embedded oxide particles afforded a method of extending coating life. Coating modifications incorporating more aluminum were considered as the "Aluminum Enrichment" Group.

The influence of chromium in improving oxidation is also well recognized. Kaufman[11] has shown that an eight-weight-percent addition of chromium to stoichiometric NiAℓ improved the oxidation resistance at 1800°F by a significant degree. Seybolt[12] determined that chromium added to NiAℓ promoted the formation of the more stable α alumina on exposure at elevated temperatures, while NiAℓ without chromium tended to produce the less stable γ alumina as the surface oxide. Thus, the addition of chromium, to alumide coatings containing oxide particles, offered promise of improved performance. The modifications incorporating chromium were identified as the "Chromium Enrichment" Group.

In all, 15 coating compositions were investigated and compared with a baseline coating (the General Electric CODEP C-2 coating on NASA VIA and a reference coating, CODEP C-2 on Rene' 100). The coatings were applied by a vapor process simulating the coating of engine components containing small-diameter cooling holes. The prevention of hole plugging during coatings was a vital consideration; therefore, some of the test pieces incorporated holes of different diameters to simulate engine hardware.

The program was divided into two tasks. In Task I, the various coatings were screened in a low-velocity burner rig at 2000°F (1366°K), cycling once per hour. Selected systems were subsequently tested in a high-velocity burner rig at Mach 0.5 and 2000°F (1366°K). A failure criterion of 3 mg/cm^2 weight loss was established. Subsequent evaluation was by metallographic, X-ray diffraction, electron microprobe, and electron microscope technique. Ballistic impact testing was also conducted. Based on these results, the two best coatings were selected for further investigation under Task II. A flow sheet outlining the Task I program is presented in Figure 1.

Under Task II, modifications to improve the selected coatings were screened in low-velocity burner rigs at 2000°F (1366°K), cycling ten times per hour for up to 500 hours. The two best coatings were selected and tested at 2000°F (1366°K) for 2000 hours, cycling once per hour. Specimens were removed at 500, 1000, and 1500 hours to monitor the progress of coating degradation. Evaluation was by the same techniques described in Task I. In addition, tensile and stress-rupture specimens were evaluated for the effects of the coatings on mechanical properties, and oxidation/erosion bars were coated for evaluation in the Mach 1 burner rig at NASA-Lewis. Task II is outlined on the flow sheet in Figure 2.

SECTION 3.0

INVESTIGATION - TASK I

3.1 Materials

3.1.1 Test Specimens

The test specimens of NASA VIA alloy were all Government-furnished materials; these included:

a. 150 paddle-wheel test specimens per NASA Sketch No. 98B-3, Figure A-1*

b. 40 specimens (1 inch X 2 inches X 0.10 inch thick) (2.54cm X 5.08cm X 0.25cm thick) for ballistic evaluation

c. 20 cast and machined-to-size wedge specimens per NASA Drawing CB-301680, Figure A-2

d. 18 stress-to-rupture test bars, 0.252 inch (0.64cm) diameter, cast to size with 1/2 inch No. 13NC threads

Paddle-wheel specimens of Rene' 100 (General Electric version of IN100) were provided from material on hand. 20 cast and machined-to-size wedge specimens of IN100 per NASA Drawing CB-301680 were Government-furnished material.

NASA VIA alloy has a nominal composition in weight percent of 9.0 Ta, 5.5 W, 7.5 Co, 6.0 Cr, 5.5 Aℓ, 2.0 Mo, 1.0 Ti, 0.13 C, 0.13 Zr, 0.02 B, and 0.5 each of RE, Hf, and Cb; while, Rene' 100 has a nominal composition in weight percent of 15.0 Co, 9.5 Cr, 5.5 Aℓ, 4.2 Ti, 3.0 Mo, 1.0 Fe, 1.0 V, 0.18 C, 0.06 Zr, 0.015 B, and 0.5 each of Mn and Si.

The paddle-wheel specimens were to be evaluated in preliminary testing as solid specimens, while screening tests were to be preformed on both solid specimens and specimens with EDM-machined holes (0.012, 0.200, and 0.040 inch in diameter by 0.250 inch deep) (0.03cm, 0.05cm, 0.10cm in diameter by 0.64cm deep) along the leading edge. The hole patterns are illustrated in Figure A-3. 20 paddles were prepared with holes by EDM machining. Ten specimens for coating and screening tests had six holes each (two holes of each size), while the remaining ten specimens had three holes each (one of each size) for metallographic examination in the as-coated condition.

---

*Figures with a letter prefix are located in the appendix with the corresponding letter designation, e.g., Figure A-1 is the first figure in Appendix A.

3.1.2 Pack Materials

The constituents of the coating packs included the following:

a. $A\ell_2O_3$ Filler - GE Specification A50TF100

b. Ammonium Fluoride - GE Specification A50TF101

c. CODEP B Powder - GE Specification B50TF93, Class B

d. CODEP C Powder - GE Specification B50TF93, Class C

e. Chromium-Aluminum Powder; Cr-89.8%, $A\ell$-8.4%

f. Chromium-Aluminum Powder; Cr-84.7%, $A\ell$-12.2%

g. Chromium-Aluminum Powder; Cr-74.5%, $A\ell$-24.7%

3.1.3 Particles - Embedment

$A\ell_2O_3$ - 2-10μM, Wall Colmonoy, White Stop-off

TiO_2 - 2μM, Wall Colmonoy, Green Stop-off

$A\ell_2O_3$ - 2μM, Electronics Division, Union Carbide Corporation

Y_2O_3 - 1-2μM, American Potash and Chemical Corporation

Y_2O_3 - 2-10μM, American Potash and Chemical Corporation

ThO_2 - 1-2μM, American Potash and Chemical Corporation

La_2O_3 - 1-2μM, American Potash and Chemical Corporation

MnO - 1-2μM, Manganese Chemicals Company

Cr - 1-3μM, Federal Mogul

3.2 Test Facilities

3.2.1 M&PTL Low-Velocity Burner Rig

The M&PTL burner rig, Figure A-4, is a natural-gas-burning, dynamic-oxidation tunnel. A set of eight selas gas burners is located at the front of the tunnel with the specimens positioned in a rotating fixture approximately 2 feet (61cm) into the tunnel. Cycling is accomplished by forcing cool air at a high velocity into the tunnel with simultaneous reduction of the burner flame.

Temperature control is maintained by adjusting airflow and natural gas input. Gas stream velocity is approximately 0.05 Mach at 2000°F (1366°K). Rotational speed of the specimens within the tunnel is 36 rpm. Monitoring techniques for temperature measurement are optical and will be discussed fully in the next section.

3.2.1.1 Temperature Measurement - M&PTL

Temperature measurement in the M&PTL burner rig tests was accomplished primarily through use of a Leeds and Northrup optical pyrometer and numerous control checks with an Ircon infrared measuring device. In addition, a platinum-platinum rhodium thermocouple attached to a metal panel was suspended just aft of the specimens for monitoring temperature.

Use of instrumented test paddles was considered as a possible temperature control device in the tunnel. However, investigation into their accuracy and dependability cast considerable doubt as to their usefulness in this type of test. At the present time, the best 10-mil (0.25mm) sheathed thermocouples available offer an accuracy of ± 3/4 percent. Therefore, at our test temperature of 2000°F (1366°K), an accuracy of ± 15°F (8°K) would be the best possible. In reality, according to our instrumentation group, a range of ± 25°F (14°K) would be more realistic. Placement of the thermocouples on the paddles presented additional problems in that their location on the surface would alter the flow pattern and, thus, possibly create a hot spot condition. On the other hand, embedding the thermocouples beneath the surface $\approx$ 2 mils (0.05mm) would not truly indicate the surface temperature. For the above reasons, and the fact that at temperatures above 1500°F (1088°K) optical measurements of temperature are the accepted standards, instrumented paddles were not utilized.

Optical readings were taken at least twice each day with either the pyrometer or infrared device. The Ircon infrared instrument included an adjustable emissivity correction. This was adjusted to a 0.85 emissivity for the coating. The normal location for reading the temperature of the paddles during testing was at a spot near the leading edge and approximately 0.4 inch (1.0cm) below the tip. Trailing edge temperatures, which visually appeared significantly hotter than the leading edge, were estimated by optical means to be 20-30°F (11-17°K) higher. Constant surveillance of the cycle characteristics was provided by the aft thermocouple.

3.2.2 EPPI Burner Rig

The high-velocity burner rig was located at EPPI Precision Products Inc., Clarendon Hills, Illinois. The facility, Figure A-5 consists of a 15-inch-long (0.38m) burner which uses Type-A jet fuel for burning. Test specimens rotate on a fixture in front of the burner. Cycling is accomplished by removing the specimens from the gas stream and blasting with cold air if necessary to maintain desired cooling rates.

Temperature control is maintained by adjusting the airflow and fuel input, which are automatically controlled to preset values and constantly monitored by the operator. Gas stream velocity at 2000°F (1366°K) is calculated to be 0.5 Mach, although actual measurements have not been conducted. Rotational speed of the test specimens was maintained at a constant speed of 1750 rpm.

Monitoring of the temperature was accomplished with a Leeds and Northrup optical pyrometer. Constant temperature measurement was conducted during heatup, with periodic checks and recordings thereafter.

3.2.3 Ballistic Impact Facility

The ballistic impact facility, Figure A-6, consisted of a modified Benjamin air rifle using 0.174-inch (4.3mm) diameter steel ball projectiles at velocities up to 650 feet (198m) per second. Velocity of the projectile was determined with an elapsed-time counter and controlled with bottled air pressure cylinders. Induction coils were utilized to bring specimens to the 1800°F (1225°K) testing temperature as shown in the above figure. Single specimens were held in a rigidized vise-type fixture for impacting.

3.3 Coating Compositions

3.3.1 Coating Combinations

Coating combinations selected for investigation are complied in Table I. The first two combinations, CODEP C-2/NASA VIA and CODEP C-2/R'100, were selected to serve as a baseline coating and a reference coating, respectively. In addition, applying the same coating process to both the Rene' 100 and the NASA VIA alloy provided a basis for comparison between the two alloys and a measure of severity between the test facilities.

The basis for selection of the three modification groups; "Inert Oxide Particle Embedment", "Chromium Enrichment". and "Aluminum Enrichment" are discussed in the Introduction.

3.3.2 Coating Processes

Most turbine airfoils for the hot sections of advanced engines, for which the NASA VIA alloy would be an active candidate, incorporate cooling holes in their design. Since these holes are often quite small [0.010 to 0.020 inch diameter (0.25-0.5mm)], the coating process must be capable of coating these holes without becoming plugged with coating compounds. In-house experience with the coating of such hardware had demonstrated that the conventional pack-type CODEP processes could not assure 100 percent freedom from hole plugging. This led to a process in which the parts to be coated are not in direct contact with the pack. They are suspended above the pack mixture, and coating is effected by the rising vapors generated within the pack. This was the basic process used in all the coating modifications under investigation.

3.3.2.1 Pack Preparation

The pack itself consisted of a mixture of 40 percent alloy powder, 60 percent oxide filler, and an ammonium fluoride activator. Except for the chromium-enrichment modifications, the alloy powders were ternary alloys of titanium, aluminum, and carbon of either intermediate aluminum, or high aluminum activity. CODEP "C" and CODEP "B" are General Electric designations for powders of intermediate and high aluminum activity, respectively.

For the chromium-enrichment coatings, three chromium-aluminum powders were used: (1) 89.9 Cr-8.4 Aℓ, (2) 84.7 Cr-12.2 Aℓ, and (3) 74.5 Cr-24.7 Aℓ. The filler consisted of a 50-50 mixture of aluminum oxide and chromium oxide. The chromium oxide was incorporated in the pack mixture to reduce the aluminum deposition rate so that a codeposition of both aluminum and chromium would take place. Several process variations and a number of activators were investigated. A second method of chromium enrichment involved the embedment of discrete chromium particles in the outer coating layer.

3.3.2.2 Slurry Preparation

The introduction of oxide particles into the coating is accomplished by a relatively simple method. A slurry is prepared consisting of the oxide powder, a binder, and a solvent in approximately the following:

Oxide Powder - 200 grams

Nicrobraz Cement - 50 cc

Acetone - 50 cc

Precise proportions were not defined, because minor adjustments to facilitate spraying were necessary depending on the type of oxide. The ingredients were mixed in a high-speed blender with a rotating cutter for a period of 5 minutes (minimum) and then transferred to the spray can of a Devilbiss paint spray gun. Prior to the application of the slurry, the specimens were degreased, liquid honed, and rinsed with acetone. Using the air-operated Devilbiss spray gun at a line pressure of 40-50 psi (2.8-3.5 Kg/cm^2), a smooth, opaque, adherent coating was applied free of wrinkles, blisters, or other surface discontinuities. Coating thickness varied from 10-15 mils (0.25-0.38mm). After spraying, the slurry coating was allowed to dry in air for a minimum of 30 minutes.

In the case where metallic chromium particles were introduced (NC4-Cr), the slurry composition consisted of the following:

$Aℓ_2O_3$ - 50 grams

TiO_2 - 50 grams

Cr	-	100 grams
Nicrobraze cement	-	50 cc
Acetone	-	50 cc

Where two oxides were used together, the weight percentages of each are listed in Table I.

3.3.2.3 Processing Procedures

Processing of the test specimens was conducted in Inconel coating boxes (6 X 6 X 5 inches) (15.2 X 15.2 X 12.7cm), Figure A-7. A thermocouple tube, sealed at the end which extends into the center of the box, provided monitoring of the internal temperature throughout the coating cycle. The bottom of the box was filled with the pack mixture to a depth of one inch (2.54cm). The paddle-wheel specimens were mounted in a holding fixture, and the fixture was buried in the pack mixture leaving the entire airfoil section exposed.

After positioning the specimens, the box was covered with a lid and inserted into the forward section of an atmosphere-controlled retort, Figure A-8, mounted in a Harper furnace, Figure A-9, and set at a temperature to produce the desired processing temperature inside the coating box. Pack reactions were carried out at 1925°F (1324°K) for 4 hours.

Coating thickness control was exercised by weight gain measurement of control coupons, weight gain of the paddle specimens themselves, and metallographic examination. Thickness-control panels were placed both within the pack mixture and at several levels above the pack mixture.

3.3.3 Processing Results

The results of processing the various coatings are presented in Table II. Included are the overall coating thickness, outer coating layer thickness, inner diffusion zone, and volume fraction of embedded particles. The coating thicknesses presented in this table are the average of a minimum of ten readings taken at 500X magnification along the periphery of a polished section of the paddle airfoil. The volume fraction of the particles in the outer coating layer was based on a comparison with standards for which the particle volume fraction had been determined by the point-intercept method. These standards were for volume fraction embedment levels of 10, 20, and 30 percent. From Table II, the volume fractions of particles observed in the coatings were low in comparison with the target percentages. Only the two CODEP C-2 coatings met the target of 25 volume percent. The thoria-containing, NC2-T, modification exhibited the best particle embedment with 35 volume percent. The chromium-enrichment coating, NC4-Cr, had a nonuniform $A\ell_2O_3$ particle and chromium particle embedment totalling 30 volume percent. Yttrium oxide additions to the coating NC1-Y and NC1-AY proved unsatisfactory, due to

their masking tendencies during aluminum deposition. Apparently, the bisque of Y_2O_3 forms a tightly-bonded layer at the surface of the substrate during processing which greatly hampers aluminum deposition. As a result, coating thicknesses obtained with the 2-10 μM particles were only 0.8-1.0 mil (20-25 μM), while the 1-2 μM particles limited coating thicknesses to 0.4-0.6 mil (10-15 μM). Longer processing times and higher coating temperatures were not helpful.

Lanthanum-oxide additions to the coating NC3-L and NC14-L appeared acceptable during initial processing and evaluation; however, subsequent X-ray diffraction data revealed that the activator, NH_4F, was reducing the oxide and forming LaF_3. This reaction will be discussed more fully in a later section of the report.

Coating modifications using manganous-oxide additions, NC5-Y, NC6-T, and NC7-L, presented processing difficulties. In all cases, the MnO was reduced by the activator and/or hydrogen to Mn. As a result, the entire bisque sporadically bonded to the surface forming a porous layer ≈ 15 mils (0.37mm) thick, which was difficult to remove without damaging the underlying coating. Use of lower-activity activating agents such as $NH_4C\ell$ provided no improvement.

The chromium-enrichment group (NC8-Cr, NC9-Cr, and NC10-Cr) showed generally low weight gains and correspondingly thin coatings. These systems were designed to codeposit chromium and aluminum from selected Cr-Aℓ alloys (75-25, 85-15, and 90-10 weight percent combinations, respectively) to produce a protective coating. Several processing modifications were tried, but all were unsuccessful to varying degrees. Different activators including NH_4F, $NH_4C\ell$, KI, and CrF_3 were evaluated, with CrF_3 producing the best results. Temperature and time-cycle modifications at temperatures up to 2100°F (1421°K) and times up to 8 hours produced little improvement. Chromium levels in the final systems using CrF_3 activation and a cycle of 2000°F (1366°K)/4 hours were 7 wt/o, 11 wt/o, and 15 wt/o with thicknesses of 1.1, 1.0, and 0.8 mils (28 μM, 25 μM, and 20 μM), respectively.

As mentioned previously, the coating process which was used in this program involved suspending specimens above the pack mixture where they are coated by the rising vapors generated within the pack. The coatings produced by this type of processing differ from those produced within the pack mixture. Primary differences are in weight gain and coating thickness achieved under standard conditions. In general, both weight gain and thickness of the coating are approximately 40 percent less with the vapor process as compared with in-pack results. Examples of this behavior are included below:

Coating System	Weight Gain (mg/cm^2)[1]		Thickness, Mils (μM)[1]	
	Vapor	Pack	Vapor	Pack
NASA VIA/C-2	3.16	5.62	1.6(41)	2.0(51)
R'100/C-2	4.84	6.95	1.8(46)	2.5(64)
NC11-A	4.12	6.54	1.7(43)	2.3(58)
NC4-Cr	4.32	6.88	1.8(46)	2.2(56)

(1) All data points are the average of at least five separate coating runs.

Photomicrographs representative of the more successful systems are shown in Figures 3 through 6. Particle embedment varied from 10 percent for the NC1-Y, NC1-AY, and NC1-2Y, up to 30-35 percent for NC2-T.

Electron microscope examination, to determine particle volume fraction and particle size, was conducted. At magnifications of 10,000X and 20,000X, too few particles were present in a given field to make an accurate determination of volume. Moreover, magnification at 500X appeared to be satisfactory for volume fraction determination. The electron microscope did prove valuable in determining particle distribution and size.

In CODEP C-2 coating, Figure 7, the $A\ell_2O_3$ particles are shown to be concentrated at the outer edge of the coating and the TiO_2 at the interface of the outer coating layer and the inner diffusion zone. Identification of oxide particles was determined primarily through size differences: 2-10 μM for $A\ell_2O_3$ and < μM for TiO_2. Particle embedment, both in the grain boundaries and within the grains, was brought out in the NC11-A coating, Figure 8. Similarly, the distribution of $A\ell_2O_3$ particles at grain boundaries and within grains in the NC4-Cr coating is illustrated in Figure 9, top, and a large chromium particle in Figure 9, bottom.

3.4 Burner Rig Test

3.4.1 Testing Procedure

At the initiation of the program, it had been agreed that four combinations, CODEP C-2/Rene' 100 (reference system), CODEP C-2/NASA VIA (baseline system), NC4-Cr, and NC11-A would be evaluated first in a high-velocity burner rig test under subcontract to EPPI Precision Products, Inc. Concurrently, the same systems would be tested in the low-velocity M&PTL burner rigs to determine if a correlation existed between the two types of tests. The low-velocity flame tunnels were to be used for screening the other coating modifications, according to group. Each group consisted of three or four modifications (NC1 - NC3 constituted the first group; NC5 - NC7, the second; NC8 - NC10, the third; and NC11 - NC14, the fourth). The best coating from each group would subsequently be tested in the EPPI burner rig.

For the EPPI burner rig test, three paddle specimens were prepared with a given coating (two solid specimens and one with EDM holes). The two solid paddles were to be placed on test first. After 250 hours at 2000°F (1366°K), with a 3-minute cooling cycle every hour, one of these paddles would be removed and replaced with the specimen containing the EDM holes. If no failure occurred, these specimens would remain on test for 550 hours more, or a total of 800 hours for the solid specimen and 550 hours for the one with holes. Whenever one specimen of a given coating system failed, both specimens were to be removed and replaced with a different coating modification based on its performance in the M&PTL burner rig. From this initial 800-hour test, the better coatings were to be selected for testing in a second 800-hour test.

Before discussing the test results, some observations of the first EPPI test are in order. Specimen temperature was monitored by an optical pyrometer at the center of the airfoil leading edge. During the early stage of the testing, 159 hours, a member of the M&PTL staff was observing the test and noted that the temperature at the lower airfoil trailing edge was significantly higher than at the location where the temperature was being monitored. The temperature at the trailing edge was estimated to be approximately 2100°F. Because of the design of the holding fixture, it was difficult to obtain an accurate reading. At this point, a CODEP C-2-coated R'100 airfoil had sustained a weight loss in excess of 3 mg/cm^2 and was removed. Failure was observed in a localized area at the lower airfoil trailing edge, whereas the coating on the balance of the airfoil appeared unaffected visually, Figure 10. The other coating modifications all showed evidence of attack in this area, but not to the extent of failure. Examination of the weight change data revealed a sharp increase in weight loss between 111 and 128 hours, indicating a possible overtemperature during that period. Modifications were made in the test setup which produced a more uniform temperature profile by repositioning the burner flame and changing the specimen holder to allow the hot gases to flow more readily between the specimens. These modifications were not fully effected until some 300 hours of testing had accumulated. Continued testing to 800 hours indicated that the modifications lowered the temperature at the lower trailing edge but still not to the level at the center of the leading edge, the result being further localized attack. In an attempt to correct this situation for the second EPPI test, the paddle specimens were modified by removing the lower trailing edge section to eliminate the hot spot occurring in this area. A wedge section approximately 1/8 inch wide at the base and 1/2 inch long was removed.

This difficulty was not experienced in the M&PTL burner rig; consequently, the paddle specimens did not require modification for this test.

3.4.2 Coating Performance

The results of the initial screening tests in the EPPI and M&PTL burner rigs are presented in Tables III and IV, respectively. Only the NC4-Cr and NC11-A coatings survived 550 hours with the coating intact. All coatings showed moderate-to-severe attack in the lower trailing edge section of the airfoil and metal loss in some cases due to the higher temperature in that location. Other than $A\ell_2O_3$, none of the oxides proved to be beneficial. The addition of MnO appeared to be particularly detrimental. Performance of the coatings in the EPPI burner rig paralleled their performance in the M&PTL rig, except for the NC3-L coating which failed early in the EPPI rig.

The chromium-enrichment coatings (NC8-NC10) and the aluminum-enrichment coatings (NC12-14) did not warrant testing in the EPPI burner rig because of their poor performance in the M&PTL rig. The chromium-enriched coatings spalled severely after a relatively few hours of testing. Similar results were obtained with the Y_2O_3, ThO_2, and La_2O_3 additions to the aluminum-enriched coatings.

Metallographic examination of sections from specimens from the EPPI test, taken through the center of the airfoil where the 2000°F (1366°K) temperature was monitored, revealed that the coating on the leading edge and mid-airfoil sections was intact on all specimens, Table V. However, except for the NC4-Cr and NC11-A coatings which were intact, all other combinations failed at the trailing edge section.

For the second test series, the following coatings were selected for testing at 2000°F (1366°K) in the EPPI burner rig and a comparative test in the M&PTL burner rig.

a) NC4-Cr - chromium enrichment through dispersed $A\ell_2O_3$ chromium particles

b) NC11-A - Aluminum enrichment with dispersed $A\ell_2O_3$ particles

c) NC11-A (Modified) - Same as (b) with addition of chromium particles

d) CODEP C-2 - baseline

Selection of the first two compositions was based on their excellent performance in both the EPPI and M&PTL burner rigs as described above. Coating composition (c), the modified NC11-A, was selected in an effort to combine the higher aluminum content of composition (b) with the chromium enrichment of composition (a). The last composition, CODEP C-2, was included to provide an in-test basis for determining coating improvement and to generate additional baseline data.

Each of the compositions described above was represented by two coated paddle specimens in both the EPPI and M&PTL burner rigs. Cumulative weight changes are presented in Figures 11 and 12, respectively. Testing at the EPPI, Figure 11, was stopped after 662 hours due to the specimens exceeding the 3 mg/cm^2 weight loss criterion. Again, localized attack had occurred at the lower trailing edge despite the airfoil modification made to alleviate the condition. Aside from the local attack, the balance of the airfoils of the NC11-A and NC11-A (Modified) appeared intact.

In the M&PTL burner rig, the NC4-Cr and CODEP C-2 coatings exceeded the failure criterion after 800 hours, whereas the NC11-A and NC11-A (Modified) showed no evidence of coating failure and the weight change was still positive. Testing continued until 1568 hours before the 3 mg/cm^2 loss criterion was reached, at which point the testing was terminated. Localized failure, as found in the EPPI rig was not observed.

Because of the type of failure in the EPPI test, it is difficult to establish a severity factor between the two test facilities. At an intermediate point in the test schedule, prior to deterioration of the lower trailing edge at EPPI, the two facilities indicated equivalent rank and weight change for the four compositions, except for the NC4-Cr coating.

Coating	Weight Change, Gram	
	EPPI - 261 Hours	M&PTL - 297 Hours
NC11-A	+ 0.012 + 0.010	+ 0.038 + 0.037
NC11-A Mod.	+ 0.017 + 0.016	+ 0.037 + 0.033
NC4-Cr	- 0.063 - 0.064	- 0.102 - 0.115
C-2	- 0.210 - 0.184	- 0.084 - 0.090

In the other three cases, the EPPI rig appears to be about twice as severe as the M&PTL rig. Additional evidence for this estimate will be covered under the section on metallographic examination.

The continued overheating of the lower trailing edge in the EPPI test prompted an investigation of the temperature being experienced in that area. A study was conducted comparing the metallographic structure of the base alloy after exposure in the EPPI rig with bare specimens exposed statically at several temperature levels. Temperatures of 2050°F (1394°K) and 2150°F (1450°K) were selected for exposure times up to 300 hours. Sections were taken every 50 hours for metallographic examination and compared with a bare 360-hour EPPI specimen. The static oxidation effects at 2050°F (1394°K) after 300 hours are shown in Figure 13, in comparison with the leading, center, and trailing edge sections of the 360-hour bare EPPI specimen, Figure 14. Note that the coarsening of the gamma prime structure in the static test at 2150°F (1450°K) (Figure 13, bottom) is virtually the same as that of the EPPI center airfoil section (Figure 14, center). The grosser coarsening at the lower trailing edge section of the EPPI specimen (Figure 14, bottom) would indicate a temperature in excess of 2150°F (1450°K). On this basis, it is evident that the major portion of the weight loss sustained by the specimens in the EPPI rig is attributable to the localized over-temperature condition.

3.4.3 Evaluation

3.4.3.1 Metallography

Metallographic examination of the best performing compositions at EPPI (NC4-Cr and NC11-A) revealed the coatings to be totally intact at the leading

edge sections, where the 2000°F (1366°K) temperature had been monitored (Figure 15). Further sectioning confirmed that coating penetration or failure was confined to the lower trailing edge sections.

In Figure 16, the condition of the NC11-A coating on the leading edge and trailing edges from the M&PTL test after 1568 hours is compared with the NC11-A leading edge coating from the EPPI test after 662 hours. Whereas the coating is intact on the EPPI rig specimen, virtually all of the outer layer of the leading edges tested in the M&PTL rig has been lost. The center photograph shows a more severe attack on the trailing edge coating as evidenced by the presence of massive oxides. The latter two photographs demonstrate the extent of coating degradation associated with a weight loss of 3 mg/cm^2. Comparing this degree of degradation with the relatively intact condition of the EPPI-tested NC11-A coating, it is apparent that, in the latter case, the 800-hour goal would have been achieved readily had it not been for the lower trailing edge overtemperature.

Comparative severity of the two test facilities can only be approximated from the metallographic results. Examination of metallographic sections after 800 hours in the M&PTL burner rig revealed a level of degradation somewhat less extensive than that achieved in the EPPI facility. An equivalent level of degradation would be anticipated between 1000 and 1200 hours, where weight losses of 1.0 - 1.5 mg/cm^2 (Figure 12) had occurred. On this basis, the severity of the EPPI burner rig is judged to be between one and a half and two times that of the M&PTL burner rig. Accordingly, the projected 2000-hour test under Task II would be equivalent to at least 1000 hours in the EPPI burner rig.

3.4.3.2 Electron Microprobe Analysis, As-Coated

Microprobe results for as-coated compositions are compiled in chart form in Table VI. It must be pointed out that these data are not quantitative, but rather approximations of material concentrations from the traces.

Additive layers of the coating systems were primarily nickel and aluminum with only minor diffusion from alloying elements in the NASA VIA substrate. The systems which contained embedded chromium particles were an exception to this, in that the chromium level in the coating was at or near base-material levels. Generally, all alloying elements of the substrate were present in the diffusion zone of the coating, with a sharp decrease noted when entering the additive layer. One significant point which should be brought out is the large increase in aluminum concentration in the two optimized systems, NC11-A duplex and NC4-Cr duplex, prepared with a high-activity aluminum pack.

3.4.3.3 X-Ray Fluorescence Analysis

Studies in X-ray diffraction and microprobe of the behavior pattern for coatings tested at EPPI indicated several anomalies which needed more extensive

investigation. In particular, the behavior of chromium and the presence of iron in the coating could not be fully explained by microprobe and/or X-ray diffraction. X-ray fluorescent analysis, which would provide relative intensities of alloying elements in the coating before and after testing, was considered necessary at that time. Results from this analysis on paddle test specimens of three coating systems [NC11-A (Mod.), NC4-Cr, and R'100/C-2], plus the base alloy NASA VIA, are presented in Table VII.

Two of the compositions selected contained chromium as embedded particles in the outer coating layer. Chromium behavior, which is particularly significant in terms of coating protection, will be discussed first. Relative intensity increased twofold in the NC4-Cr system over the base alloy, while the NC11-A modified system (also containing chromium additives) showed a minor increase in the as-coated condition. After testing (EPPI rig, 662 hours), both systems showed significant decreases in chromium content with NC4-Cr remaining slightly higher and NC11-A (Modified) dropping below substrate level. Depletion of chromium in this manner is explained by the formation of a $NiCr_2O_4$ spinel-type oxide. With a high level of chromium in the coating, outward diffusion from the base material is retarded, thus maintaining the desired chromium level in the matrix. In contrast, the R' 100/C-2 system, which contained no chromium additions and showed only a minor indication as-coated, exhibited a chromium level nearly that of the matrix after 250 hours in the EPPI rig. This chromium must have diffused outward from the base alloy, thus depleting the region under the coating and making it more prone to attack if coating failure occurs.

Iron levels increased dramatically in all compositions after EPPI testing. This increase in intensity exceeded any base material content and could only be a function of the test conditions. The burner rig at EPPI uses an iron-base nozzle which apparently erodes and/or oxidizes, and the resulting product is deposited on the coating surface. The effect of the iron on coating protection is unknown, although it is not believed to be detrimental. Presence of iron of this intensity will help explain the strong indication of $MA\ell_2O_4$ reported in the following section on X-ray diffraction analysis.

3.4.3.4 X-Ray Diffraction Analysis

X-ray diffraction analyses of coated paddles included all coating systems which were tested in the EPPI burner rig. A complete listing of the results for the nine compositions, as processed, and after their respective EPPI exposures, is included in Tables B-I through B-IX. Analyses of the coating modifications, as processed, showed the coatings to be basically $NiA\ell$ with differences attributed to process variations and/or particle additions to the outer coating layer. Specific points of interest were:

- As-coated NC11-A (Modified) coating showed an increase in aluminum level as evidenced by the possible presence of a $Ni_2A\ell_3$ phase in the outer coating layer with 42 w/o $A\ell$ shown by electron microprobe analysis.

- Phases after exposure were $NiA\ell$, $Ni_3A\ell$, $A\ell_2O_3$, $MA\ell_2O_4$, and particles.

- For exposures longer than 300 hours, those coatings processed with CODEP B retained a strong $NiA\ell$ presence with some $Ni_3A\ell$, while those processed with CODEP C showed a strong $Ni_3A\ell$ and a weak $NiA\ell$.

- Chromium additions to the coatings were observed as free Cr in compositions NC4-Cr and NC11-A (Modified), with the intensity being much greater than in other systems.

- All particle additions (ThO_2, $A\ell_2O_3$, TiO_2, and La_2O_3), which were part of the coating modifications, were identified as phases in the coating.

- Lanthanum oxide additions to the coating compositions were largely reduced by the ammonium fluoride activator and hydrogen in the coating process to a LaF_3 phase. On exposure, oxidation of LaF_3 to La_2O_3 proved deleterious to the coating.

X-ray diffraction patterns of the coating compositions after EPPI testing generally showed a decrease in aluminum and chromium intensity with the $NiA\ell$ degrading into $Ni_3A\ell$. All particle additions retained their identity with the exception of La_2O_3, which was identified as LaF_3 with indication of $LaA\ell_2O_3$ as well. In addition, a phase $MA\ell_2O_4$ was found in each composition after testing. Initially, the phase was believed to be $NiA\ell_2O_4$; however, X-ray fluorescent studies, which were discussed previously, uncovered substantial iron indications and made it probable that $FeA\ell_2O_4$ is also present.

3.5 Ballistic Impact Testing

Coating compositions of primary interest were ballistic impact tested, to determine if the coating improvements altered properties of the basic $NiA\ell$ coating layer. All testing was conducted with a modified Benjamin air rifle using steel balls, 0.174 inch (0.44cm) in diameter and weighing 0.3576 gram. Initial testing was conducted at room temperature and 1800°F (1255°K) at velocities of 200 - 650 feet (60.9-198m) per second. Final selected velocities of 400 feet (121.9m) per second at room temperature, and 500 feet (152.5m) per second at 1800°F (1255°K), were determined to be the velocities necessary to produce fine coating cracks without fracture of the base metal. Actual impact energies to produce cracking were calculated using the kinetic energy equation $E = 1/2\ M\ V^2$, neglecting rebound velocities and other variables such as angle trajectory, bending moments, and deformation of the pellet. In this particular case, the impact energy for the specimens was determined as

1.96 foot-poundals (0.083j) for the 400 fps (121.9 mps) velocity and 3.06 foot-poundals (0.129j) for the 500 fps (152.5 mps) velocity. Projectile velocities were monitored by an elapsed-time counter during all tests.

Five compositions were selected for M&PTL burner rig testing after ballistic impact damage. One specimen from each of the five compositions evaluated was impacted at room temperature and the other at 1800°F (1255°K). Macro pictures of all impacted compositions used for burner rig testing are shown at 15X magnification in Appendix C. No significant differences were observed among the other four compositions in comparison with the basic aluminide composition of NASA VIA/C-2.

This testing arrangement, together with the respective velocities and impact energies, is listed below:

Coating System	Impact Temperature °F	Velocity FPS(mps)	Energy foot-poundals (Joule)
NC11-A (Mod.)	RT	400(121.92)	1.96(0.083)
NC11-A (Mod.)	1800(1255°K)	500(152.4)	3.06(0.129)
NC11-A	RT	400(121.92)	1.96(0.083)
NC11-A	1800(1255°K)	500(152.4)	3.06(0.129)
NC4-Cr	RT	400(121.92)	1.96(0.083)
NC4-Cr	1800(1255°K)	500(152.4)	3.06(0.129)
NASA VIA/C-2	RT	400(121.92)	1.96(0.083)
NASA VIA/C-2	1800(1255°K)	500(152.4)	3.06(0.129)
NC3-L	RT	400(121.92)	1.96(0.083)
NC3-L	1800(1255°K)	500(152.4)	3.06(0.129)

Evaluation of oxidation-tested specimens after impact consisted of visual inspection of the impacted areas at 30X magnification, to determine if cracking accelerated the oxidation attack. M&PTL testing was conducted for 286 hours under the typical conditions described for other testing in the program with the results following the same trend. Coating systems NC11-A and NC11-A (Modified) exhibited the least severe attack in the impact areas. Systems NC3-L and NASA VIA/C-2 not only showed attack in the impact area, but attack of the overall coating as well. In general, all impact areas appeared to have sustained greater oxidation attack than the overall coating, as evidenced by a blue oxide and excessive oxide growth.

Metallographic examination of the cracked areas after burner rig testing showed that attack had proceeded down the open cracks but not through the diffusion area of the coating. No lateral oxidation was observed along the coating/base material interface. The attack was relatively mild.

3.6 Summary of Results - Task I

The initial phase of this program, identified as Task I, was basically a screening phase which included testing and evaluating of 15 coating modifications, a baseline coating composition, and a reference composition.

The basic approach involved improvement of an in-house-developed aluminide coating by:

(1) The incorporation of fine reactive oxides in the outer coating layer through embedment

(2) Increasing the chromium level in the coating by pack composition and embedment

(3) Increasing the aluminum level in the coating

Particle embedment studies of the various reactive oxides and metallic particles incorporated in the addition layer of the coatings comprised the first work in the program. Actual volume fraction levels of particles added to the coating compositions were less than the goals set forth in the program. In general, embedment levels averaged $\approx$ 25%, with the best system being NC2-T at 25-40%. Only one composition, baseline system NASA VIA/C-2, actually achieved the proposed goal of 30%. Although embedment was not at the proposed levels, it was sufficiently high to substantially influence the results.

Preliminary testing of all coating compositions was conducted in the M&PTL low-velocity burner rig. From this testing, the best composition of each modification group was selected for more extensive testing in the high-velocity burner rig at EPPI. Results from the first EPPI test series demonstrated that the best compositions were NC11-A, Aℓ enrichment + dispersed $A\ell_2O_3$ particles, and NC4-Cr - chromium particle addition to the basic aluminide. These two modifications remained in test for 550 hours without failure, despite a severe hot spot condition at the lower trailing edge.

Final testing in Task I involved concurrent testing at EPPI and M&PTL of the best coating compositions. Each selected composition was represented by duplicate specimens in each test. The EPPI test was terminated at the end of 662 test hours with all specimens having exceeded the 3 mg/cm^2 weight loss criterion. The bulk of the weight loss was suffered at the lower trailing edge where the hot-spot condition persisted despite all attempts to alleviate the condition. However, conclusive results were obtained in determining the most protective system, NC11-A.

Testing of the identical coating compositions in the M&PTL rig was terminated at the end of 1568 test hours. Specimens in this rig were not subject to any abnormal test conditions and were very consistent in behavior. NC11-A (Modified) and NC11-A were the most Protective Compositions from this test.

A comparison of the severity of the two test facilities was based on visual examination, weight change, and metallographic examination. The coatings from the EPPI rig were found to be totally intact in all areas except the lower trailing edge section. Furthermore, these areas appeared to have a substantial thickness of intact coating. In the case of specimens tested at M&PTL, there was a general degradation of the coating layers in all areas after 1568 test hours.

Condition of the coatings from this test was indicative of a spent coating with little life remaining, Figure 16. These results, coupled with weight change data from an intermediate test point in the two rigs, indicated a severity factor of 1.5-2 for the EPPI rig over the M&PTL rig. There is little doubt that, had the local failure in EPPI testing not occurred, the better coating compositions would have readily exceeded the goal of 800 hours.

Electron microprobe, X-ray fluorescence, and X-ray diffraction evaluation techniques substantiated the presence of the several additives in the coating compositions and that of the high residual aluminum and chromium of the best compositions.

Ballistic impact testing demonstrated that the additives to the nickel aluminide coating layers did not appreciably alter impact properties. All compositions tested, including the basic aluminide, showed cracking to the same degree under equivalent temperatures and impact energies.

SECTION 4.0

INVESTIGATION - TASK II

4.1 Coating Process Parameters Modifications

Under Task II of the program, three coating compositions [NC11-A, NC11-A (Mod.), and NC4-Cr] were selected for coating improvement studies. Since the processing parameters originally used for the above coatings produced thicknesses in the range of 1.3 - 1.6 mils (33-41μM), an obvious approach to achieve longer life was to increase coating thickness. This was undertaken by several methods:

1. Higher processing temperatures
2. Longer processing times
3. Higher aluminum activity packs

One of the methods of achieving higher aluminum activity was to process the parts within the pack mixture rather than outside the pack. As reported in Section 3.3.3, the weight gain and thickness of the coating are approximately 40 percent less with the vapor process as compared with nominal in-pack results. A coating thickness of 2.0 mils (51μM) minimum was considered the goal.

A second approach was to increase the volume fraction of embedded particles since the burner rig tests indicated the particle-rich areas of the coatings to be more oxidation resistant. Several methods were investigated:

1. Conducting a duplex cycle in which the slurry coating was applied prior to each cycle
2. Lowering the processing temperature but extending the processing time
3. Using a lower aluminum activity pack at a lower processing temperature but for an extended processing time
4. Using a lower processing temperature for a first cycle, followed by a second cycle to increase coating thickness

The latter three methods were based on an in-house investigation on another program in which it was demonstrated that a reduction in coating build-up rate promoted the entrapment of particles.

Based on the above approaches, 15 coating/process modifications were investigated. These modifications are described in Table VIII; several items in the table require clarification. In the coating designated NC11-C, the "C" refers to a pack mixture of intermediate rather than high aluminum activity which was used to reduce the rate of coating buildup, thereby increasing particle entrapment. The notation of "(Mod.)" after a coating system indicates that a slurry of Al_2O_3 and chromium was applied. "VPH" refers to those coating cycles in which the specimens were held above the pack, whereas "PACK" denotes processing within the pack mixture.

As presented in Table VIII, most of the modifications produced coating thicknesses in excess of 2.0 mils (51μM) and yet some did not achieve the desired effects. In particular, the 1800°F (1255°K)/16-hour processing did not result in an increase in embedded particles. Actually, particle entrapment dropped off under this cycle. Also, attempts to increase particle entrapment above 25-30 volume percent by other cycle modifications were unsuccessful. Apparently, this level of entrapment was the maximum that could be achieved with the "size" of particles used in the coating slurries.

4.2 M&PTL Burner Rig Screening

The 15 candidate modifications were given a preliminary screening in three low-velocity burner rigs at 2000°F (1366°K) so that the two best modifications could be selected for a 2000-hour cyclic test at 2000°F (1366°K). To expedite the screening, the severity of testing was augmented by increasing the frequency of cycling from once per hour to ten times per hour. It was anticipated that the more severe testing would discriminate among the various modifications within 200-300 hours. For many of the modifications some 500 hours of testing was needed before a decision could be made as to the two best systems for the final test.

Three burner rig tests were conducted to complete the screening of the 15 modifications. In each test series, eight paddles were tested simultaneously. An NC11-A coated paddle was included for comparison purposes in two of the tests. A bare NASA VIA alloy paddle was run in each test to monitor the severity of the individual burner rigs. Dummy specimens filled out the balance of the test sites. The latter was coated specimens which had a tip section removed for metallographic examination of the as-coated structure. Weight change data were not recorded.

Results from the three burner rig tests are presented in Tables IX, X, and XI. In tests No. 1 and No. 3, all of the coatings showed weight gains varying from 0.6 to 2.0 mg/cm^2, though test No. 1 was significantly more severe than test No. 3 on the basis of the weight loss of the bare specimen, which was three times as great in test No. 1 as in test No. 3. Moreover, at the completion of test No. 1, all of the specimens showed visual evidence of coating attack to various degrees in the top section of the airfoils whereas after Test No. 3, the coatings were intact visually. Test No. 2 was the most severe due to the burner rig operating at metal temperatures

of 2050 to 2100°F (1394 - 1427°K) (cycle range) for a period of approximately 40 hours. This occurred between the 287- and 377-hour weigh-in periods. Note the severe loss in weight that occurred for all specimens except the NC11-A-S1 and NC11-A(Mod.)-D1 specimens. The latter actually gained weight during this interval. However, it had 146 hours less burner rig time than the other coatings, being a replacement for the R'100/C-2 specimen. The test was terminated at 377 hours because most of the specimens showed signs of coating failure in the top airfoil sections. The NC11-A-S1 and NC11-A(Mod.)-D1 coated specimens were transferred to test No. 3 to accumulate additional test time.

An extensive metallographic examination was conducted on all the coated paddles. Sections were examined from the top, center, and bottom of the airfoils. Because of the differences in the severity of testing, it was difficult to assess accurately the performance on an intertest basis. However, by comparing sections which experienced equivalent temperatures based on surface oxide appearance and matrix structural changes, the NC11-A-S1 and NC11-A-D1 systems were selected. The selection of the former was made on its outstanding performance in test No. 2 under an overtemperature condition. The latter choice was more difficult because, in that same test, the NC11-A(Mod.)-D1 coating had performed equally well under the overtemperature condition though it had had 146 hours less test time. Overall, testing had indicated little difference in performance between the NC11-A and NC11-A(Mod.) coatings. Since the former is a simpler system, the decision was made to select NC11-A-D1 as the second choice.

The condition of the selected coatings after 500 hours of burner rig testing is shown in Figures 17-20. In Figure 17, the leading edges at 100X are presented and, in Figure 18, the trailing edges. Both leading edge and trailing edge coating structures at 500X are shown in Figures 19 and 20. Note that much of the coating of both compositions is still present, and that attack appears to be preferentially in the areas where the concentration of embedded particles is low or absent.

4.3 Final 2000°F (1366°K) Test

4.3.1 Preparation and Procedure

Final testing of the selected coating modifications was conducted at 2000°F (1366°K) for 2000 hours in two M&PTL burner rigs. A total of 20 paddle-wheel specimens, some with EDM holes, was processed - 10 with the NC11-A-S1 coating and 10 with the NC11-A-D1. Processing details are presented in Table XII. One specimen of each of the coating modifications was sectioned for metallographic examination and electron microprobe analysis, a second specimen of each was submitted for XRD analysis.

The testing procedure was as follows:

1. Specimen temperature was monitored optically on the leading edge at a point approximately 0.4 inch (1.0cm) below the tip of the airfoil. Optical measurements were made with the L&N and Ircon optical pyrometers. The latter instrument was set for an emissivity of 0.85. Agreement between the optical and Ircon was within 10°F (5.6°K).

2. The specimens were cycled once per hour to 900°F (755°K) or below. On burner rig No. 5, a temperature of 900°F (755°K) was attained during cooldown; and, on rig No. 4, a temperature of 875°F (748°K) was attained, as measured with an Ircon No. 300 series Model T.

3. The test schedule of specimens in the burner rigs is presented in Table XIII. At the end of each 500-hour period, the specimens were photographed, and one specimen of each coating system was removed and replaced with a specimen of the same system. The test specimens were submitted for metallographic examination, microprobe analysis, and XRD.

4. Specimens were weighed at approximately 100-hour intervals. Measurement periods varied because the burner rigs operated continuously including the weekends. Failure criterion was 3 mg/cm^2.

5. An uncoated specimen was included with each group of test specimens to compare the relative severity of the two burner rigs and to indicate if the same degree of severity was maintained in the individual burner rigs as the testing progressed. The uncoated specimen in burner rig No. 5 was removed after 1500 hours and replaced with a standard NC11-A coating. In rig No. 4, the uncoated specimen continued on test for the full testing period. Examination of these specimens provided a measure of the oxidation behavior of the uncoated alloy and the structural changes induced by the extended exposure at 2000°F (1366°K).

4.3.2 Coating Performance

Cumulative weight changes of the coated specimens are presented graphically in Figures 21 and 22, and in Figure 23 for the uncoated specimens. In burner rig No. 5 (see Figure 21), the performance of each coating modification was highly reproducible, and there was only slight variation between modifications. The specimens with the EDM holes tended to show greater weight loss than the solid specimens. Such behavior could be anticipated, since some of the holes were only partially coated.

Based on an airfoil surface area of 40 cm^2, weight losses after 2000 hours on the NC11-A-S1 coated specimens were 1.15 mg/cm^2 for the solid specimen and 2.67 mg/cm^2 for the one with the EDM holes. Both weight losses were under the 3.0 mg/cm^2 failure criterion. The NC11-A-D1 coated specimens, both solid, had weight losses of 1.91 and 1.97 mg/cm^2.

In burner rig No. 4 (see Figure 22), coating performance was very similar, though burner conditions appeared to be slightly less severe. Weight losses for the NC11-A-S1 coatings, both solid specimens, were 0.92 and 1.09 mg/cm^2, while the NC11-A-D1 coated specimen with EDM holes showed a loss of 1.57 mg/cm^2, and the one without holes showed a loss of 0.70 mg/cm^2.

The slightly less severe burner conditions are reflected in the performance of the uncoated specimens during the first 1500 hours of testing, Figure 23. For the first 1000 hours, the weight losses were in very close agreement. However, after 1000 hours there appears to be a slight divergence. This may have been the result of modification and rewiring of the burner rigs to incorporate additional safety controls which occurred at approximately 1100 hours of testing.

Significant observations during the course of testing are recorded in Table XIV. The pinpoint attacks on the airfoil trailing edge tips and on the upper portion of the trailing edges were not unexpected. Both the leading and trailing edges of the paddles heat up more rapidly during the heat-up cycle and cool more rapidly during the cool-down cycle. The trailing edges, being thinner than the leading edges, overtemperature during heatup. Optical measurements at approximately 0.4 inch (1.0cm) below the tip registered temperatures of 2050 - 2060°F (1394 - 1400°K). Also, under steady state operation, the trailing edges ran 20 - 30°F (11 - 17°K) hotter than the leading edges where the 2000°F (1366°K) temperature was monitored. Optical measurements on the leading edge at 1.0 inch (2.54cm) and 1.5 inches (3.81cm) below the airfoil tip gave readings of 1970 - 1980°F (1350 - 1355°K) and 1950 - 1960°F (1339 - 1345°K) respectively, during steady state operation.

Under steady state operation, the temperature normally fluctuated over a range of 15 - 20°F (8.4 - 11.0°K). To compensate for this fluctuation, the temperature controller was set so that the leading edges reached a peak fluctuation temperature of 2005 - 2010°F (1369 - 1372°K).

4.4 Evaluation

4.4.1 Metallographic Examination

The coated specimens were sectioned for metallographic examination, as coated and after approximately 500, 1000, 1500, and 2000 hours of testing. Sections were taken at 0.4, 1.0, and 1.5 inches (1.0, 2.54, and 3.81cm) below the airfoil tip on the solid specimens and thru the holes of the EDM-drilled specimens. The critical section for examination was at the 0.4-inch (1.0cm) level, where the 2000°F (1366°K) temperature was being monitored. Examination was made also of those areas that showed visual evidence of coating attack. The uncoated specimen was sectioned after approximately 1500 hours of testing.

4.4.1.1 As-Coated Specimens

The structure of the NC11-A-S1 coating, as-processed, is shown in Figure 24 (top) and of NC11-A-D1 in Figure 24 (bottom) at 500X magnification. Both coatings are 2.3 - 2.4 mils (58 - 61μM) thick, with a particle-embedment level of 20 -25 volume percent in the NC11-A-D1 coating and 15 - 20 volume percent in the NC11-A-S1 coating. Uniformity of particle entrapment was not achieved, as illustrated by some grains in the coatings being devoid of particles. However, it must be realized that only one plane through an individual grain is being examined - other planes may contain particles.

Penetration of the NC11-A-S1 coating into the EDM-drilled holes is shown in Figure 25 at 100X magnification. This section through a 0.020-inch (0.05cm) hole shows the coating at the leading edge and to a depth of 0.185 inch (0.47cm) where an irregularity of the drilled hole occurred. There is little evidence of embedded particles in the coating within the holes. The NC11-A-D1 coating, not shown, was not significantly different.

4.4.1.2 After 2000°F (1366°K)/500 Hours

The two specimens removed after ~ 500 hours were an NC11-A-S1-coated solid specimen from burner rig No. 5 and an NC11-A-D1-coated specimen with EDM holes from burner rig No. 4. Weight gains were 0.44 and 0.40 mg/cm^2, respectively. Figure 26 (top) shows the NC11-A-S1 leading edge section to have sustained little or no coating degradation. Some aluminum depletion has occurred as indicated by the presence of the "white" phase in the coating (subsequently identified to be gamma). This is confirmed by microprobe analysis in a subsequent section. Coating-thickness measurements reveal a growth in thickness of about 0.4 mil (10μM). On the trailing edge, Figure 26 (bottom), some degradation has occurred and the amount of "white" phase has reached a significant level. One area, Figure 27, shows oxidation attack into the diffusion zone. This is from the area where a pinpoint attack was observed and is attributed to the overtemperature during heatup.

The leading and trailing edges of the NC11-A-D1-coated specimen, Figure 28, reveal less effect of the 500-hour exposure, especially on the trailing edge. In both cases, "white" phase transformation was less pronounced. However, this specimen also had a pinpoint attack on the airfoil tip near the trailing edge, Figure 29. It appeared to be associated with a defect at the parting line of the casting, though this section also overtemperatures during heatup in the burner rig. Examination of a section through the 0.020-inch (0.05cm) EDM hole, Figure 30, indicated that the coating had penetrated to nearly the full depth of the hole (0.234 inch (0.59cm) versus 0.250 inch (0.64cm)). Though there is little evidence of particle entrapment at the entrance section of the hole, Figure 30 (top), there appears to be a significant amount near the exit of the hole. Where no coating was present, a considerable amount of alloy depletion and scaling took place.

4.4.1.3 After 2000°F (1366°K)/1000 Hours

At the 1000-hour test point, both of the specimens removed had EDM-drilled holes (an NC11-A-S1 coating from burner rig No. 4 and an NC11-A-D1 coating from burner rig No. 5, after 995 and 1013 hours, respectively). Corresponding weight changes were -0.04 and +0.19 mg/cm^2. The NC11-A-S1 coating on the leading and trailing edges, Figure 31, had undergone a considerable change. More than 50 percent of the outer coating layer had transformed to the "white" phase on the leading edge and about 90 percent on the trailing edge. The concentration of oxide particles has decreased. However, there has been little reduction in thickness of the outer coating layer.

In contrast, the NC11-A-D1 coating, Figure 32, had fully transformed to the "white" phase, both at the leading edge, Figure 32 - top, and the trailing edge, Figure 32 - bottom. Attack of the leading edge coating is evident, though there has been little reduction in outer layer thickness. On the other hand, significant attack has occurred at the trailing edge, and the outer layer has been materially reduced. A local trailing edge area, where the attack has penetrated the coating, is shown in Figure 33 at 100X magnification. This represents one of the pinpoint attack areas previously mentioned.

The condition of the coated EDM holes is shown in the next group of Figures, 34-36. For each of the holes (0.012, 0.020, and 0.040 inch) (0.03, 0.051, and 0.10cm), the leading edge section and the section at maximum depth of coating protection are illustrated. In the 0.012-inch (0.03cm) hole (Figure 37), the NC11-A-S1 coating had penetrated to a depth of 0.168 inch (0.43cm) and was essentially intact over that distance. Virtually all of the coating had transformed to the "white" phase. Where the hole was uncoated, gross scaling and alloy depletion occurred. Coating protection extended to a depth of 0.200 inch (0.51cm) in the 0.020-inch (0.05cm) hole, Figure 35. The coating appears to be in much the same condition as that in the 0.012-inch (0.03-cm) hole. Since the 0.012-inch (0.03-cm) hole is 1/4 inch (0.64cm) below the tip, and the 0.020-inch (0.05 cm) hole, 7/16 inch (1.1cm), both would experience essentially the same exposure. Coating in the 0.040-inch (0.10cm) hole penetrated the full depth, 0.250 (0.64cm) inch (Figure 36), though little coating remains at the extreme depth. Still, there is no evidence of oxidation attack or alloy depletion. There has been less transformation to the "white" phase. The NC11-A-D1 coating performance in the EDM holes was virtually the same as the NC11-A-S1, except that the depth of penetration was 0.020 - 0.030 inch (0.05 - 0.076cm) less.

4.4.1.4 After 2000°F (1366°K)/1500 Hours

After 1483 hours, an EDM-drilled specimen with the NC11-A-S1 coating was removed from burner rig No. 5; and, after 1495 hours, a solid specimen with the NC11-A-D1 coating was removed from burner rig No. 4. Weight losses were 1.31 and 0.52 mgs/cm^2, respectively. The uncoated specimen from burner rig No. 5 was also removed. It had lost 252 mgs or 6.3 mgs/cm^2.

The condition of the NC11-A-S1 coating from a section through the 0.012-inch (0.03cm) hole is shown in Figure 37 for both the leading and trailing edges at 500X. Considerable degradation of the other layer of the coating had occurred at the edge of the hole, Figure 37 - top, while at the trailing edge, Figure 37 - bottom, most of the outer coating layer was still intact though reduced in thickness. There was only partial transformation to the "white" phase. A 100X magnification of the leading edge section at the 0.012-inch (0.03-cm) and 0.020-inch (0.05cm) holes (Figure 38) shows the coating to be intact in areas adjacent to the holes.

The uncoated specimen, which was removed from burner rig No. 5 at the same time as the NC11-A-S1 specimen, illustrates the extent of metal loss and alloy depletion at the trailing edge, 0.4 inch (1.0cm) below the tip, Figure 39 - top, and 1.5 inches (3.8cm) below the tip, Figure 39 - bottom. The extent of alloy depletion at the corresponding leading edge sections, Figure 40, was significantly lower, indicating that the very tip of the lower trailing edge experienced approximately the same temperature as the top leading edge section.

The NC11-A-D1 coating after 1495 hours showed some degradation in local areas of the leading edge, Figure 41 - top, but confined only to the upper portion of the outer coating layer. At the trailing edge, the degradation was more severe, progressing well into the inner diffusion zone, Figure 41 - bottom. The rounded appearance of some of the void areas would indicate that melting had taken place at some point during testing. Overall, the coating was still protective as illustrated in a 100X view of the trailing edge, Figure 42.

4.4.1.5 After 2000°F (1366°K)/2000 Hours

At the conclusion of the 2000-hour test in burner rig No. 5, one specimen of each coating system which had logged 2000 hours was sectioned for metallographic examination. Weight losses on these specimens were 1.15 mgs/cm^2 for the NC11-A-S1 coating and 1.9 mgs/cm^2 for the NC11-A-D1. Both were solid specimens. Sections were taken at 0.4, 1.0, and 1.5 inches (1.0, 2.54, and 3.81cm) below the airfoil tip. Examination was made around the periphery of each section; photomicrographs were taken of the leading and trailing edges of each cross section at 100X magnification and of the leading edge, trailing edge, and center convex sections at 500X magnification (Figure 43 - 52).

The trailing edge views of the NC11-A-S1 coating are shown in Figure 43 at 100X. Only the section at the 0.4-inch (1.0cm) location shows a small local coating breakthrough, Figure 43 - top; the coating was still providing protection at the other locations, Figure 43 - center and bottom. The corresponding leading edge sections all appear to be intact, Figure 44. At higher magnification (500X), a continuous "gray" phase is seen along the surface of the leading and trailing edge sections and scattered islands of the same phase in the region below, Figure 45 - top and bottom. Analysis of this layer will be discussed under the electron microprobe sections

4.4.2.1 and 4.4.2.2. In the convex center section, Figure 45 - center, the coating is virtually intact with a high concentration of oxide particles still evident. At the 1.0-inch (2.54-cm) level, Figure 46 - top, much of the coating at the leading edge is still intact with many oxide particles still present, but voids have formed in the inner diffusion zone. In the center convex section, Figure 46 - center, the coating is virtually intact, though much of the outer layer has transformed to the "white" phase. The trailing edge section, Figure 46 - bottom, appears to have the same continuous "gray" layer as was observed at the 0.4-inch (1.0-cm) level. At the 1.5-inch (3.81-cm) level, Figure 47, the coating is intact at all three sections with little reduction in thickness of the outer coating layer. Again, we see the darker phase where the oxide particles are more concentrated, Figure 47 - center.

On the NC11-A-D1 coating, Figures 48 and 49, there were some pinpoint coating penetrations on both the leading and trailing edges, which would account for the greater weight loss that this specimen experienced. At 500X magnification, Figure 50, the 0.4-inch (1.0-cm) level shows thicker layers of the "gray" phase noted in Figure 45 and severe degradation of the coating in the center convex section, Figure 50 - center. At the 1.0-inch (2.54-cm) level, Figure 51, only the trailing edge section shows the continuous "gray" phase, the coating being intact at the leading edge and center convex sections. The appearance of the coating at the 1.5-inch (3.8-cm) level, Figure 52, is very similar to that at the 1.0-inch (2.54-cm) level.

Overall, both the NC11-A-S1 and NC11-A-D1 coatings were highly successful in providing protection to the NASA V1A alloy. Exposure temperature appears to be very critical as shown by the marked difference in coating behavior near the tip area where the temperature was 2000°F (1366°K) and above and the root section which experienced 40-50°F (22-28°K) lower temperatures. The coatings remained fully intact after 2000 hours in the latter areas. Though the evidence is not conclusive, it would appear that the oxide particles prolong coating life.

4.4.2 Electron Microprobe Analysis

Electron microprobe analysis was made on the coatings at the convex leading edge section, 0.4 inch (1.0cm) below the tip and approximately 1/8 inch (0.32cm) back. Analysis was made of the as-coated condition and after testing intervals of approximately 500 hours. The as-coated, 500- and 1000-hour specimens were scanned for the principal elements (Aℓ, Cr, Ni, Ta, W, and Ti); the 1500- and 2000-hour specimens, for Aℓ and Cr only. Elemental traces were made only for Aℓ and Cr.

4.4.2.1 Elemental Scans

The elemental scans are shown in Appendix D, Figures D-1 to D-10. Though Ti scans were made, they are not presented in the figures because of titanium's low concentration in the alloy and in the coating. It tended to segregate at

the interface of the outer coating and the inner diffusion zone. It was also observed to segregate where Ta and W were present. Both Ta and W were found to be highly segregated in the inner diffusion zone of the coating and in the matrix, Figures D-1 and D-2. This concentration of W and Ta at the same sites intensified with increased exposure time, Figures D-3 to D-6. The significant changes with time were in the aluminum and chromium concentrations.

In the as-coated condition, the aluminum level was high in the outer coating layer, falling rapidly through the inner diffusion zone to a uniform level in the matrix, Figures D-1 and D-2. After 500 hours, the aluminum level dropped in the outer coating layer, and that of the inner diffusion zone leveled off with the matrix, Figures D-3 and D-4. At 1000 hours, a very high aluminum level at the surface is seen, indicative of oxide formation, Figures D-5 and D-6. In some areas of the outer coating layer, the concentration appears to be at base material level, 5-6 W/O, indicating transformation of the NiAℓ phase to gamma. After 1500 hours, the depletion of aluminum in the outer coating layer becomes more pronounced, Figures D-7 and D-8 - left center. These areas correspond with the "gray" phase as shown optically in Figure 37 after 1500 hours and in Figure 45, top and bottom, after 2000 hours. A trace at the center of the convex surface, however, shows the aluminum level to be still high. An additional 500-hour exposure did not produce significant change, Figures D-9 and D-10.

Chromium levels as-processed and after exposure were the same for the two coating systems. As-processed, there was an increase of chromium in the inner diffusion zone and a sharp gradient drop to the surface, Figures D-1 and D-2. After 500 hours exposure, the concentration in the outer coating layer leveled off with that of the matrix, Figures D-3 and D-4, with some tendency to segregate. After 1000 hours, the segregation became more pronounced, but the concentration in the coating remained at the same level, Figures D-5 and D-6. The same condition persisted after 1500 hours, but there was also evidence of increased chromium in the surface scale, Figures D-7 and D-8. After an additional 500 hours, there is further chromium concentration at the surface and in islands below the surface corresponding to the "gray" phase areas observed optically in Figure 50, top.

4.4.2.2 Elemental Traces

The elemental traces for aluminum and chromium illustrate more definitively the concentration levels in the coating and matrix. Since the distribution of the oxide particles was not uniform, traces were made in areas where the particle volume fraction was high and where it was low or void of particles. The path of the electron microprobe beam was directed into the different areas of interest, in order that areas with and without particles be fully distinguished. Beginning with the NC11-A-S1 coating, Figure D-11, aluminum levels of 40 - 50 percent were recorded in the particle-rich areas and of 20 - 25 percent in the particle-free areas. The latter would approximate closely the actual aluminum level in the individual grains, indicative

of a NiAℓ composition. Chromium varied from 12 to 15 percent in the inner diffusion zone and dropped to 2-3 percent at the coating surface. The initial 500-hour exposure dropped the aluminum level drastically, down to 20 - 25 percent in the particle-rich areas, and as low as 8 - 10 percent in a particle-free area that had transformed to the "white" phase indicative of gamma, Figure D-12. After 1000 hours, there was a further loss of aluminum down to 15 percent in the particle-rich areas and only 8 percent where the transformation to the "white" phase had occurred. In the latter case, the high Aℓ concentration at the surface indicates $A\ell_2O_3$ or $NiA\ell_2O_4$ scale formation. For a more precise analysis of aluminum concentration, a number of spot point count measurements was made on individual grains of both the "white" and "dark" phases, with and without particles. These results on NC11-A-D1 are summarized as follows:

Coating Section	Appearance	Average Counts	Percent Aluminum
Outer Layer Inside Hole	White-No Particles	730	~ 6.5
Outer Layer Convex Surface	White-No Particles	800	~ 7.0
Outer Layer Convex Surface	Dark-No Particles	1650	~14.0
Outer Layer Convex Surface	White-Particles	1680	~14.0
Outer Layer Convex Surface	Dark-Particles	2900	~24.0

Apparently, the oxide particles affected the count even though efforts were made to manipulate the probe in areas between particles. The results confirm the "white" phase to be gamma and the "dark" phase to be predominantly gamma prime, $Ni_3A\ell$. At 1500 hours, the aluminum level dropped to that of the matrix. An additional 500 hours of exposure produced oxidation within the coating, as evidenced by the very high aluminum peak, Figure D-12, far right.

The changes in chromium were less drastic, Figure D-13, but of significant interest. In the particle-rich areas, the chromium had leveled off after 500 hours exposure at approximately 8 percent, while a particle-free grain contained about 6 percent, Figure D-13 - lower left. With an additional 500 hours, the chromium level in the outer coating layer remained about the same and then dropped to about 5 percent after 1500 hours. In all cases, it remained high at the original inner diffusion zone/matrix interface, holding at about 15 percent. Little further change occurred after 2000 hours except for a chromium concentration at the surface indicating its presence in the surface scale.

The behavior of the NC11-A-D1 coating was not significantly different, Figures D-14 through D-16. In the as-coated condition, Figure D-14, the aluminum concentration across the outer coating layer was flatter than in the NC11-A-S1 in the particle-rich areas. Chromium concentration, though, was nearly identical in pattern. After 500 hours exposure, Figure D-15, the aluminum level in the particle-rich area was somewhat higher (25 - 35 percent); it was also higher in the particle-free zone (~ 18 percent). This higher aluminum persisted through the 1500-hour exposure, the two levels becoming equivalent at the 2000-hour exposure. At 1500 hours, a trace through the center convex section (where the coating was fully intact) showed a significantly higher aluminum concentration, Figure D-15 - right, center. The chromium traces followed the same pattern as those for NC11-A-S1 in the outer coating layer and inner diffusion zone. However, as the matrix structure coarsened during exposure, the chromium became more and more segregated, as reflected by the numerous spikes in the 1500- and 2000-hour specimens.

4.4.3 X-Ray Diffraction Analysis

X-ray diffraction patterns, Table XXV, were made on the convex side of the paddle airfoil approximately 1/2 inch (1.27cm) below the top of the paddle. Both final systems (NC11-A-S1 and NC11-A-D1) were evaluated as-coated and after 500-, 1000-, 1500-, and 2000-hour exposures. In addition, the oxide layer was removed from the tested paddles by vapor honing with the underlying surface then being subjected to X-ray diffraction analysis.

4.4.3.1 Phase Identification

In the as-coated condition, See Table XV, only $NiA\ell$ and $\alpha A\ell_2O_3$ patterns were obtained for both coatings, the $NiA\ell$ corresponding to the aluminum in the particle-free areas. After 500 hours, as-exposed, patterns for $Ni_3A\ell$, $\alpha A\ell_2O_3$, and $NiA\ell_2O_4$ were obtained, the latter phase being relatively weak. After removal of the scale, by vapor honing only $Ni_3A\ell$ and $\alpha A\ell_2O_3$, patterns were found. There was no evidence of residual $NiA\ell$. The same patterns were obtained after 1000, 1500, and 2000 hours plus lines indicative of the gamma phase. In the as-exposed condition, the intensity of the $NiA\ell_2O_4$ phase increased with increasing exposure time. This was noted visually during testing by the gradual increase in the blue-colored scale formation with increasing test time.

Since the X-ray patterns for $Ni_3A\ell$ and gamma are very similar, the presence of $Ni_3A\ell$ can only be confirmed by one of the superlattice lines which coincides with one of the $A\ell_2O_3$ lines. Therefore, in Table XV, $Ni_3A\ell$ and gamma are listed together. However, based on the aluminum content from the electron microprobe analysis, gamma can be presumed to be the predominant phase present after the 1500- and 2000-hour exposures.

4.4.4 Effect of Coatings on Mechanical Properties

The mechanical properties evaluated for the effects of coatings were tensile strength, ultimate and yield, elongation, reduction of area, and stress rupture. Tensile testing was conducted at 1400°F (1033°K) and 1800°F (1255°K). Stress rupture was performed at 1800°F (1255°K) at a stress level of 29,000 psi (199.9×10^6 nt/m^2); test results are presented in Tables XVI and XVII, respectively.

Since only two specimens of each coating were tested in each condition, definitive conclusions could not be made. From the limited data, it would appear that the coatings do not degrade the mechanical properties nor affect the ductility.

4.5 Summary of Results - Task II

Fifteen coating process modifications were investigated to increase coating thickness and volume fraction of entrapped particles. In all cases, a thickness of 1.9 mils (48μM) or higher was achieved in a single-cycle VPH process of 4 hours at 2000°F (1366°K) or above and of a two-cycle VPH process of 4 hours each at 1925°F (1324°K). An 1800°F (1255°K)/16-hour cycle and a two-cycle process of 2 hours at 1900°F (1311°K) followed by 2 hours at 2000°F (1366°K) yielded thicknesses of 1.7 - 1.8 mils (43 - 47μM). All of the modifications involving processing in the pack mixture produced thicknesses of 2.1 mils (53μM) or above. Highest volume functions of embedded oxide particles, 25-30%, were obtained with the two-cycle VPH and in-pack processes. Poorest particle embedment was with the 1800°F (1255°K)/16-hour treatments.

Burner rig screening of the coatings produced by the above processing modifications resulted in the selection of a single-coating cycle of 2000°F (1366°K)/4 hours, and a double-coating cycle of 1925°F (1324°K)/4 hours each. For the screening test, the former (NC11-A-S1) produced a coating thickness of 1.9 mils (48μM) with a oxide particle volume function of ~ 10% and the latter (NC11-A-D1) 2.3 mils (58μM), with a volume function of particle of ~ 25%, Table XVIII.

In processing the first groups of paddle specimens for the 2000-hour burner rig tests, thicker coatings [2.3 - 2.4 mils (58 - 61μM)] were produced by both processes with volume fractions of embedded particles of 15 - 20 and 20 - 25 percent for NC11-A-S1 and NC11-A-D1, respectively, Figure 30. Greater thicknesses were also reflected in coating weight gains above 6.0 mg/cm^2, Table XXII.

In subsequent coating runs, KZ and HZ-IZ, there was a significant drop in weight gain with a corresponding decrease in coating thickness. A satisfactory explanation for this drop could not be established. Consequently, the latter specimens were only used as replacements in the test program.

However their performance for comparable test periods did not appear to be appreciably different from that of the thicker coatings.

The throwing power of the two coating cycles was demonstrated on the specimens with the EDM holes. Coatings were produced to a depth of ~ 0.170 inch (4.2μM) in the 0.012-inch (0.3-μM) diameter holes, ~ 0.200 inch (5.0μM) in the 0.020-inch (0.5-μM) diameter holes, and the full 0.250-inch depth in the 0.040-inch (1.0-μM) diameter holes. The number of test specimens was too limited to determine significant coating depth[4] difference between the two processes.

Both coating modifications satisfactorily passed the 2000-hour cycle tests at 2000°F (1366°K), cycling once per hour to 900°F (755°K) or below. Weight losses were well below the 3 mg/cm^2 criterion. Some specimens showed isolated localized attack down to the substrate in areas which tended to overtemperature during the heat-up cycle in the burner rig. The specimens with the EDM holes showed greater weight losses than the solid ones. This was not unexpected, since the smaller-diameter holes were not fully coated.

During the initial phase of the testing, the weight increase was parabolic, reaching a plateau between 500 and 800 hours. With continued exposure, there was a gradual loss in weight to between 1200 and 1500 hours where a net loss was experienced. Weight loss then increased at an accelerated rate for the balance of the test. Coating behavior followed a fairly definite pattern. During the initial period of continuous weight gain, the coating surfaces were dull gray with blue areas beginning to appear after 500-800 hours. The bluish areas were confined to the upper airfoil section, in particular at the leading and trailing edges where somewhat higher temperatures were experienced. The bluish areas tended to increase as the specimens began to lose weight and became more pronounced as the weight loss accelerated.

Metallographic examination, microprobe analysis, and X-ray diffraction at 500-hour intervals revealed the corresponding structural and compositional changes that had occurred. During the first 500-hour period, the protective oxide film was predominately αAl_2O_3 with minor amounts of $NiAl_2O_4$. All of the outer coating had transformed from $NiAl$ to Ni_3Al. After 1000 hours, increasing amounts of $NiAl_2O_4$ were present in the scale and some of the Ni_3Al has degenerated to γ. After 1500 hours, little or no Ni_3Al could be detected in the coating, and the oxide film had become predominately $NiAl_2O_4$.

Transformations also occurred in the structure and composition of the substrate material adjacent to the coating. The first 500 hours of exposure produced pronounced segregation of tantalum and tungsten in the same areas. A corresponding segregation of chromium became evident after 1500 hours and increased in concentration after 2000 hours. The segregation of chromium appeared to coincide with the coarsening of the grain structure. Aluminum diffusion from the coating into the substrate apparently was minor, there being little evidence of an increase in the aluminum level.

The above transformations had little effect on the mechanical properties. Tensile tests at 1400°F (1033°K) and 1800°F (1255°K) and stress-rupture tests at 1800°F (1255°K) showed little or no effect for either coating.

SECTION 5.0

DISCUSSION

This investigation identified an aluminide coating composition, NC11-A, for NASA VIA alloy, that met the goals of a 2000-hour life at 2000°F (1366°K) under low-velocity cyclic conditions and an 800-hour life at 2000°F (1366°K) under high-velocity cyclic conditions. The latter was a projected life based on the intact condition of the coating in the area where the 2000°F (1366°K) temperature was being maintained when the test was terminated (after 662 hours, due to a localized overtemperature condition). Two processing cycles were developed that produced coatings of equivalent performance: a single-cycle of 2000°F (1366°K) for four hours (NC11-A-S1) and a two-cycle process of 1925°F (1322°K) for four hours each (NC11-A-D1). These processes produced coating thicknesses of 2.0 - 2.5 mils (51 - 65μM) and volume fractions of embedded $A\ell_2O_3$ particles of 15-25 percent; the higher volume fractions were achieved with the two-cycle process. In both processes, the coating was produced by vapor phase deposition above the pack mixture to simulate the coating of hardware containing small cooling holes which could become plugged if the part were submerged in the pack mixture. The throwing power of the processes was demonstrated, in that EDM holes of 0.012-inch (0.03-cm) diameter were effectively protected to a depth of 0.170 inch (0.43cm), 0.020-inch (0.05-cm) diameter holes were effectively protected to a depth of 0.200 inch (0.51cm), and 0.040-inch (0.10-cm) diameter holes were effectively protected to a depth of 0.250 inch (0.64cm).

The above coatings were the culmination of a series of studies to improve an in-house-developed aluminide coating incorporating a dispersion of $A\ell_2O_3$ and TiO_2 particles (CODEP C-2) by: (1) substituting other reactive metal oxide particles as dispersoids, (2) increasing the aluminum level of the coating, and (3) increasing the chromium level.

Of basic interest was the role of oxide particles in benefitting coating life. As discussed in the INTRODUCTION, it had been postulated that oxidation behavior may be structure sensitive with the fine-grained structure produced by the $A\ell_2O_3$ particles in CODEP C-2 being more resistant to attack than the coarse-grained structure obtained in the absence of particles. These studies generated no support for this concept. The other reactive metal oxides, Y_2O_3, La_2O_3, and ThO_2 all promoted grain refinement, but the resultant coatings were all short lived. In the case of La_2O_3, it was found that the fluoride activator used in the coating process reduced the La_2O_3 to LaF_3. As an embedded particle, the fluoride proved very detrimental to oxidation resistance and resulted in premature failure. On the other hand, where the coating structure was refined by the aluminum oxide particles, a relatively short time exposure at elevated temperature produced grain growth, thus negating possible beneficial effects of a fine-grained structure. The negative results with Y_2O_3 and ThO_2 could not be explained, particularly the ThO_2, which yielded the highest volume fraction of particle embedment.

The addition of MnO along with the other oxide particles to improve oxide scale adherence did not prove successful. During processing, the MnO was reduced by the hydrogen and the fluoride activator, causing the slurry coating to sinter to the surface and preventing the transfer of manganese to the coating. Thus, the anticipated beneficial effect of manganese could not be evaluated.

Chromium enrichment by codeposition from a pack mixture containing Cr-Aℓ alloy powder failed to produce satisfactory coatings. Only the chromium particle embedment process resulted in a high performance coating, NC4-Cr. Though the improvement can be attributed to the actual embedment of chromium particles, it is also highly probable that some chromizing occurred simultaneously during the coating process from chromium particles in the slurry coating. The beneficial effect of chromium would be in the $NiCr_2O_4$ spinel formed on exposure. One problem with the NC4-Cr coating was the lack of consistency in results, an indication that further development effort was needed to improve coating uniformity.

The best performance improvement was achieved by aluminum enrichment combined with a very fine dispersoid of $A\ell_2O_3$ particles, NC11-A. Whereas the oxide particles in the baseline CODEP C-2 coating were 2-10μM in size, those in the NC11-A coating were 2μM or finer. In areas where these particles reached a concentration of 20-25% in the outer coating layer, the overall aluminum level rose above 40%, reducing the corresponding nickel concentration. The diffusion of chromium and other elements from the substrate also contribute to a lower nickel concentration. The lower nickel concentration appeared to be a factor in longer coating life. Since the activity of an element is directly related to its concentration, a low-nickel and high-aluminum concentration formation of $A\ell_2O_3$ at elevated temperature will predominate. NiO or $NiA\ell_2O_4$ will only begin to form when the aluminum has dropped below a certain critical level, $\sim$ 14.0%. This is readily observed in the bottom views of Figures 16, 19, and 20, which show attack in areas that are devoid of particles, whereas the particle-rich areas are intact. An earlier stage of aluminum depletion is seen in Figure 28, in which only a small transformation to gamma (white phase) has occurred where the oxide particle concentration is high, Figure 28 - top, in contrast with the more extensive transformation, Figure 28 - bottom, where the particles are less concentrated.

In addition to their influence on elemental activity, the $A\ell_2O_3$ particles appear to fulfill several other roles in prolonging coating life. The particles tend to be more concentrated near the surface than uniformily distributed throughout the outer layer. Thus, an intermittent oxide layer is already present prior to exposure. Consequently, less aluminum is needed to maintain the protective surface oxide film. The oxide film that first forms is highly adherent and appears to be anchored by the oxide particles. During the first 500 hours of exposure at 2000°F (1366°K), there was no observable evidence of oxide spalling. Only with the formation of the $NiA\ell_2O_4$ spinel, which began after approximately 500 hours, did the first evidence of spalling appear. Apparently, the particles were less effective in anchoring the $NiA\ell_2O_4$ spinel.

The subsequent stages of coating transformation are less clearly understood. Here the role of chromium may have increased significance. In the as-processed condition, the chromium concentration in the outer coating layer of the NC11-A-S1 coating varied from 2-3% at the surface to about 9% at the outer coating layer/inner diffusion zone interface, Figure D-11. Within the inner diffusion zone, the concentration varied from 12-14%. After 500 hours of 2000°F (1366°K) exposure, the chromium concentration in the outer coating layer leveled out at between 8 and 9%, Figure D-12, and after 1000 hours experienced a slight drop to between 7 and 8%. During the same period, the aluminum level had dropped to about 14% in the $A\ell_2O_3$ particle-rich areas and approximately 7% in the particle-free areas. In spite of the low aluminum level in the latter case, oxidation resistance was still very high. Apparently, a highly-oxidation-resistant, gamma-type alloy had formed. In a recent study on the behavior of nickel-base superalloys by Kvernes and Kofstad[13], a nickel - (9%)Cr - (6%)Aℓ alloy was found to have exceptional oxidation resistance at 1200° and 1300°C (1473° and 1573°K). This composition is very close to that observed above.

Subsequent exposure for 1500 and 2000 hours produced a continuous gray surface layer and islands of the same phase within the residual coating, Figures 45, 50, 51 - bottom, and 54 - bottom. The original outer coating layer is no longer evident, and only the inner diffusion zone remains. Aluminum and chromium in these areas remain at 6-7%, constituting a gamma composition that is unusually oxidation resistant.

The performance of the coatings in the EDM holes warrants comparison with that of the exterior coating. These internal coatings were essentially free of embedded oxide particles, yet their performance was very similar to the exterior coatings. This would be due, in part, to oxidizing conditions within the holes more nearly approaching those under static conditions, since the coatings were not exposed directly to the alternate hot gas and cooling air impingement during the burner rig heating and cooling cycle. Moreover, heating and cooling rates within the holes would be slower than on the exterior surface, and the actual cyclic temperature range would be lower, thereby reducing thermal shock. Consequently, there would be less tendency for the protection oxide film to spall and degrade.

The processes, as-developed, are directly applicable to turbine blades and vanes incorporating cooling holes and internal passages. In current and advanced configurations of these components, cooling holes normally do not extend more than 0.150 inch (0.38cm) deep, though depths up to 0.250 inch (0.63cm) may be encountered in some applications. Retention of hole dimension is critical to the successful operation of air-cooled hardware. Thus, these processes afford protective coatings in dimensionally critical areas.

In assessing the future possibilities of the NC11-A coating, one must bear in mind that this investigation covered primarily the oxidation behavior of the coating and very limited mechanical property effects. Much more must be known before engine evaluation would be warranted. The coating performance

in a hot-corrosion environment is a first consideration. Behavior under thermal shock must be established. Additional high-velocity burner rig testing is needed as well as an extensive mechanical properties effects study. Further processing studies should be conducted to demonstrate coating reproducibility and particle distribution uniformity.

SECTION 6.0

CONCLUSIONS

1. An improved aluminide coating, NC11-A, was developed for NASA VIA alloy with a projected protective life of 800 hours at 2000°F (1366°K) under high-velocity cyclic testing and 2000 hours at 2000°F (1366°K) under low-velocity cyclic testing.

2. Two processing cycles were developed for NC11-A that yielded essentially equivalent performance, a single cycle of 2000°F (1366°K) for four hours and a double cycle of 1925°F (1322°K) for four hours each.

3. Coating performance of the NC11-A coating was at least double that of the baseline CODEP C-2 coating which outperformed the reference coating, CODEP C-2, on IN 100.

4. Oxide particles, other than $A\ell_2O_3$, were not beneficial as dispersoids in the coating but were actually detrimental. Ultra-fine $A\ell_2O_3$, = 2μM, at volume fractions of 15-25%, contributed to increased coating life.

5. Aluminum enrichment of the coating was definitely beneficial through the formation of hyperstoichiometric $NiA\ell$ in the presence of $A\ell_2O_3$ particles, which retarded the conversion to $Ni_3A\ell$ during elevated-temperature exposure.

6. Good performance was achieved through chromium enrichment with dispersed chromium particles although reproducibility was not consistent. Chromium enrichment by codeposition from Cr-$A\ell$ alloy powder was not successful.

7. Testing in the high-velocity burner rig at EPPI was $1\frac{1}{2}$-2 times more severe than testing in the low-velocity burner rig at M&PTL.

8. Mechanical properties, tensile and stress-rupture, are not appreciably affected by the improved aluminide coatings.

SECTION 7.0

REFERENCES

1. Collins, H.E., "Development of High Temperature Nickel-Base Alloys for Jet Engine Turbine Bucket Applications". Contract NAS3-7267, NASA CR-54507 (June, 1967).

2. Stetson, et al, "Evaluation of Coatings for Cobalt- and Nickel-Base Superalloys". Contract NAS3-940 1, NASA CR-72714 (July 1970).

3. Moore, V.S., Brentnall, W.D., and Stetson, A.R., "Evaluation of Coatings for Cobalt and Nickel-Base Superalloys". Contract NAS3-9401, Vol. I NASA CR-72359 (January, 1969).

4. Wlodek, S.T., "The Oxidation of Ni-2% ThO_2". R62FPD140, General Electric Company, Evendale, Ohio (May, 1962).

5. Pettit, F.S. and Felton, E.J. J. Electrochemical 500.111, 135 (1964).

6. Mincher, A.L., E.I. duPont de Nemours Co., Technical Report AFML-TR-65-442, (January, 1966).

7. Wasielewski, G.E., "Nickel-Base Superalloy Oxidation". AFML-TR-67-30, (January, 1967), General Electric Company.

8. Wukusick, C.S. and Collins, J.E., "An Iron Chromium-Aluminum Alloy Containing Yttrium", Materials Research, (1964) 4, p637.

9. Wasielewski, G.E. and Wukusick, C.S., "Nickel-Base Superalloy Oxidation". R69AEG266, (February, 1969).

10. Wasielewski, G.E., "Oxidation of Nickel and Cobalt Superalloys 'State of the Art' Review". R68AEG141, (January, 1968).

11. Kaufman, M., "Hot Corrosion Reactions in Codep Coated Superalloys", General Electric Co., Lynn, Massachusetts. (February, 1968).

12. Seybolt, A.U., et al., "Investigation of the Basic Parameters Affecting the Properties of Intermetallic Compounds". WADC-TD-184, Part VI. (June, 1965).

13. Kremes, I. and Kofstad, P., "Studies on the Behavior of Nickel-Base Superalloys at High Temperatures". AFML TR-70-103, (July, 1970).

Table I. Improved Aluminide Coating Compositions.

Coating Designation	Purpose	Additive Metallics		Embedded Oxides			
		By Vapor Deposition(1)	By Embedment	Composition	Wt %(2)	Particle Size	Volume Fraction Goal
Codep C-2/NASA V1A	Baseline	Al + Ti	-	Al_2O_3 + TiO_2	50/50	2 - 10μM	20 - 40
Codep C-2/R'100	Reference	Al + Ti	-	Al_2O_3 + TiO_2	50/50	2 - 10μM	20 - 40
NC1-Y	Oxide Particle Embedment	Al + Ti	-	Y_2O_3	100	≅ 2μM	40 - 60
NC1-AY	"	Al + Ti	-	Y_2O_3	100	2 - 10μM	40 - 60
NC2-T	"	Al + Ti	-	THO_2	100	≅ 2μM	40 - 60
NC3-L	"	Al + Ti	-	La_2O_3	100	≅ 2μM	40 - 60
NC5-Y	"	Al + Ti	-	Y_2O_3 + MnO	75/25	≅ 2μM	30 - 45
NC6-T	"	Al + Ti	-	THO_2 + MnO	75/25	≅ 2μM	30 - 45
NC7-L	"	Al + Ti	-	La_2O_3 + MnO	75/25	≅ 2μM	30 - 45
NC4-Cr	Chromium Enrichment	Al + Ti	Cr (1-3μ) (50 wt/o)	Al_2O_3 + TiO_2	25/25	≅ 2μM	30 - 45
NC8-Cr	"	Cr + Al	-	Al_2O_3 + TiO_2	50/50	≅ 2μM	40 - 60
NC9-Cr	"	Cr + Al (3)	-	Al_2O_3 + TiO_2	50/50	≅ 2μM	40 - 60
NC10-Cr	"	Cr + Al	-	Al_2O_3 + TiO_2	50/50	≅ 2μM	40 - 60
NC11-A	Aluminum Enrichment	Al	-	Al_2O_3	100	≅ 2μM	30 - 45
NC12-Y	"	Al	-	Y_2O_3	100	≅ 2μM	30 - 45
NC13-T	"	Al	-	THO_2	100	≅ 2μM	30 - 45
NC14-L	"	Al	-	La_2O_3	100	≅ 2μM	30 - 45

(1) Major metallic deposited is aluminum with titanium deposited in trace amounts only.

(2) Weight percent of slurry applied prior to embedment.

(3) Three chromium and aluminum concentrations; 75/25, 85/15, and 75/25 weight percents, respectively.

Table II. Coating Characteristics.

Mount	Coating System[1]	Coating Thickness						Particle Embedment[4] and Comments
		OCL[2]		DZ[3]		Total		
		Mils	μM	Mils	μM	Mils	μM	
Baseline								
A1796	CODEP C-2	0.8	20.3	0.7	17.8	1.5 - 1.6	38 - 41	25 v/o evenly distributed
A1795	CODEP C-2/R'100	0.9	22.9	1.0	25.4	1.9 - 2.0	48 - 51	25 v/o evenly distributed
Inert Particle Embedment								
A1897	NC1-Y	0.6	15.2	0.5	12.7	1.0 - 1.1	25 - 28	10 v/o surface entrapment only
A3056	NC1-AY	0.3	7.62	0.2	5.08	0.4 - 0.6	10 - 15	10 v/o uniform
A2102	NC2-T	0.7	17.8	0.6	15.2	1.3 - 1.4	33 - 36	30 - 35 v/o uniform
A1962	NC3-L	0.7	17.8	0.6	15.2	1.3 - 1.4	33 - 36	15 v/o uniform
A5161	NC5-Y	1.4	35.5	0.3	7.62	1.7 - 2.0	43 - 51	MnO reaction
A5163	NC6-T	1.2	30.5	0.4	10.2	1.6 - 2.6	41 - 66	MnO reaction
A5164	NC7-L	1.3	33.0	0.4	10.2	1.7 - 2.0	43 - 51	MnO reaction
Chromium Enrichment								
A2430	NC4-Cr	0.8 - 1.2	20.3 - 30.5	0.6	15.2	1.4 - 1.8	36 - 46	15 v/o inert particles 15 v/o Cr particles
A6641	NC8-Cr	0.9	22.9	0.2	5.08	1.1 - 1.3	28 - 33	Minimal < 5 v/o
A6640	NC9-Cr	0.8	20.3	0.2	5.08	0.9 - 1.1	23 - 28	Minimal < 5 v/o
A6639	NC10-Cr	0.6	15.2	0.2	5.08	0.8 - 0.9	20 - 23	Minimal < 5 v/o
Aluminum Enrichment								
A1692	NC11-A	0.9	22.9	0.6	15.2	1.5 - 1.6	38 - 41	15 v/o nonuniform
A4101	NC12-Y	0.6	15.2	0.5	12.7	1.1	28	10 - 15 v/o nonuniform
A4099	NC13-T	0.7	17.8	0.6	15.2	1.3	33	20 v/o uniform
A4102	NC14-L	0.8	20.3	0.7	17.8	1.5 - 1.6	38 - 41	15 v/o uniform

(1) See Table I for coating system compositions
(2) OCL - Outer coating layer (contains particles)
(3) DZ - Diffusion zone
(4) Particle embedment determined by use of standards for which volume percentages of particles were determined by the point intercept method.

Table III. EPPI Burner Rig Test No. 1 Results Temperature 2000°F(1366°K), Mach 0.5 Fuel JP-5.

Coating	Specimen	Hours	Weight Loss (Gm)	Remarks
CODEP C-2/R'100	1	159	0.222	Severe oxidation and metal loss - lower T.E. only
	2	159	0.269	Severe oxidation and metal loss - lower T.E. only
CODEP C-2/NASA VIA	1	250	0.201	Severe attack - lower T.E. only
	2	250	0.178	Severe attack - lower T.E. only
NC4-Cr	1	250	0.129	Attack lower T.E. only - intact
	2	390	0.202	Severe attack - lower T.E. only
	EDM Holes	550	0.170	Attack lower T.E. only - coating intact
NC11-A	1	250	0.116	Attack lower T.E. only - coating intact
	2	421	0.207	Attack lower T.E. only
	EDM Holes	550	0.197	Attack lower T.E. only - coating intact
NC3-L	1	108	0.238	Severe spalling T.E. section
	2	231	0.225	Severe spalling T.E. section
	EDM Holes	171	0.140	Spalling on both L.E. and T.E. sections
NC7-L	1	203	0.242	Severe attack and metal loss - lower T.E.
	2	203	0.174	Severe attack and metal loss - lower T.E.
NC5-Y	1	100	0.275	General attack
	2	100	0.078	Removed with Specimen 1
NC2-T	1	157	0.216	Severe attack - lower T.E.
	2	157	0.068	Removed with Specimen 1
NASA VIA - Uncoated	1	201	0.162	Severe attack - lower T.E.; general attack balance
	2	201	0.177	Severe attack - lower T.E.; general attack balance

Table IV. M&PTL Burner Rig-Screening Test - 2000°F(1366°K)

System	Weight Change (GM) at Indicated Hours[1]				
	50	100	125	175	250
NASA VIA/C-2	+0.0142	+0.0138	+0.001	-0.0077	-0.0747[2]
R100/C-2	+0.0179	-0.2262[2]	---	---	---
NC1-Y	-0.1153	-0.3637[2]	Failed - Severe Oxidation		
NC2-T	-0.2077	-0.4731	Failed - Oxidation Accompanied by Spalling		
NC3-L	+0.0026	+0.0051	+0.0017	-0.0005	-0.0315
NC4-Cr	+0.0287	+0.0249	+0.0079	-0.0035	-0.0579[2]
NC5-Y	-0.2017	Failed - Spalling		---	---
NC6-T	-0.1797	Failed - Spalling		---	---
NC7-L	-0.0001	-0.0648	-0.1287	Failed - Oxidation	
NC8-Cr	Failed - Completely Spalled Coating Layer				---
NC9-Cr	Failed - Completely Spalled Coating Layer				---
NC10-Cr	Failed - Completely Spalled Coating Layer				---
NC11-A	+0.0153	+0.0173	+0.0139	+0.0140	-0.0191[2]
NC12-Y	-0.2164	Failed - Oxidation & Spalling			---
NC13-T	-0.1236	Failed - Oxidation Accompanied by Spalling			
NC14-L	+0.0019	-0.0948	---	Failed - Severe Oxidation	

(1) Hours are approximate - Specimens were included in 3 separate tests

(2) Tunnel overtemperature, 2130°F(1439°K)

Table V. Survey of Coating Thicknesses After EPPI Burner Rig Test No. 1 - 2000°F (1366°K).

Coating System	As-Coated Thickness (Mils)/μM	Exposure Time (Hr)	After-Exposure Thicknesses(Mils)(μM) L.E.(1)	M.A.(2)	T.E.(3)	Comments
CODEP C-2/R'100	2.0(51)	159	1.7(43)	2.2(56)	0.0 - 1.0(25.4)	Severe attack on T.E. only
CODEP C-2/NASA VIA	1.6(40.6)	250	1.4(35.5)	1.7(43)	0.0 - 1.2(30.5)	Severe attack on T.E. only
NC4-Cr	1.6(40.6)	550	1.5(38)	1.6(40.6)	0.8(20.3) - 1.4(35.5)	Coating intact after exposure
NC11-A	1.6(40.6)	550	1.6(40.6)	1.8(45.6)	0.4(10.2) - 1.2(30.5)	No coating failure after exposure
NC3-L	1.4(35.5)	231	1.0(25.4)	1.2(30.5)	0.0	Complete failure at T.E.
NC5-Y	1.3(33)	100	1.0(25.4)	1.1(28)	0.0	Coating shows general severe attack
NC6-T	1.3(33)	157	1.2(30.5)	1.2(30.5)	0.0 - 0.8(20.3)	Severe attack on T.E.
NC7-Y	1.3(33)	203	1.0(25.4)	1.2(30.5)	0.0	Complete failure at T.E.
NC11-C	1.6(40.6)	209	1.5(38)	1.8(45.6)	1.2(30.5) - 1.3(33)	Coating intact
CODEP C-2/R'100/PK	1.7(43)	280	1.5(38)	1.6(40.6)	0.6(15.2) - 1.1(28)	Coating attack apparent on T.E.

(1) Leading edge area of the paddle test specimen
(2) Midairfoil areas of the paddle test specimen
(3) Trailing edge area of the paddle test specimens

Table VI. Microprobe Results As-Coated Specimens.

System	Area of Trace	Element Concentrations, %(1)					
		Aℓ	Cr	Ti	Ta	Ni	Misc.
NASA VIA (Base Alloy)	Random	≈ 5	≈ 6	≈ 1	≈ 9	63 - 64	Bal
NC4-Cr	Diffusion Zone(2)	5 - 15	8.0 - 6	1.0 - 3	9 - 6	64 - 48	W: 7 - 5
	Additive Layer(3)	15 - 25	6.0 - 6	3.0 - 1	6 - 0	48 - 40	W: 5 - 0
NC11-A	Diffusion Zone	5 - 18	6.0 - 5	1.5 - 1	9 - 6	65 - 48	W: 6 - 8
	Additive Layer	18 - 30	5.0 - 1	1.0 - 0.5	6 - 0	48 - 65	W: 8 - 0
NASA VIA/C-2	Diffusion Zone	5 - 12.5	5.5 - 3	1.0 - 4	9 - 3	65 - 50	W: 4 - 4
	Additive Layer	13 - 24	3.0 - 1	4.0 - 0	3 - 0	50 - 45	W: 4 - 0
R'100/C-2	Diffusion Zone	5 - 15	12.5 - 5	3.0 - 5	---	60 - 56	W: 8 - 8
	Additive Layer	15 - 25	5.0 - 1	5.0 - 0	---	56 - 45	W: 8 - 3
NC7-L	Diffusion Zone	5 - 10	4.0 - 2	1.0 - 2	5 - 4	68 - 50	La: 0 - 3
	Additive Layer	10 - 25	2.0 - 0	2.0 - 0.5	4 - 0	50 - 10	La: 3 - 40
NC1-Y	Diffusion Zone	7 - 20	5.0 - 4	1.0 - 2	9 - 7	63 - 54	Y: 0
	Additive Layer	20 - 21	4.0 - 0.5	2.0 - 0.5	7 - 0	54 - 60	Y: 5 - 30
NC11-A (Mod.)	Diffusion Zone	6 - 30	6.2 - 3	---	9 - 5	55 - 55	W: 6.5 - 5.5
	Additive Layer	30 - 38	3.0 - 7	---	5 - 0	55 - 47	W: 5.5 - 1
NC11-A (Duplex) (Optimized System)	Diffusion Zone	6 - 22	6.0 - 4	1.0 - 1	9 - 12	62 - 50	W: 5.5 - 10
	Additive Layer	22 - 42	4.0 - 0	1.0 - 0	9 - 0	62 - 58	W: 7 - 0
NC4-Cr (Duplex) (Optimized System)	Diffusion Zone	6 - 20	7.0 - 4	1.0 - 1	9 - 7	55 - 50	W: 5 - 1
	Additive Layer	20 - 42	4.0 - 6	1.0 - 0	7 - 0	50 - 38	W: 1 - 0

(1) Concentrations are not quantitative but approximations from microprobe traces
(2) That original base material which has been influenced by inward diffusion of aluminum
(3) Layer formed by outward diffusion of nickel and deposition of aluminum from coating powders

Table VII. X-Ray Fluorescence Analysis[1] of Coated and Uncoated NASA VIA Alloy.

Voltage - 50 KVP
Current - 50 MA

Coating System	Condition	Elements and/or Phases (Relative Intensity)									
		MoKα	CbKα	TaLα	NiKβ	CoKβ	NiKα	CoKα	FeKα	CrKβ	CrKα
None	As Received	38	12	44	100+	59	100+	100+	6	12	51
NC4-Cr on NASA VIA	As Coated	21	6	13	100+	66	100+	100+	4	30	100+
NC4-Cr on NASA VIA	Tested 662 Hrs EPPI Rig	34	10	44	100+	45	100+	100+	98	19	81
NC11-A (Mod.) on NASA VIA	As Coated	38	3	9	100+	62	100+	100+	3	16	68
NC11-A (Mod.) on NASA VIA	Tested 662 Hrs EPPI Rig	15	5	24	100+	46	100+	100+	100	9	39
R'100/C-2	As Coated	21	---	---	100+	55	100+	100+	---	---	10
R'100/C-2	Tested 250 Hrs EPPI Rig	32	---	---	100+	77	100+	100+	63	8	38

(1) X-ray fluorescence work was conducted with the following equipment:
- Model GE XRD-5
- Dual Counter Tube
- Tungsten Target X-Ray Tube
- LiF Analyzing Crystal

Table VIII. Coating Processing Parameter Variations, Improvement Studies.

Basis Coating	Process Cycle	Symbol	Weight Gain (mg/cm^2)	Coating Thickness (Mils)	v/o Particles	Purpose
NC11-A	VPH - 2000°F(1366°K)/4 Hours	S1	5.35	1.9 (48.2μM)	~ 10	Higher processing temperature to increase thickness
NC11-A	VPH - 2050°F(1394°K)/4 Hours	S2	5.77	2.1 (53.3μM)	~ 10	Higher processing temperature to increase thickness
NC11-A	VPH - Gas Manifold 1800°F(1255°K)/16 Hours	S3	3.75	1.8 (45.6μM)	~ 5	Lower temperature and longer time to increase particle entrapment
NC11-A (Mod.)	VPH - 2000°F(1366°K/4 Hours	S4	6.84	---	---	Higher processing temperature to increase thickness
NC11-C	VPH - Gas Manifold 1800°F(1255°K)/16 Hours	S5	6.80	1.7 (43.1μM)	~ 5	Lower temperature and longer time plus lower-activity pack to increase particle entrapment
NC4-Cr	VPH - Gas Manifold 1800°F(1255°K)/16 Hours	S6	6.13	1.7 (43.1μM)	~ 10	Lower temperature and longer time to increase particle entrapment
NC11-A (Mod.)	VPH - Gas Manifold 1800°F(1255°K)/16 Hours	S7	5.55	---	---	Lower temperature and longer time to increase particle entrapment
NC11-A	VPH - Two Cycles 1925°F(1324°K)/4 Hours	D1	8.36	2.3 (58.4μM)	~ 25	Increase particle entrapment Increase coating thickness
NC11-A	VPH - 1 1900°F(1309°K)/2 Hrs 2 2000°F(1366°K)/2 Hrs	D2	4.44	1.7 (43.1μM)	~ 20	1 Increase particle entrapment 2 Increase coating thickness
NC11-A (Mod.)	VPH - Two Cycles 1925°F(1324°K)/4 Hours	D1	9.62	2.4 (60.9μM)	~ 25	Increase particle entrapment Increase coating thickness
NC11-A (Mod.)	VPH - 1900°F(1309°K)/2 Hours 2000°F(1366°K)/2 Hours	D4	6.20	1.8 (45.6μM)	~ 15	1 Increase particle entrapment 2 Increase coating thickness
NC11-C NC11-A	PACK - Two Cycles 1900°F(1309°K)/4 Hours	D5	8.32	2.2 (55.9μM)	~ 25	1 Increase particle entrapment 2 Increase coating thickness
NC11-C (Mod.) NC11-A (Mod.)	PACK - Two Cycles 1900°F(1309°K)/4 Hours	D6	8.19	2.3 (58.4μM)	~ 25	1 Increase particle entrapment 2 Increase coating thickness
NC4-Cr NC11-A (Mod.)	VPH - 1850°F(1283°K)/4 Hours PACK - 1900°F(1309°K)/4 Hours	D7	7.5	2.1 (53.3μM)	~ 30	1 Increase particle entrapment 2 Increase coating thickness
NC11-C (Mod.) NC11-A	PACK - Two Cycles 1900°F(1309°K)/4 Hours	D8	8.2	2.2 (55.9μM)	~ 25	1 Increase particle entrapment 2 Increase coating thickness

Notes:
1. All processing in hydrogen atmosphere
2. Gas Manifold - hydrogen flow through pack
3. Basis Coatings:
   a. NC11-A - High Aℓ activity pack - $Aℓ_2O_3$ slurry
   b. NC11-A (Mod.) - High Aℓ activity pack - $Aℓ_2O_3$ + Cr slurry
   c. NC11-C - Intermediate Aℓ activity pack - $Aℓ_2O_3$ slurry
   d. NC11-C (Mod.) - Intermediate Aℓ activity pack - 4% alloy powder concentration
   e. NC4-Cr - Intermediate Aℓ activity pack - $Aℓ_2O_3$, TiO_2, Cr slurry
4. VPH - Parts processed above pack mixture
5. PACK - Parts processed in pack mixture

Table IX. Test No. 1, Coating Optimization Cyclic Dynamic Oxidation, 2000°F(1366°K)/10 Cycles/ Hour.

Basis Coating	Coating Cycle	Accumulative Weight Change - Gram						
		Hours						
		50	146	216	287	377	442	503
(1) NC11-A (Mod.)	D4	+0.0162	+0.0297	+0.0402	+0.0506	+0.0763	+0.0815	+0.0804
(2) NC11-A	S3	+0.0127	+0.0180	+0.0222	+0.0293	+0.0370	+0.0379	+0.0265
(3) NC11-A	D2	+0.0132	+0.0173	+0.0192	+0.0216	+0.0262	+0.0278	+0.0277
(4) NC4-Cr	S6	+0.0162	+0.0227	+0.0282	+0.0331	+0.0402	+0.0430	+0.0384
(5) NC11-C	S5	+0.0148	+0.0214	+0.0280	+0.0333	+0.0421	+0.0377	+0.0390
(6) NC11-A	Std	+0.0222	+0.0357	+0.0398	+0.0458	+0.0547	+0.0541	+0.0319
(7) NASA VIA Bare	---	+0.0118	-0.0380	-0.0698	-0.0978	-0.1283	-0.1577	-0.1853
(8) Dummy Specimen(1)	---	N.W.	N.W.	N.W.	N.W.	N.W.	N.W.	N.W.

NOTE: (1) NC11-A (Mod.) Coating - Tip Section removed for as-coated micro.

Table X. Test No. 2, Coating Refinement Cyclic Dynamic Oxidation, 2000°F(1355°K)/10 Cycles/Hour.

Basis Coating	Coating Cycle	Accumulative Weight Change, Gram					
		Hours					
		50	146	216	287	377(2)	Remarks
(1) NC11-A	S2	+0.0116	+0.0198	+0.0289	+0.0580	+0.0012	Removed
(2) NC11-A (Mod.)	S7	+0.0154	+0.0233	+0.0315	+0.0566	-0.0808	Removed
(3) NC11-A	S1	+0.0122	+0.0157	+0.0185	+0.0282	+0.0273	Transferred, Test No. 3
(4) NC11-A (Mod.)	S4	+0.0155	+0.0264	+0.0355	+0.0519	+0.0230	Removed
(5) NC11-A (Mod.)	D1	---	---	+0.0255	+0.0368	+0.0549	Transferred, Test No. 3
(6) R'100/C-2	Std	+0.0356	-0.4292(1)	---	---	---	---
(7) NC11-A	Std	+0.0222	+0.0386	+0.0459	+0.0596	-0.0224	---
(8) NASA VIA Bare	---	-0.0100	-0.0638	-0.0891	-0.1365	-0.2297	Removed
(9) Dummy Specimen(3)	---	N.W.	N.W.	N.W.	N.W.	N.W.	

Notes: (1) Removed after 146 hours; replaced with (5) NC11-A (Mod.) - D3.

(2) Test discontinued due to overtemperature of 2050 - 2100°F (1394 - 1427°K) for approximately 40 hours between 287 and 377 hours. All coatings showed some visual evidence of failure. The two visually best paddles, NC11-A-S1 and NC11-A (Mod.)-D3, were transferred to Test No. 3.

(3) NC11-A tip section removed for as-coated micro coating.

Table XI. Test No. 3, Coating Refinement Cyclic Dynamic Oxidation, 2000°F (1366°K)/10 Cycles/Hour.

Basis Coating	Coating Cycle	Accumulative Weight Change, Gram						
		Hours						
		65	126	217	312	381	404	499
(1) Combination NC11-C NC11-A	D5	+0.0184	+0.0190	+0.0209	+0.0218	+0.0239	+0.0245	+0.0263
(2) NC11-A	D1	+0.0109	+0.0136	+0.0170	+0.0194	+0.0239	+0.0239	+0.0263
(3) Combination NC11-C (Mod.) NC11-A (Mod.)	D6	+0.0330	+0.0375	+0.0394	+0.0382	+0.0383	+0.0384	+0.0393
(4) Combination NC4-Cr NC11-A (Mod.)	D7	+0.0200	+0.0247	+0.0253	+0.0372	+0.0280	+0.0265	+0.0282
(5) Combination NC11-C (Mod.) NC11-A	D8	+0.0238	-0.0308	+0.0328	+0.0390	+0.0456	+0.0488	+0.0568
(6) NASA VIA Bare	---	+0.0168	-0.0147	-0.0280	-0.0418	-0.0489	-0.0543	-0.0659
(7) NC11-A	S1	+0.0232	+0.0132(1)	---	---	---	---	---
(8) NC11-A (Mod.)	D1	+0.0549	+0.0540	+0.0346(2)	---	---	---	---

Notes: (1) Transferred from Test No. 2 - total time - 503 hours

(2) Transferred from Test No. 2 - removed after 268 hours - total time 499 hours

Table XII. Processing of NC11-A-S1 and NC11-A-D1 Coatings for 2000°F(1366°K)/2000-Hour Tests.

Specimen	Coating Modification	Run Ident.	Coating Weight Gain			
			Cycle No. 1	Cycle[1] No. 2	Total, Gram	Total Mg/Cm^2
G4160E	S1	GY	0.2683	---	0.2683	6.70
G4105B	S1	GY	0.2737	---	0.2737	6.84
G4160P	S1	GY	0.2767	---	0.2767	6.93
G4106M	S1	GY	0.2580	---	0.2580	6.45
G4106R*	S1	GY	0.2919	---	0.2919	7.29
G4106Q	S1	GY	0.2737	---	0.2737	6.84
G4092G	S1	GY	0.2876	---	0.2876	7.18
G8049Q*	S1	GY	0.3183	---	0.3183	7.97
G4161V	S1	GY	0.2479	---	0.2479	6.20
G4095-R*	D1	Hy-Jy	0.1971	0.0636	0.2607	6.53
G4105-D	D1	Hy-Jy	0.1775	0.0883	0.2658	6.64
G4105-Q	D1	Hy-Jy	0.1785	0.0804	0.2589	6.47
G4106-H	D1	Hy-Jy	0.1751	0.0784	0.2535	6.33
G4092-R*	D1	Hy-Jy	0.1944	0.0761	0.2705	6.76
G4161-W	D1	Hy-Jy	0.1730	0.0818	0.2548	6.37
G4092-F	D1	Hy-Jy	0.1740	0.0745	0.2485	6.21
G4106-J	D1	Hy-Jy	0.1700	0.0893	0.2593	6.48
G4103-X*	D1	Hy-Jy	0.2221	0.0564	0.2785	6.96
G4089-C	S1	KZ	0.1810	---	0.1810	4.53
G4092-E	S1	KZ	0.1781	---	0.1781	4.46
G4089-D	S1	KZ	0.1877	---	0.1877	4.69
G4089-E	D1	HZ-IZ	0.1308	0.0769	0.2077	5.18
G4022-V	D1	HZ-IZ	0.1129	0.0876	0.2005	5.02
G4089-F	D1	HZ-IZ	0.1135	0.0820	0.1955	4.89

* Indicates specimens containing drilled holes in leading edge.

(1) Cycle No. 2 pertains only to the dual-coating System D1.

Table XIII. Specimen Arrangement in M&PTL Burner Rigs for 2000°F(1366°K)/2000-Hour Tests.

Burner Rig No.	Specimen	Coating Modification	EDM Holes	Test Period (Hours)
5	G4160P	S1	Yes	2000
5	G4106P	S1	No	500
5	G4106R	S1	No	2000
5	G4160E	S1	Yes	1500
5	G4106M(1)	S1	---	1500
5	G4092E(2)	S1	---	500
5	G4095R	D1	Yes	1000
5	G4105D	D1	No	2000
5	G4092F	D1	No	2000
5	G4089C(3)	D1	Yes	1000
5	G4092C	Uncoated	No	1500
5	G4103-0(4)	Std	No	500
4	G4161V	S1	Yes	1000
4	G4105B	S1	No	2000
4	G4092G	S1	No	2000
4	G4189C(5)	S1	---	1000
4	G4105Q	D1	Yes	2000
4	G4161W	D1	No	1500
4	G4089F(6)	D1	---	500
4	G4092R	D1	No	2000
4	G4106J	D1	Yes	500
4	G4106H(7)	D1	---	1500
4	G4092C	Uncoated	No	2000

Notes:
(1) Replacement for G4106P
(2) Replacement for G4160E
(3) Replacement for G4095R
(4) Replacement for G4092C
(5) Replacement for G4161V
(6) Replacement for G4161W
(7) Replacement for G4106J

Table XIV. Significant Events During Burner Rig Testing, 2000°F (1366°K)/2000-Hour Tests.

Hours	Paddle	Coating	Observation
			BURNER RIG NO. 5
307	G4106Q	S1	Pinpoint attack - trailing edge tip ridge from casting
504	G4105D	D1	Pinpoint attack - trailing edge slightly below tip: Several paddles show slight blue discoloration on upper airfoil
900	---	---	All coated paddles, except G4106M (500-hr replacement) show blue discoloration on upper airfoil sections.
1102	G4106M	S1	Pinpoint attack - trailing edge top
1200	G4089E	D1	Pinpoint attack - trailing edge tip
1483	G4092F G4106R	D1 S1	Pinpoint attack - trailing edge top, blue discoloration G4106R
1642	G4106M G4106R G4092F	S1 S1 D1	Several pinpoint attacks - trailing edge top
1804	G4092E	S1	Blue discoloration, upper airfoil section. Area of discoloration increasing on other paddles.
2000	---	---	No significant change
			BURNER RIG NO. 4
102	---	---	Control chart indicated 16 hours operation at 1500°F(1088°K).
401	G4106J	D1	Pinpoint attack - trailing edge tip
503	---	---	Several paddles show blue discoloration on upper airfoil.
995	G4105B	S1	Three pinpoint attack spots - trailing edge tip. All coated paddles show blue discoloration to varying degrees on upper airfoil sections.

Table XV. X-Ray Diffraction Analysis of NC11-A-S1 and NC11-A-D1 Coatings.

Costing (NC11-A-)	Condition	Phases Observed[1]
S1	As-Coated	$NiAl$(S), α Al_2O_3(S)
S1	2000°F(1366°K)/500 Hours As-Exposed	Ni_3Al(S), α Al_2O_3, $NiAl_2O_4$(W)
S1	2000°F(1366°K)/500 Hours Scale Removed	Ni_3Al(S), α Al_2O_3(S)
S1	2000°F(1366°K)/1000 Hours As-Exposed	(Ni_3Al and γ) (S), α Al_2O_3(S), $NiAl_2O_4$(M)
S1	2000°F(1366°K)/1483 Hours As-Exposed	(Ni_3Al and/or γ) (S), α Al_2O_3(S), $NiAl_2O_4$(S)
S1	2000°F(1366°K)/1483 Hours Scale Removed	(Ni_3Al and/or γ) (S), α Al_2O_3(M)
S1	2000°F(1366°K)/2000 Hours As-Exposed	(Ni_3Al and/or γ) (S), α Al_2O_3(S), $NiAl_2O_4$(S)
S1	2000°F(1366°K)/2000 Hours Scale Removed	(Ni_3Al and/or γ) (S), α Al_2O_3(S)
D1	As-Coated	$NiAl$(S), α Al_2O_3(S)
D1	2000°F(1366°K)/500 Hours As-Exposed	Ni_3Al(S), α Al_2O_3(S), $NiAl_2O_4$(M)
D1	2000°F(1366°K)/1000 Hours As-Exposed	Ni_3Al(W), γ(S), α Al_2O_3(S), $NiAl_2O_4$(S)
D1	2000°F(1366°K)/1000 Hours Scale Removed	Ni_3Al(W), γ(S), α Al_2O_3(S)
D1	2000°F(1366°K)/1495 Hours As-Exposed	(Ni_3Al and/or γ) (S), α Al_2O_3(S), $NiAl_2O_4$(S)
D1	2000°F(1366°K)/2000 Hours As-Exposed	(Ni_3Al and/or γ) (W), α Al_2O_3(S), $NiAl_2O_4$(S)
D1	2000°F(1366°K)/2000 Hours Scale Removed	(Ni_3Al and/or γ) (S), α Al_2O_3(S)

Notes: (1) (S) Strong
(M) Medium
(W) Weak

Table XVI. Mechanical Test Data Tensile Results, Strain Rate: 0.005 In./In./Min. (0.002 Cm/Cm/Min.)

Specimen	Temperature		UTS		0.2% Yield		0.02% Yield		Percent Elongation	% Reduction of Area
	°F	°K	KSI	$nt/m^2 \times 10^7$	KSI	$nt/m^2 \times 10^7$	KSI	$nt/m^2 \times 10^7$		
NASA VIA - Bare	1400	1033	166.2	114.7	137.5	948	119.0	821	3.8	7.2
NASA VIA - Bare	1400	1033	159.9	110.1	134.8	929	107.7	742	2.3	5.6
NASA VIA + NC11-A-D1	1400	1033	154.2	106.2	131.0	903	112.8	776	3.8	3.0
NASA VIA + NC11-A-D1	1400	1033	147.0	101.2	127.7	876	108.5	749	2.6	7.9
NASA VIA + NC11-A-S1(1)	1400	1033	160.0	110.2	134.3	926	118.8	819	4.5	7.1
NASA VIA + NC11-A-S1(1)	1400	1033	157.2	108.3	131.3	906	113.0	745	2.5	13.1
NASA VIA - Bare	1800	1255	80.0(1)	55.2	72.9	50.4	53.4	36.8	---	---
NASA VIA - Bare	1800	1255	96.3	66.4	71.6	49.6	51.0	35.2	2.2	3.1
NASA VIA + NC11-A-D1	1800	1255	88.0	60.7	73.7	50.8	52.5	36.2	1.3	3.2
NASA VIA + NC11-A-D1	1800	1255	91.0	62.8	75.0	51.7	60.3	41.6	2.0	3.3
NASA VIA + NC11-A-S1	1800	1255	92.8	64.0	76.8	52.9	53.0	36.6	1.3	2.4
NASA VIA + NC11-A-S1	1800	1255	90.5	62.4	75.5	52.1	57.5	39.7	2.2	2.5

Note: (1) Grip failure - Ultimate strength based on highest load obtained; 0.2% and 0.02% yield strengths appear accurate

Table XVII. Stress-Rupture Test Results.

Test Temperature = 1800°F(1255°K)

Stress = 29,000 PSI (200 X 10^6 Nt/M^2)

Specimen	Coating	Time to Failure (Hours)	Percent Elongation	R.A. (%)
G4067-J	Uncoated	90.85	4.5	6.2
G4067-N	Uncoated	104.62	4.8	5.6
G4068-C	NC11-A-D1	89.40	4.7	6.5
G4067-B	NC11-A-D1	87.49	5.3	4.5
G4067-O	NC11-A-S1	94.16	5.3	4.2
G4067-F	NC11-A-S1	123.24	5.8	5.8

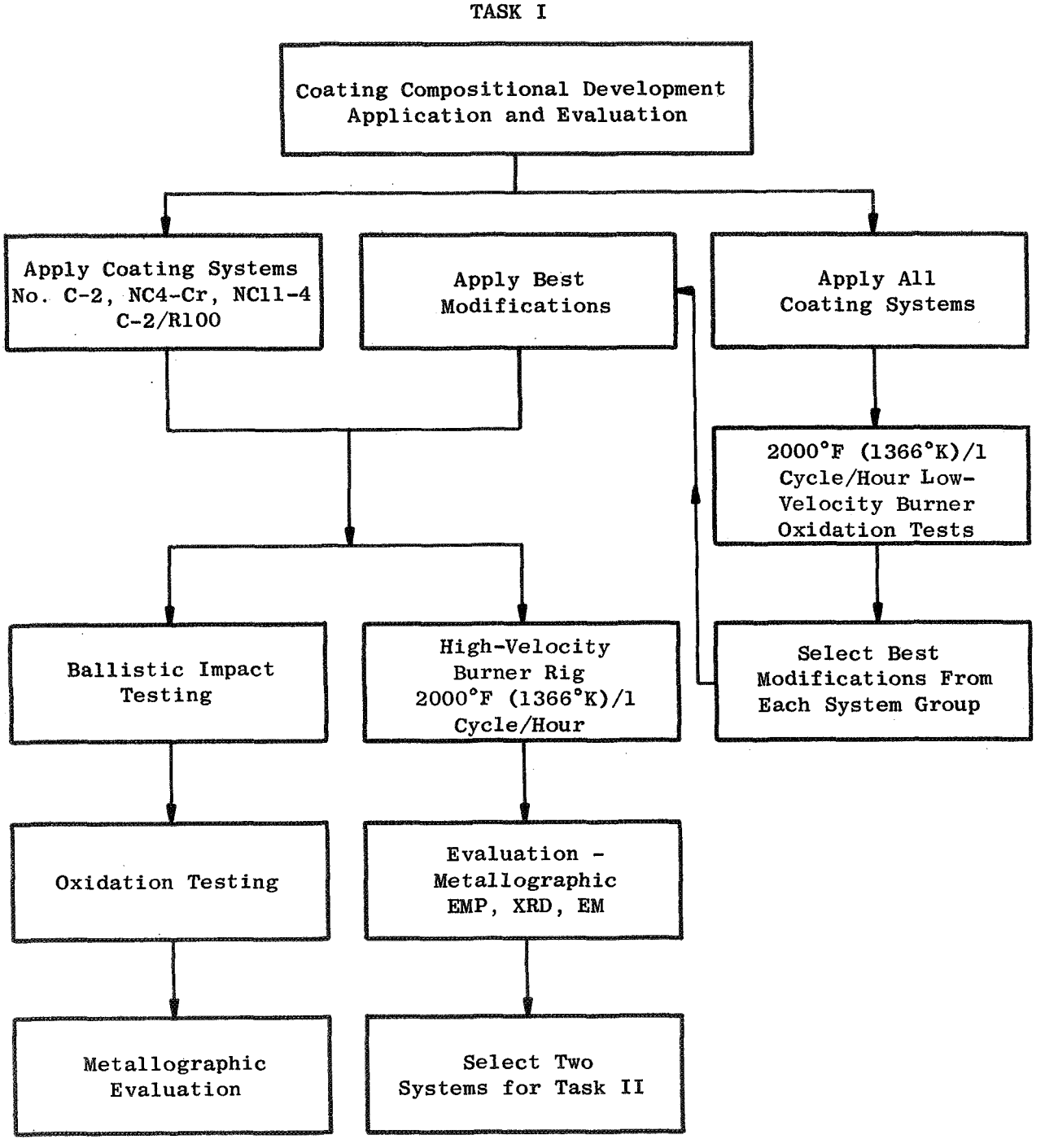

Figure 1. Flow Sheet for Task I.

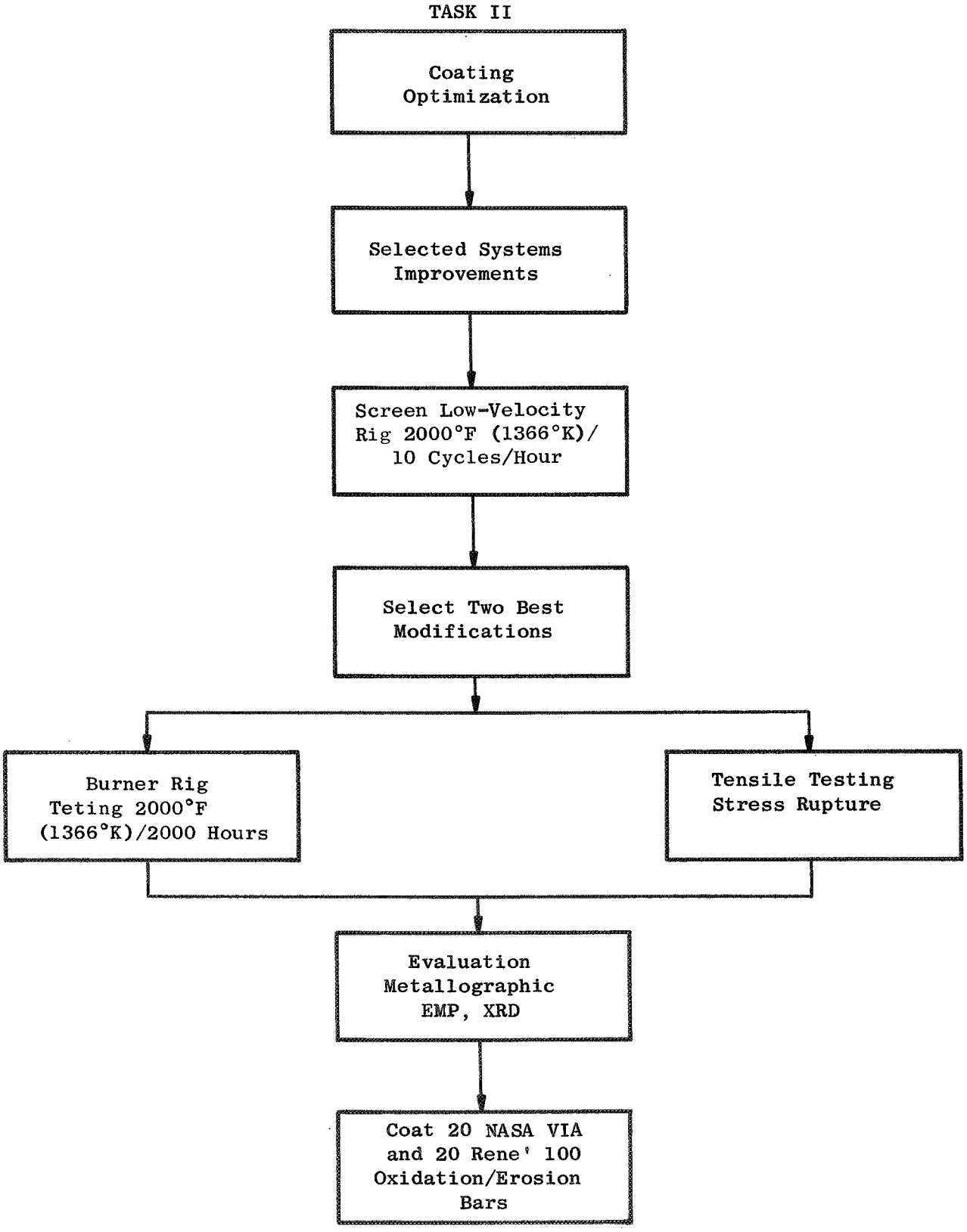

Figure 2. Flow Sheet for Task II.

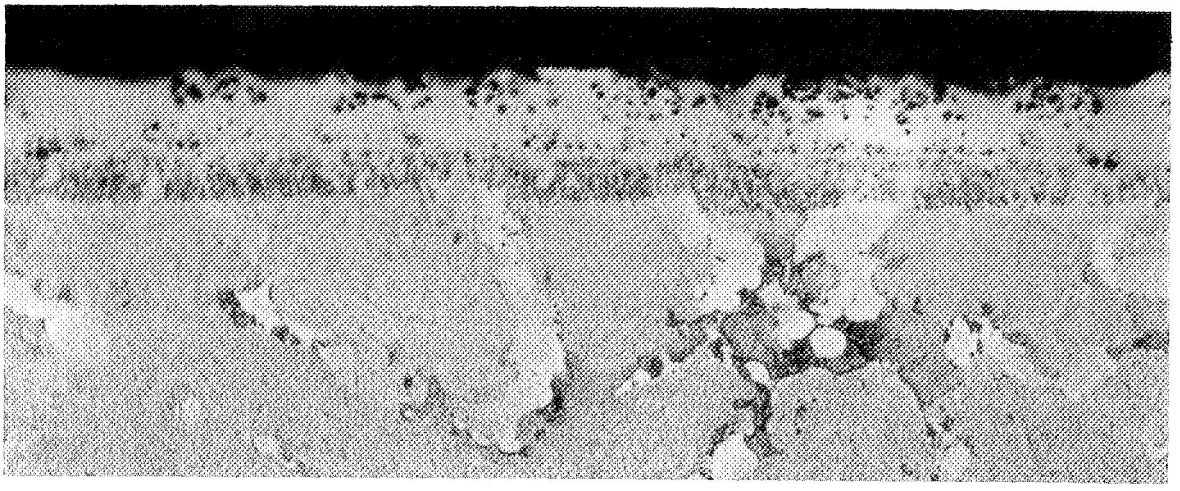

B5450 500X

Coating System: NC11-A
Coating Thickness: 1.3 Mils (33.0 μM)
Particle Embedment: Al_2O_3 ≦ 2 μM - 10 v/o

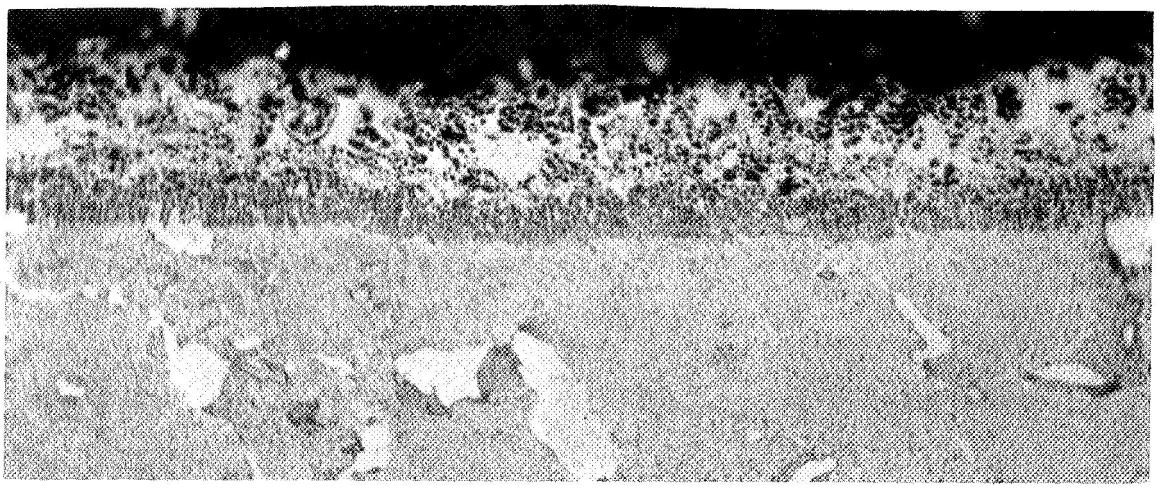

B5456 500X

Coating System: NC4-Cr
Coating Thickness: 1.6 Mils (40.6 μM)
Particle Embedment: Al_2O_3/TiO_2 ≦ 2 μM 30 v/o
Cr Powder 1-3

Figure 3. Coating Structure of Systems NC11-A and NC4-Cr.

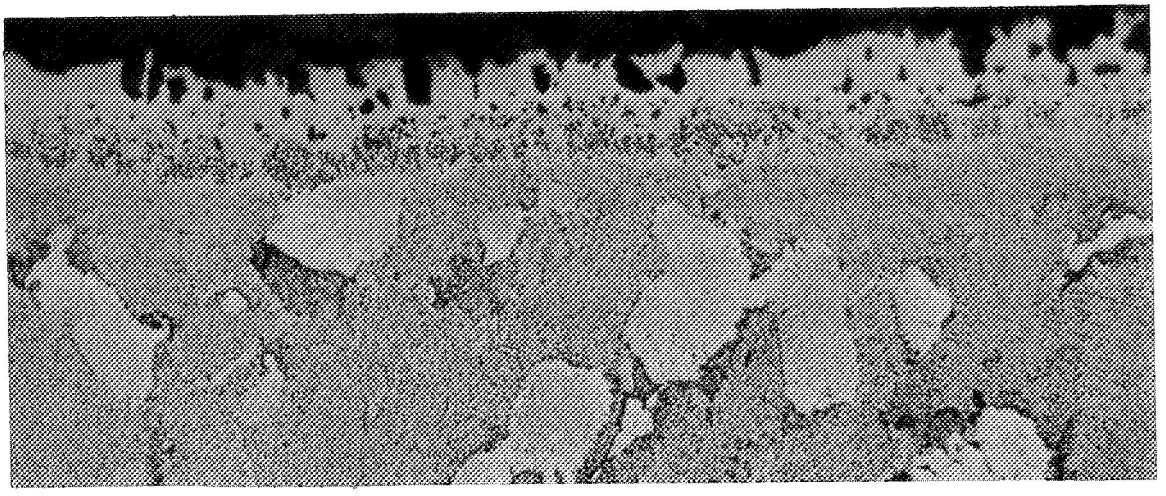

B5453 500X

Coating System: NCl-Y
Coating Thickness: 1.1 Mils (27.9 μM)
Particle Embedment: Y_2O_3 ≦ 2 μM - 10 v/o

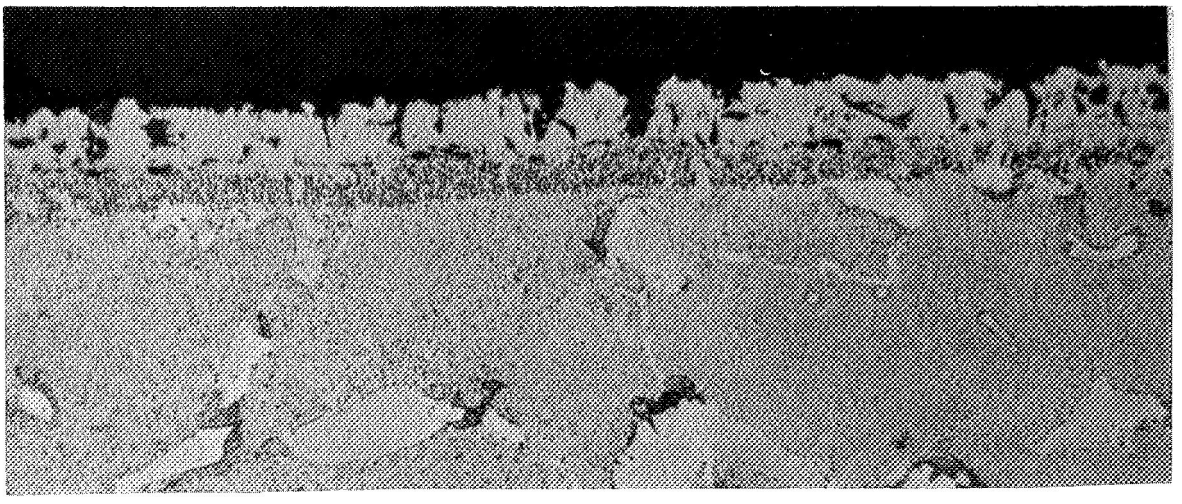

B5461 500X

Coating System: NCl2-Y
Coating Thickness: 1.1 Mils (27.9 μM)
Particle Embedment: Y_2O_3 ≦ 2 μM - 10 v/o

Figure 4. Coating Structure of Systems NCl-Y and NCl2-Y.

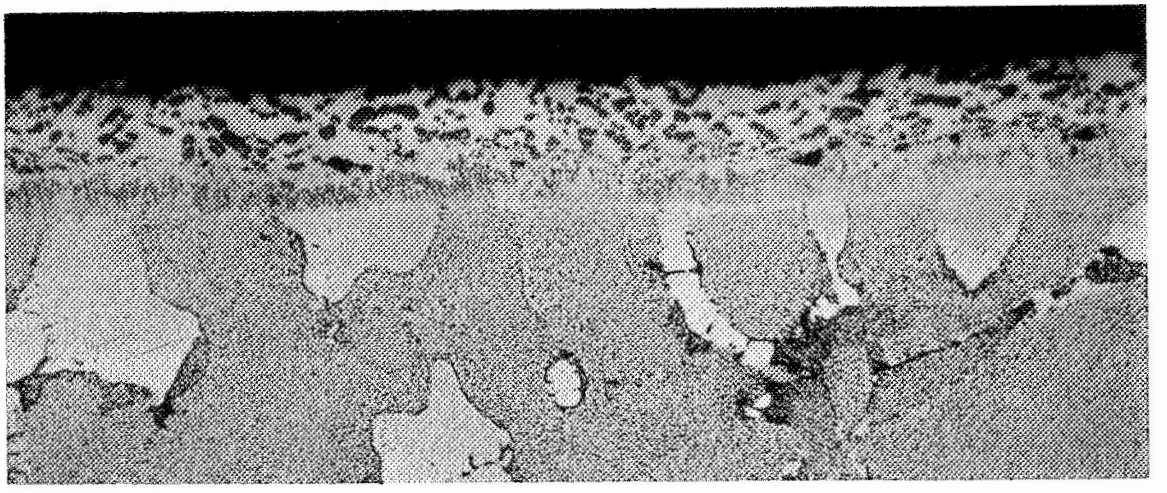

B5455

500X

Coating System: NC2-T
Coating Thickness: 1.4 Mils (35.5 μM)
Particle Embedment: ThO_2 ≦ 2 μM - 30 v/o

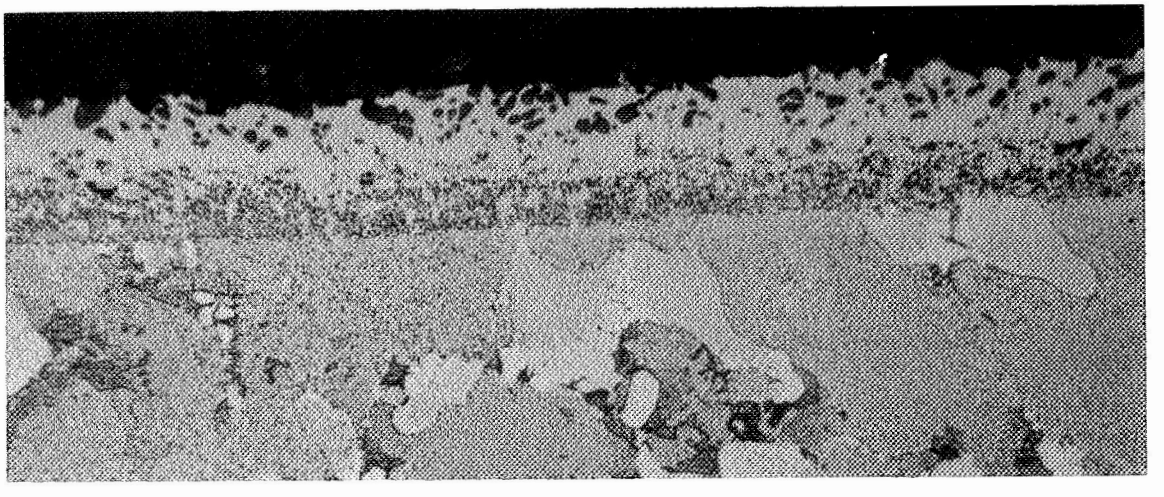

B5458

500X

Coating System: NC13-T
Coating Thickness: 1.3 Mils (33.0 μM)
Particle Embedment: ThO_2 ≦ 2 μM - 20 v/o

Figure 5. Coating Structure of Systems NC2-T and NC13-T.

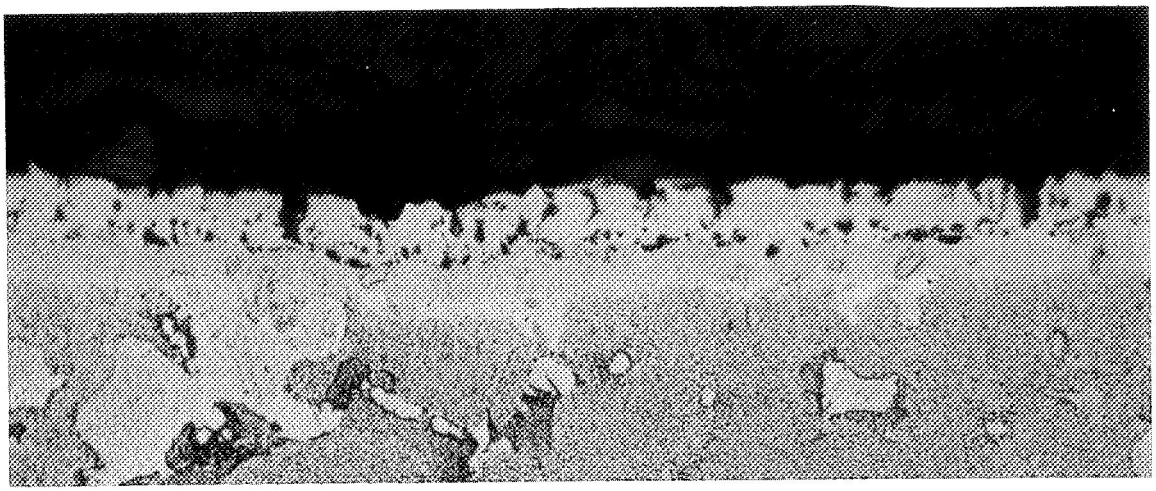

B5454 500X

Coating System: NC3-L
Coating Thickness: 1.3 Mils (33.0 μM)
Particle Embedment: La_2O_3 ≦ 2 μM - 15 v/o

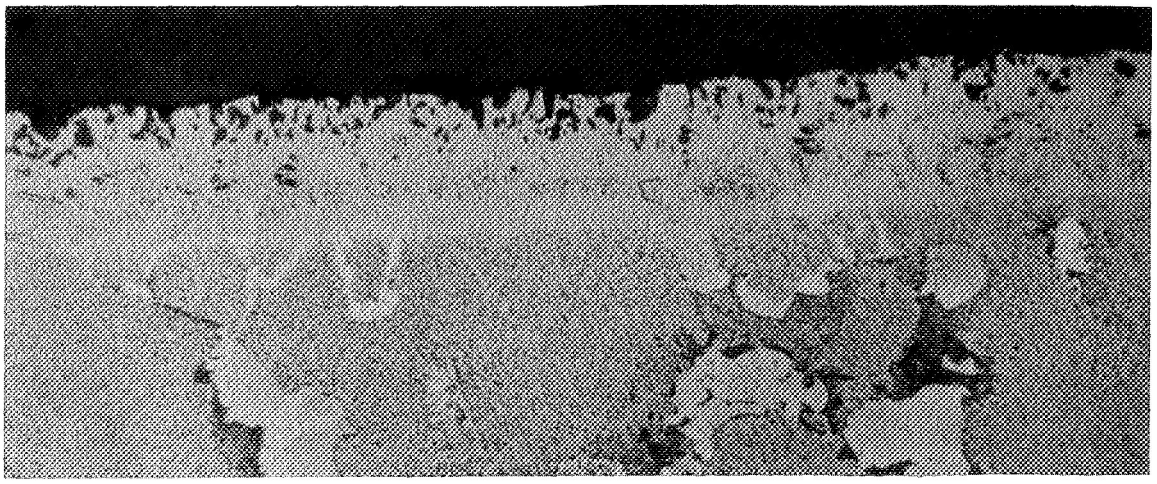

B5460 500X

Coating System: NC14-L
Coating Thickness: 1.6 Mils (40.6 μM)
Particle Embedment: La_2O_3 ≦ 2 μM - 15 v/o

Figure 6. Coating Structure of Systems NC3-L and NC14-L.

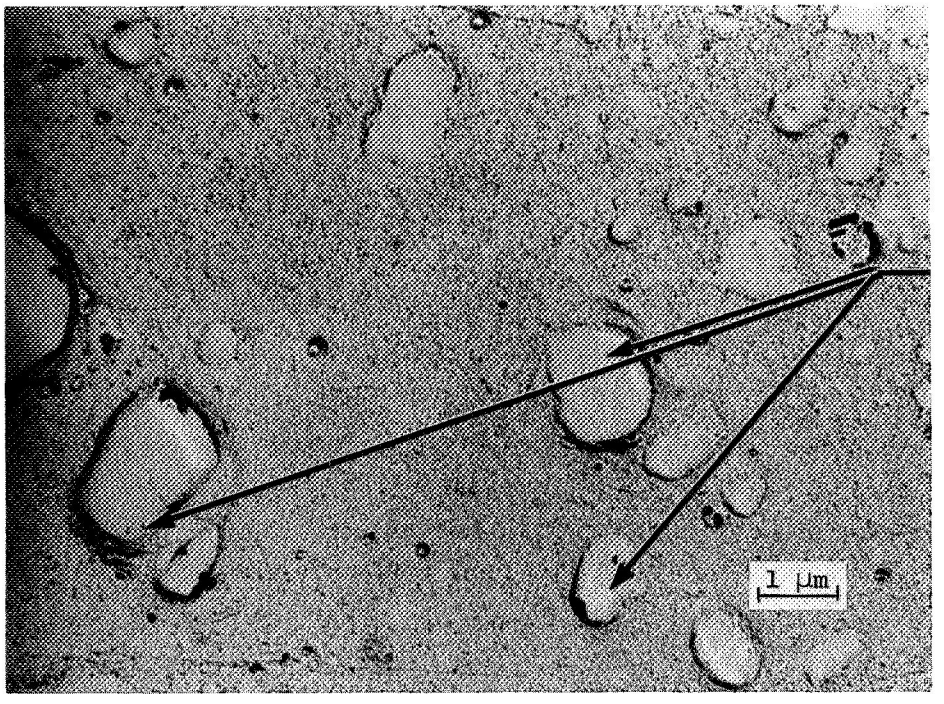

Outer Edge - Al_2O_3 Particles

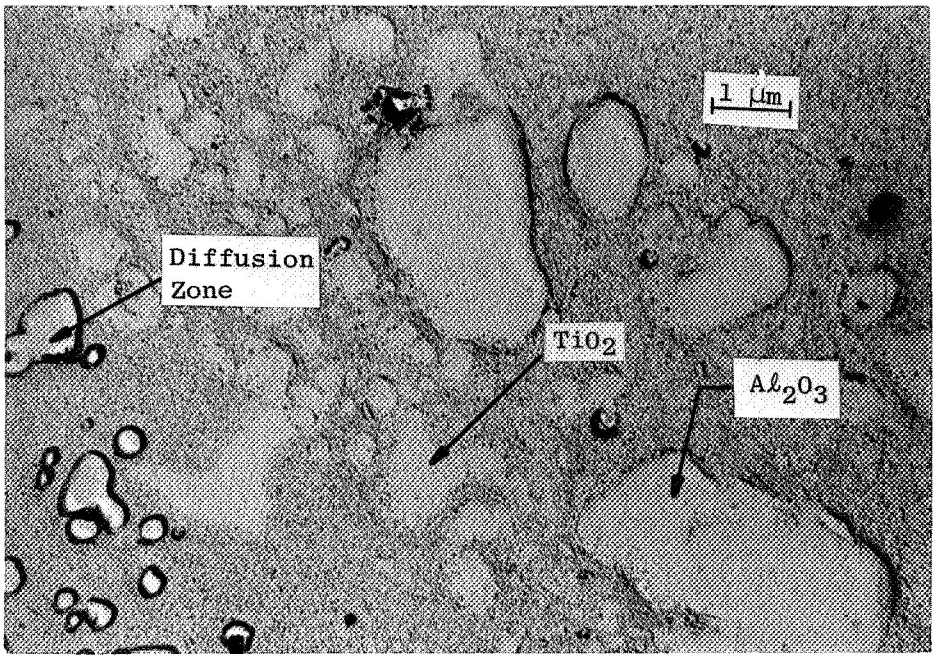

Interface - Al_2O_3 and TiO_2 Particles

Figure 7. Electron Microscopy of CODEP C-2 Coating on NASA V1A Alloy, As Coated (10,000X).

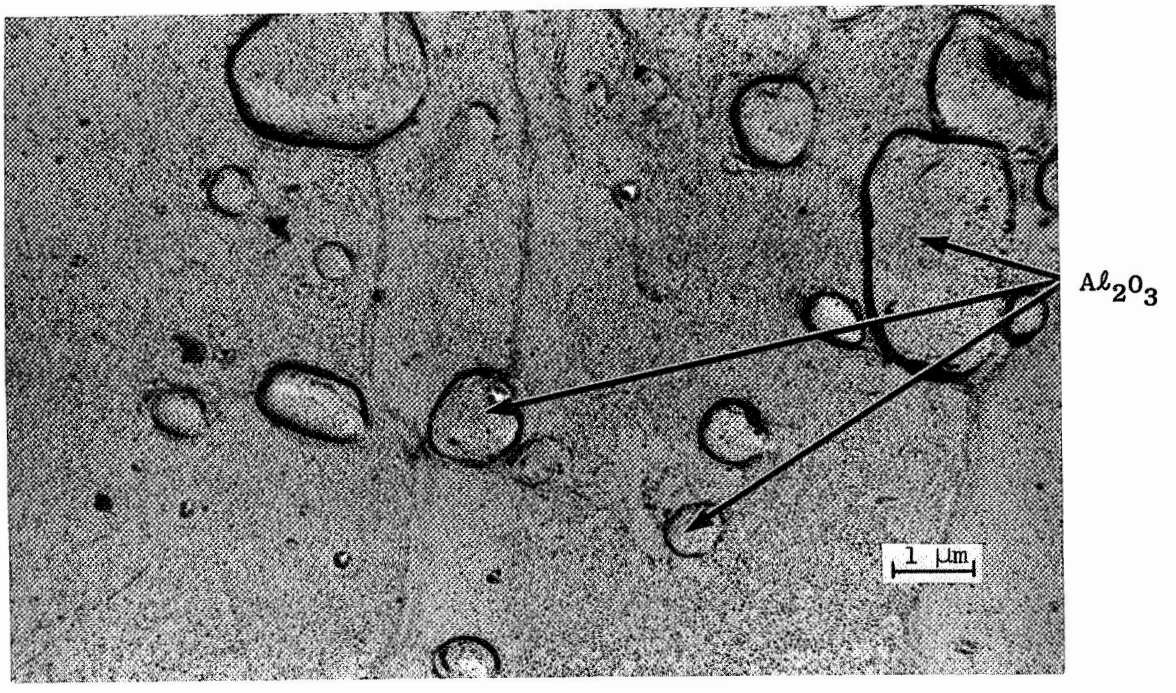

Outer Edge - Al_2O_3 Particles

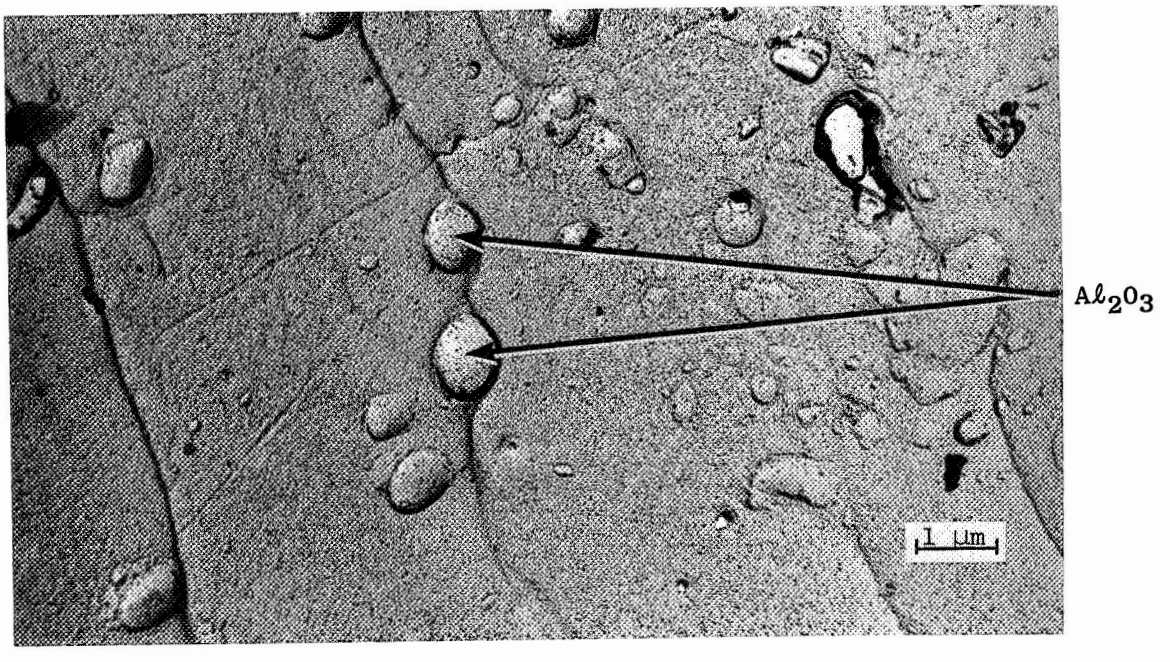

Center - Al_2O_3 Particles

Figure 8. Electron Microscopy of NC11-A Coating on NASA VIA Alloy, As-Coated (10,000).

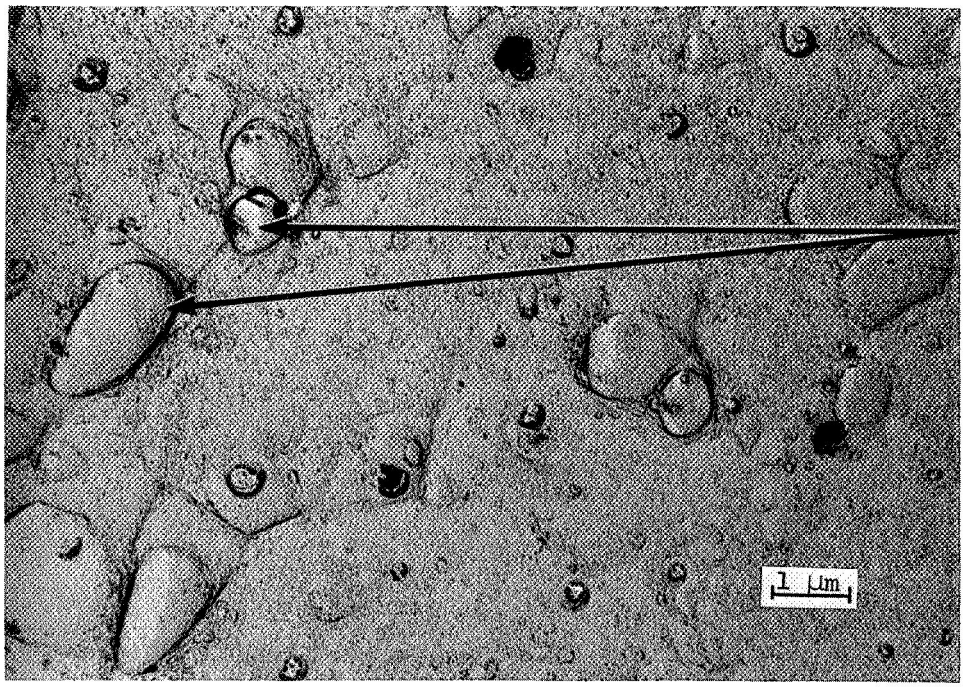

Center - Al_2O_3 Particles

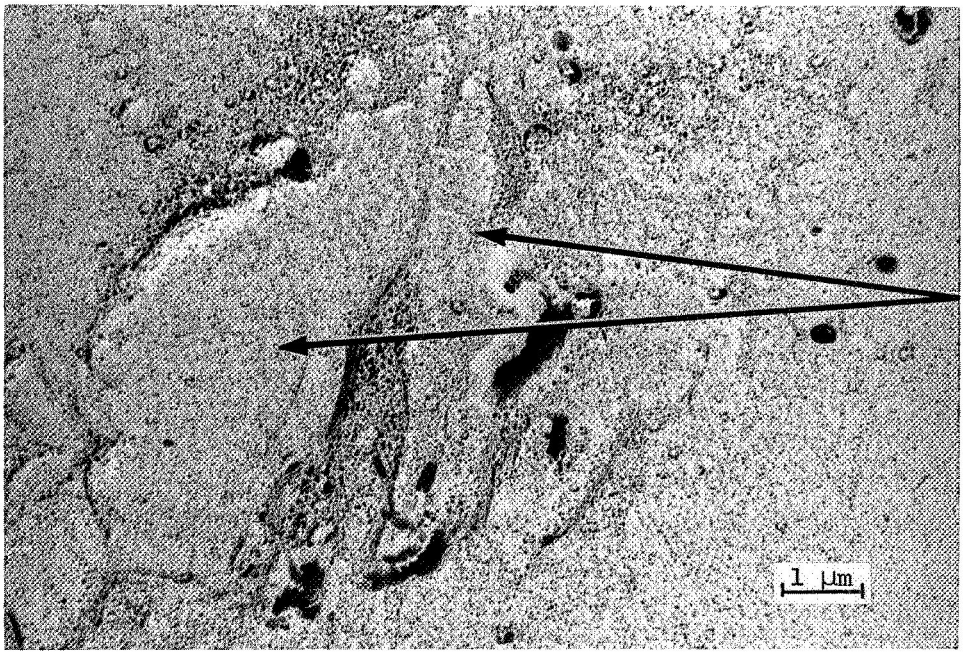

Cr Particle

Figure 9. Electron Microscopy of NC4-Cr Coating on NASA VIA Alloy, As-Coated (10,000).

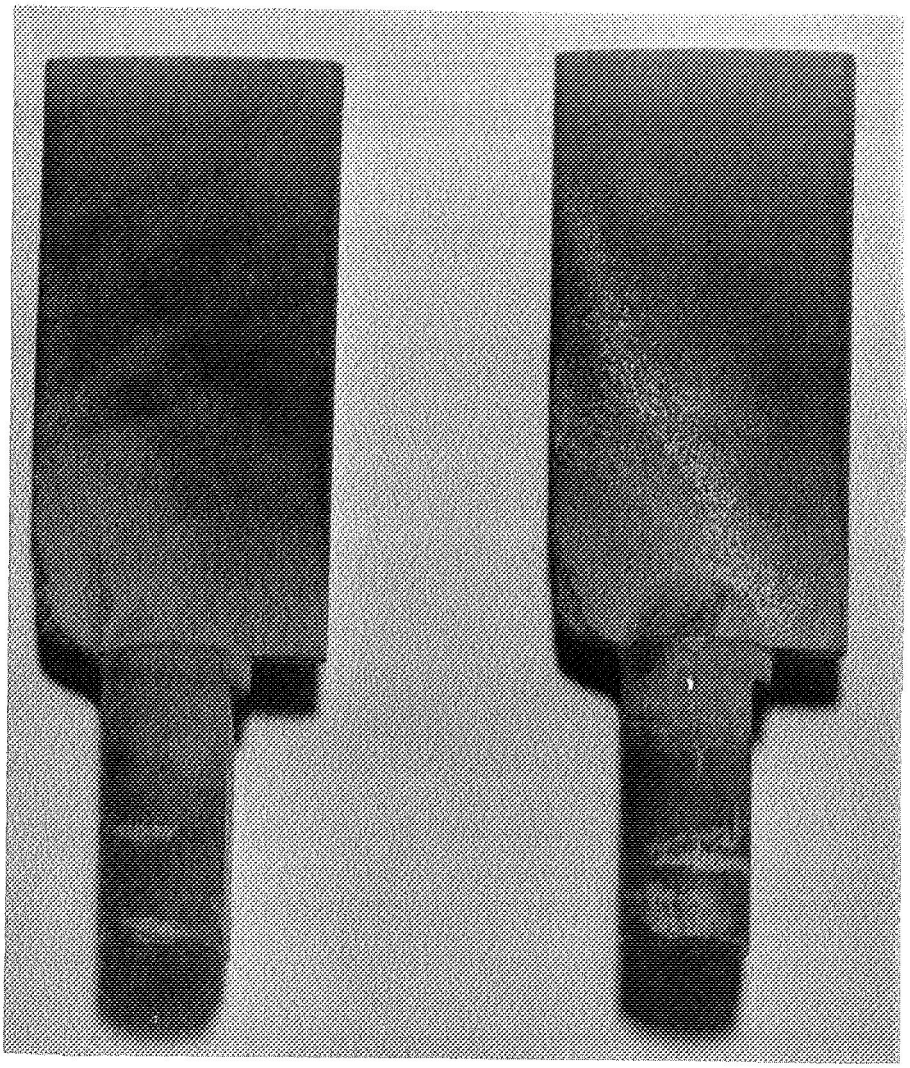

2X

Figure 10. Overtemperature Failure at Airfoil Lower Trailing Edge Due to High Stagnation Temperature; CODEP C-2 Coated Rene' 100.

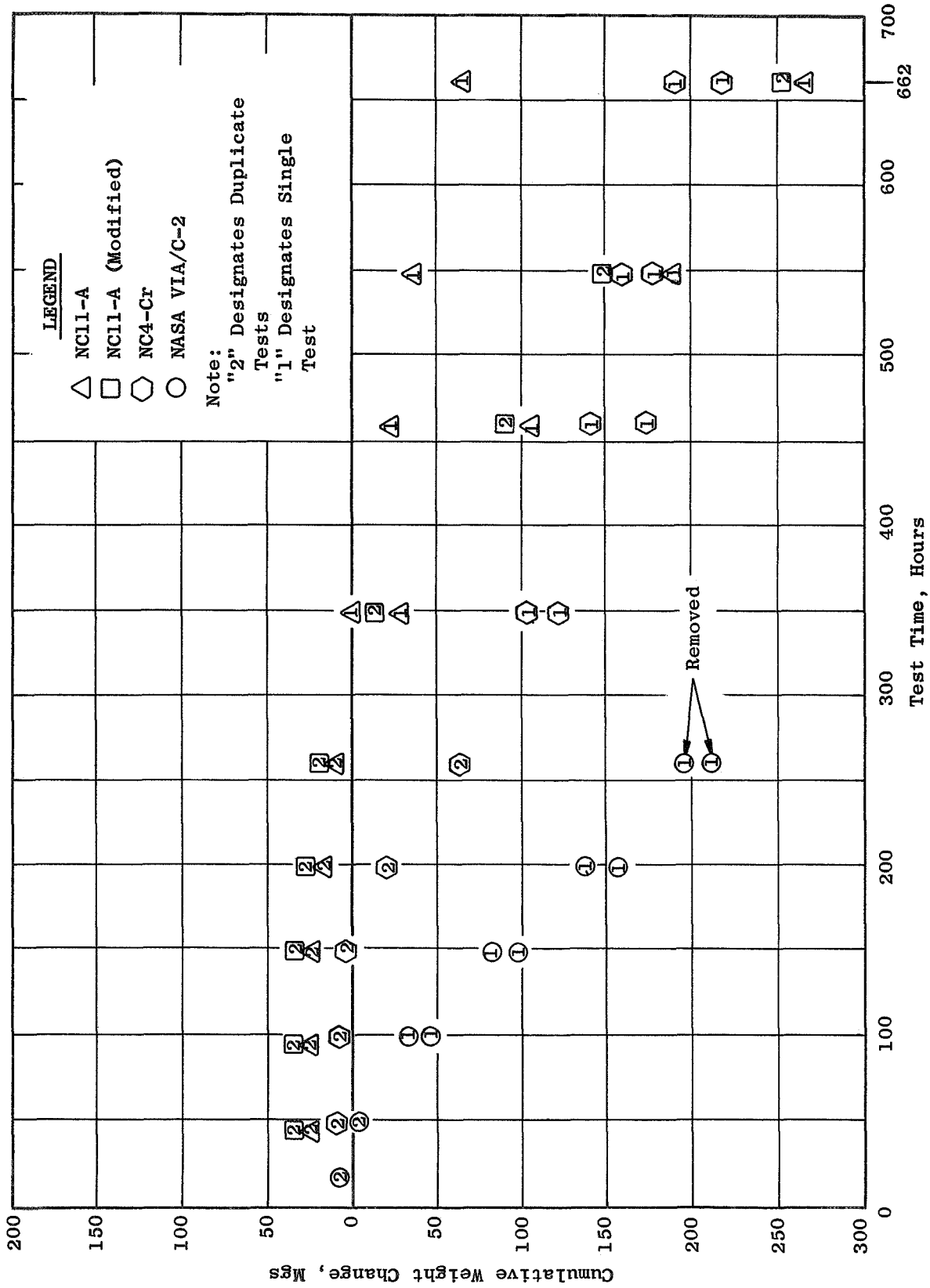

Figure 11. Cumulative Weight Change in 2000°F (1366 °K) Burner Rig Test No. 2.

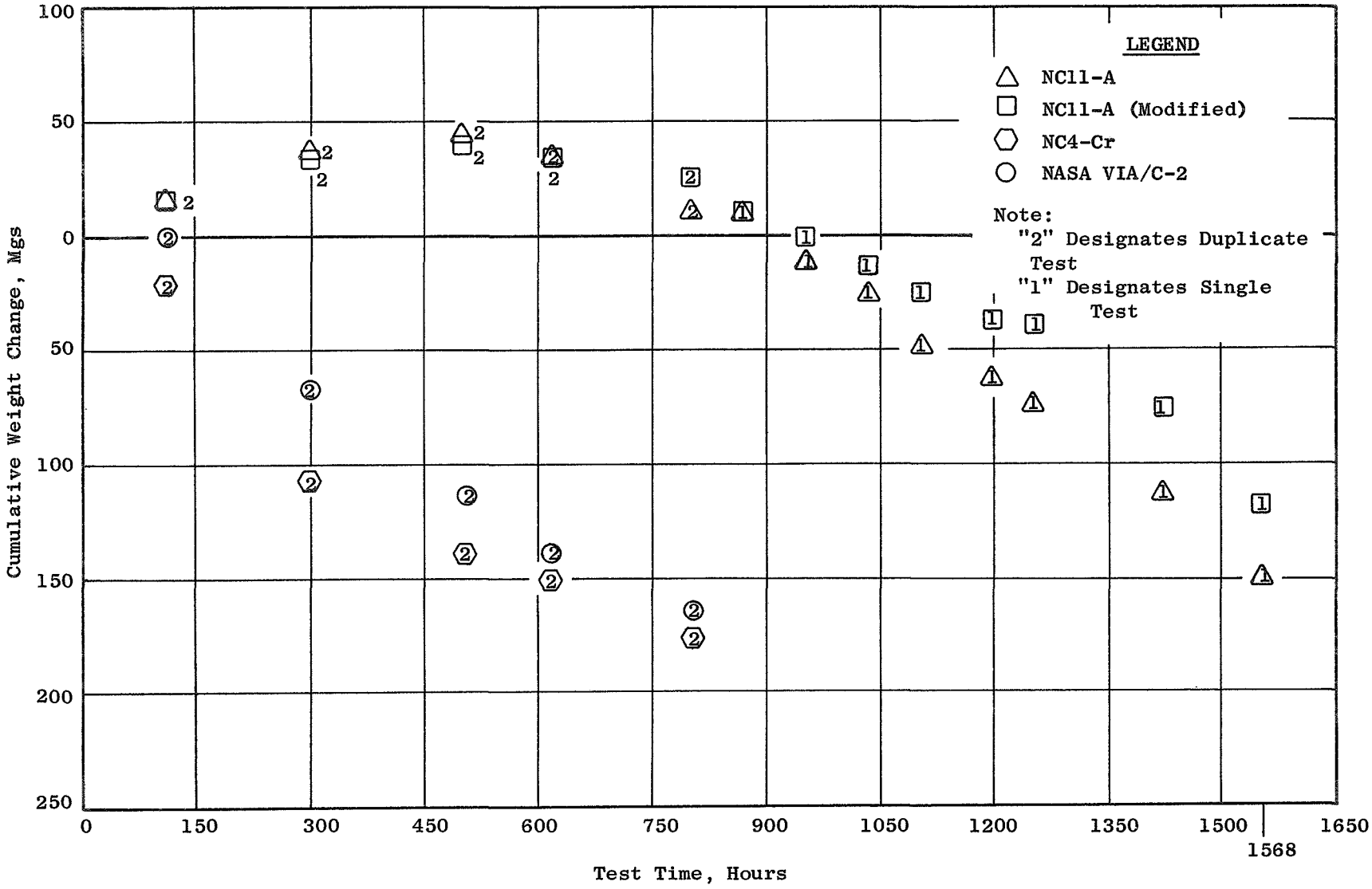

Figure 12. Cumulative Weight Change in 2000°F (1366°K) MPTL Burner Rig Test.

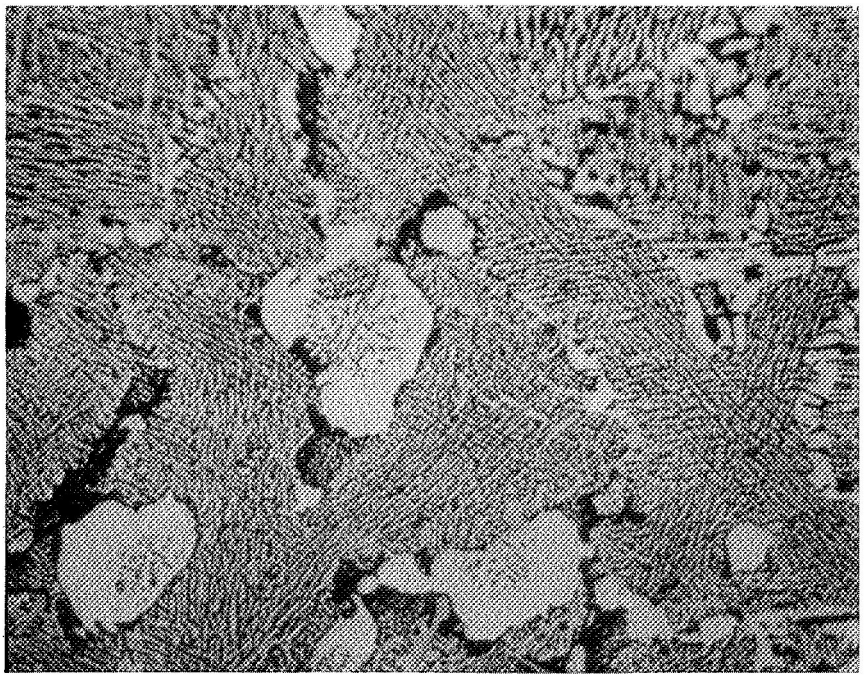

2050°F (1394°K)

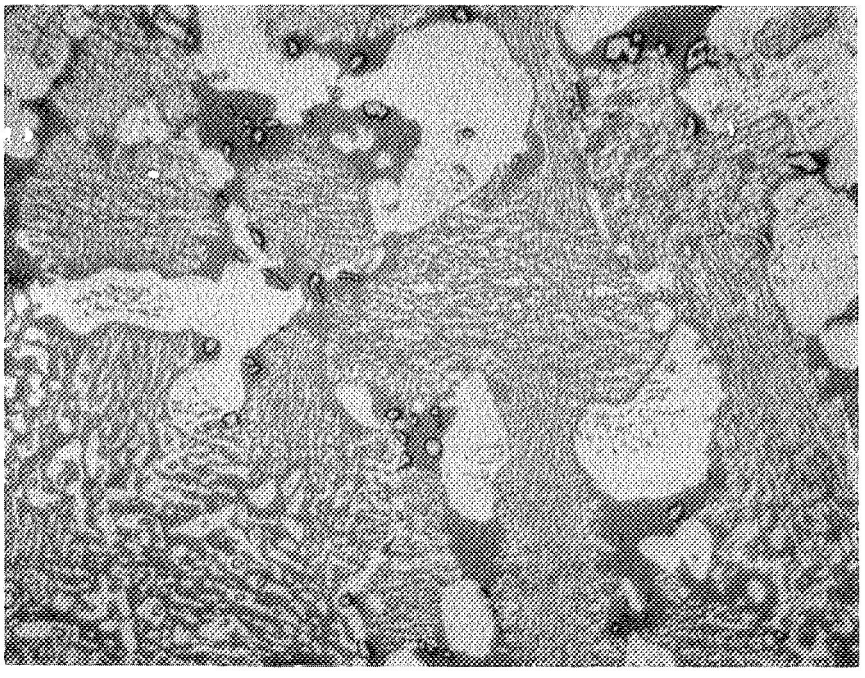

2150°F (1450°K)

Figure 13. NASA VIA Alloy Structural Changes After 300 Hours in Laboratory Static Oxidation Test (Etched 500X).

Leading Edge Section

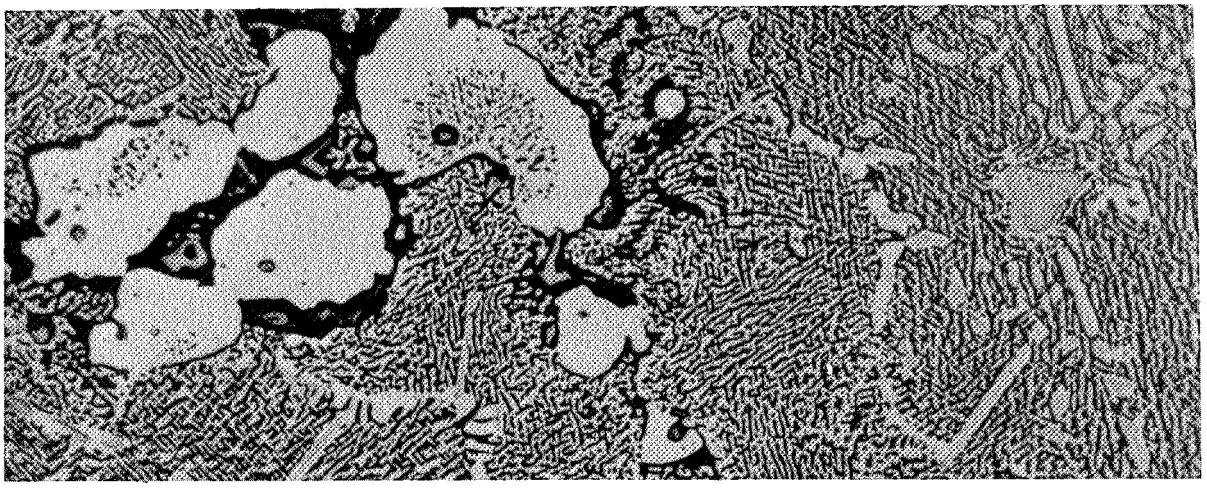

Center Airfoil Section

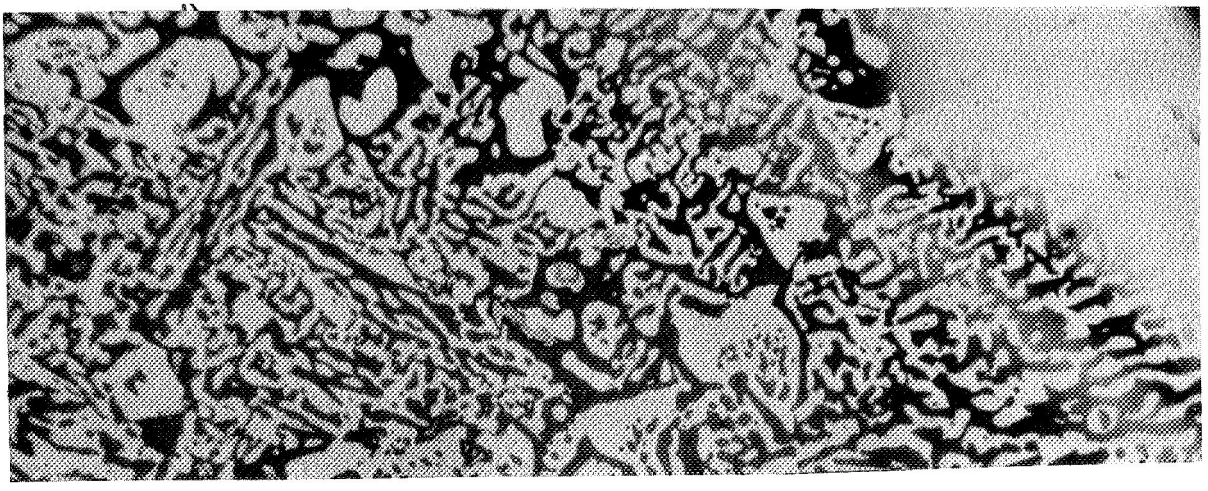

Lower Trailing Edge Section

Figure 14. NASA VIA Structural Changes After 360 Hours in EPPI Burner Rig Test - 2000°F (1366°K) Temperature Monitored at Leading Edge (Etched 500X).

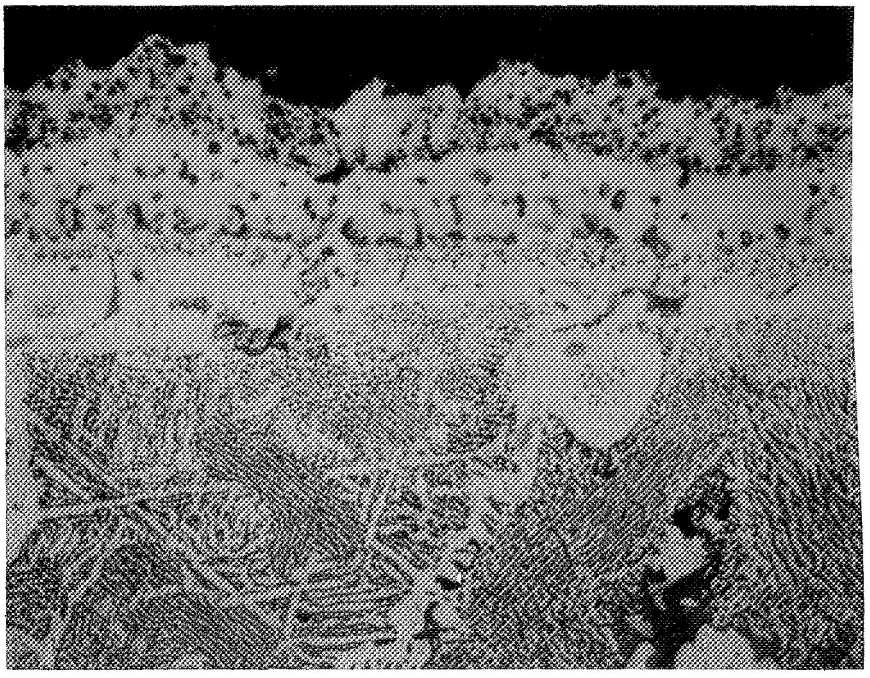

NC4-Cr - Coating 500X

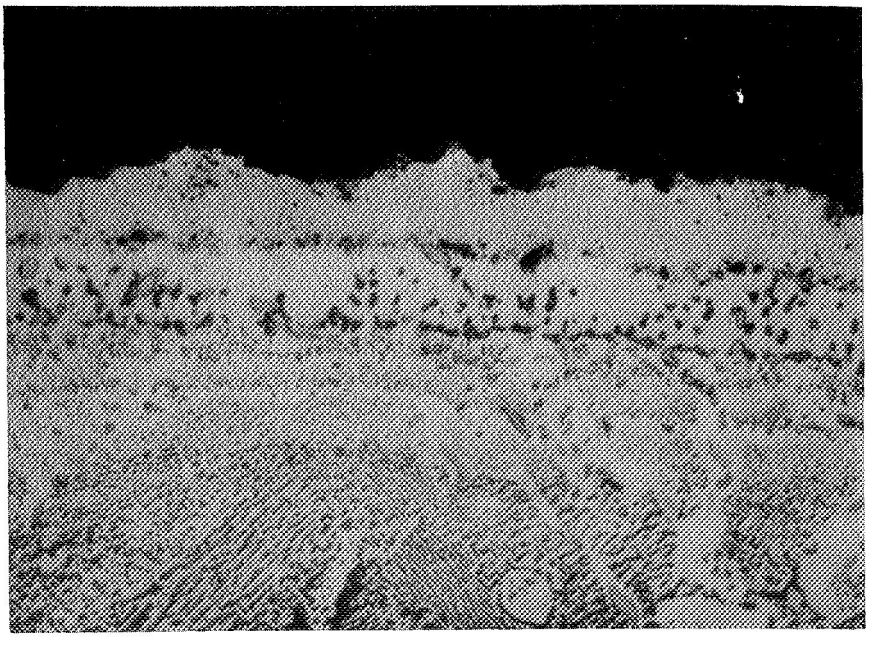

500X

NC11-A - Coating

Figure 15. Coating Structure of Leading Edge Sections Exposed at 2000°F (1366°K) in EPPI Burner Rig for 662 Hours.

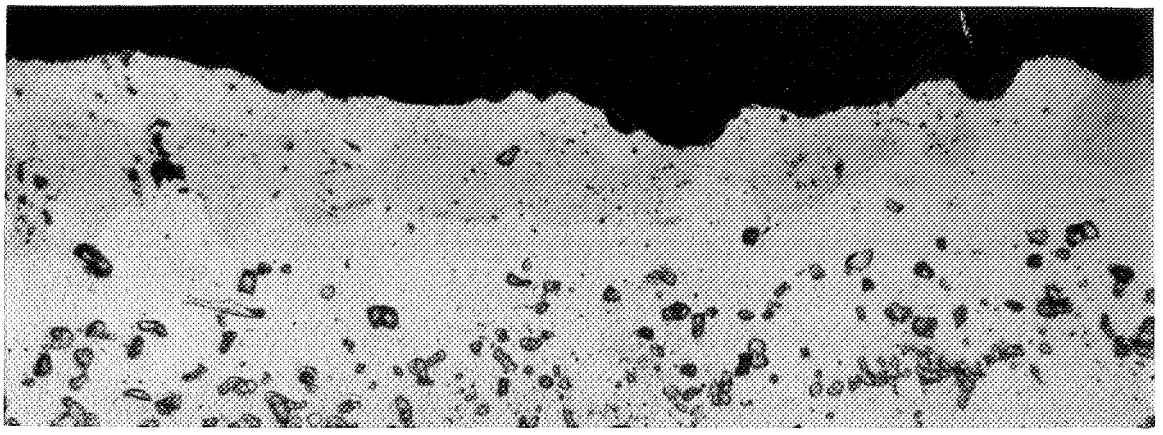

M&PTL - 1568 Hours - Leading Edge - Top Section

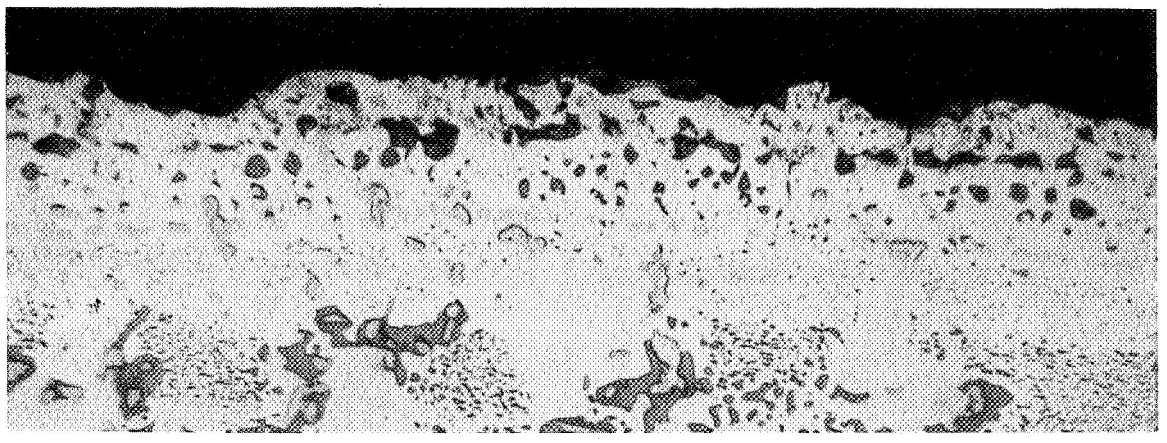

M&PTL - 1568 Hours - Trailing Edge - Top Section

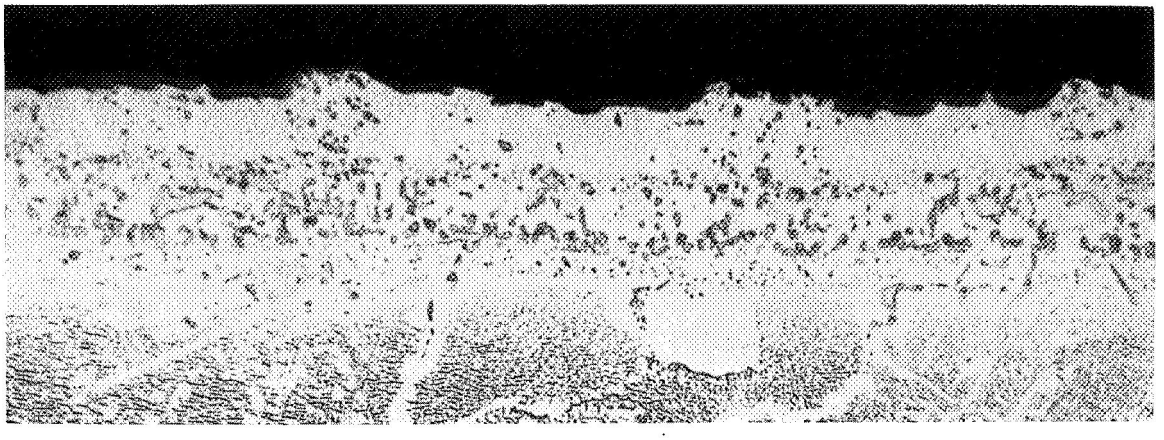

EPPI - 662 Hours - Leading Edge - Top Section

Figure 16. Comparison of Coating Structure of NC11-A Coating After EPPI and M&PTL Burner Rig Tests at 2000°F (1366°K) (Etched 500X).

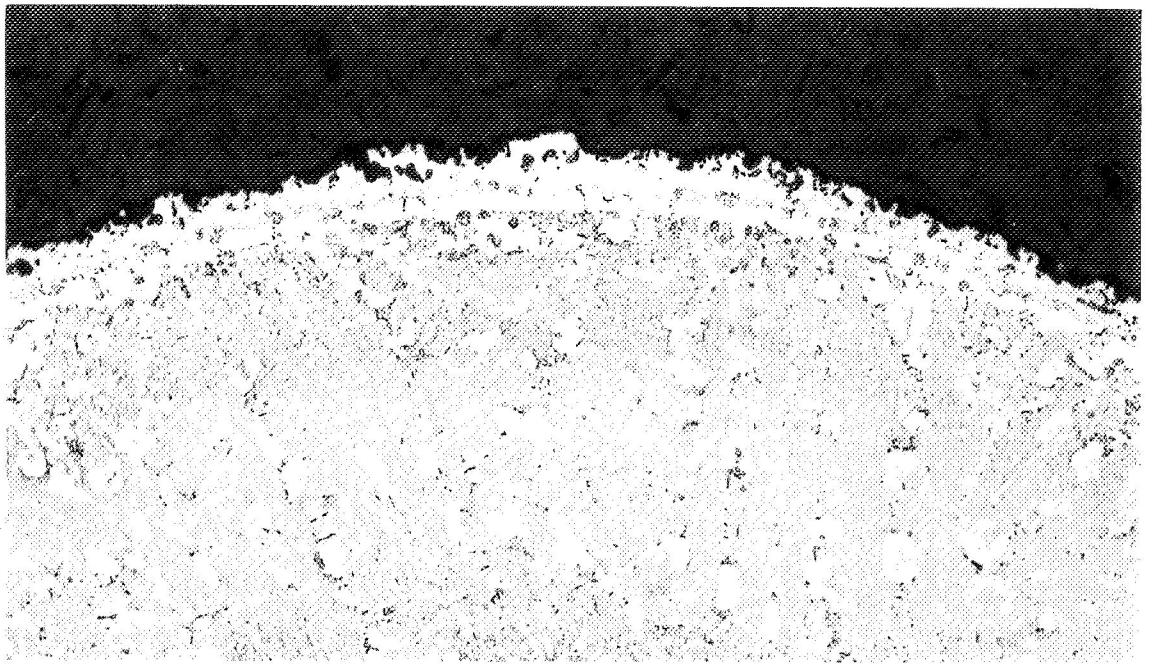

NC11-A-S1

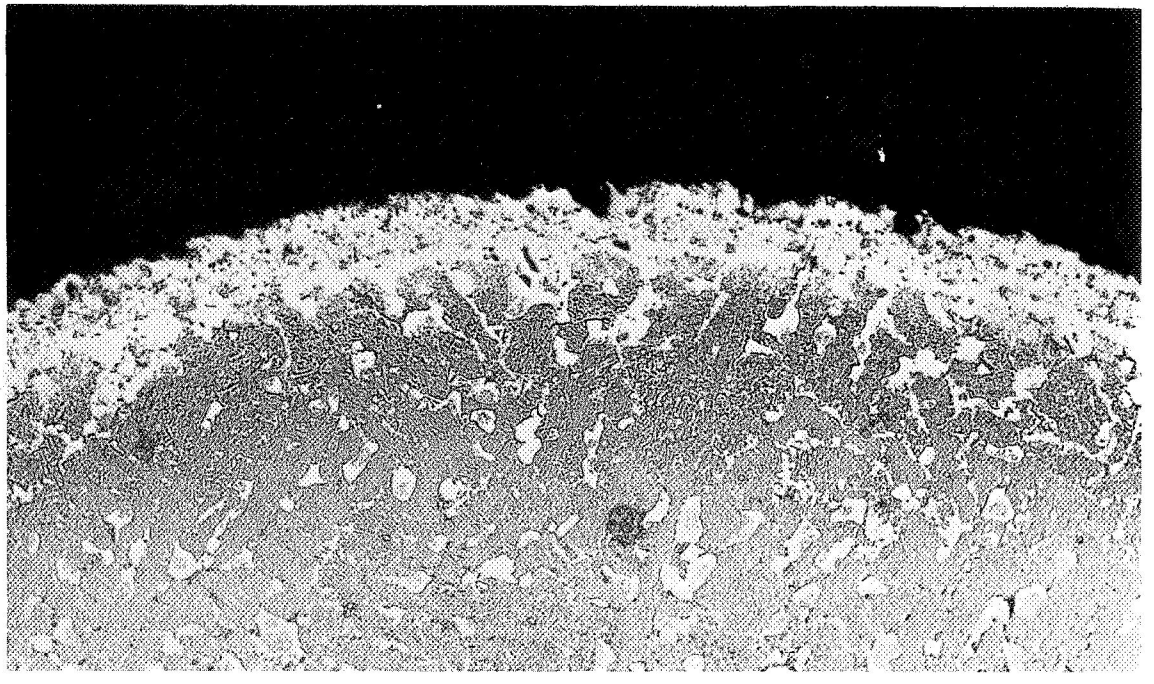

NC11-A-D1

Figure 17. Leading Edge Sections of Selected Coatings After 2000°F (1366°K)/500 Hours Burner Rig Testing, 10 Cycles/Hour (Etched 100X).

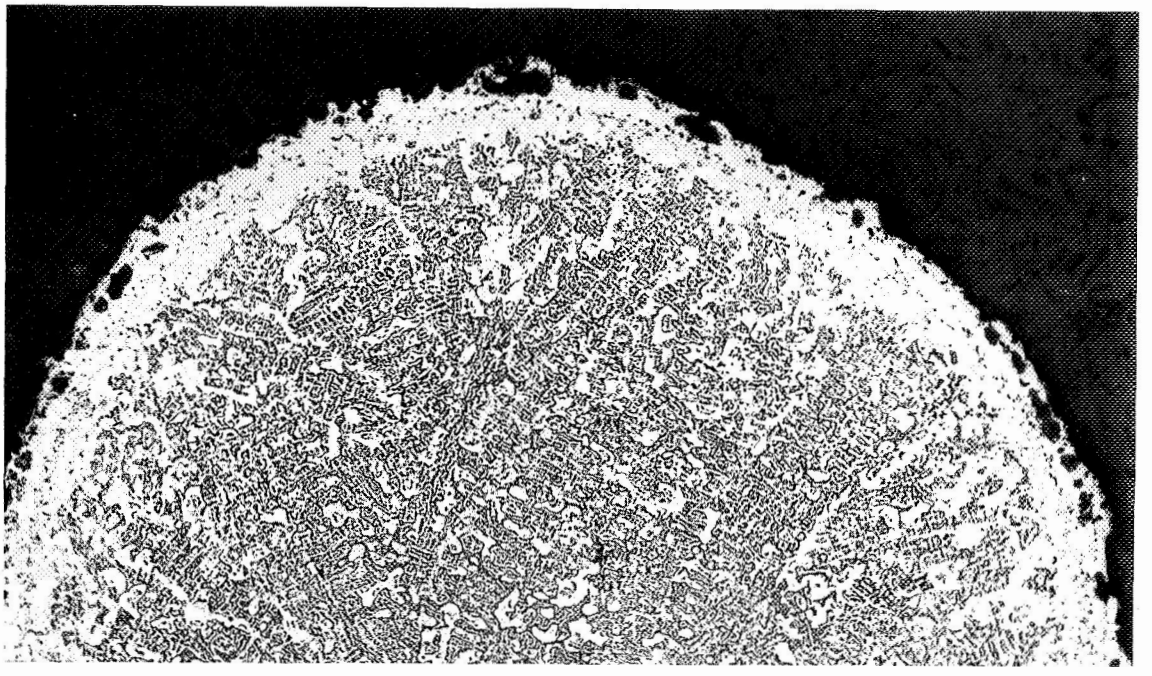

NC11-A-S1

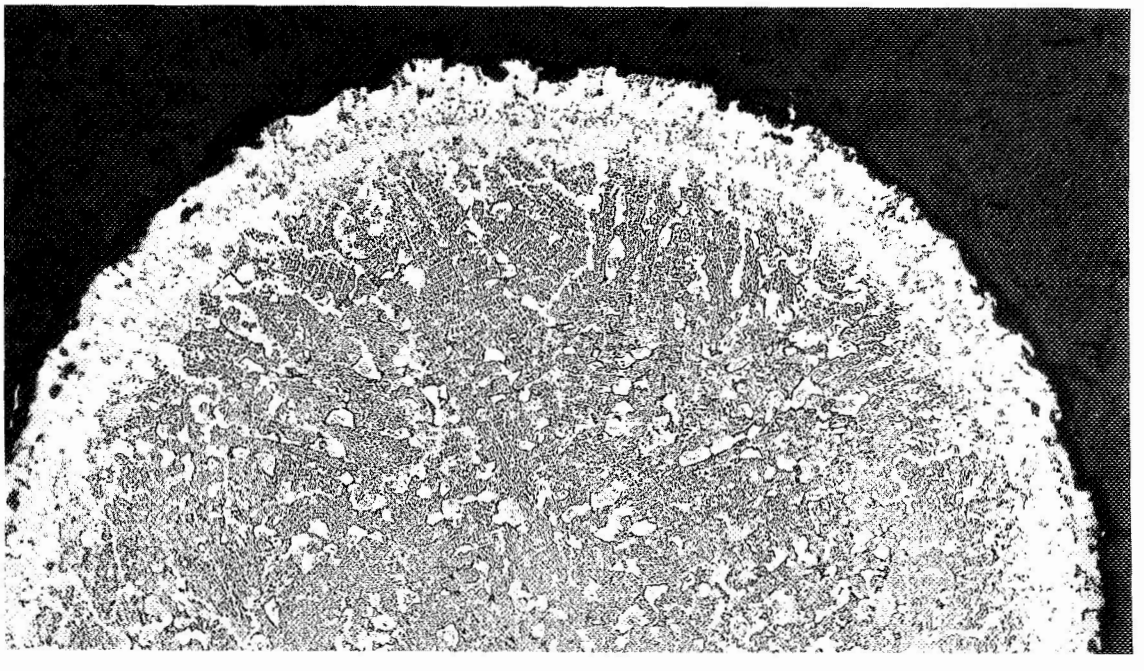

NC11-A-D1

Figure 18. Trailing Edge Sections of Selected Coatings After 2000°F (1366°K)/500 Hours Burner Rig Testing, 10 Cycles/Hour (Etched 100X).

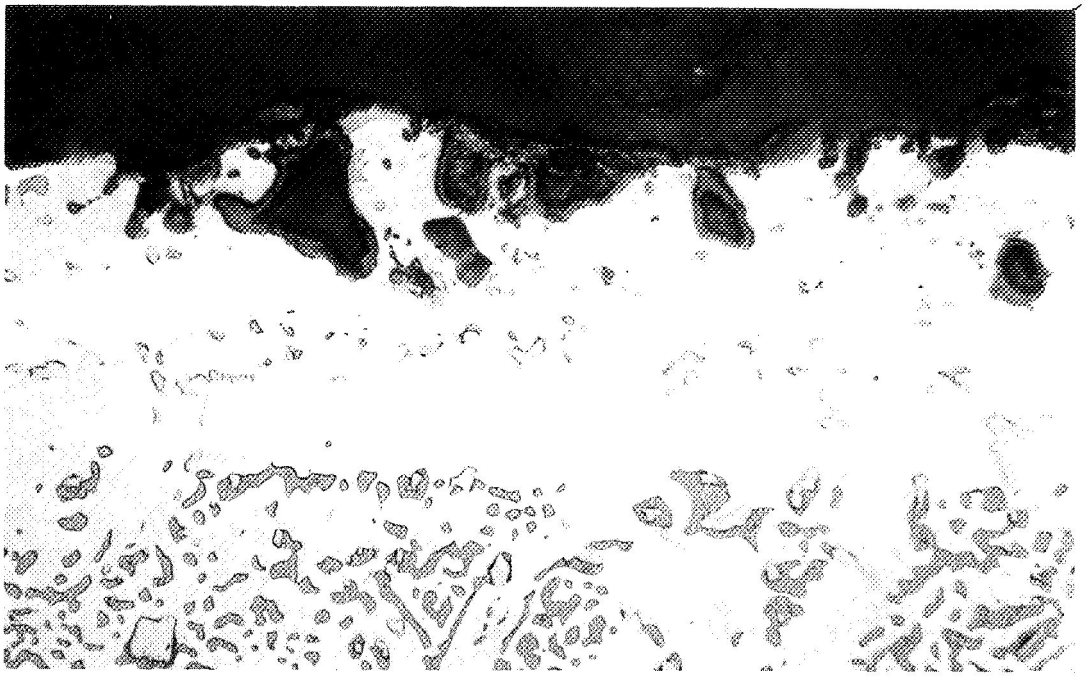

NC11-A-S1

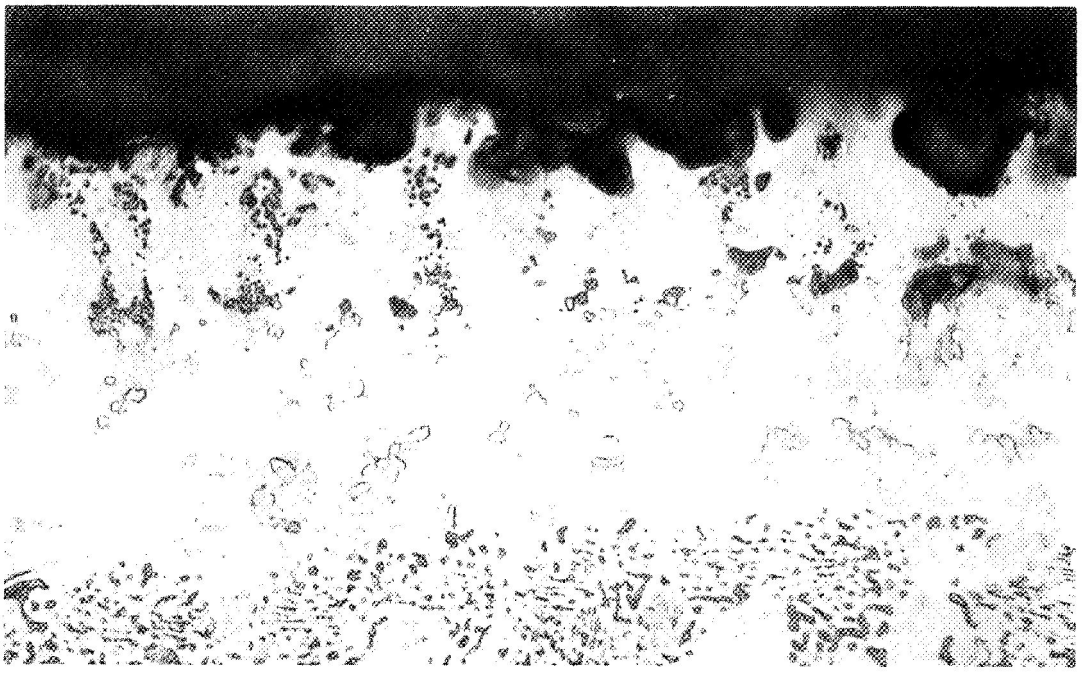

NC11-A-D1

Figure 19. Leading Edge Sections of Selected Coatings After 2000°F (1366°K)/500 Hours Burner Rig Testing, 10 Cycles/Hour (Etched 500X).

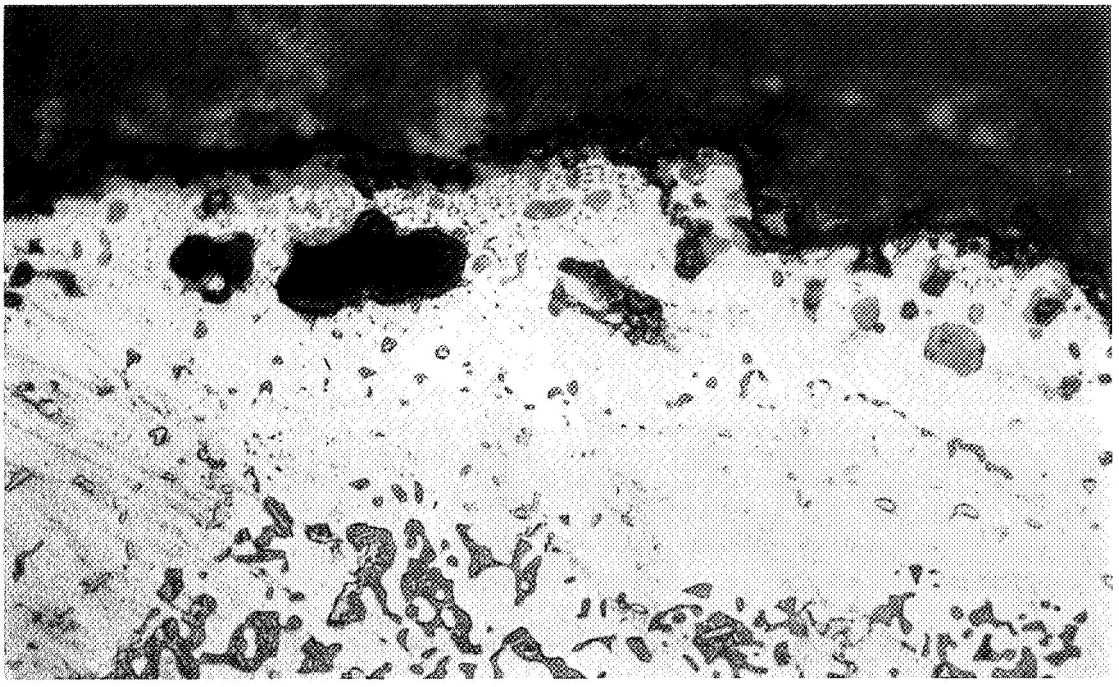

NC11-A-S1

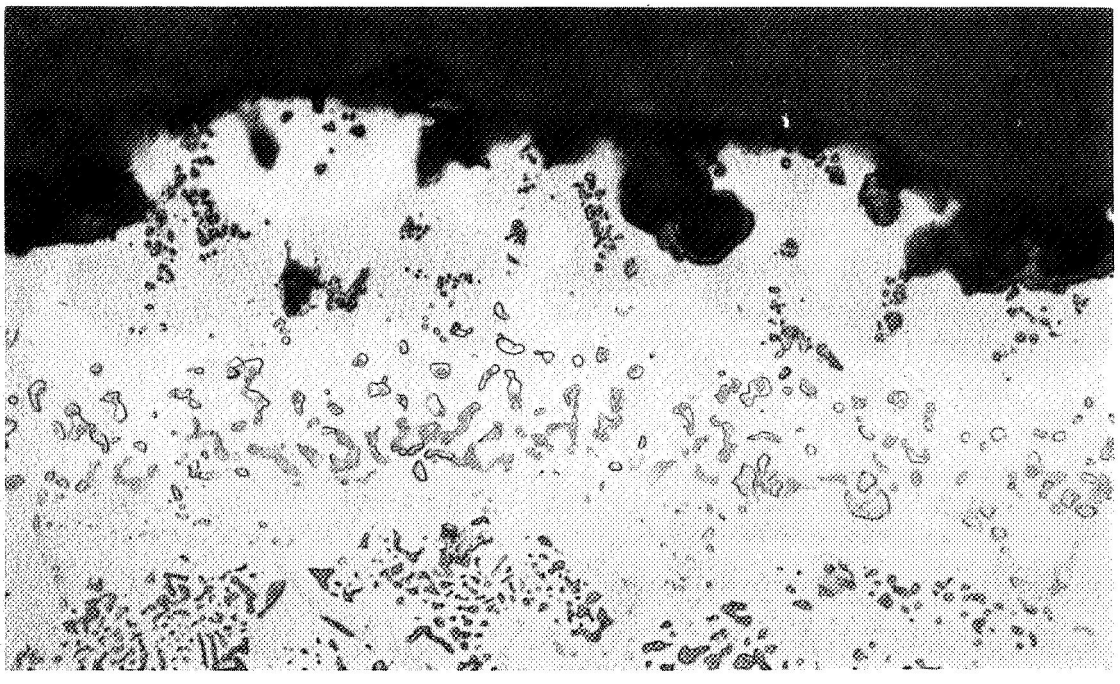

NC11-A-D1

Figure 20. Trailing Edge Sections of Selected Coatings After 2000°F (1366°K)/500 Hours Burner Rig Testing, 10 Cycles/Hour (Etched 500X).

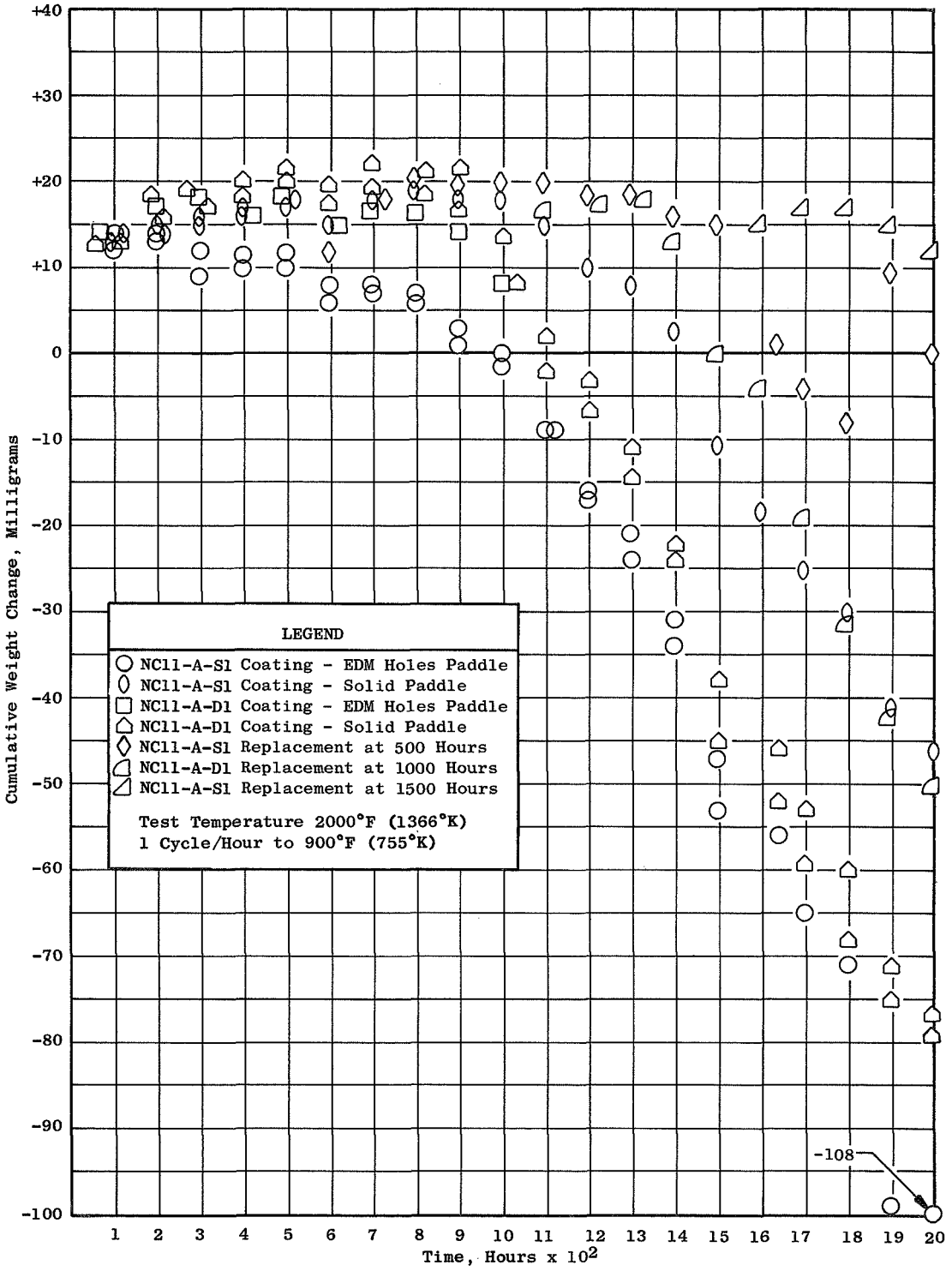

Figure 21. Cumulative Weight Changes in Burner Rig No. 5, at 2000°F (1366°K).

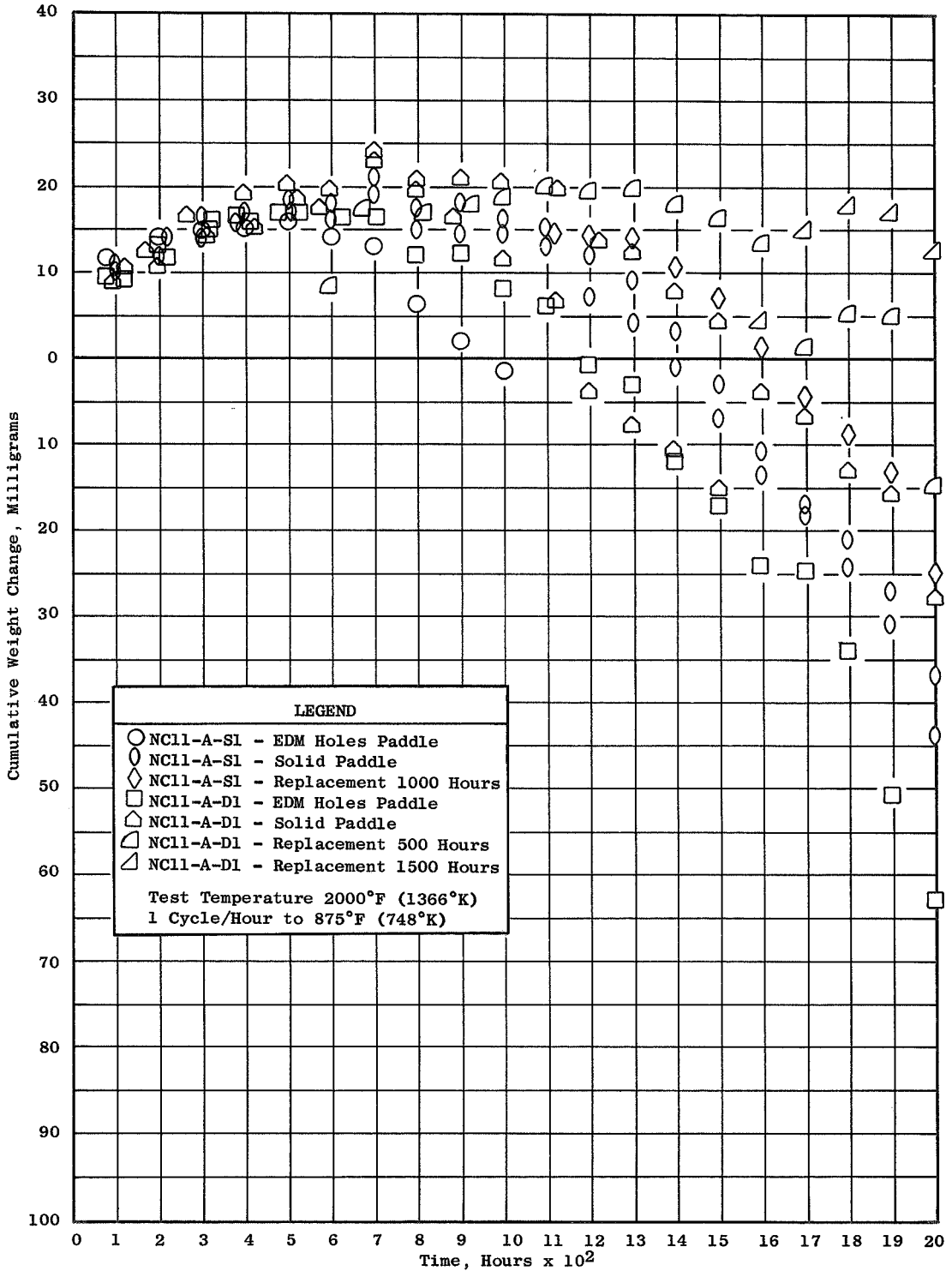

Figure 22. Cumulative Weight Changes in Burner Rig No. 4, at 2000°F (1366°K).

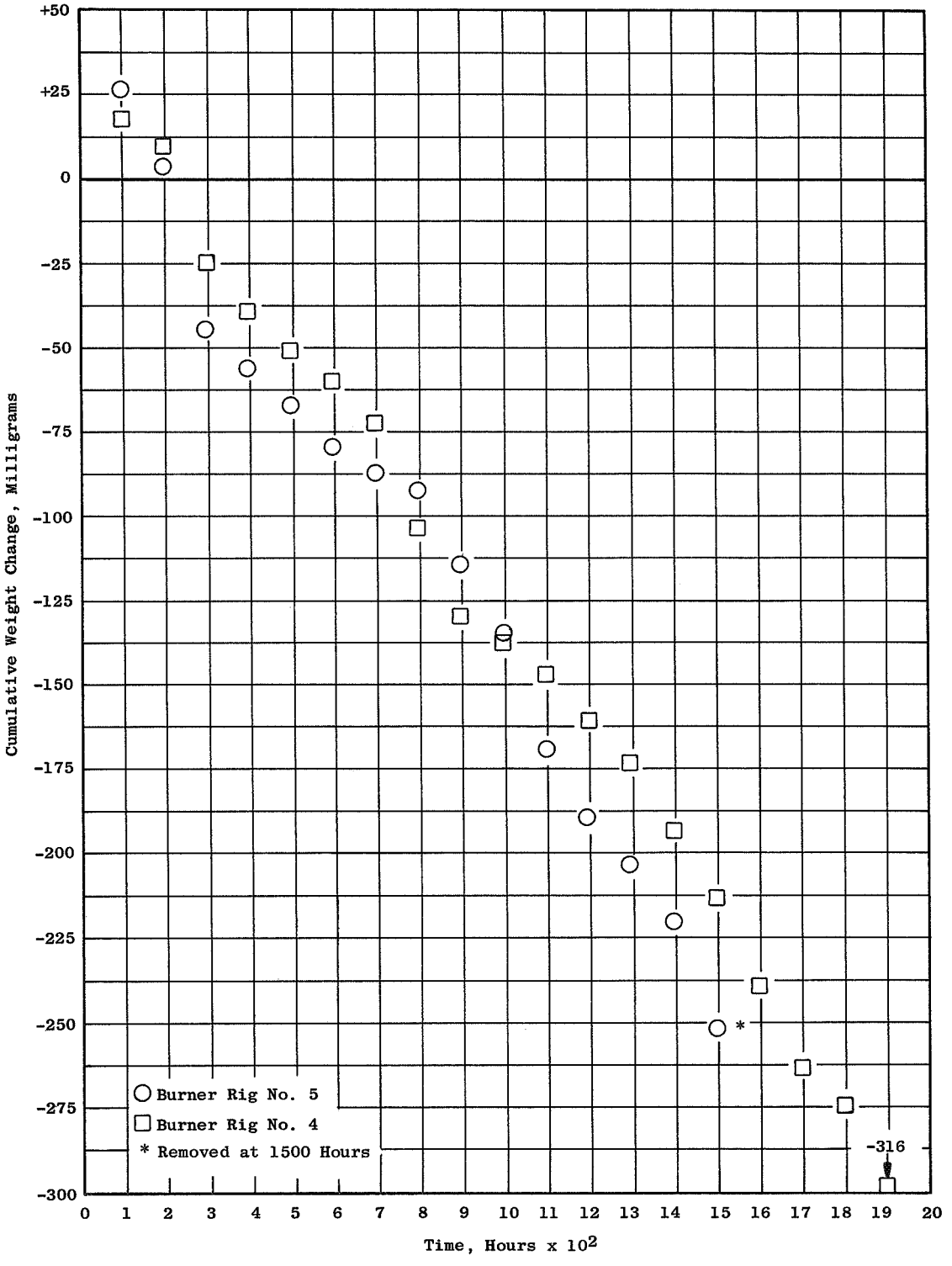

Figure 23. Cumulative Weight Changes on Uncoated NASA VIA Alloy Paddles at 2000°F (1366°K).

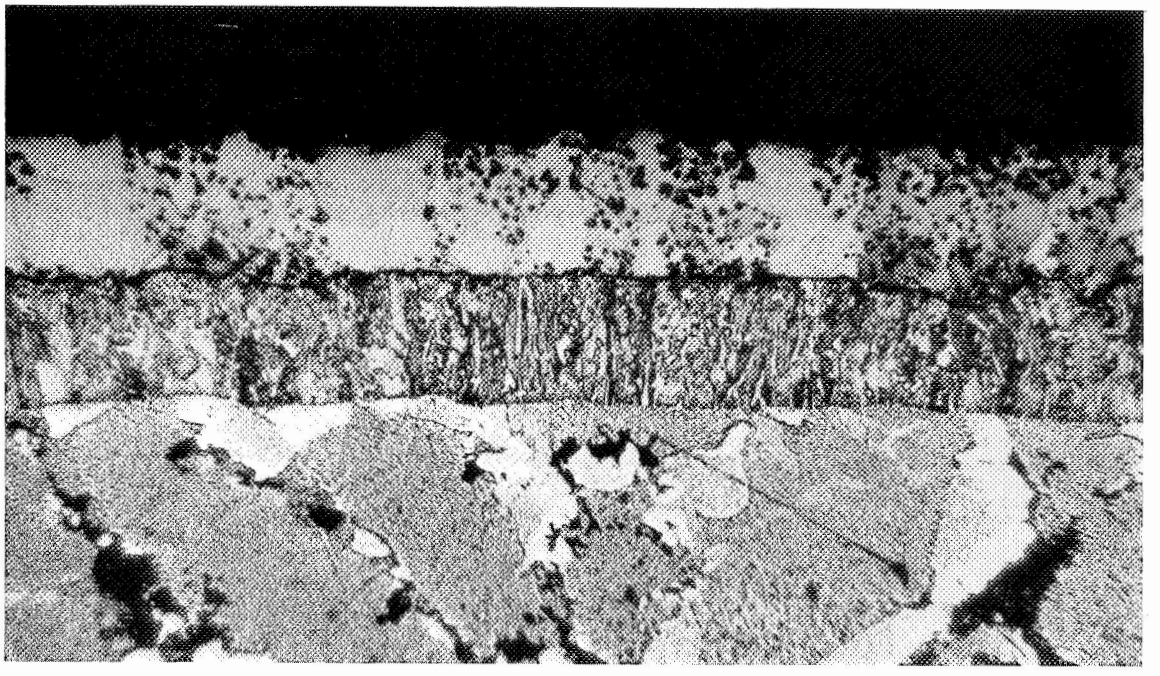

NC11-A-S1

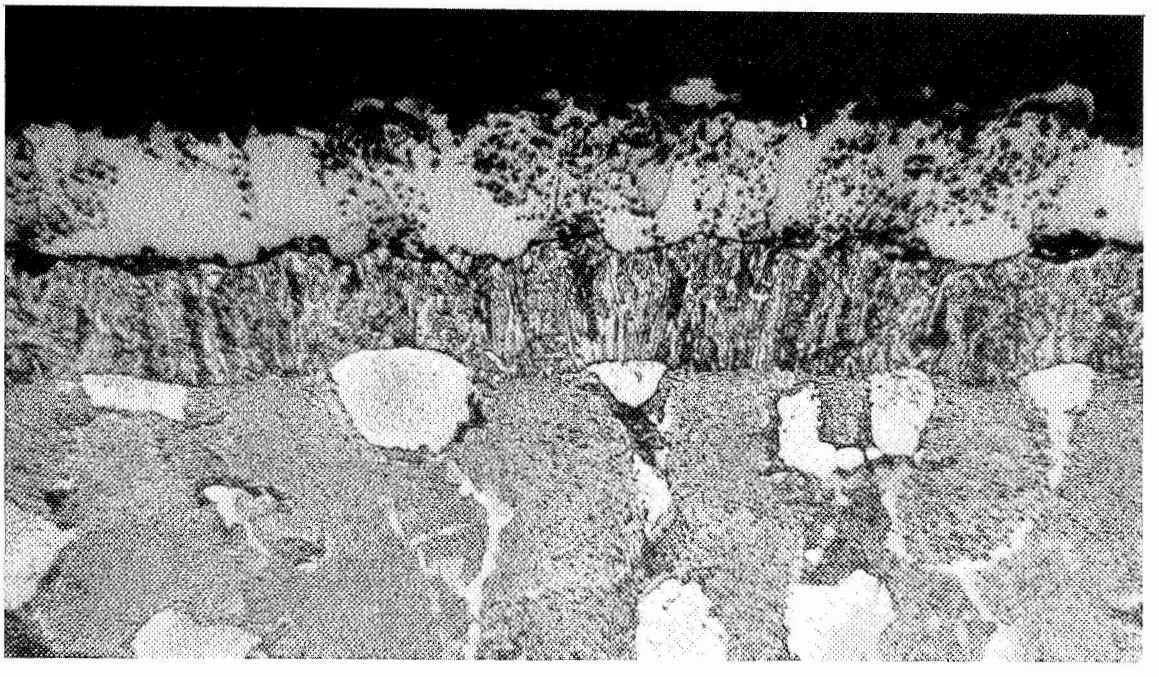

NC11-A-D1

Figure 24. Coating Structures of Systems Selected for 2000°F (1366°K)/ 2000-Hour Test (Etched 500X).

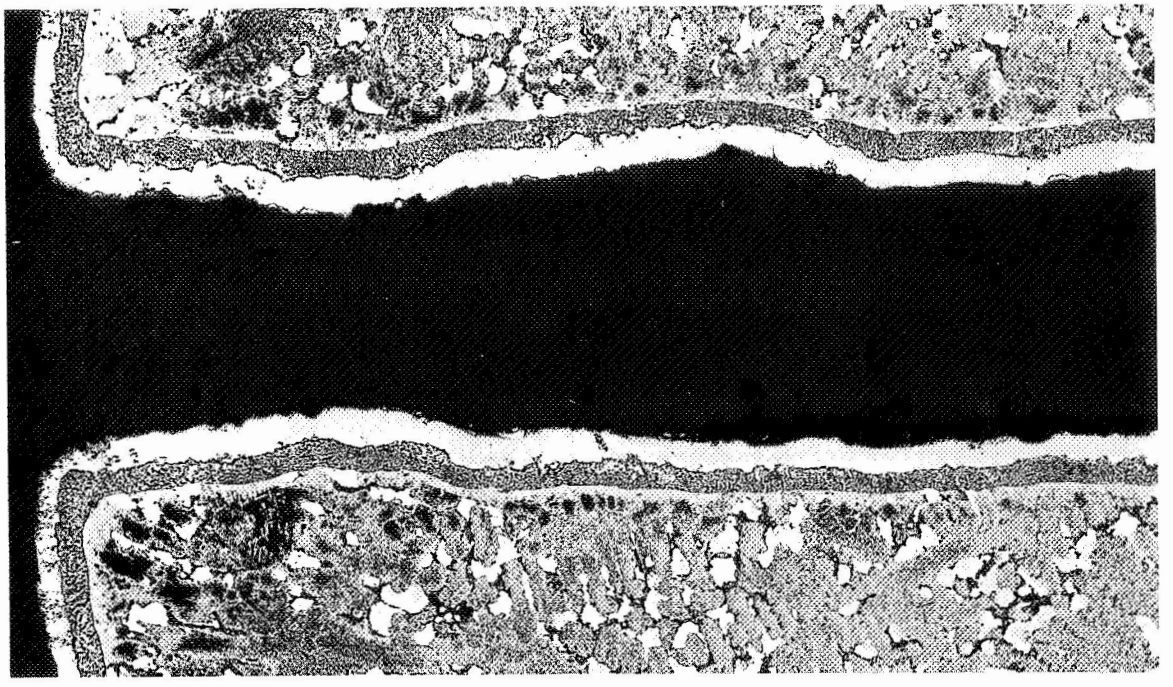

Leading Edge

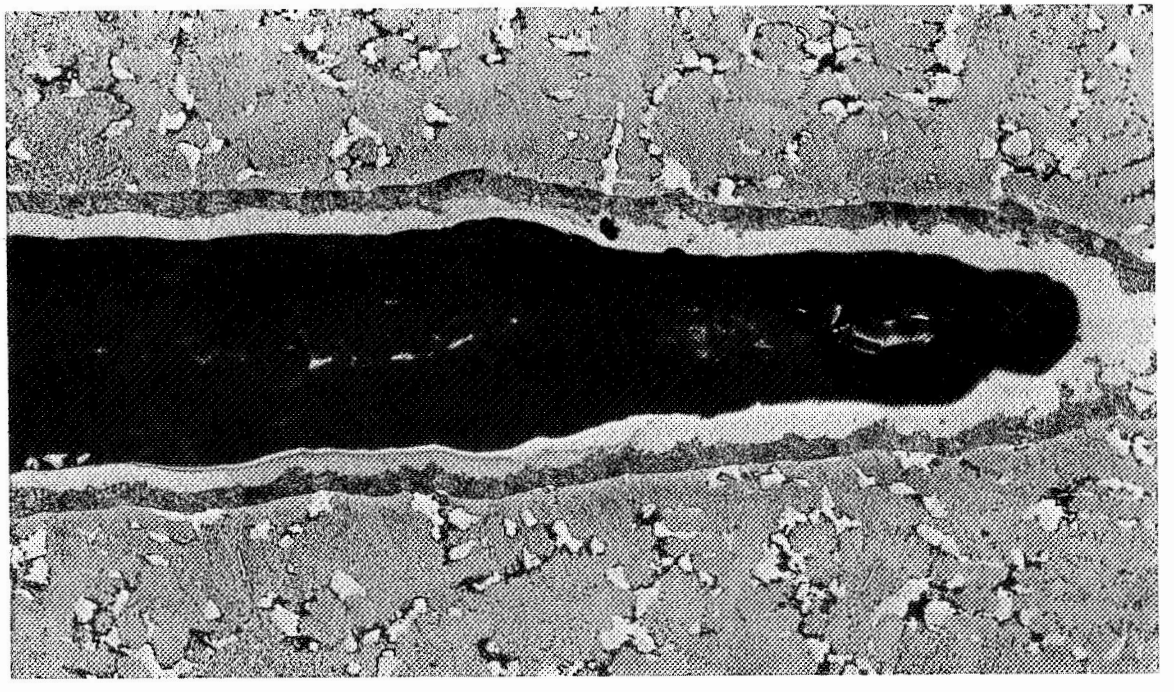

Maximum Measureable Depth - 0.185 Inch (0.47 cm)(Irregular Hole)

Figure 25. NC11-A-S1 Coating in 0.020-Inch (0.05 cm) Diameter Hole, As Coated (Etched 100X).

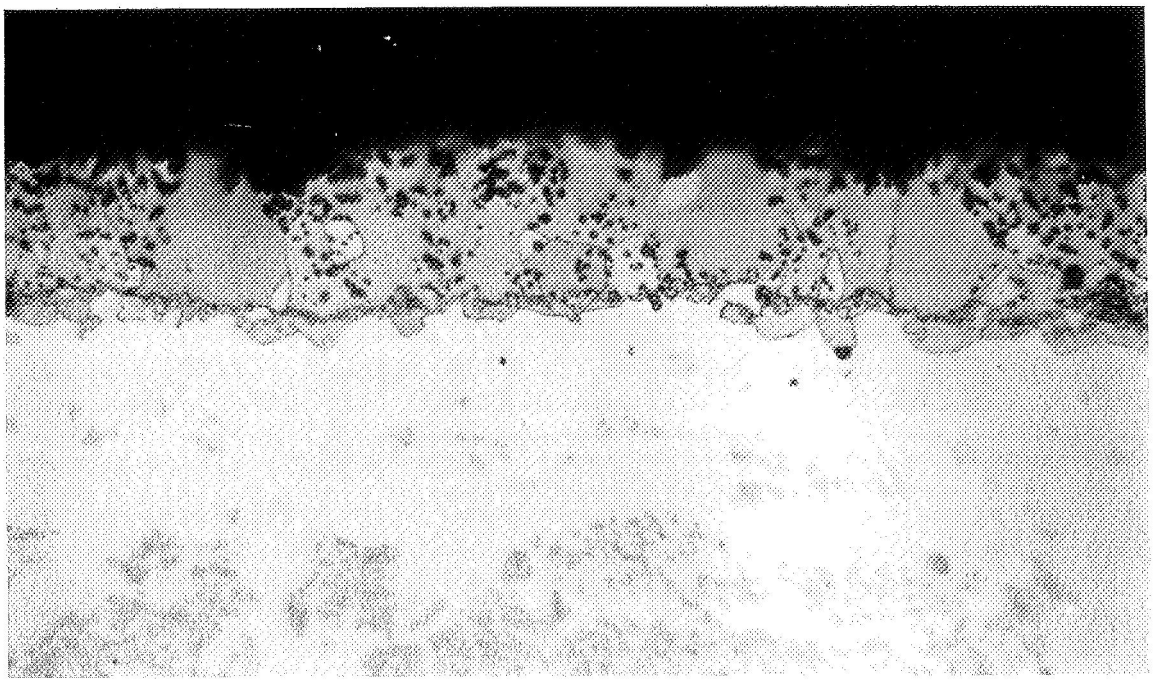

Leading Edge - 0.4 Inch (1.0 cm) Down from Tip

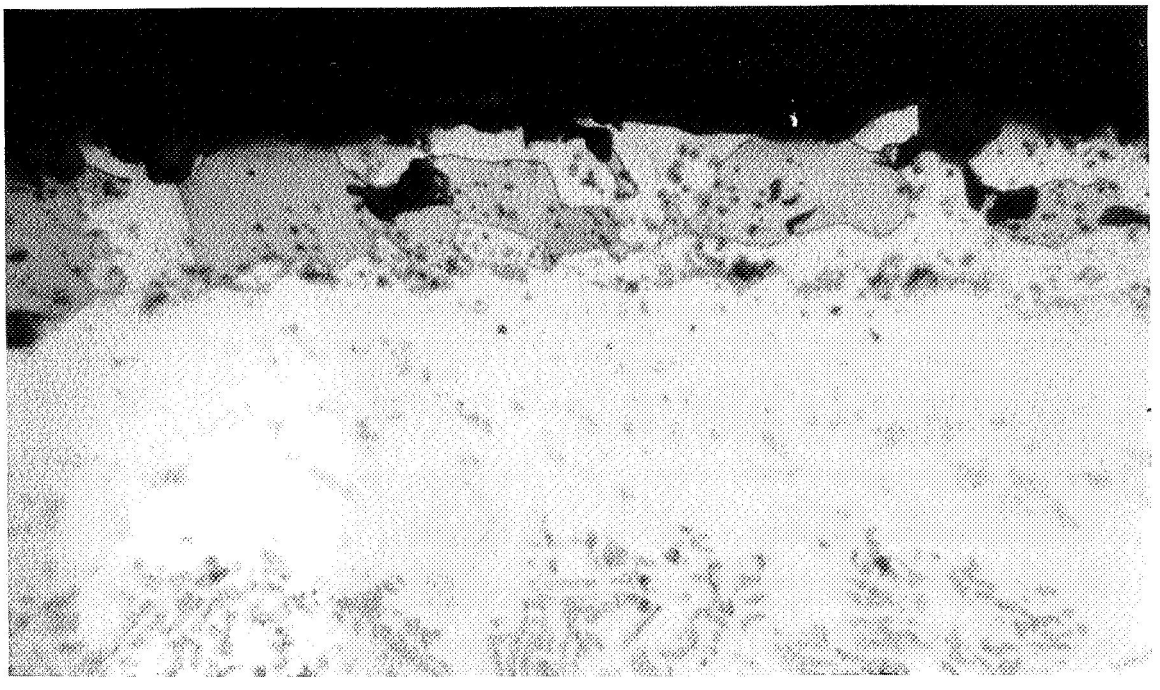

Trailing Edge - 0.4 Inch (1.0 cm) Down from Tip

Figure 26. NC11-A-S1 Coating Structure After 504 Hours at 2000°F (1366°K)(500X).

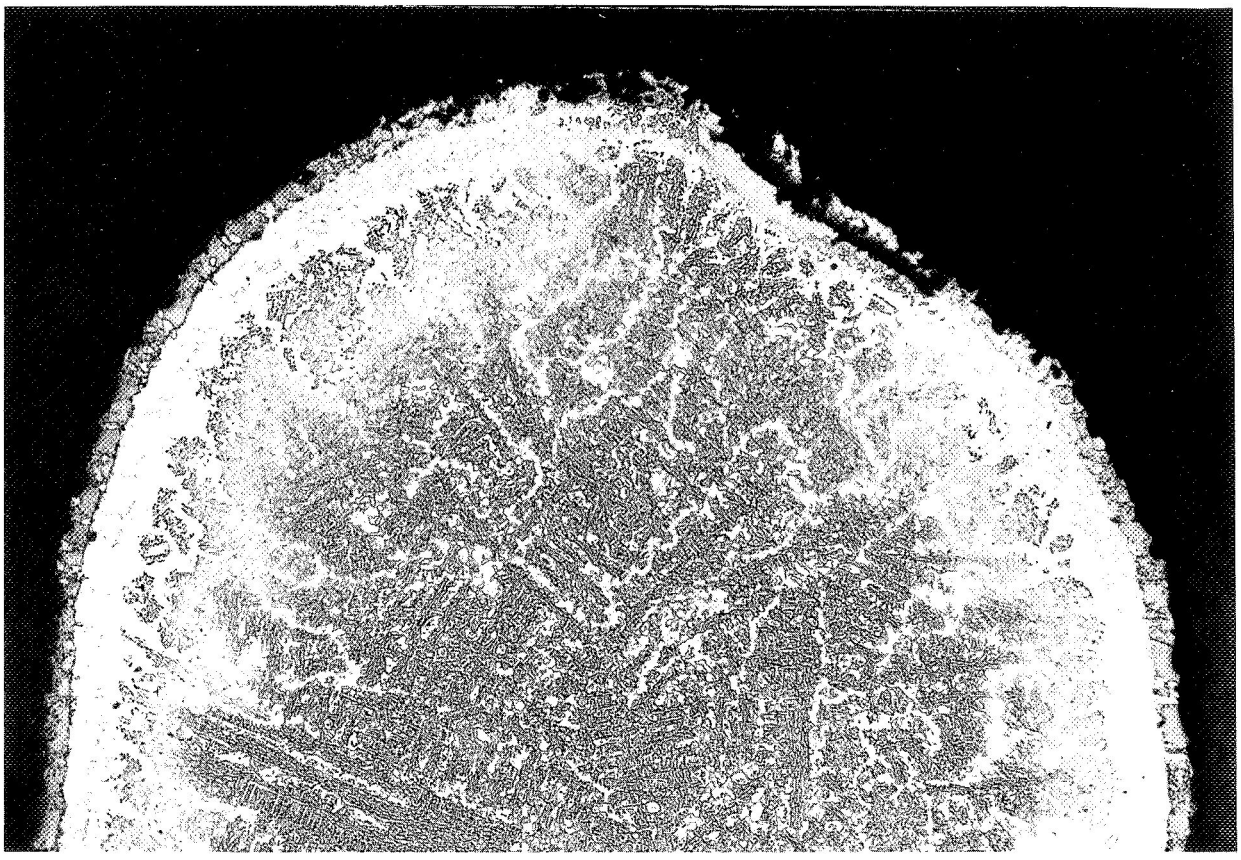

Figure 27. NC11-A-S1 Coating on Trailing Edge Section - 504 Hours at 2000°F (1366°K) - Site of Local Attack Near Tip (Etched 500X).

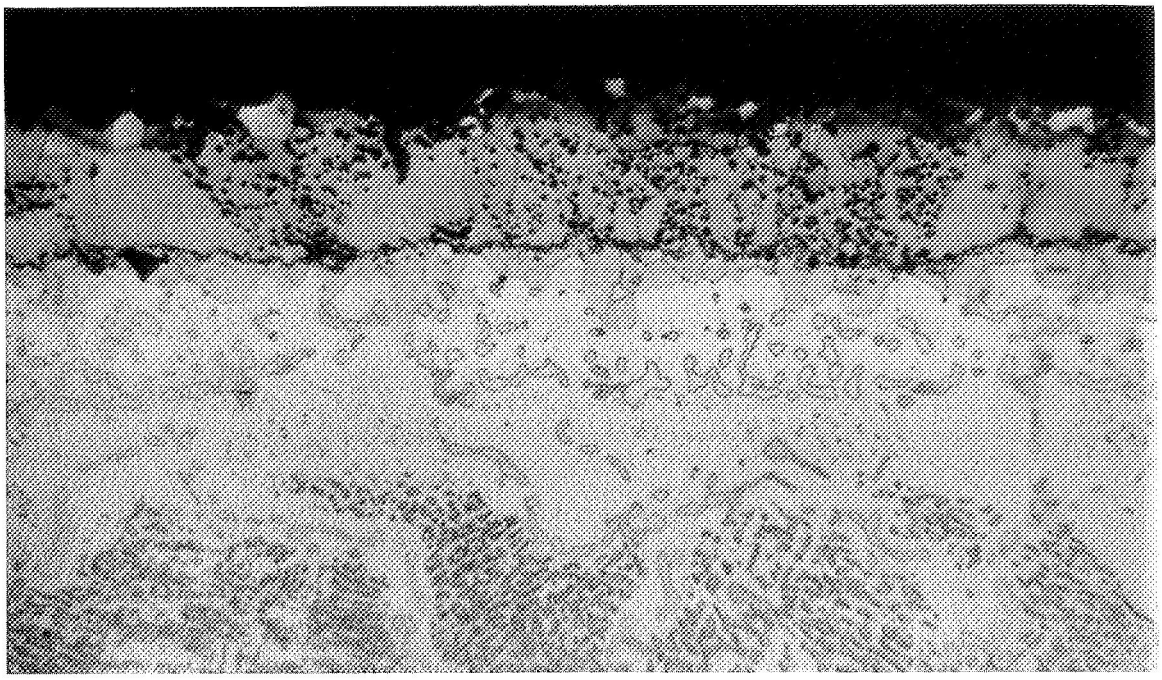

Leading Edge - 0.4 Inch (1.0 cm) Below Tip

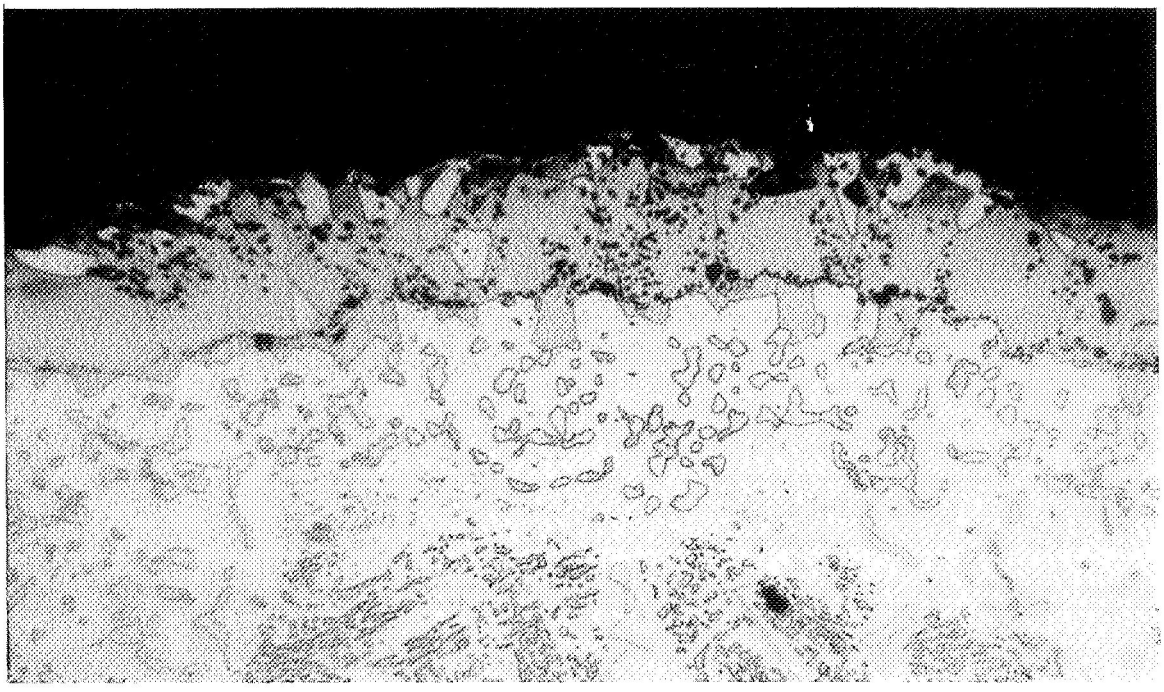

Trailing Edge - 0.4 Inch (1.0 cm) Below Tip

Figure 28. NC11-A-D1 Coating Structure After 503 Hours at 2000°F (1366°K) (Etched 500X).

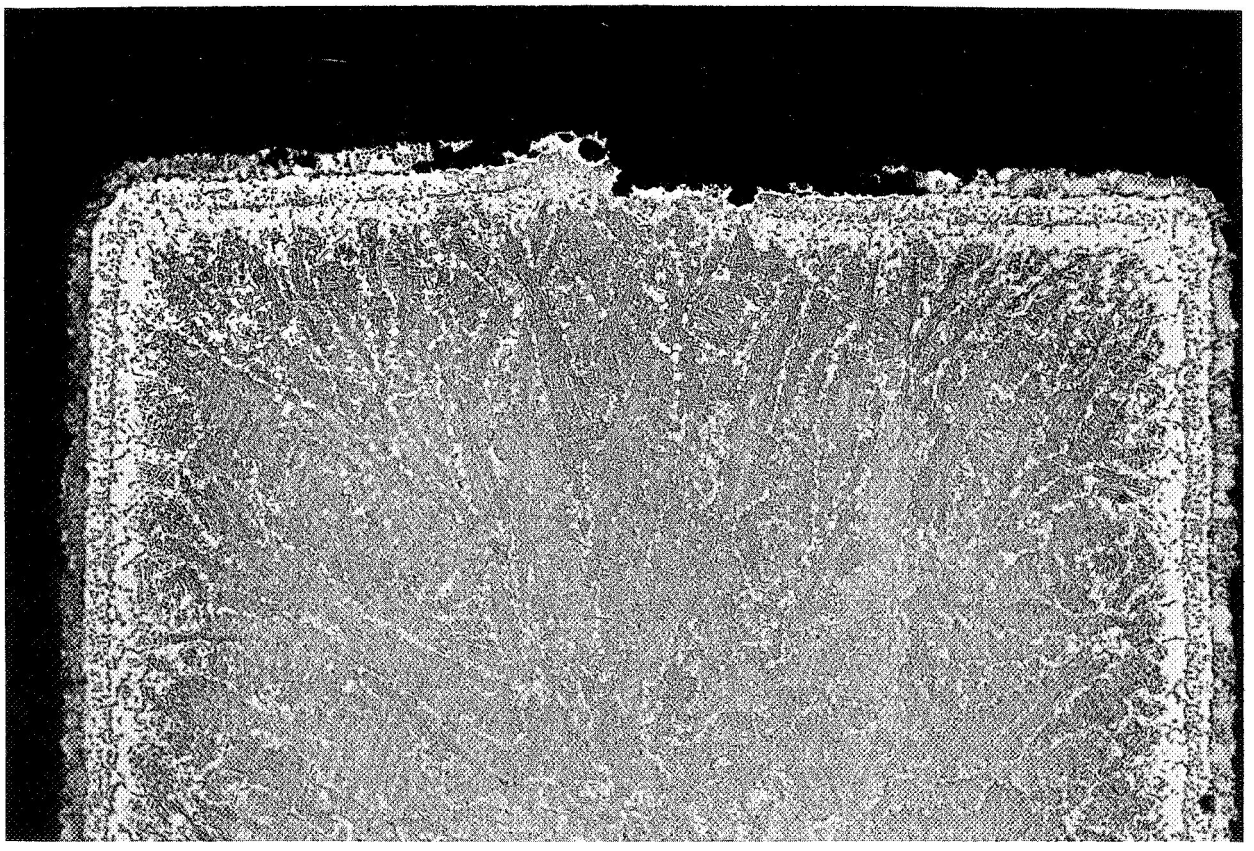

Figure 29. NC11-A-D1 Coating After 503 Hours at 2000°F (1366°K) - Local Coating Attack on Trailing Edge Airfoil Tip - Apparent Casting Imperfection (Etched 100X).

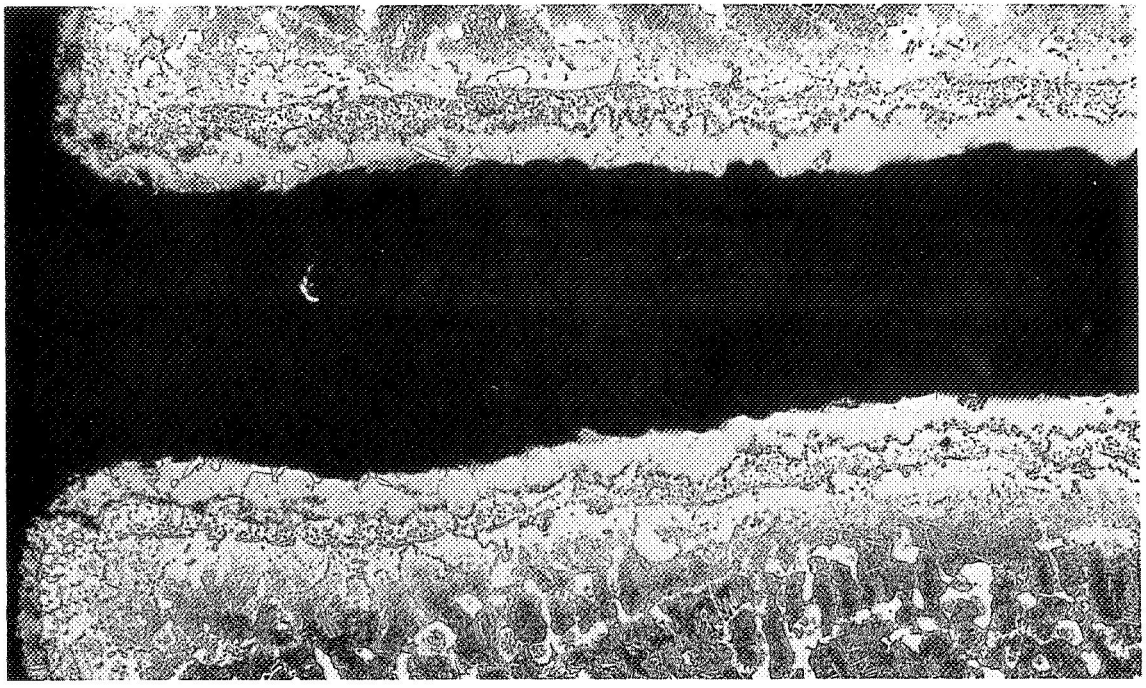

Leading Edge

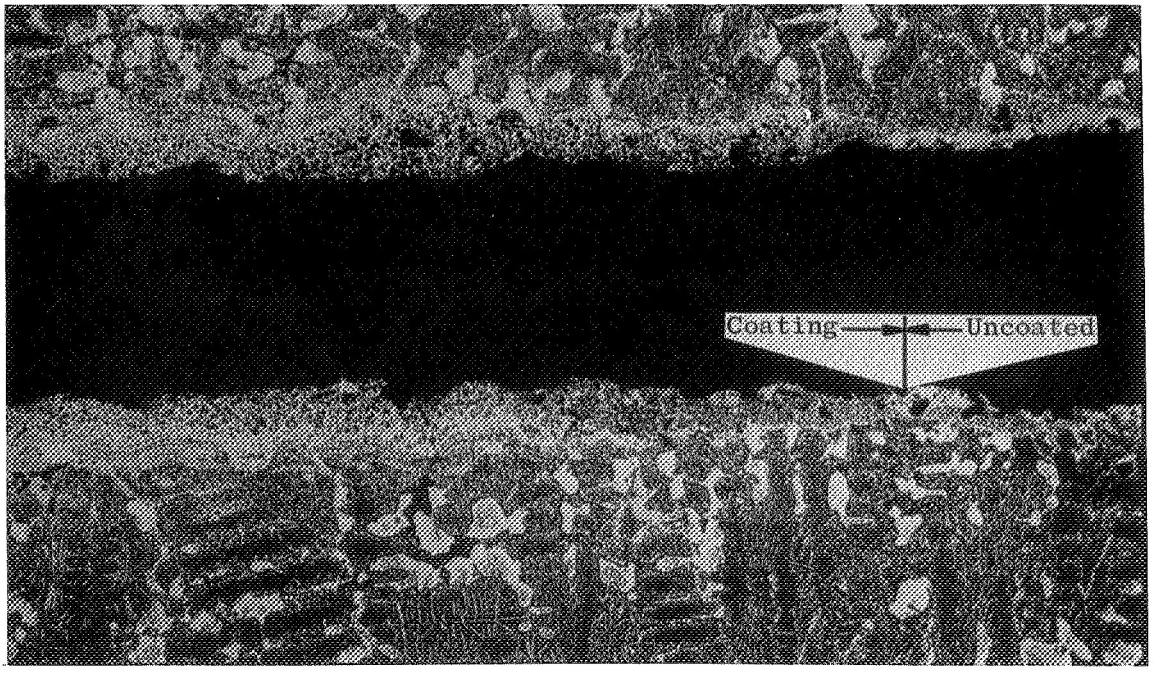

Maximum Depth of Coating Protection - 0.234 Inch (0.594 cm)

Figure 30. NC11-A-D1 Coating in 0.020-Inch (0.05 cm)-Diameter Hole After 503 Hours at 2000°F (1366°K)(Etched 100X).

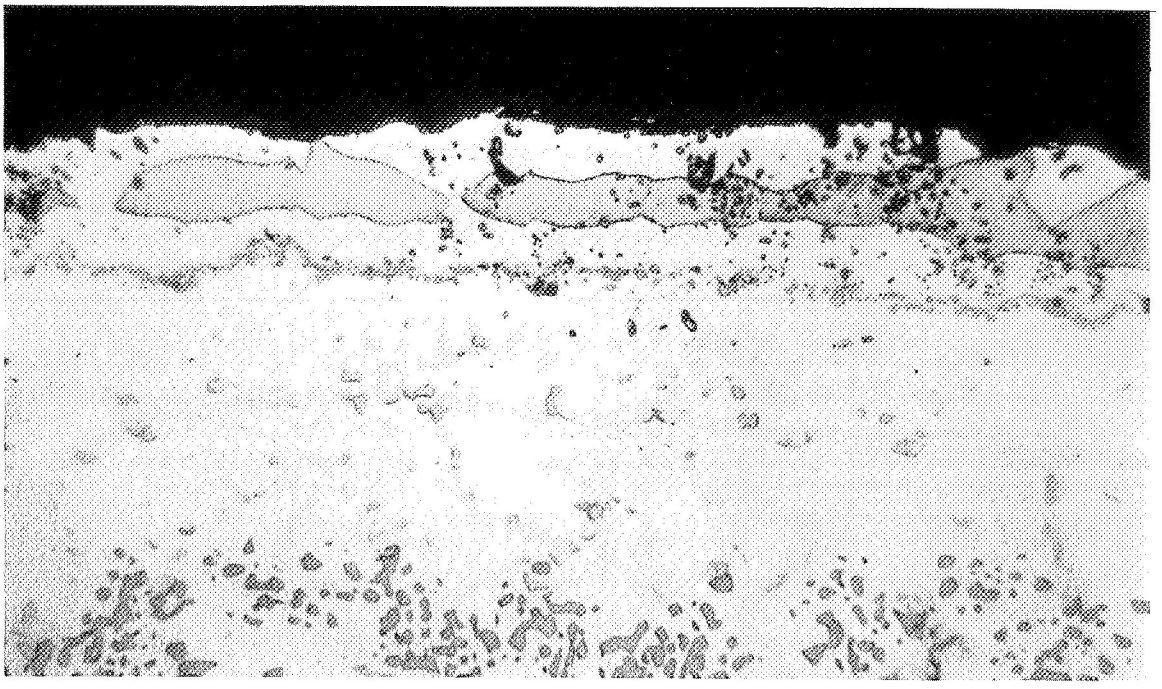

Leading Edge - 0.4 Inch (1.0 cm) Down from Tip

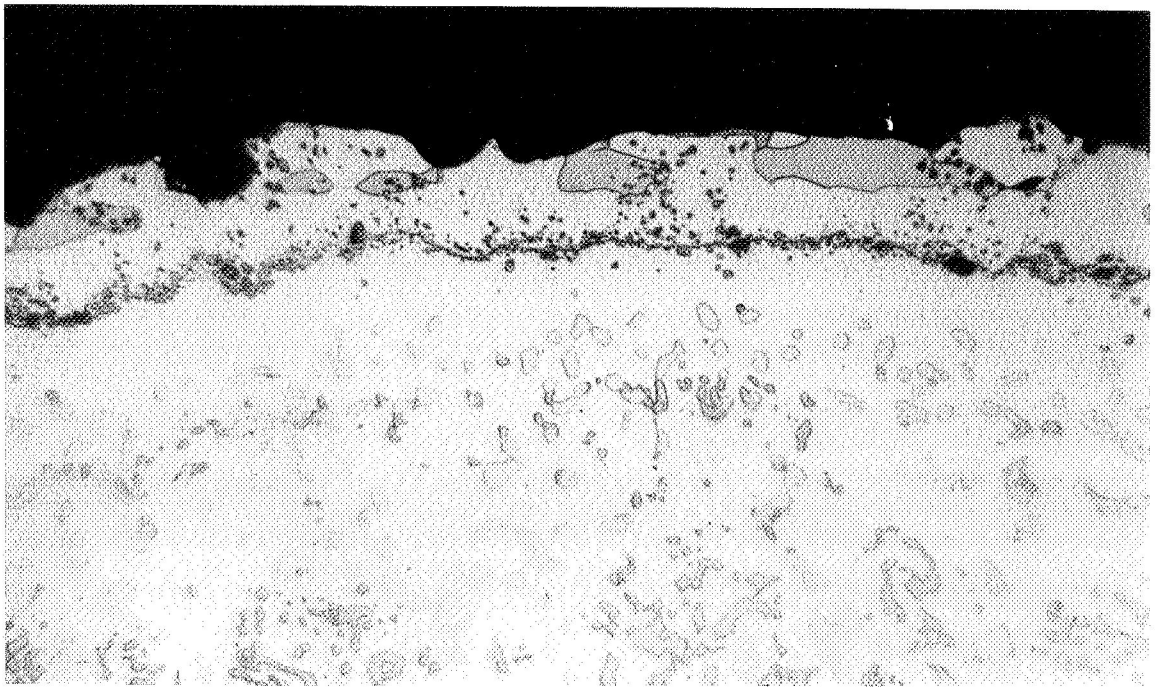

Trailing Edge - 0.4 Inch (1.0 cm) Down from Tip

Figure 31. NC11-A-S1 Coating Structure After 995 Hours at 2000°F (1366°K)(Etched 500X).

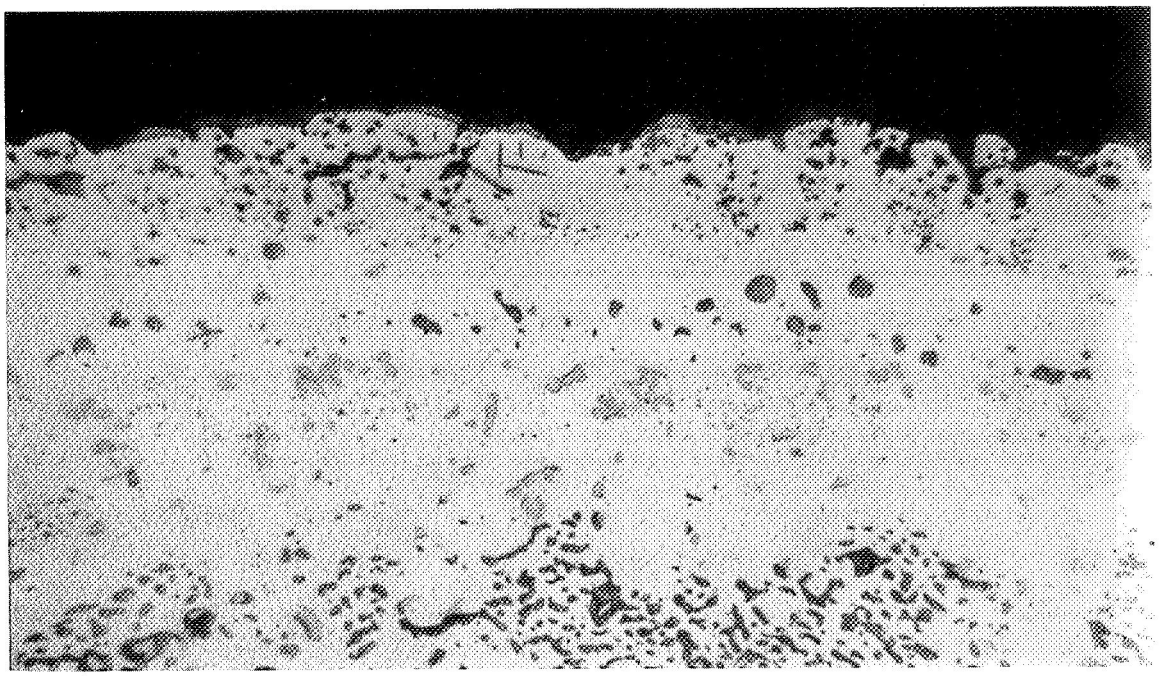

Leading Edge Section - 0.4 Inch (1.0 cm) Down from Tip

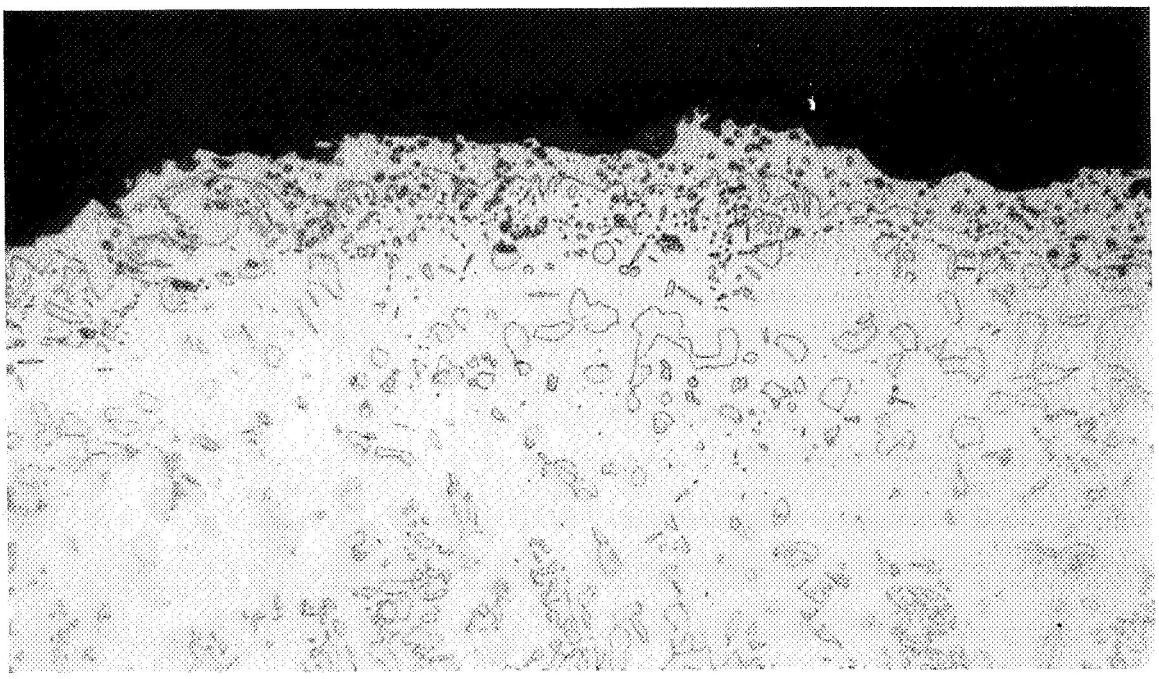

Trailing Edge Section - 0.4 Inch (1.0 cm) Down from Tip

Figure 32. NC11-A-D1 Coating Structure After 1013 Hours at 2000°F (1366°K)(Etched 500X).

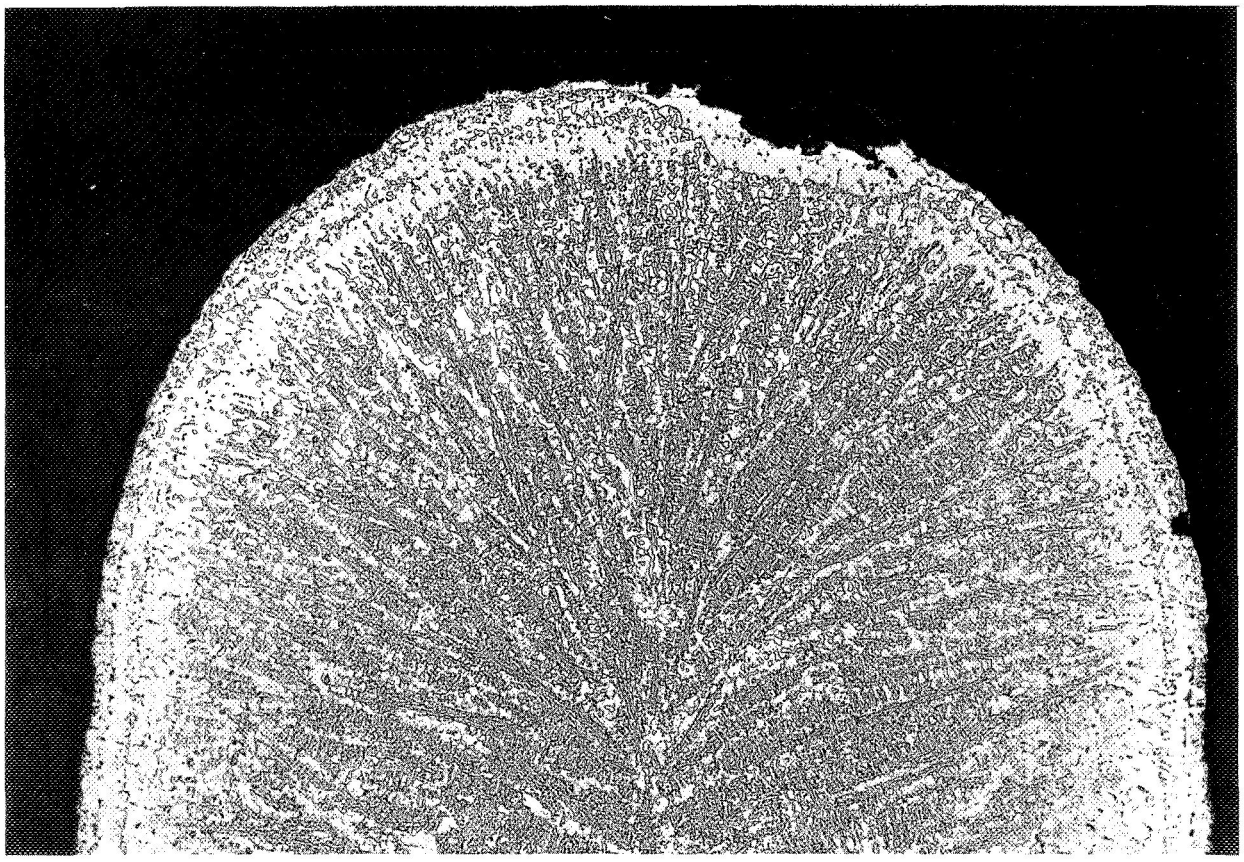

Figure 33. NC11-A-D1 Coating on Trailing Edge After 1013 Hours at 2000°F (1366°K) Showing Local Oxidation Attack (Etched 100X).

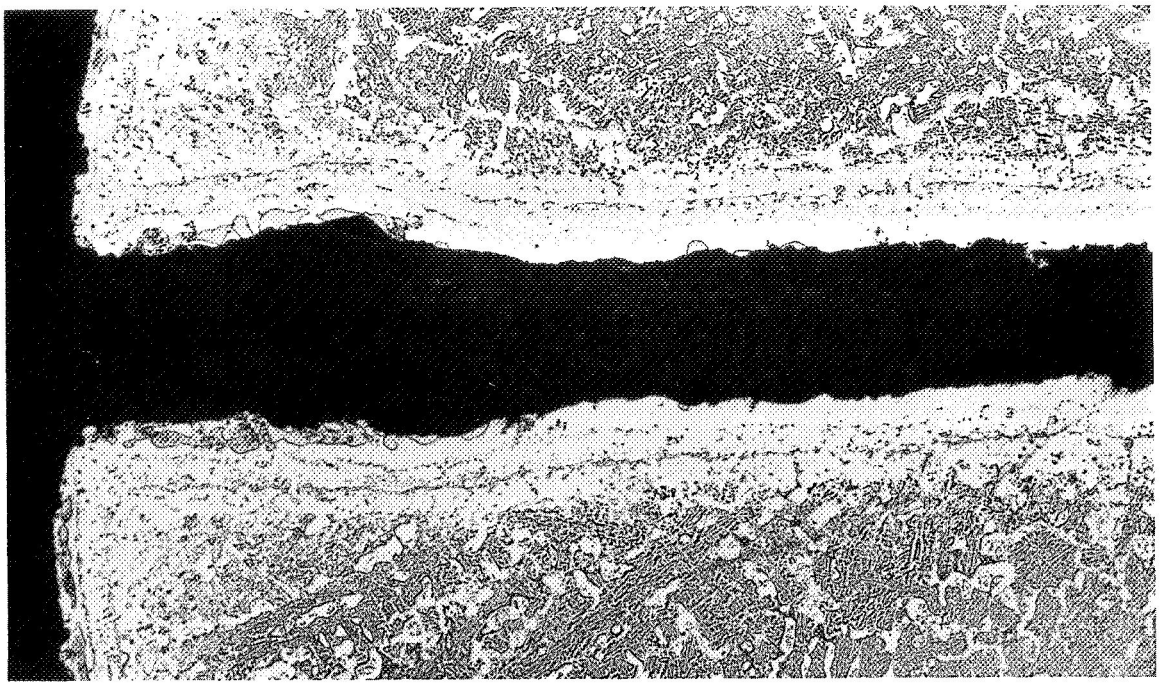

Leading Edge

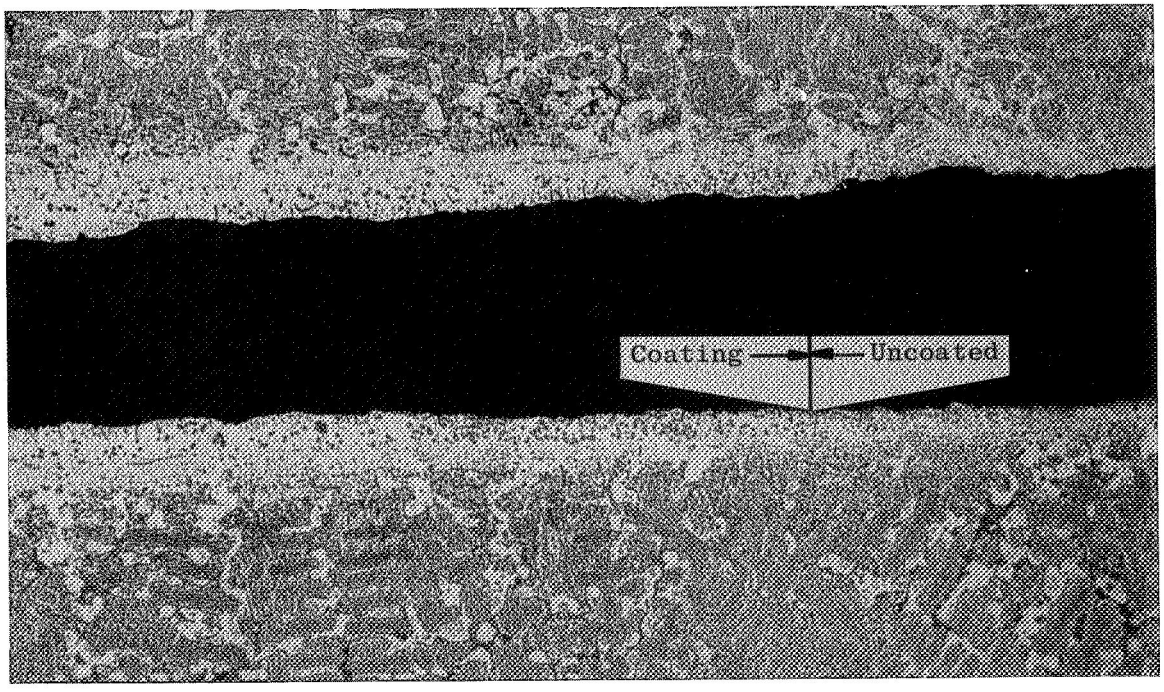

Maximum Depth of Coating Protection - 0.168 Inch (0.384 cm)

Figure 34. NC11-A-S1 Coating in 0.012-Inch (0.03 cm)-Diameter Hole After 995 Hours at 2000°F (1366°K)(Etched 100X).

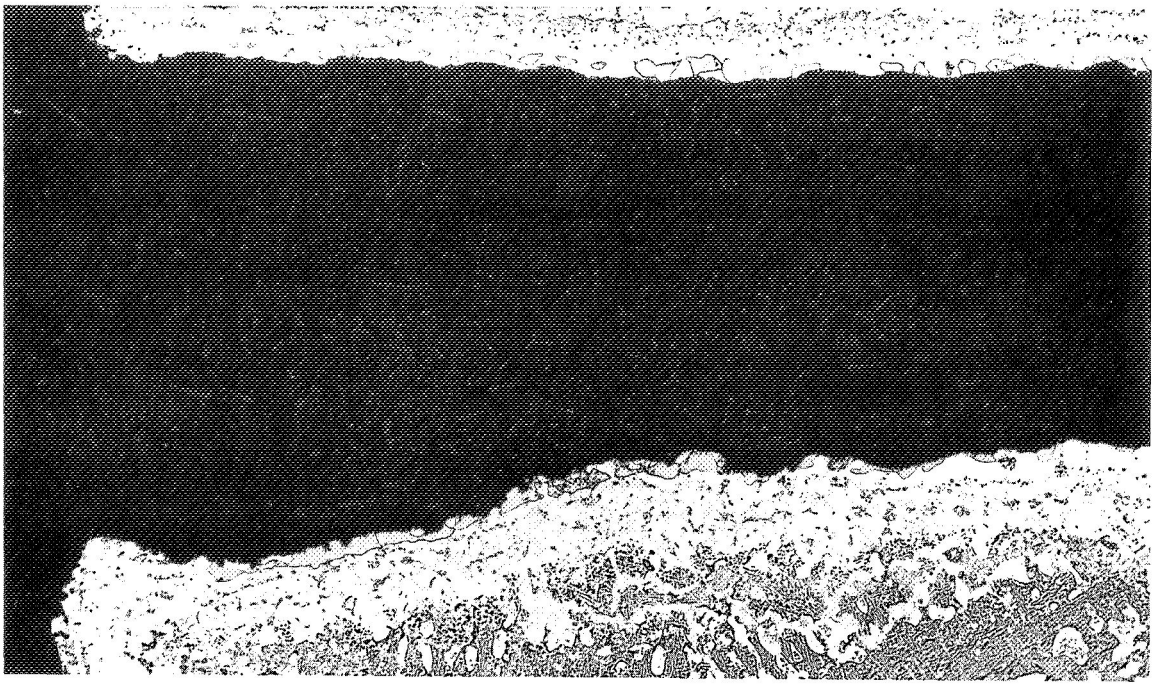

Leading Edge

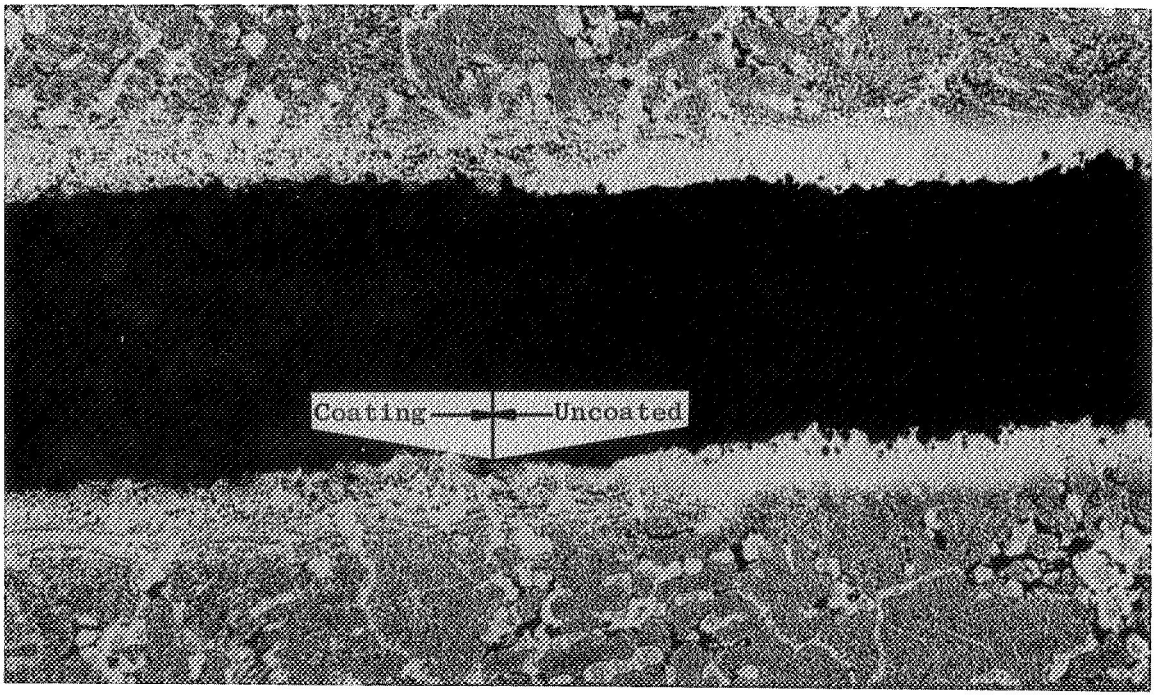

Maximum Depth of Coating Protection - 0.200 Inch (0.51 cm)

Figure 35. NC11-A-S1 Coating in 0.020-Inch (0.051 cm)-Diameter Hole After 995 Hours at 2000°F (1366°K) (Etched 100X).

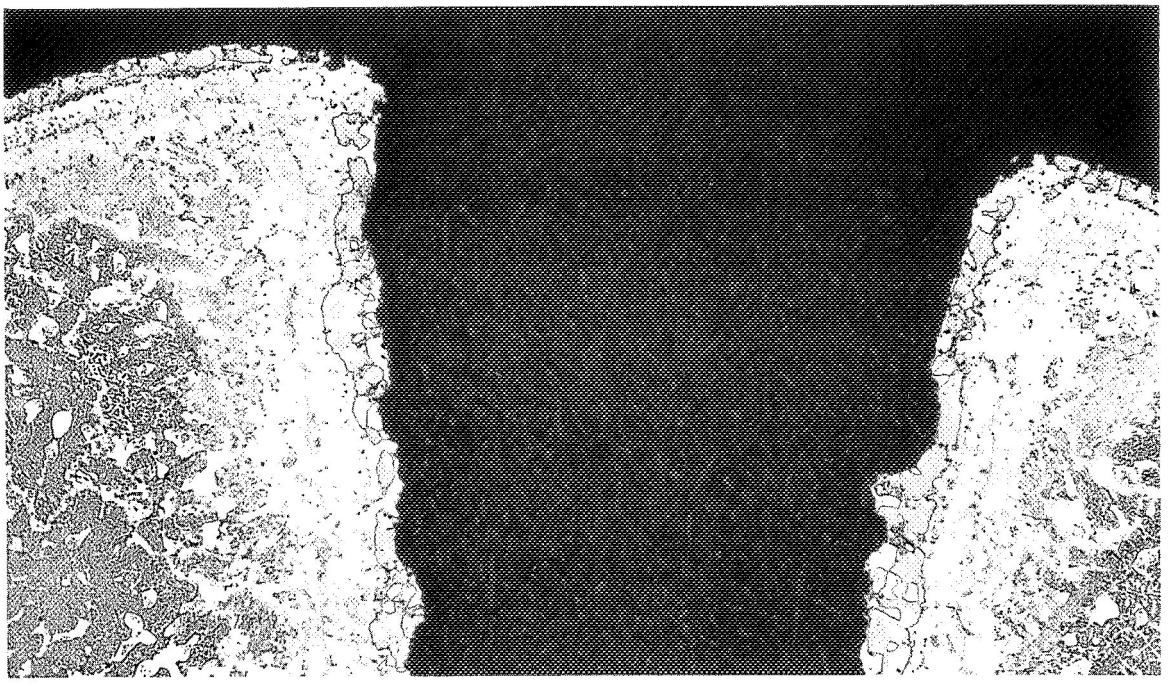

Leading Edge (Note: Polished Slightly Off Center)

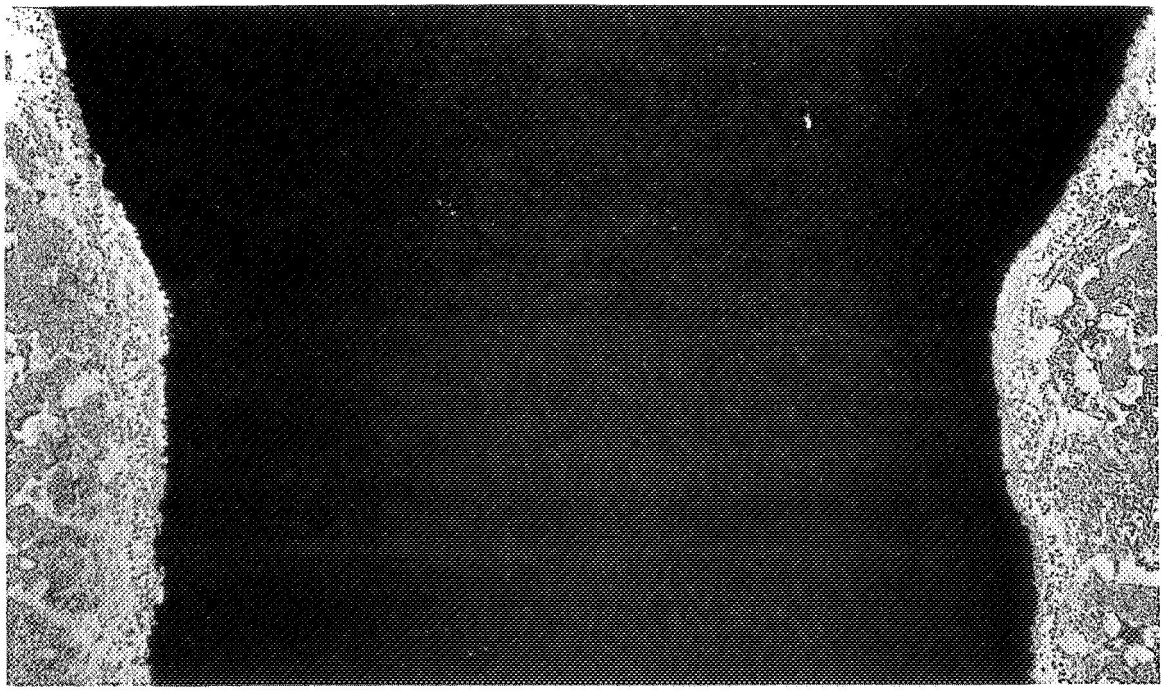

Maximum Depth of Coating Protection - 0.250 Inch (0.63 cm)

Figure 36. NCl1-A-Sl Coating in 0.040-Inch (0.10 cm)-Diameter Hole After 995 Hours at 2000°F (1366°K)(Etched 100X).

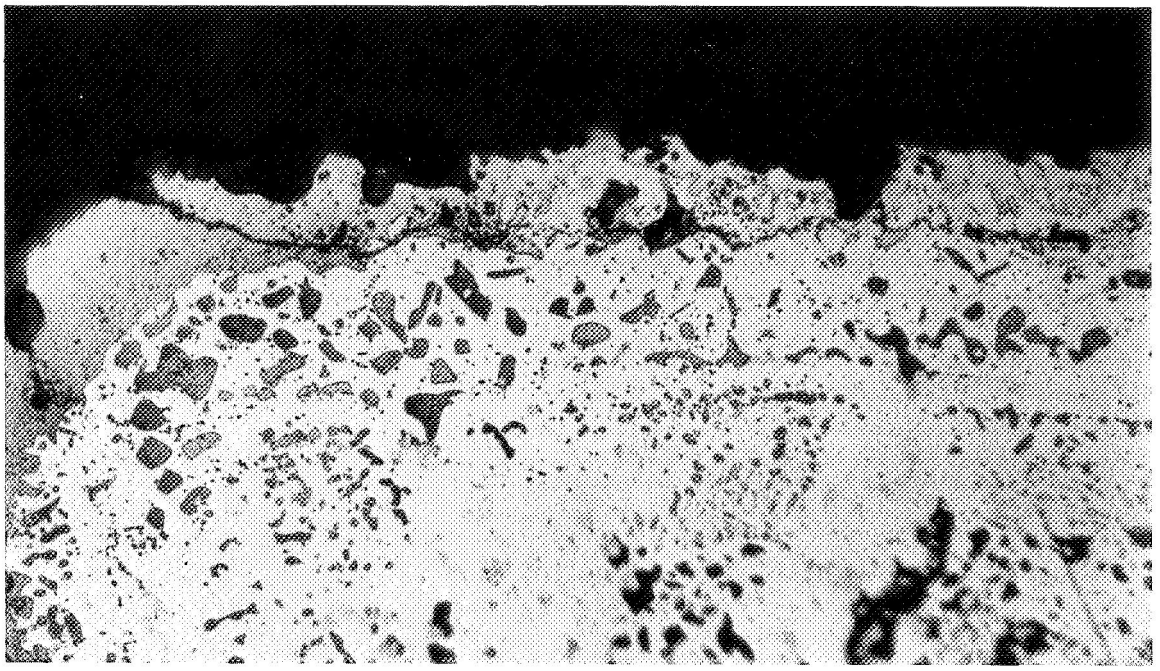

Leading Edge

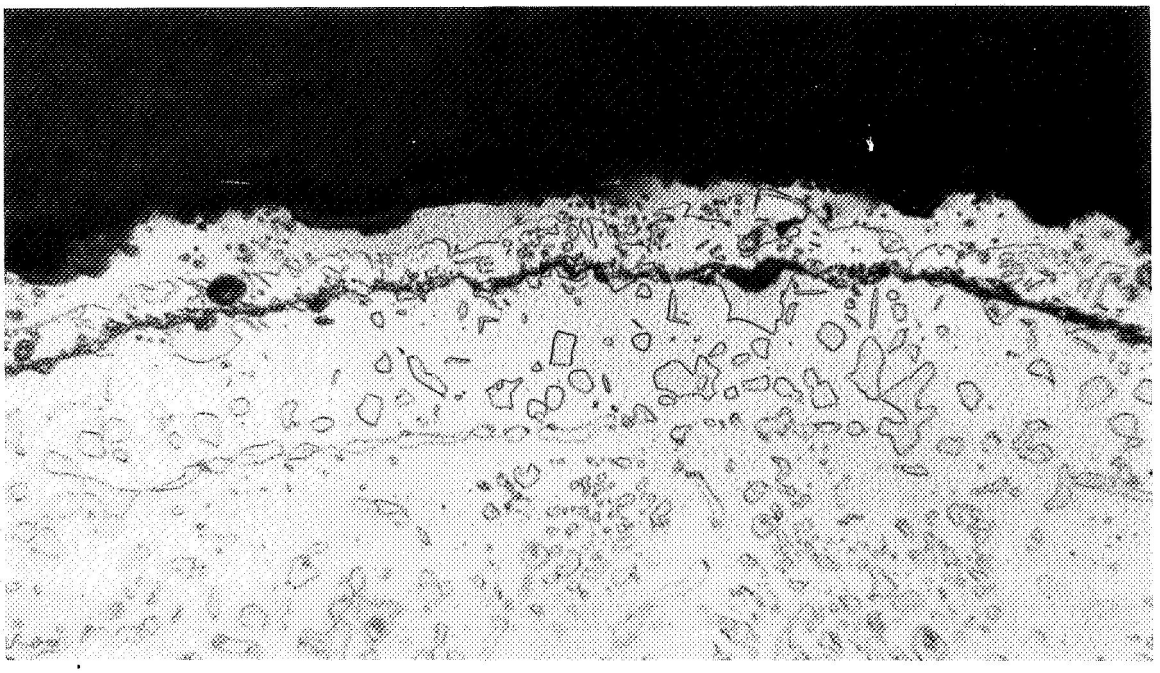

Trailing Edge

Figure 37. NC11-A-S1 Coating Structure After 1483 Hours at 2000°F (1366°K) Section Through Area of 0.012-Inch (0.030 cm)-Diameter Hole (Etched 500X).

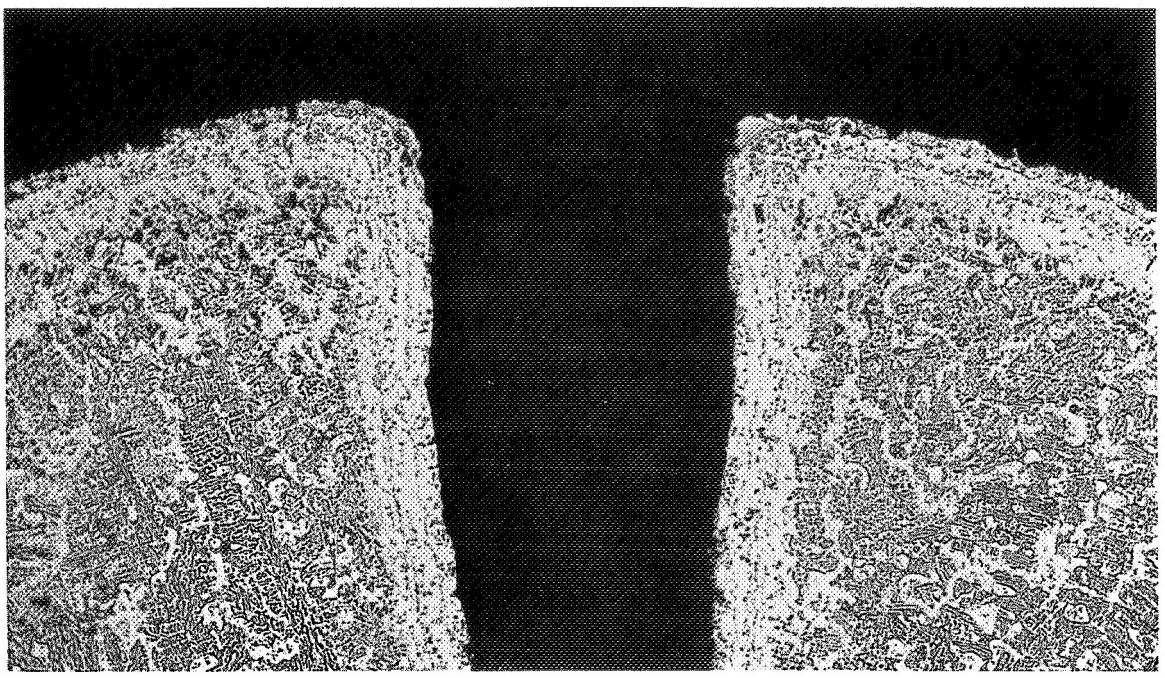

0.012-Inch (0.030 cm) Hole

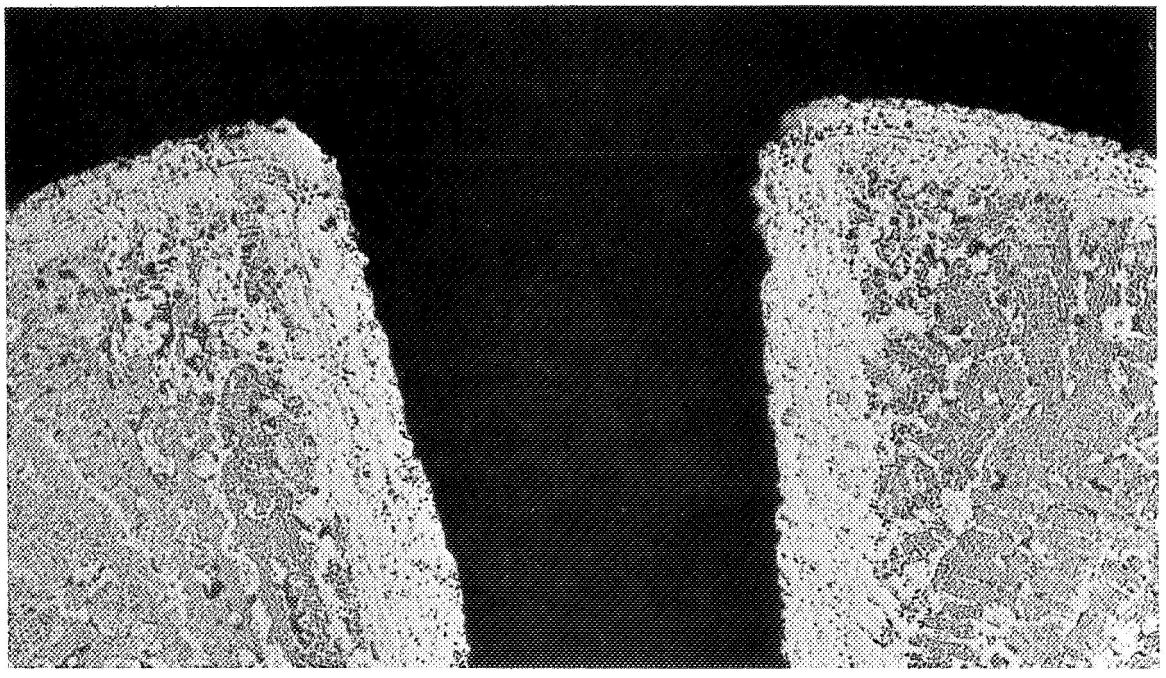

0.020-Inch (0.051 cm) Hole

Figure 38. NC11-A-S1 Coating at Leading Edge of EDM-Drilled Holes After 1483 Hours at 2000°F (1366°K)(100X).

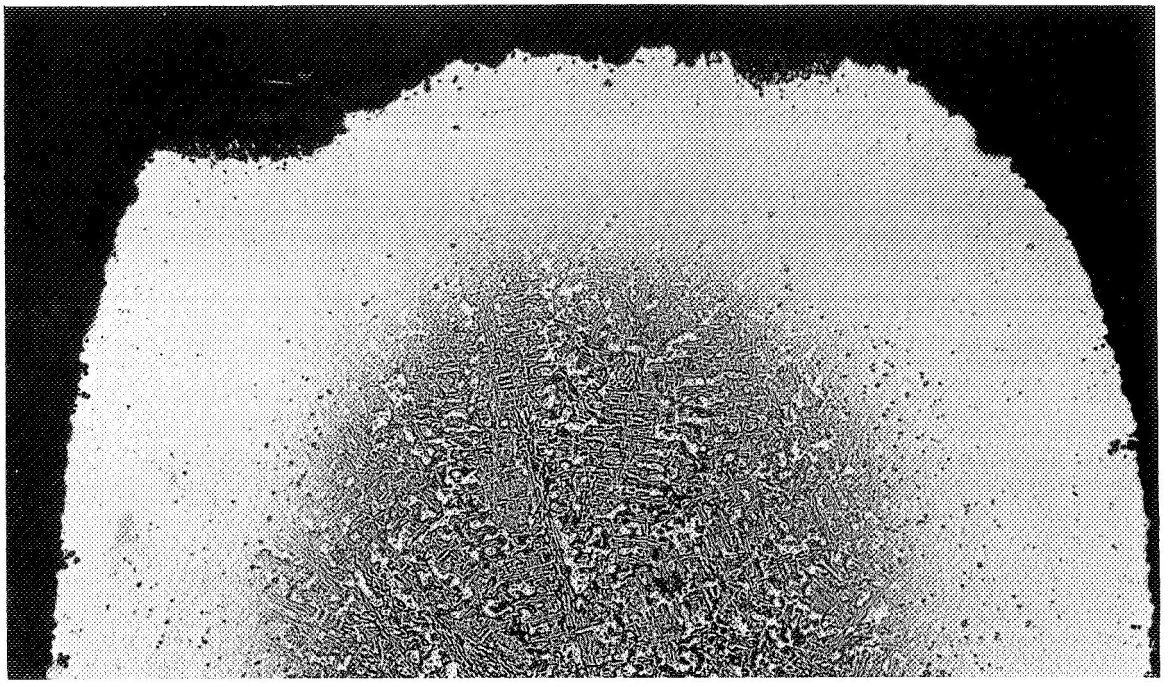

Top Section - 0.4 Inch (1.0 cm) Down from Tip

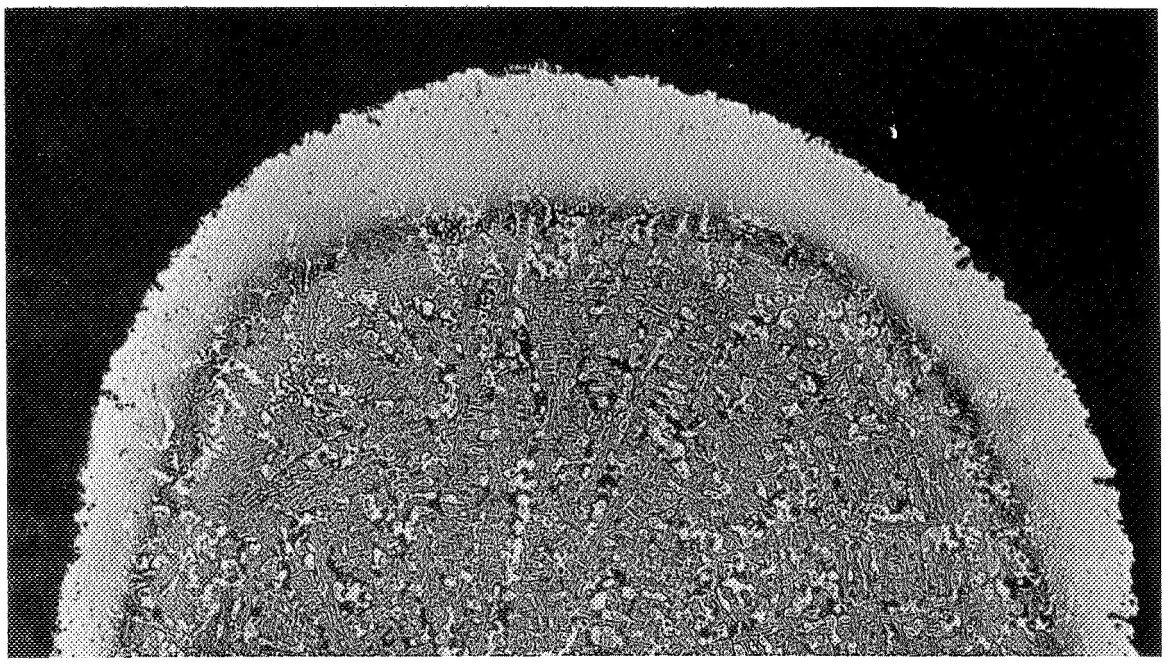

Bottom Section - 1.5 Inches (3.8 cm) Down from Tip

Figure 39. Uncoated NASA VIA Alloy Paddle After 1483 Hours at 2000°F (1366°K) - Trailing Edge. (Note: Temperature Measured at Top of Leading Edge.)(Etched 100X).

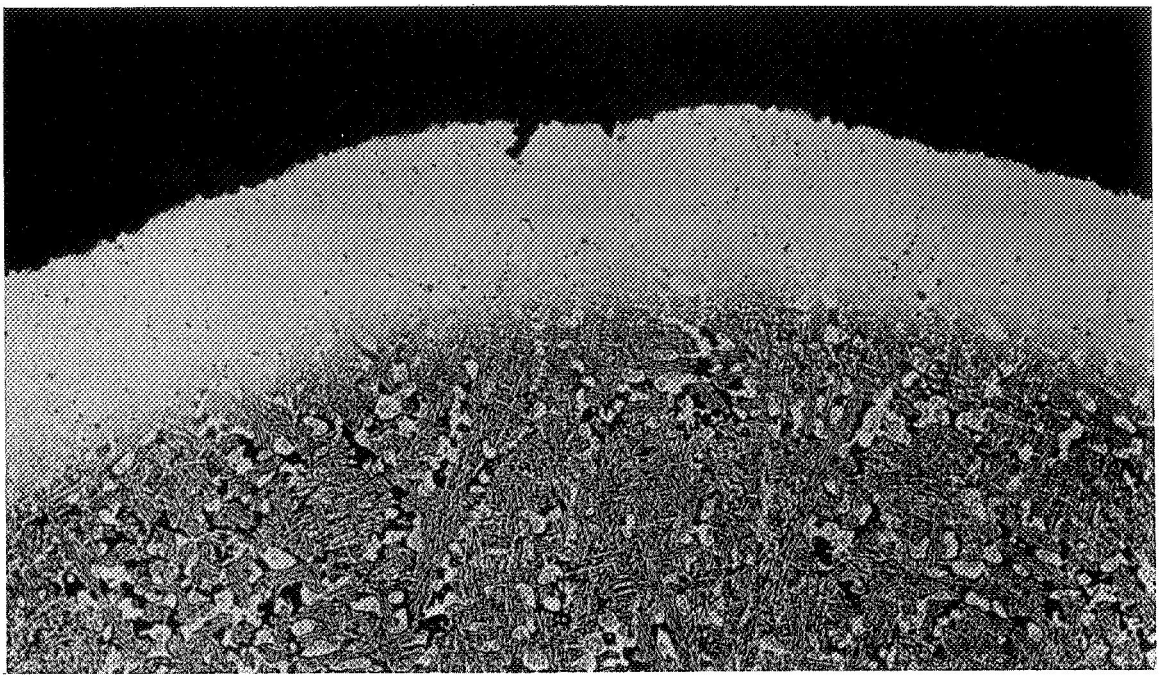

Top Section - 0.4 Inch (1.02 cm) Down from Tip

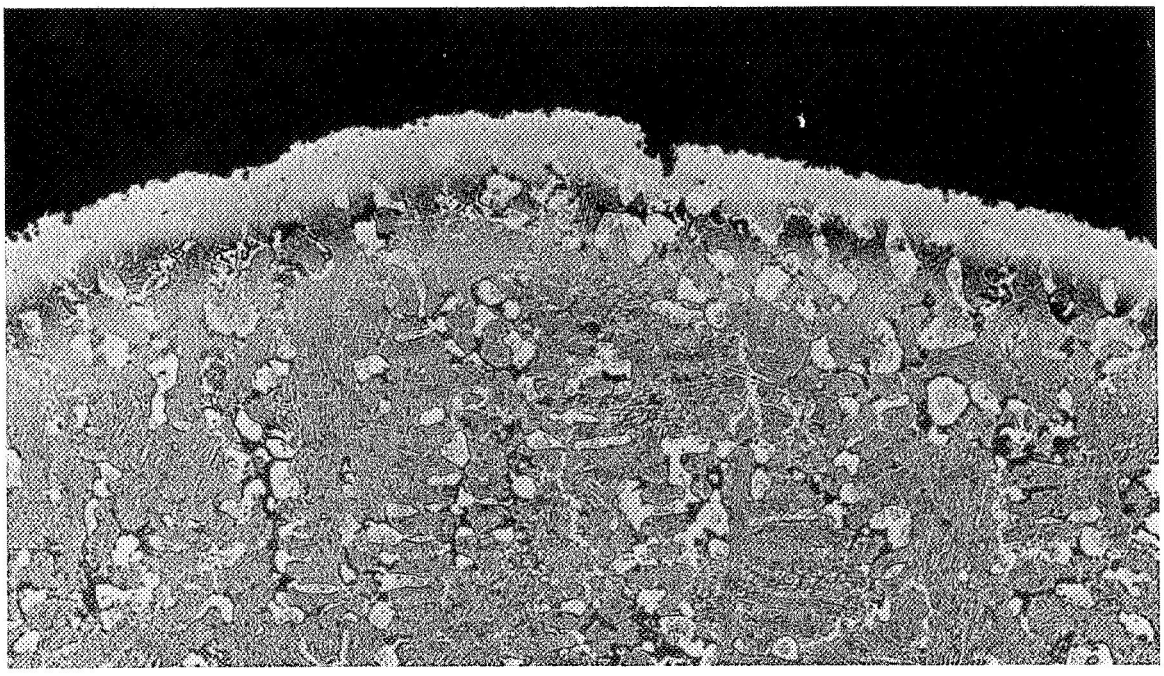

Bottom Section - 1.5 Inches (3.8 cm) Down from Tip

Figure 40. Uncoated NASA VIA Alloy Paddle After 1483 Hours at 2000°F (1366°K) - Leading Edge. (Note: Temperature Measured at Top Section.)(Etched 100X).

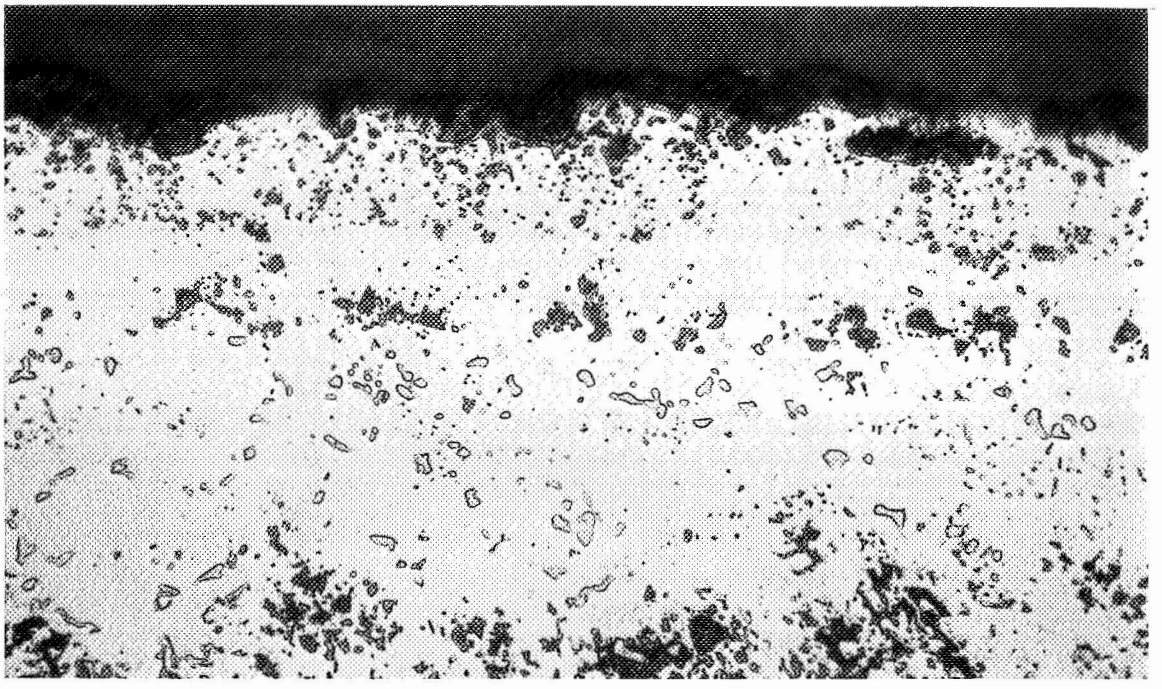

Leading Edge

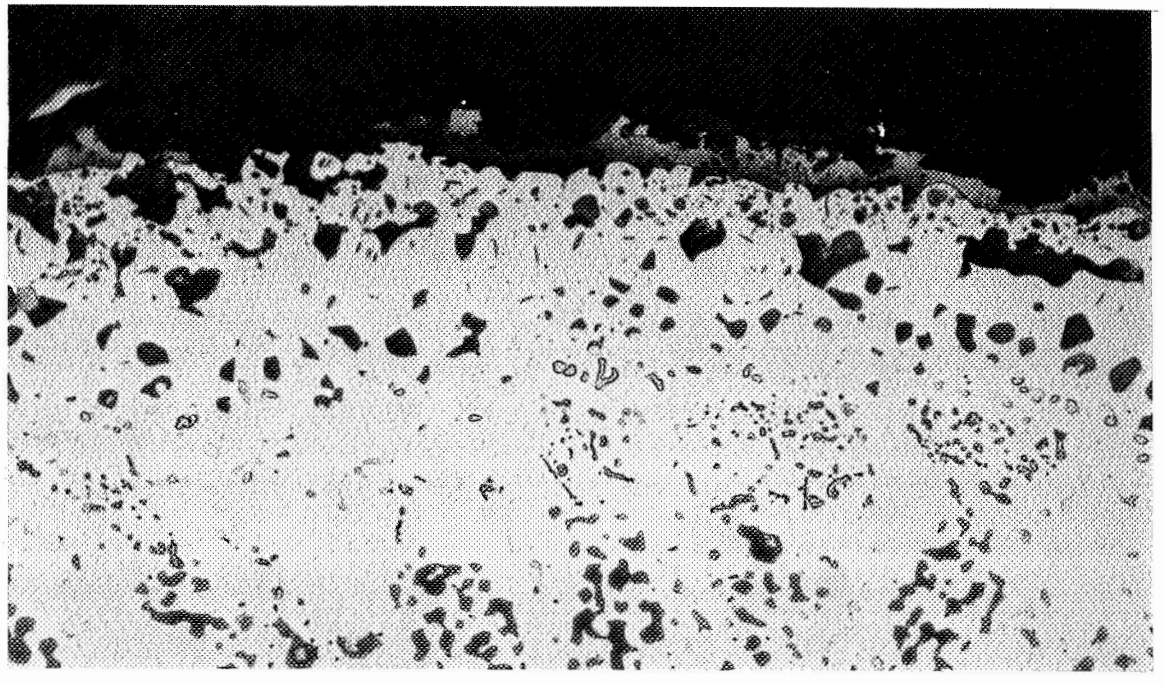

Trailing Edge

Figure 41. NC11-A-D1 Coating After 1495 Hours at 2000°F (1366°K). Section Through 0.012-Inch (0.03 cm)-Diameter Hole (Etched 500X).

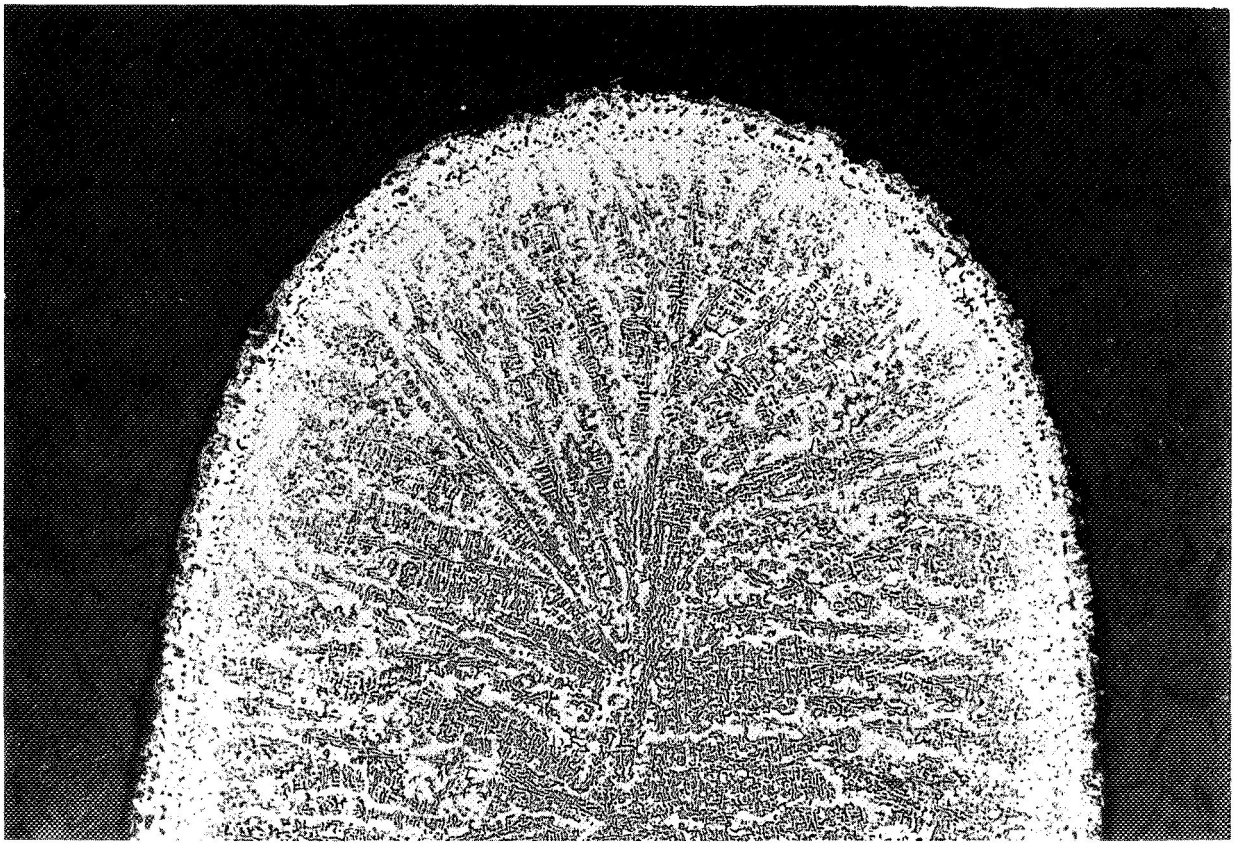

Figure 42. Trailing Edge of NC11-A-D1 Coated Specimen, 0.4 Inch (1.0 cm) Below Tip After 1495 Hours at 2000°F (1366°K) (Etched 100X).

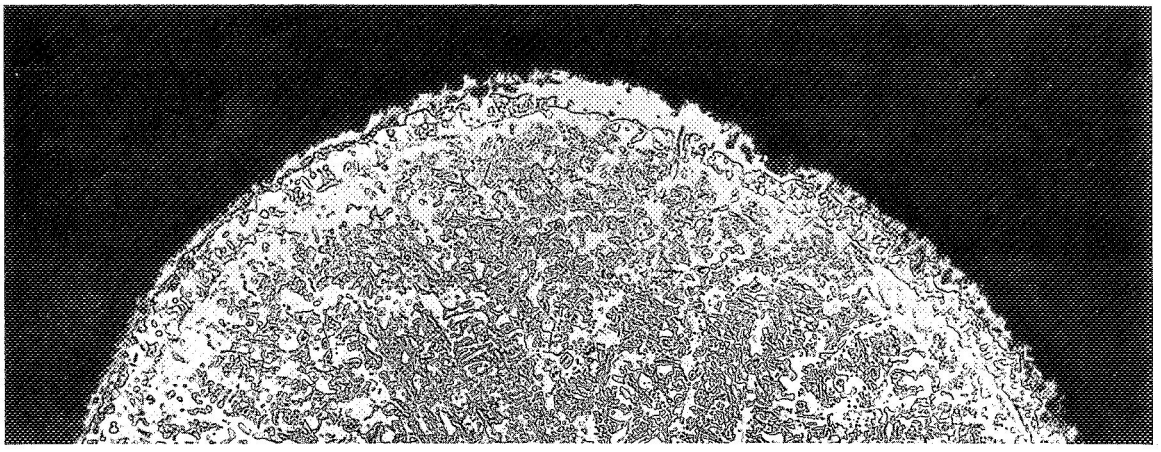

0.4 Inch (1.0 cm) Below Tip

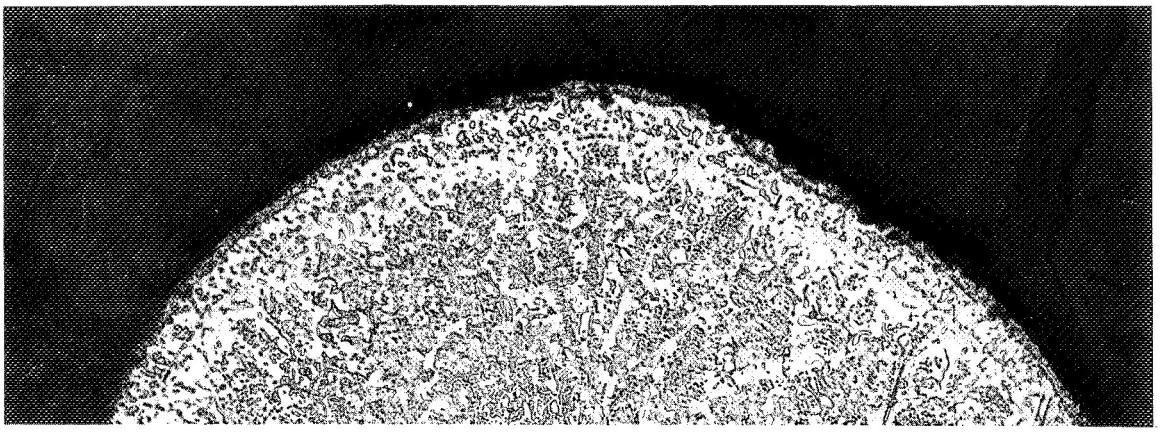

1.0 Inch (2.54 cm) Below Tip

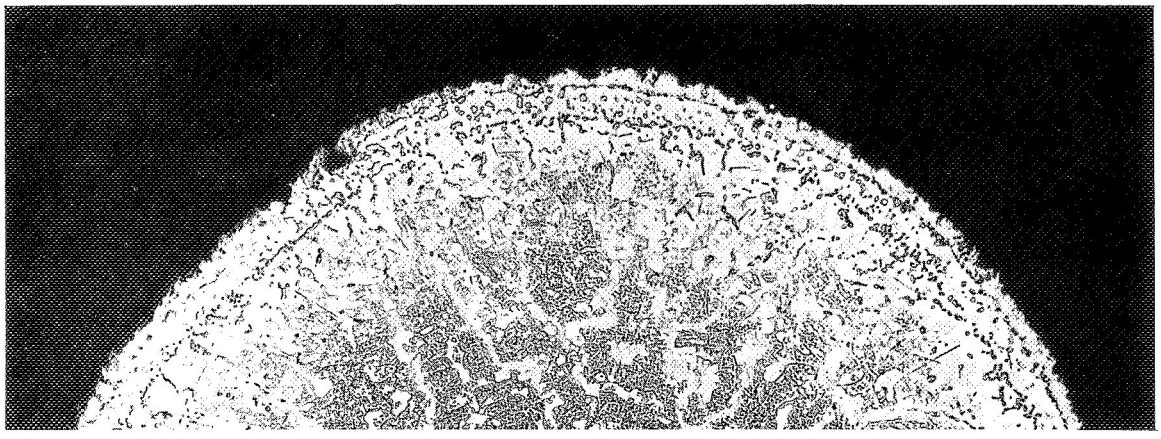

1.5 Inches (3.8 cm) Below Tip

Figure 43. NC11-A-S1 Coating on Trailing Edge Section After 2000°F (1366°K)/2000 Hours; Burner Rig No. 5 (Etched 100X).

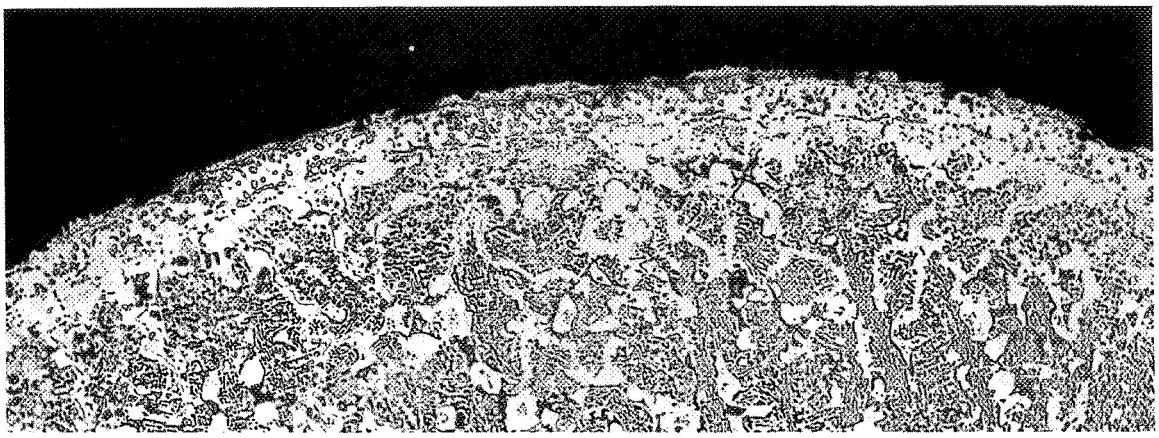

0.4 Inch (1.02 cm) Below Tip

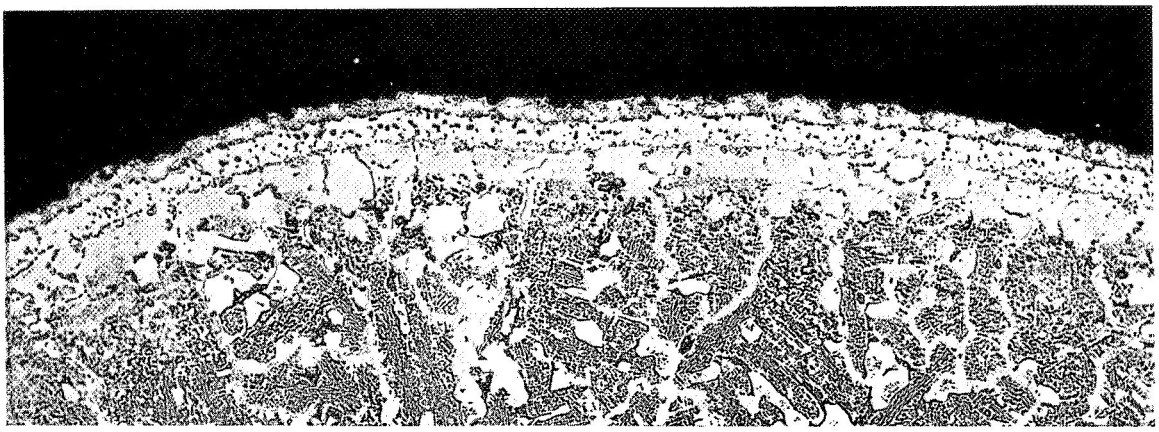

1.0 Inch (2.54) Below Tip

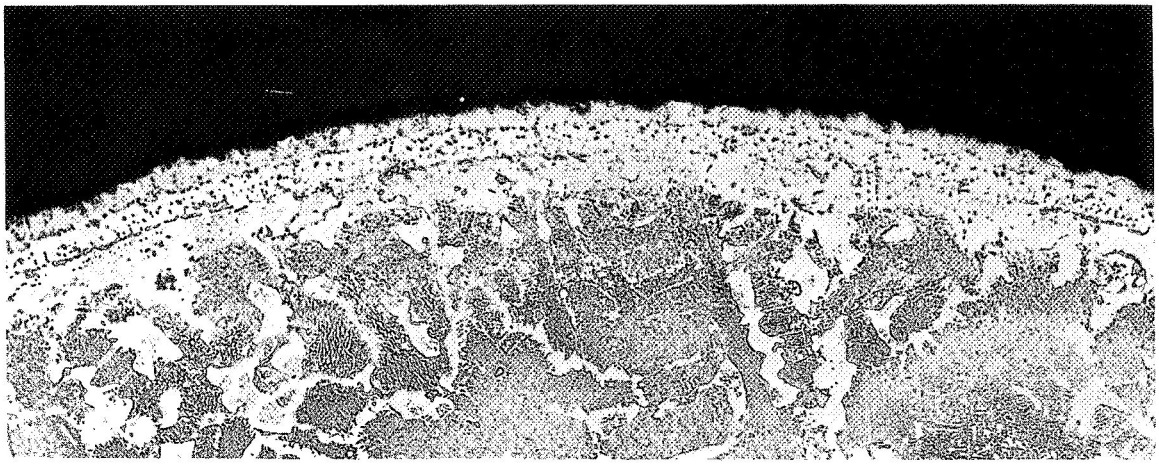

1.5 Inches (3.8 cm) Below Tip

Figure 44. NC11-A-S1 Coating on Leading Edge Sections After 2000°F (1366°K)/2000 Hours; Burner Rig No. 5 (Etched 100X).

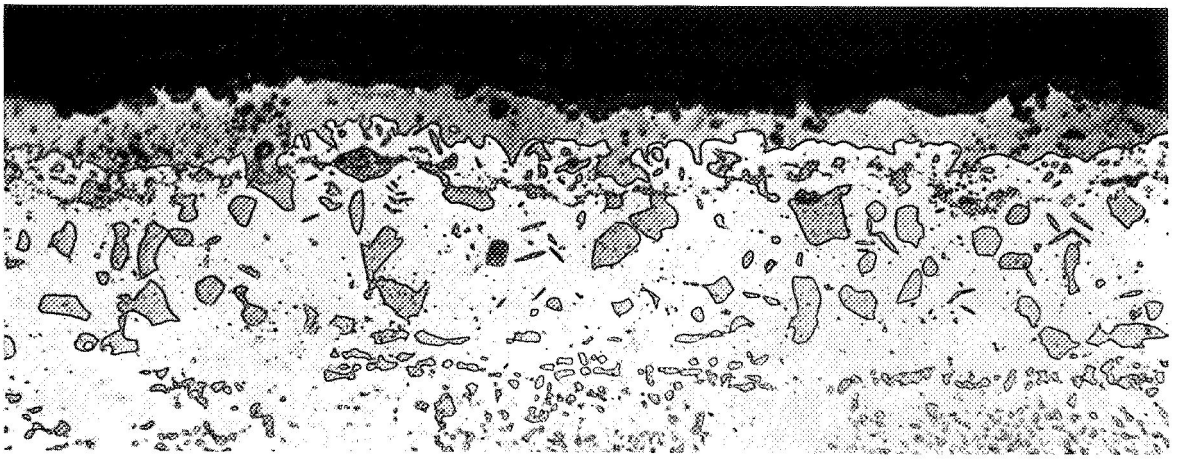

Leading Edge

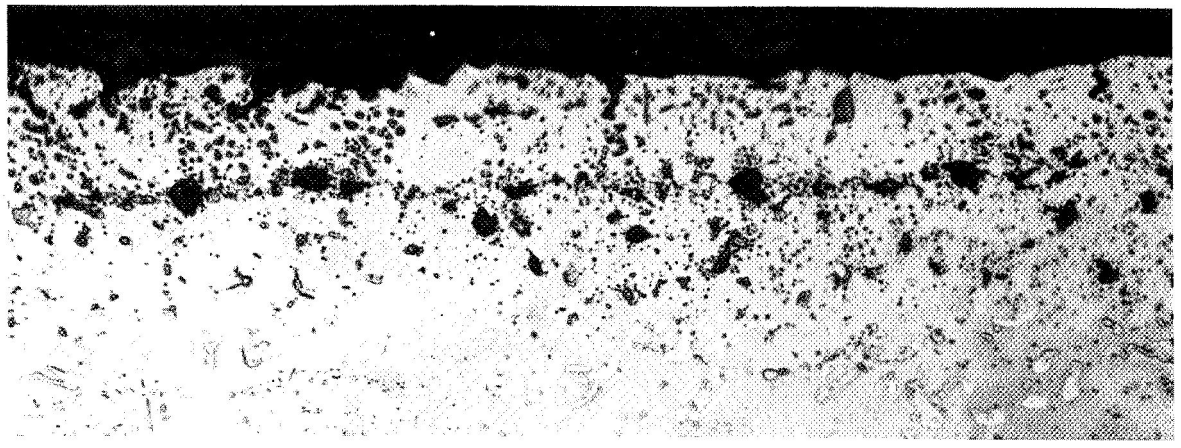

Center - Convex

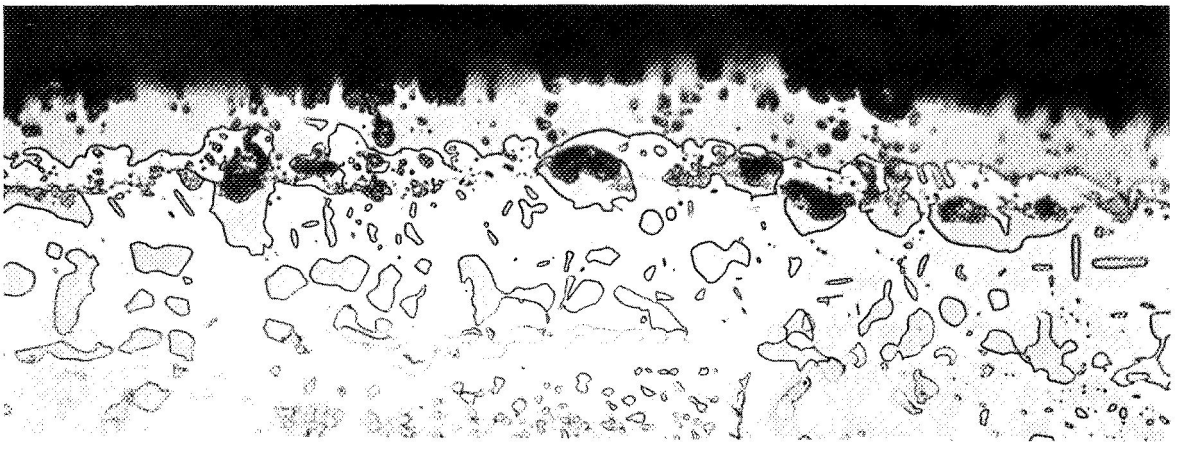

Trailing Edge

Figure 45. NC11-A-S1 Coating at 0.4 Inch (1.0 cm) Below Tip After 2000°F (1366°K)/2000-Hour Burner Rig Test (Etched 500X).

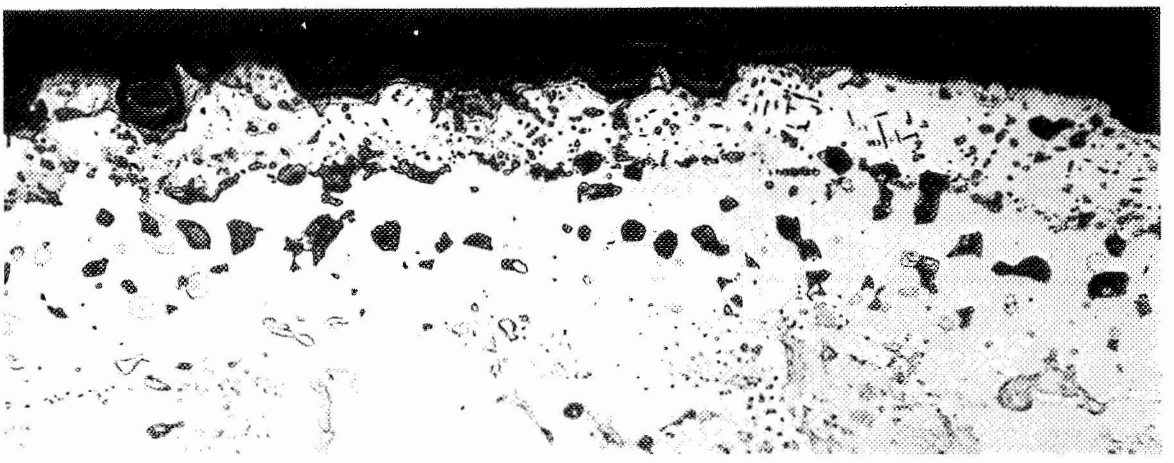

Leading Edge

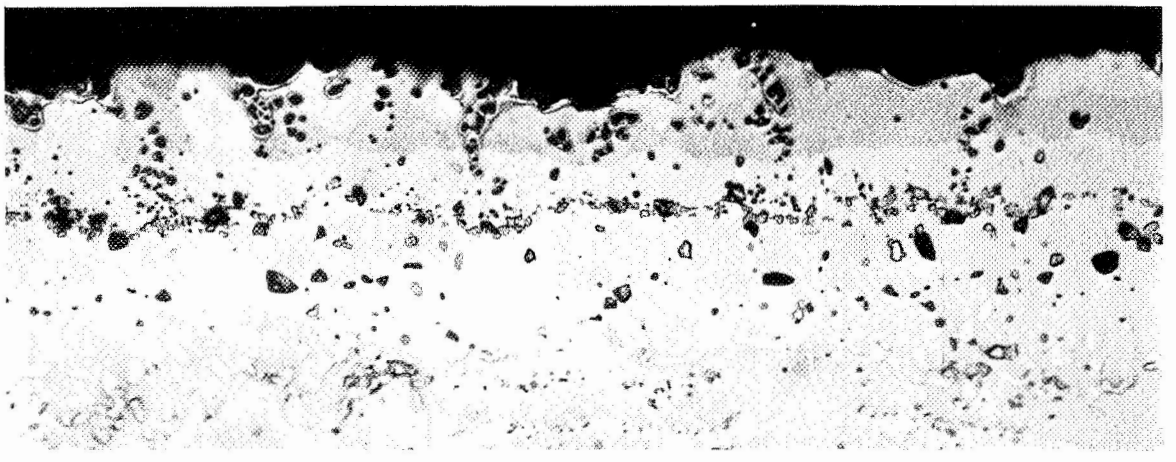

Center - Convex

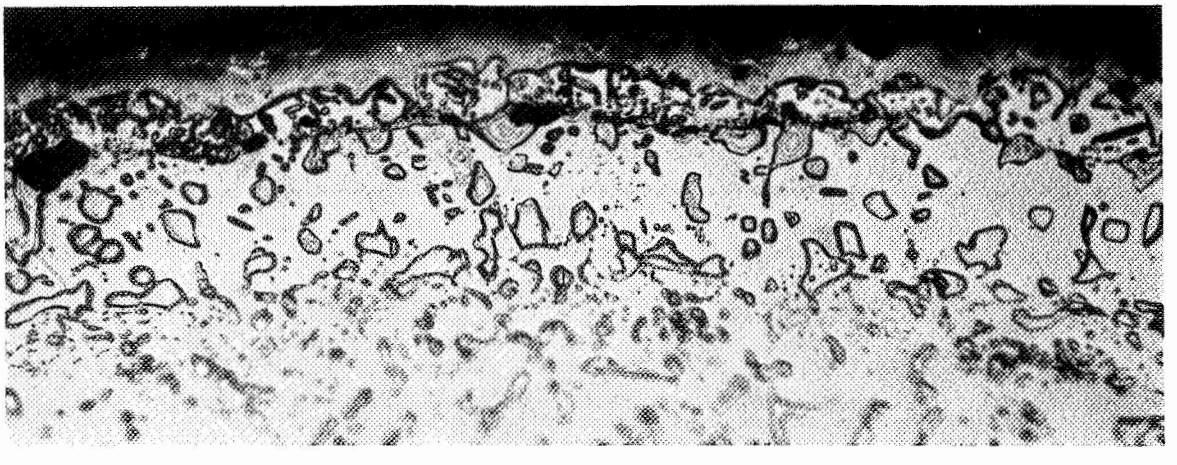

Trailing Edge

Figure 46. NC11-A-S1 Coating at 1.0 Inch (2.54 cm) Below Tip After 2000°F (1366°K)/2000-Hour Burner Rig Test (Etched 500X).

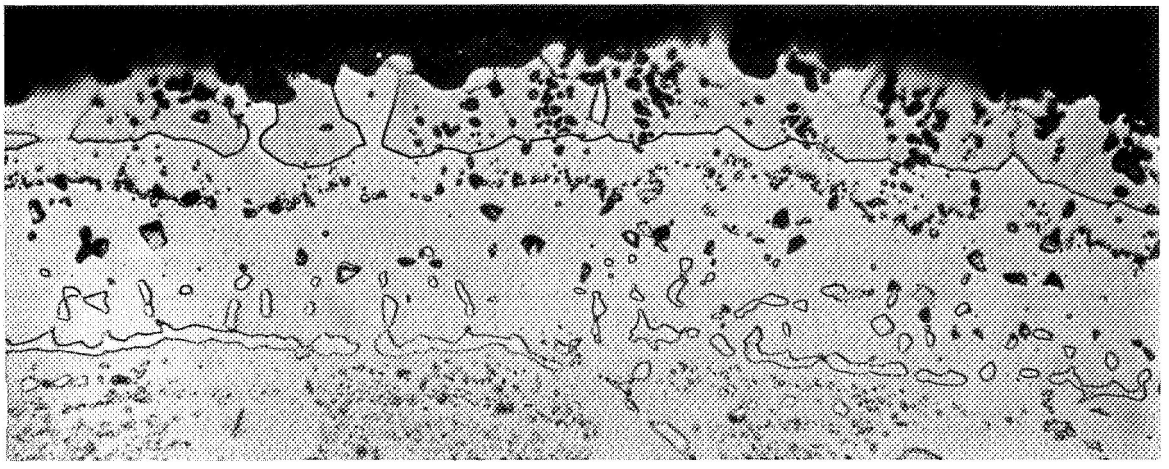

Leading Edge

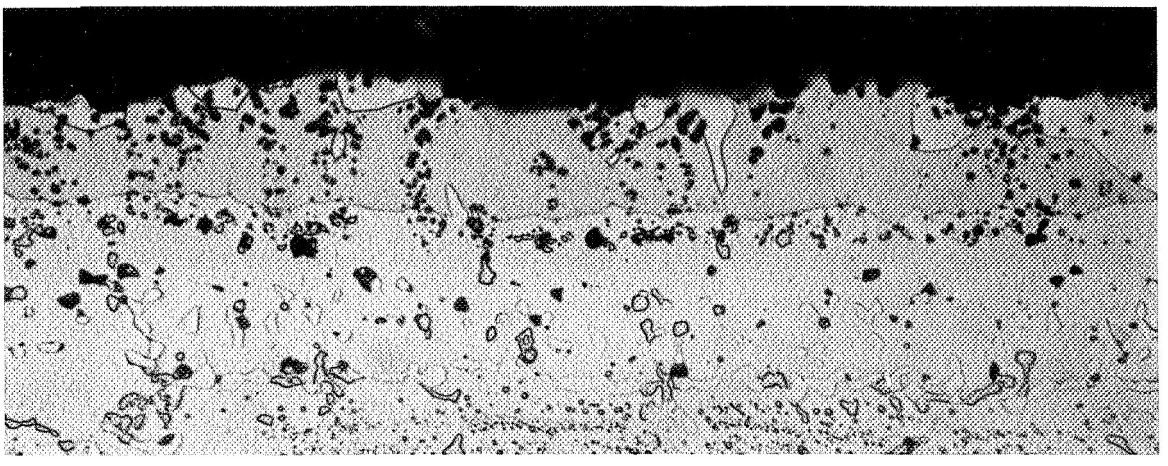

Center - Convex

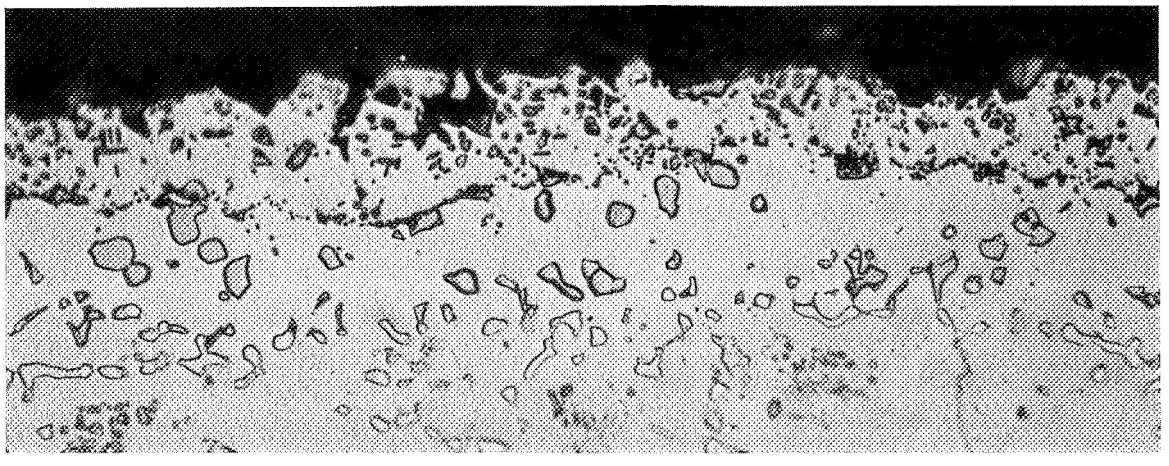

Trailing Edge

Figure 47. NC11-A-Sl Coating at 1.5 Inches (3.8 cm) Below Tip After 2000°F (1366°K)/2000-Hour Burner Rig Test (Etched 500X).

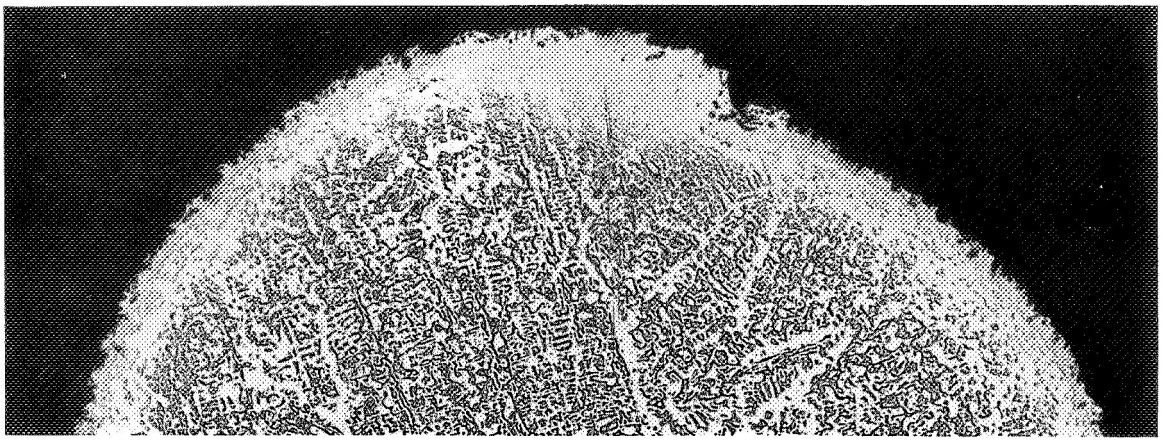

0.4 Inch (1.0 cm) Below Tip

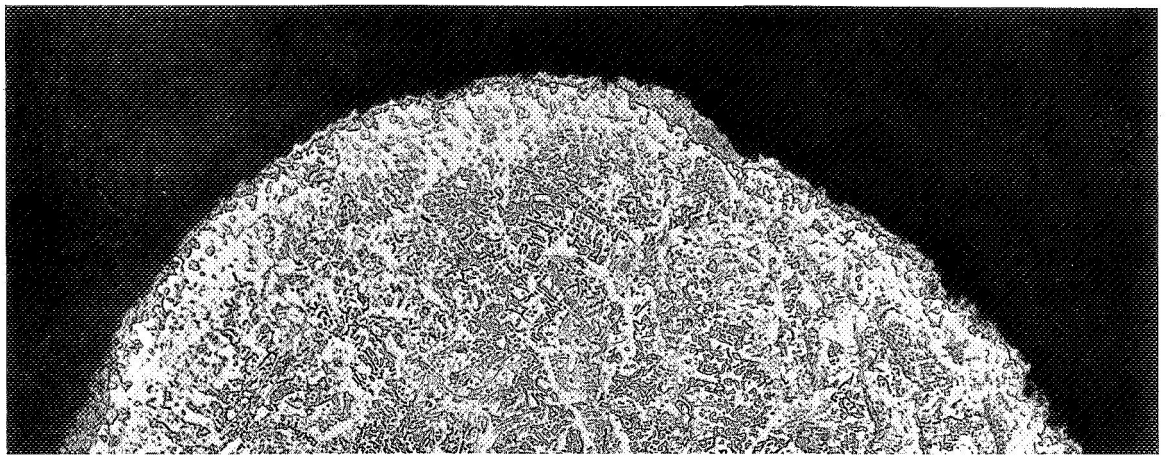

1.0 Inch (2.54 cm) Below Tip

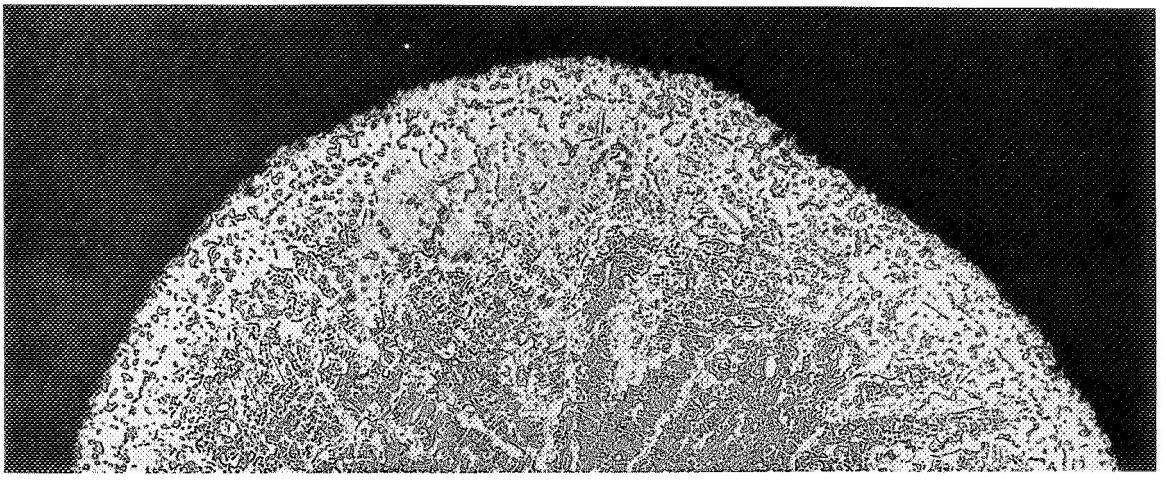

1.5 Inches (3.8 cm) Below Tip

Figure 48. NC11-A-D1 Coating on Trailing Edge Sections After 2000°F (1366°K)/2000-Hour Burner Rig Test (Etched 100X).

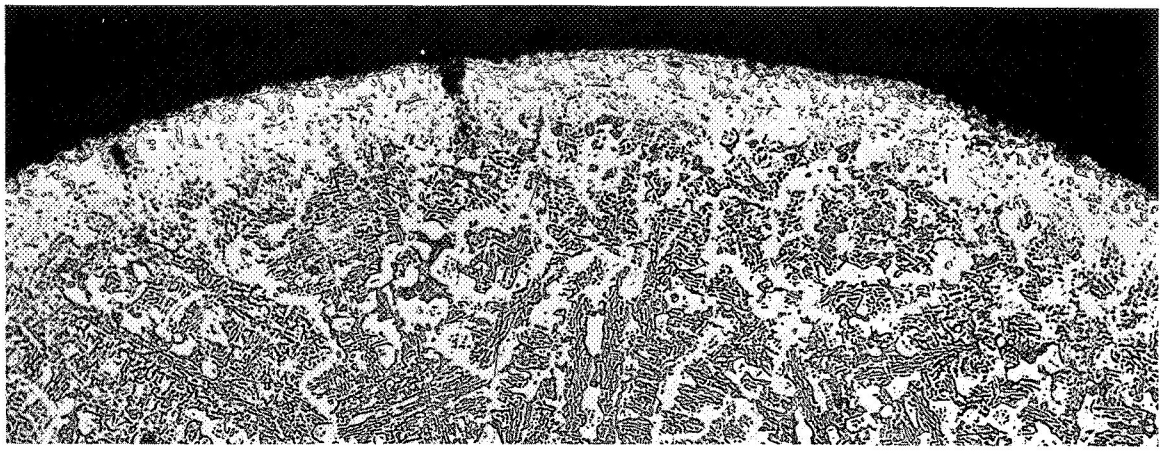

0.4 Inch (1.02 cm) Below Tip

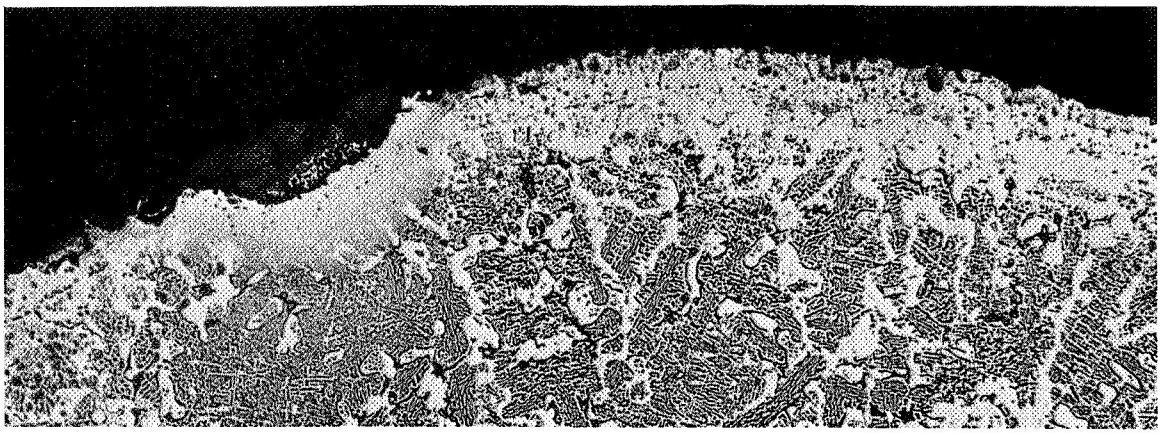

1.0 Inch (2.54 cm) Below Tip

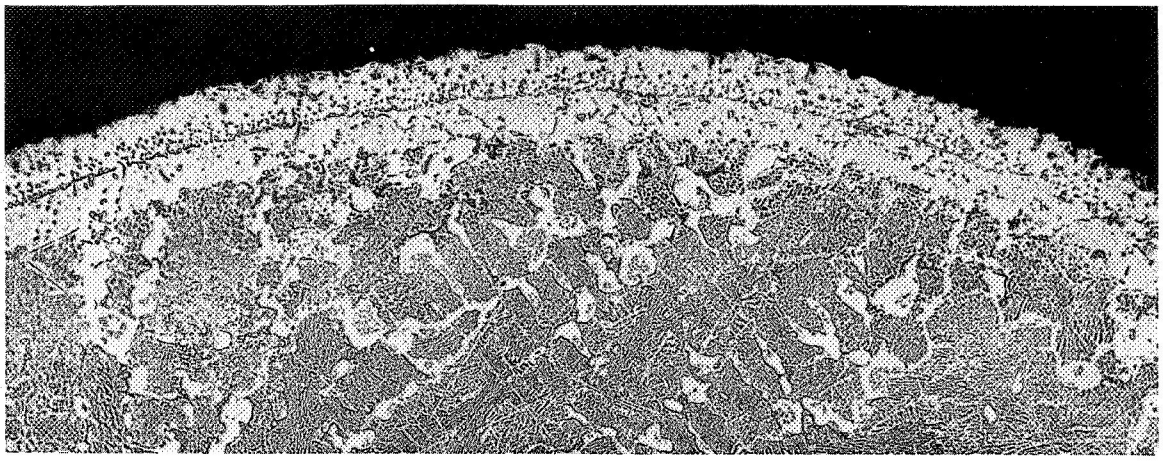

1.5 Inches (3.8 cm) Below Tip

Figure 49. NC11-A-D1 Coating on Leading Edge Sections After 2000°F (1366°K)/2000-Hour Burner Rig Test (Etched 100X).

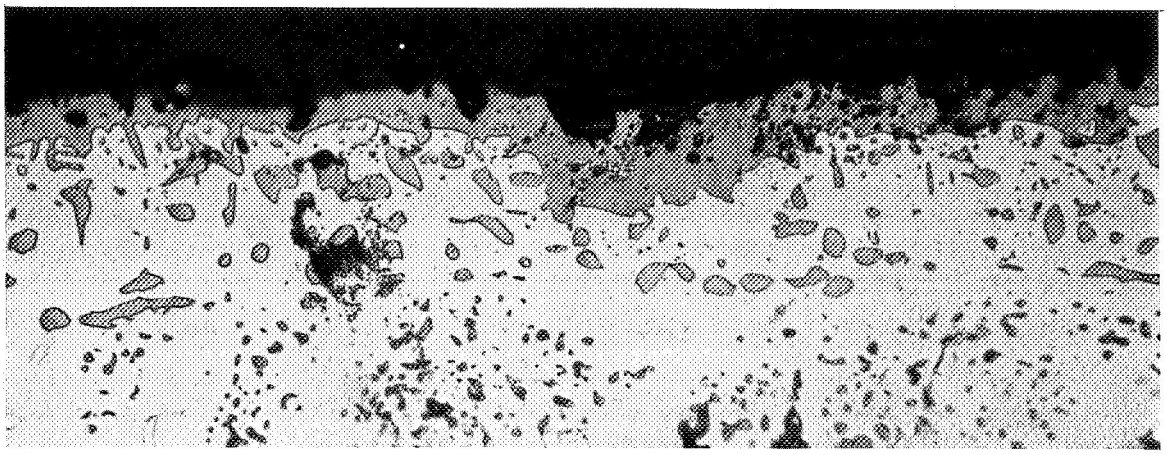

Leading Edge

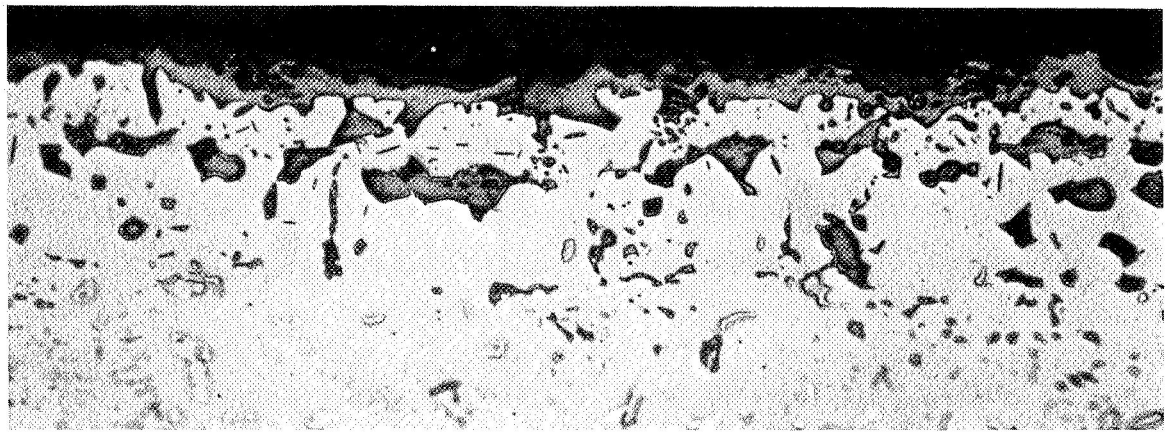

Center - Convex

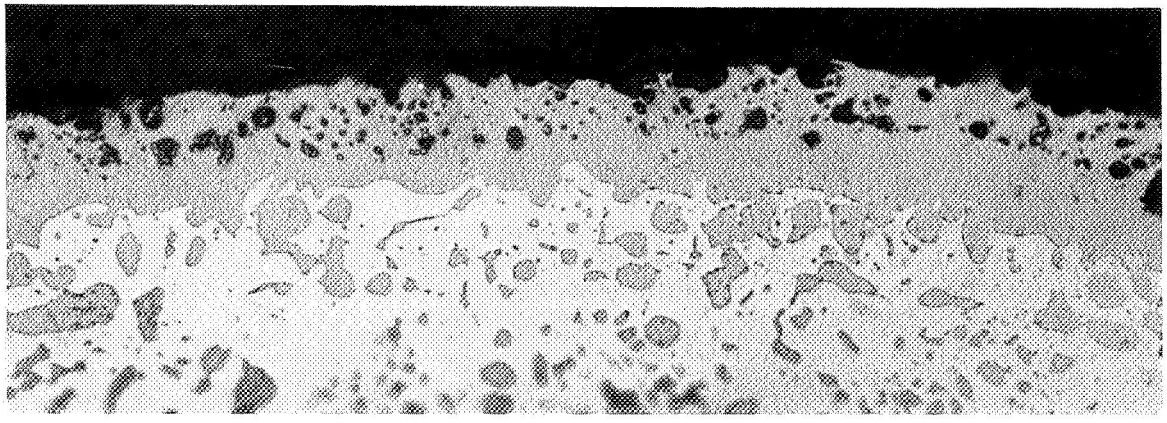

Trailing Edge

Figure 50. NC11-A-D1 Coating at 0.4 Inch (1.02 cm) Below Tip After 2000°F (1366°K)/2000-Hour Burner Rig Test (Etched 500X).

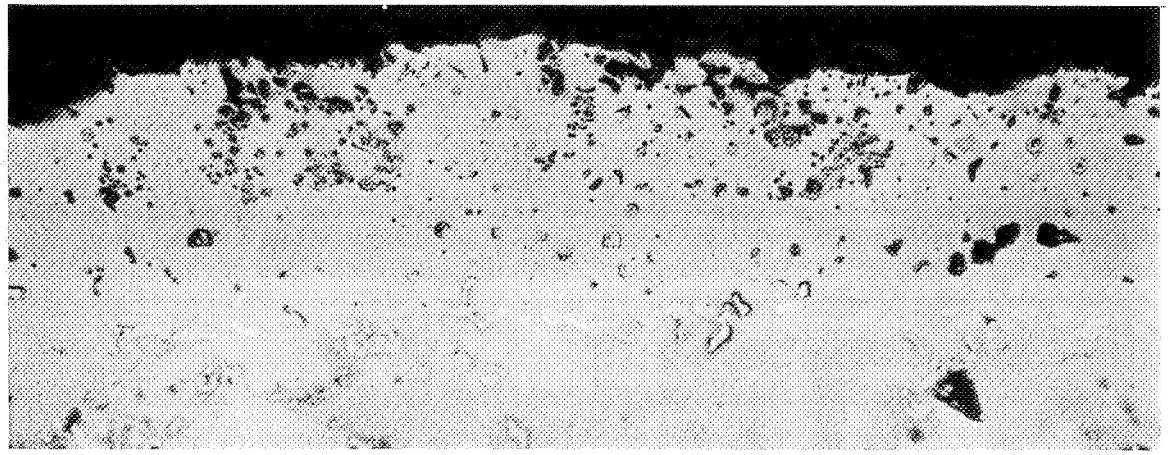

Leading Edge

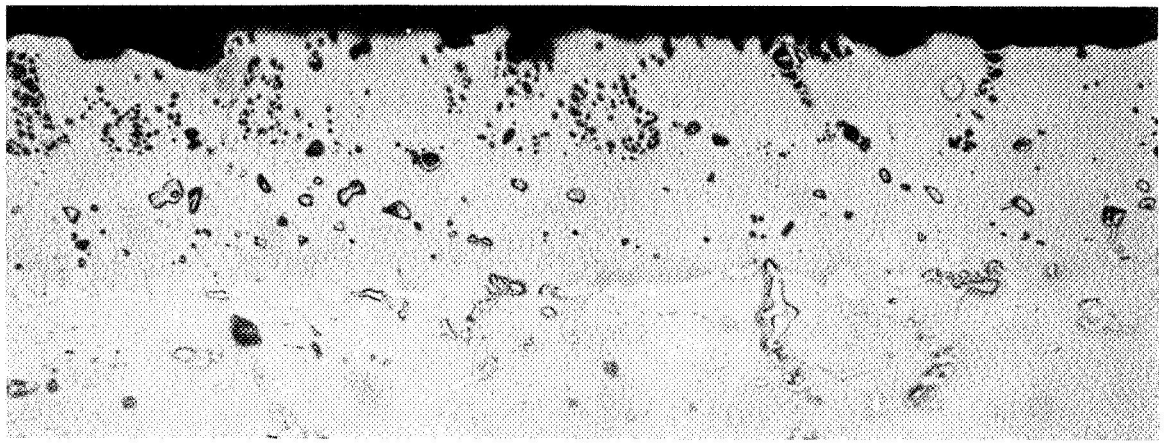

Center - Convex

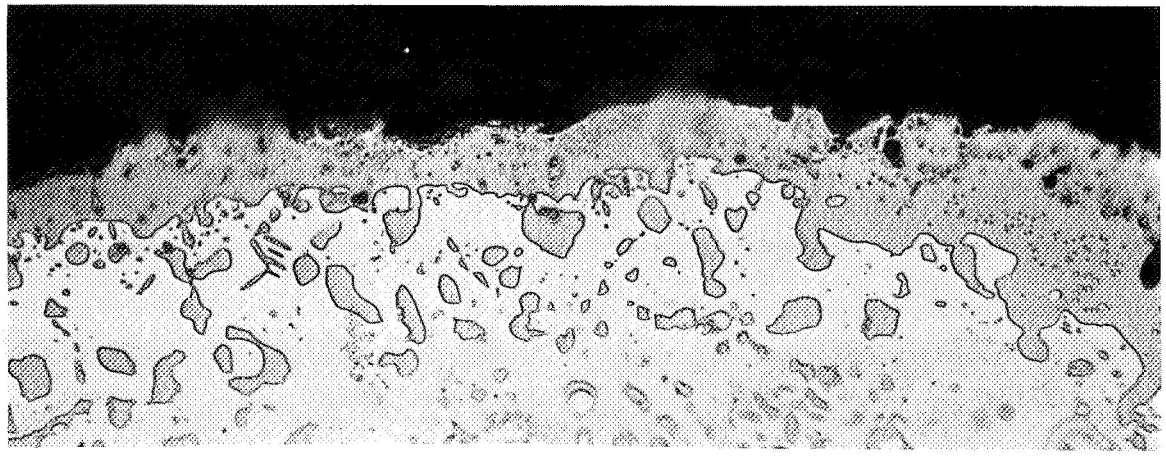

Trailing Edge

Figure 51. NC11-A-D1 Coating at 1.0 Inch (2.54 cm) Below Tip After 2000°F (1366°K)/2000-Hour Burner Rig Test (Etched 500X).

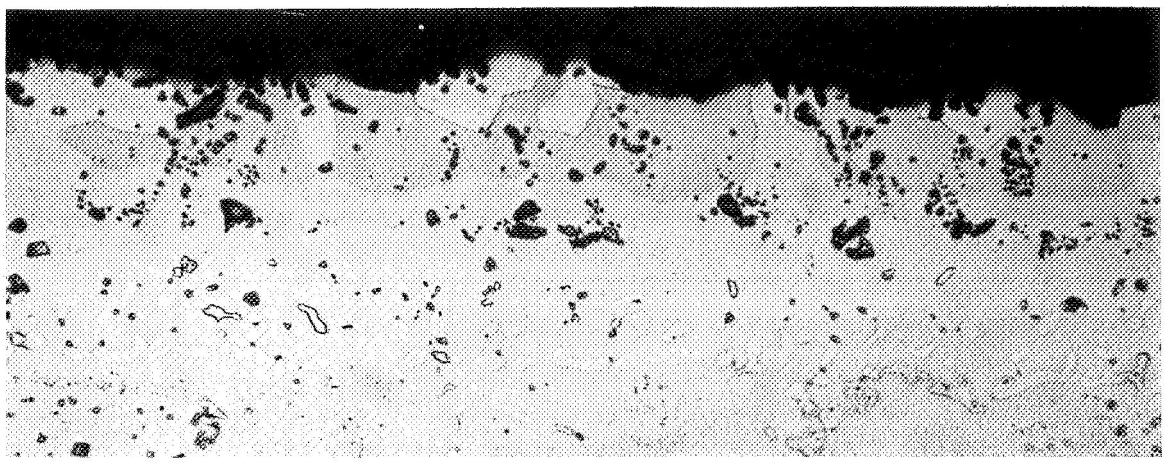

Leading Edge

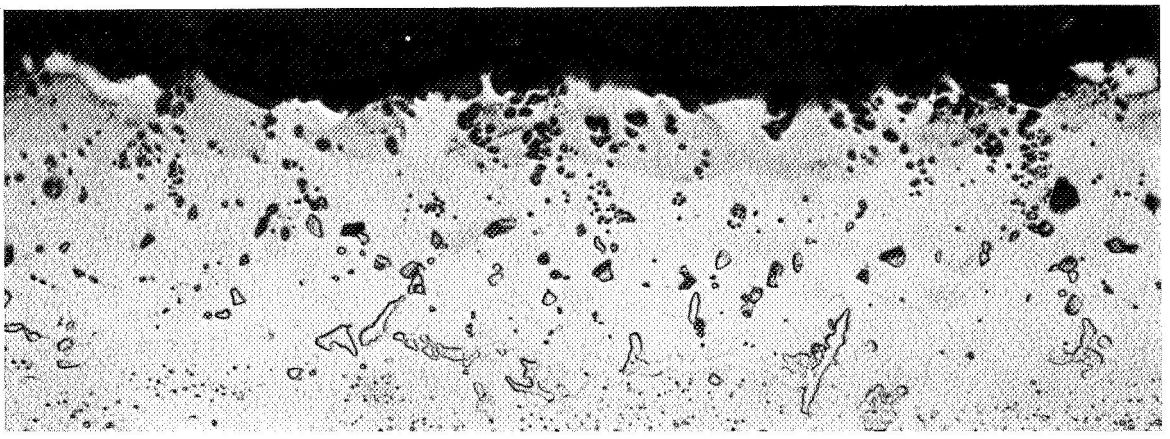

Center - Convex

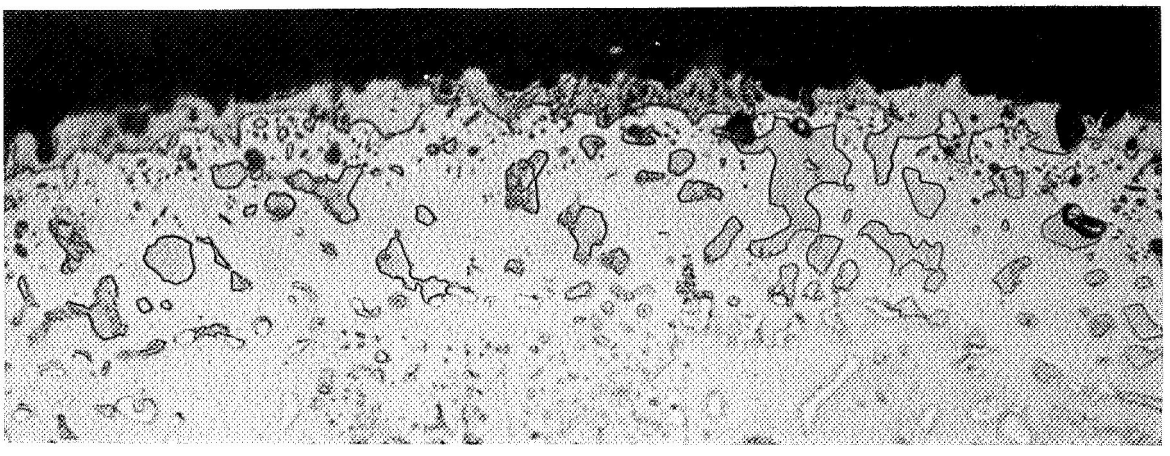

Trailing Edge

Figure 52. NC11-A-D1 Coating at 1.5 Inches (3.8 cm) Below Tip After 2000°F (1366°K)/2000-Hour Burner Rig Test (Etched 500X).

APPENDIX A

TEST SPECIMENS

TEST FACILITIES

PROCESSING FACILITIES

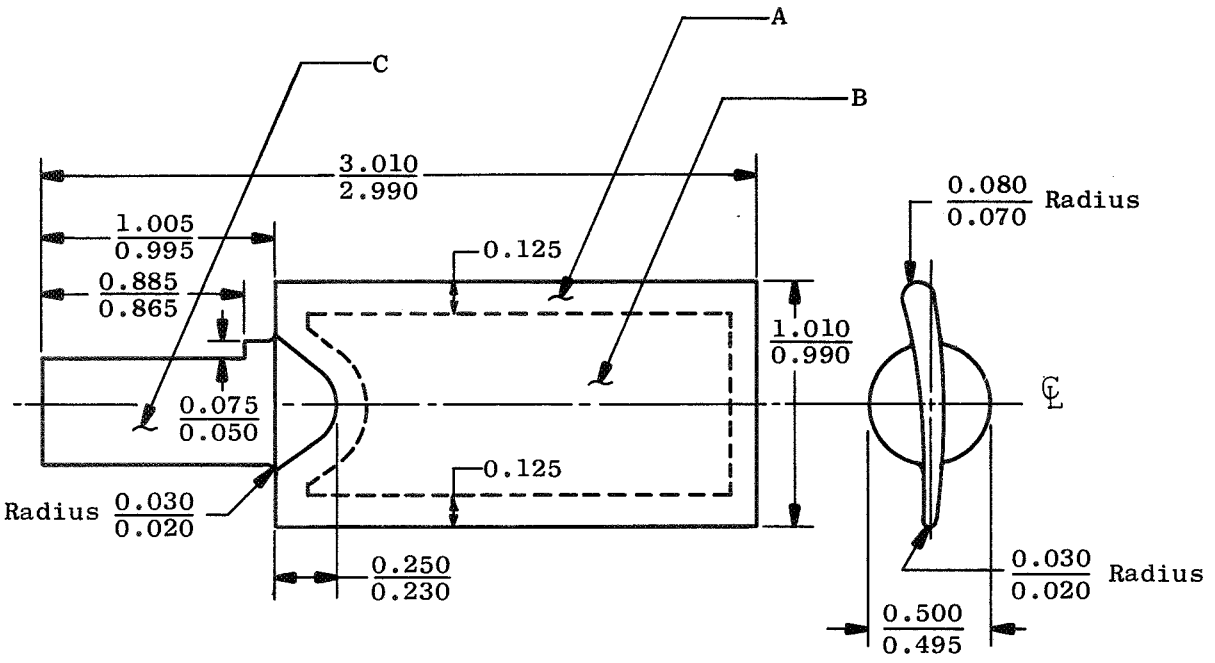

All Dimensions in Inches

Figure A-1. Simulated Airfoil Test Specimen (NASA Sketch No. 98B-3).

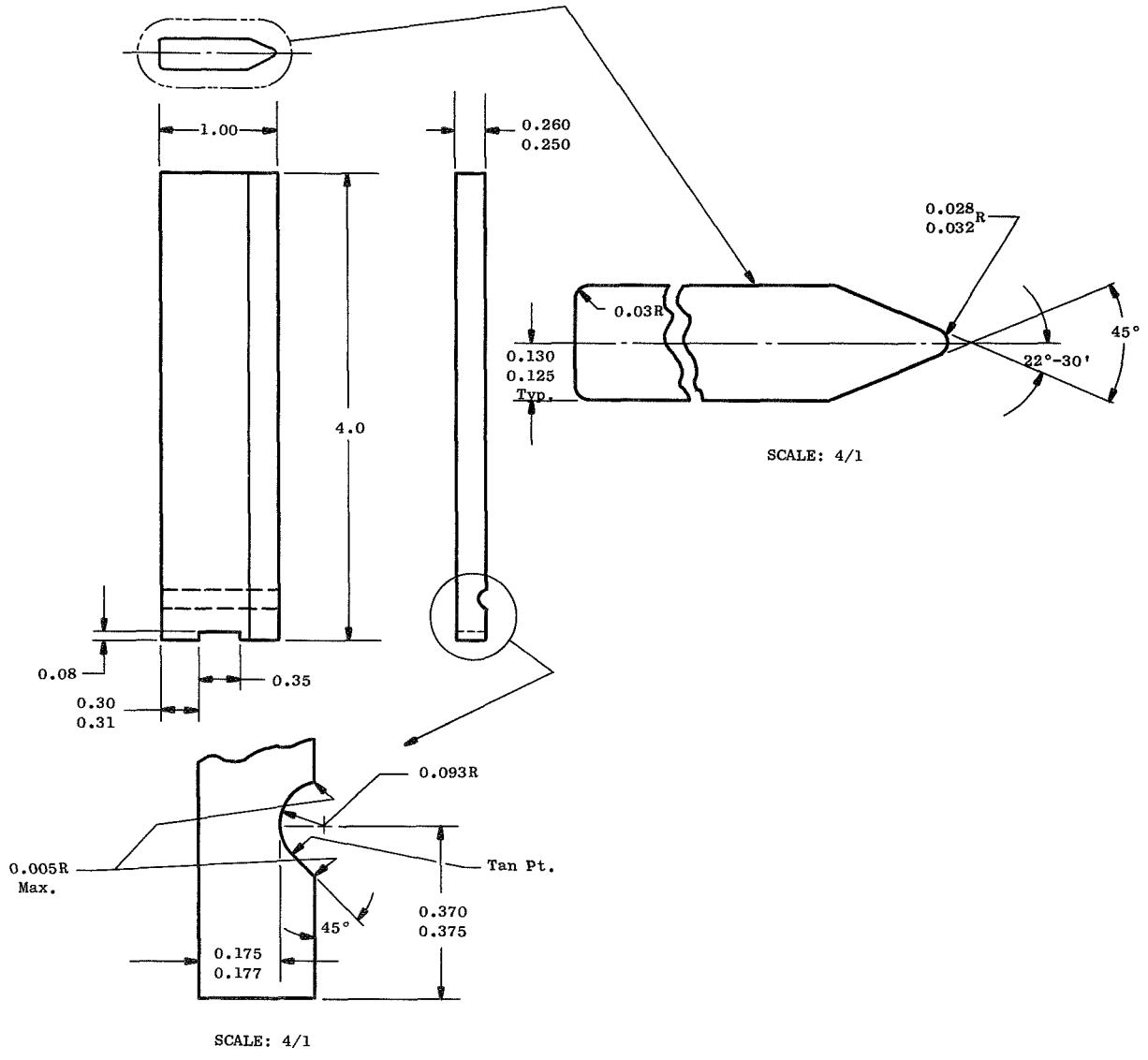

Figure A-2. Erosion Test Specimen CB-301680.

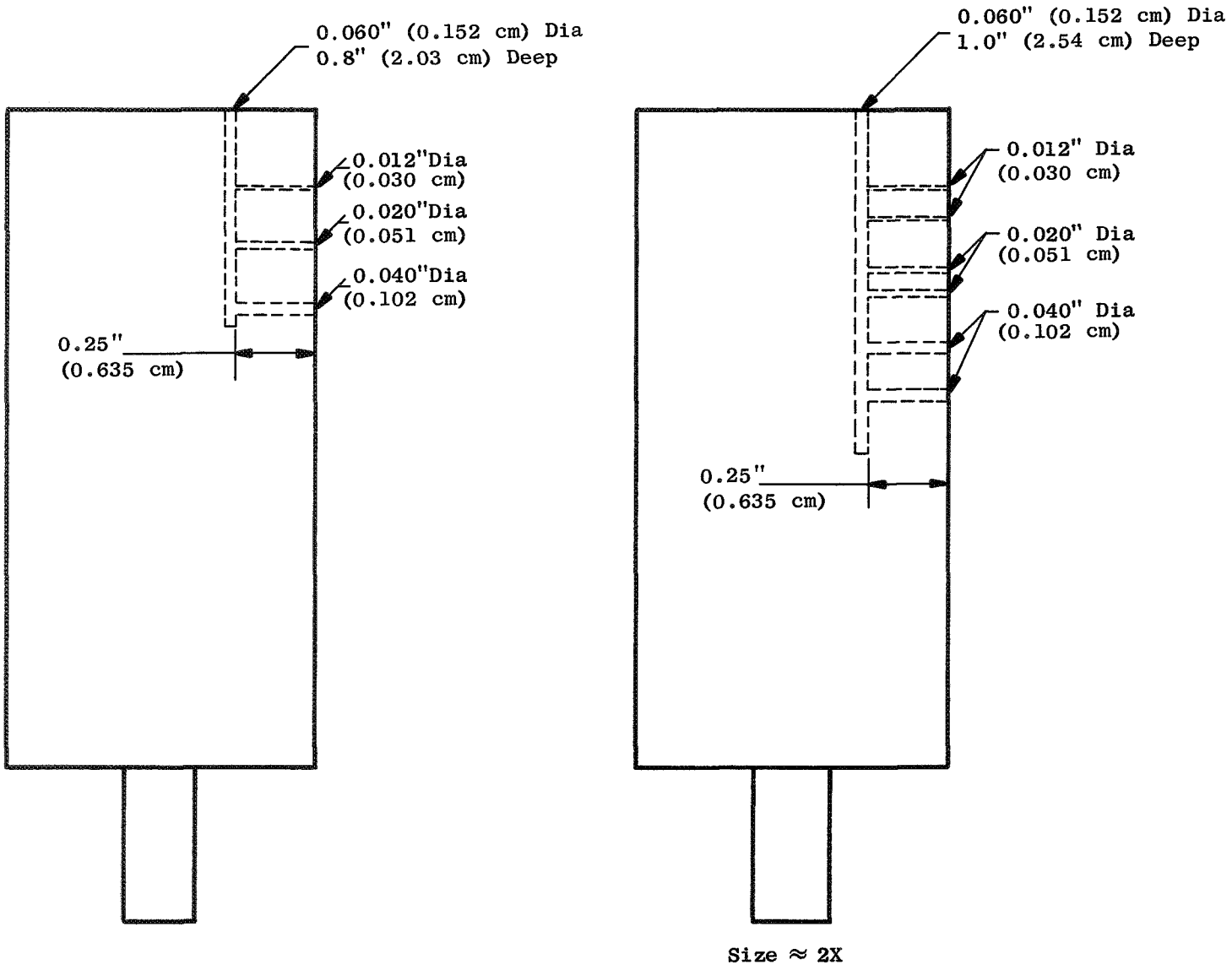

Figure A-3. EDM Hole Patterns on Paddle-Wheel Specimens.

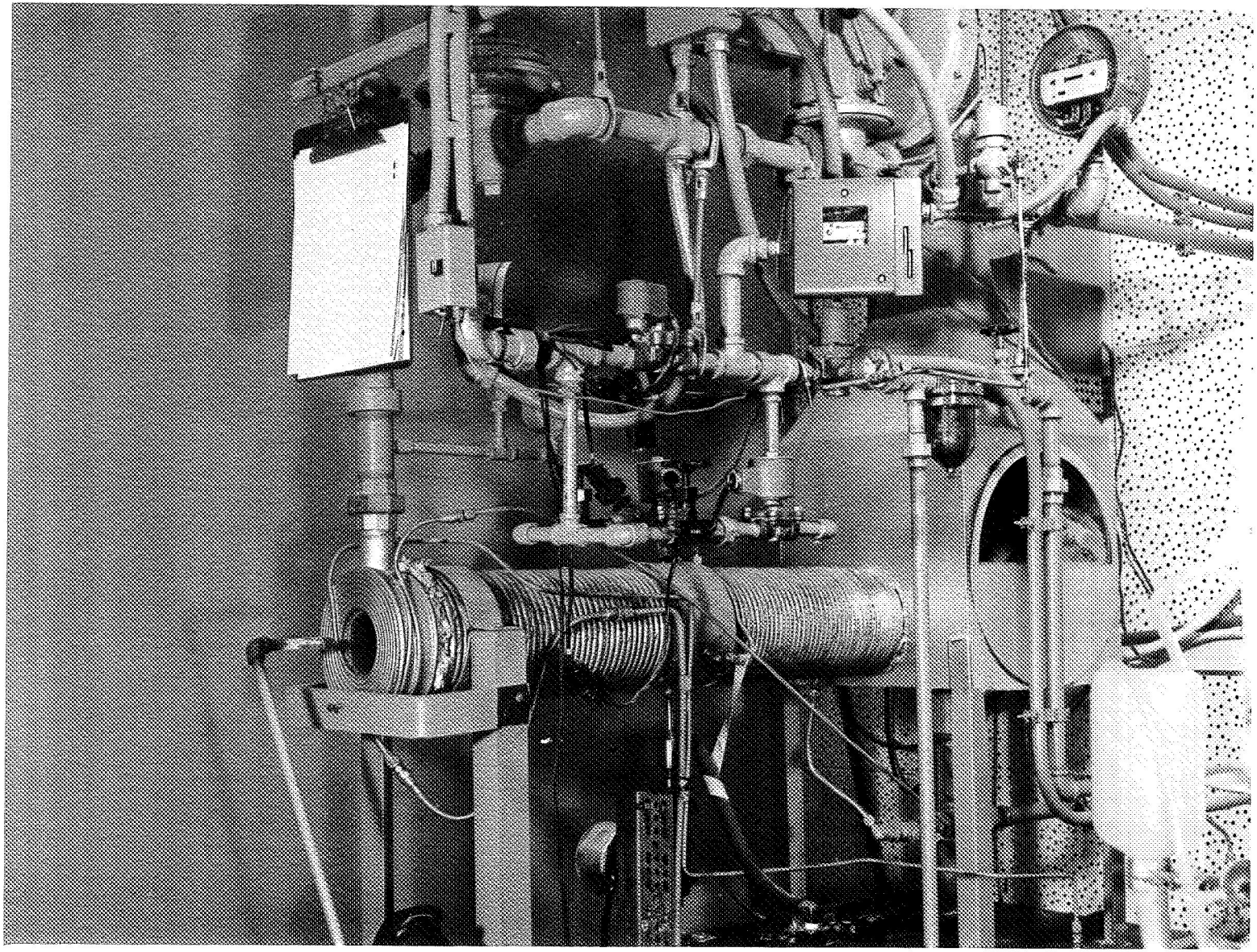

Figure A-4. M&PTL Low-Velocity Burner Rig.

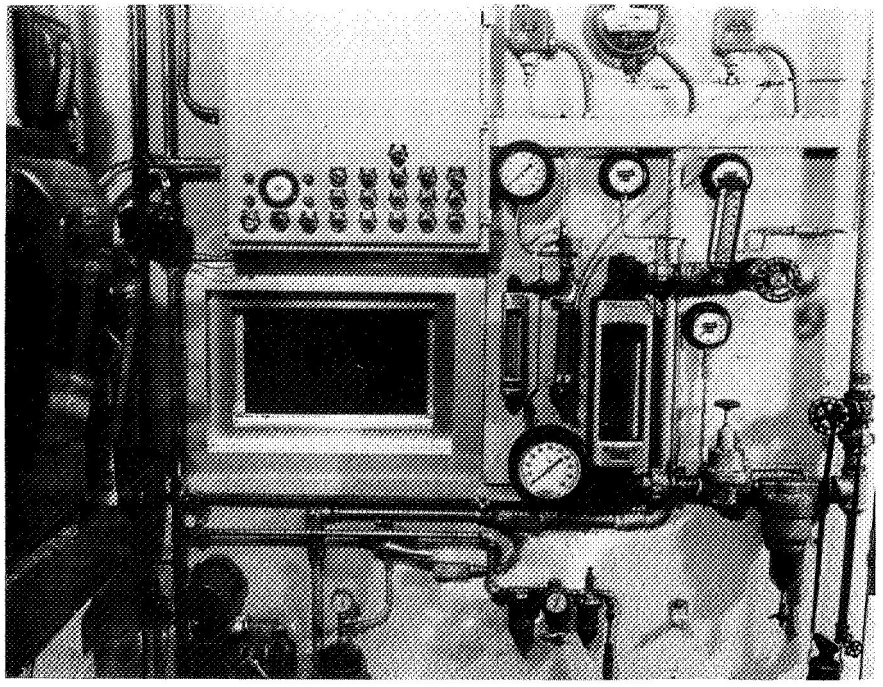

EPPI Burner Rig Control Panel

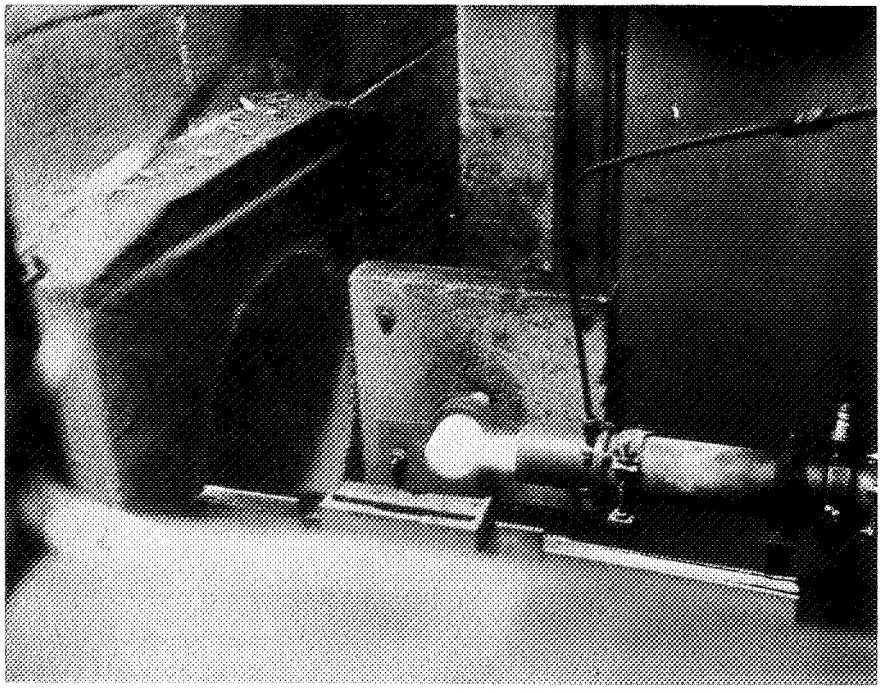

EPPI Test in Progress

Figure A-5. EPPI High-Velocity Burner Rig.

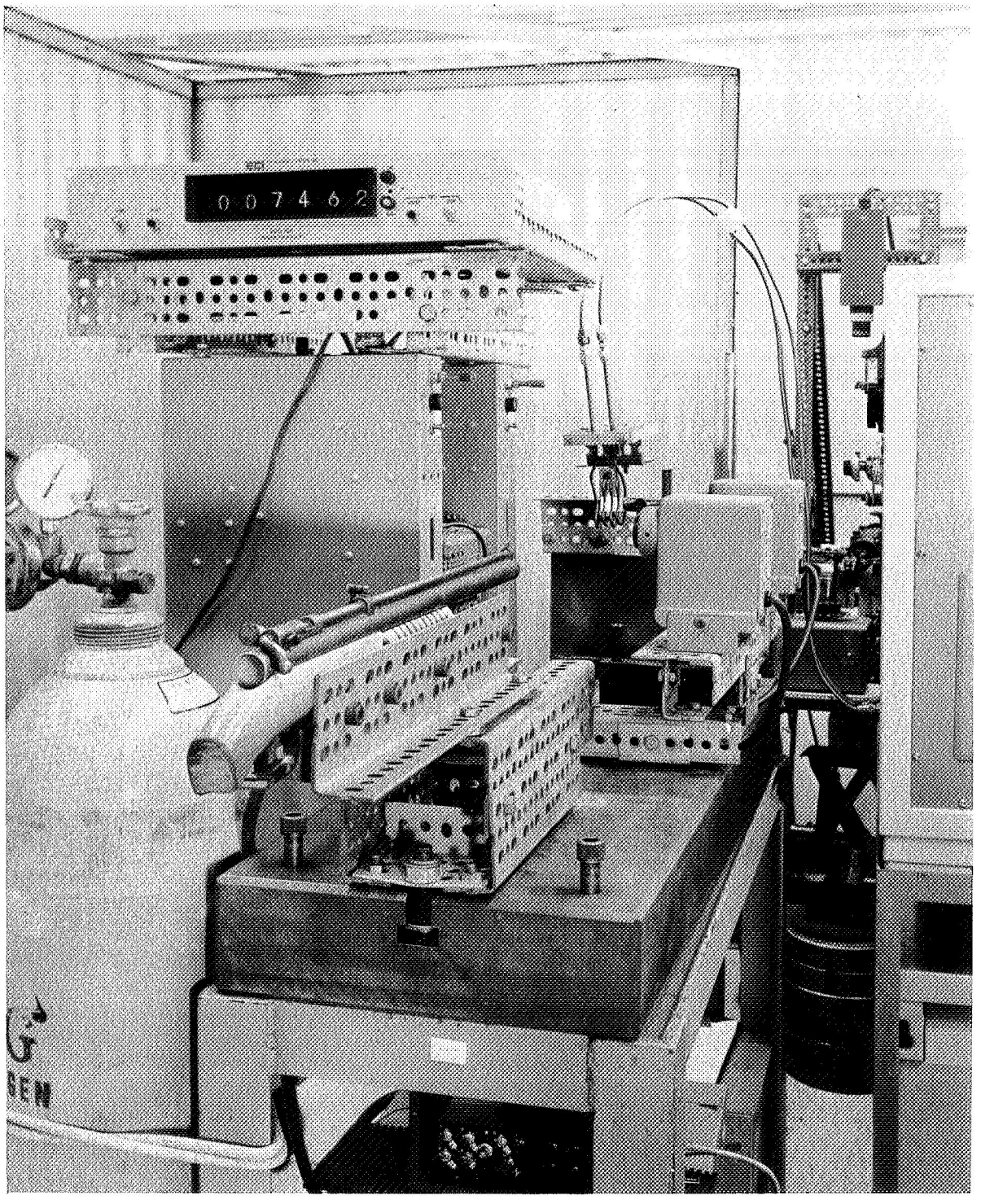

Figure A-6. Ballistic Impact Test Equipment.

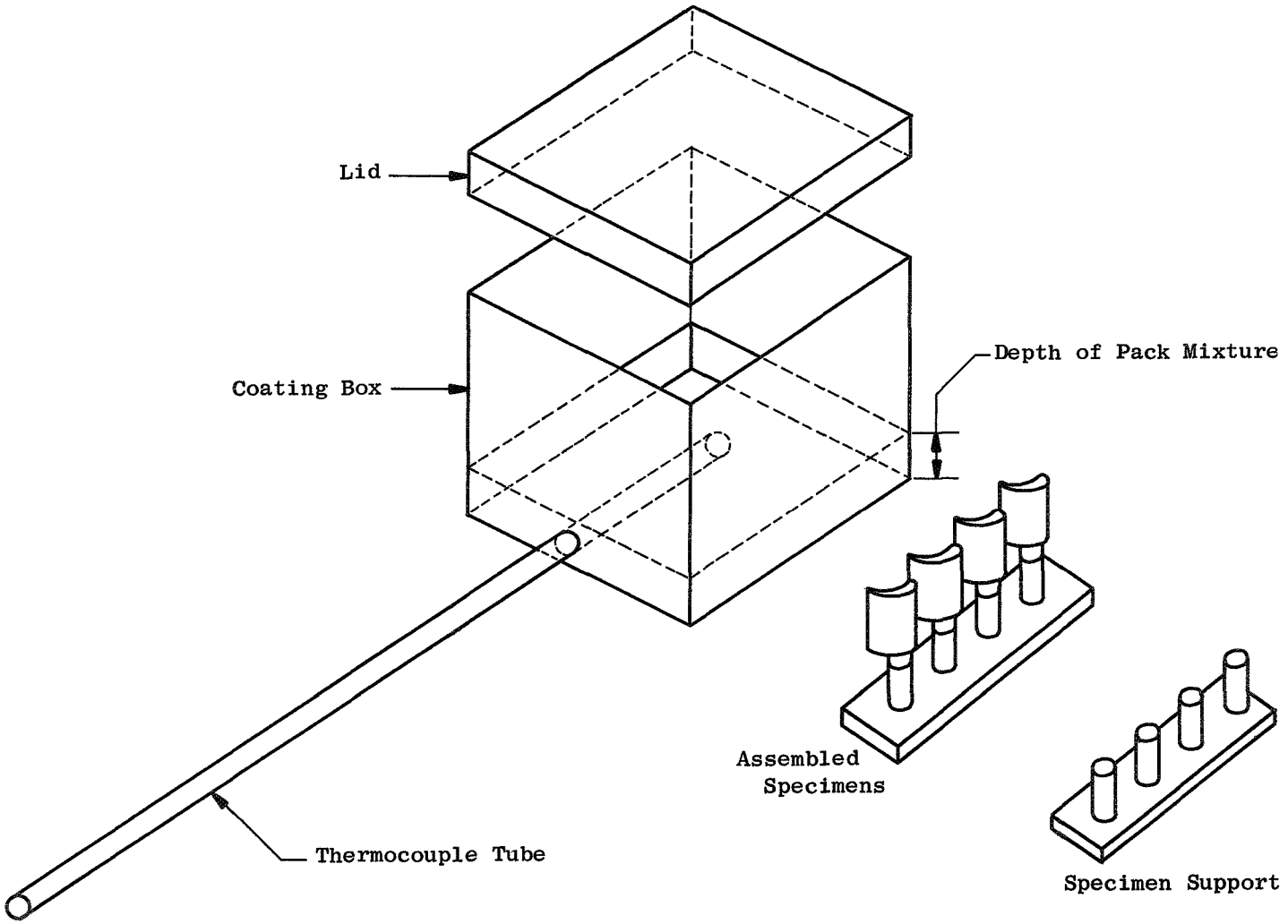

Figure A-7. Schematic of Coating Box and Specimen Support Fixture.

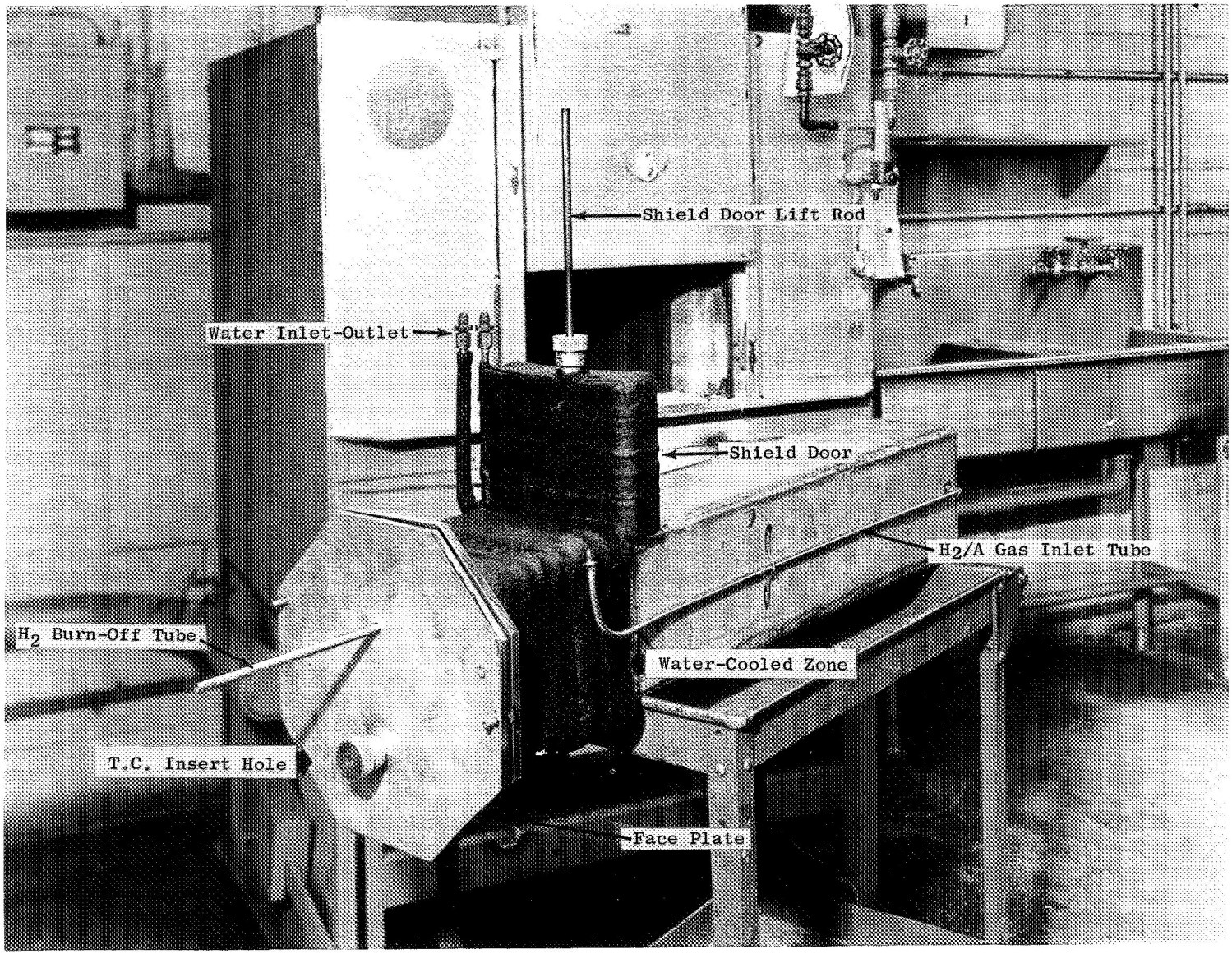

Figure A-8. Controlled Atmosphere Coating Retort.

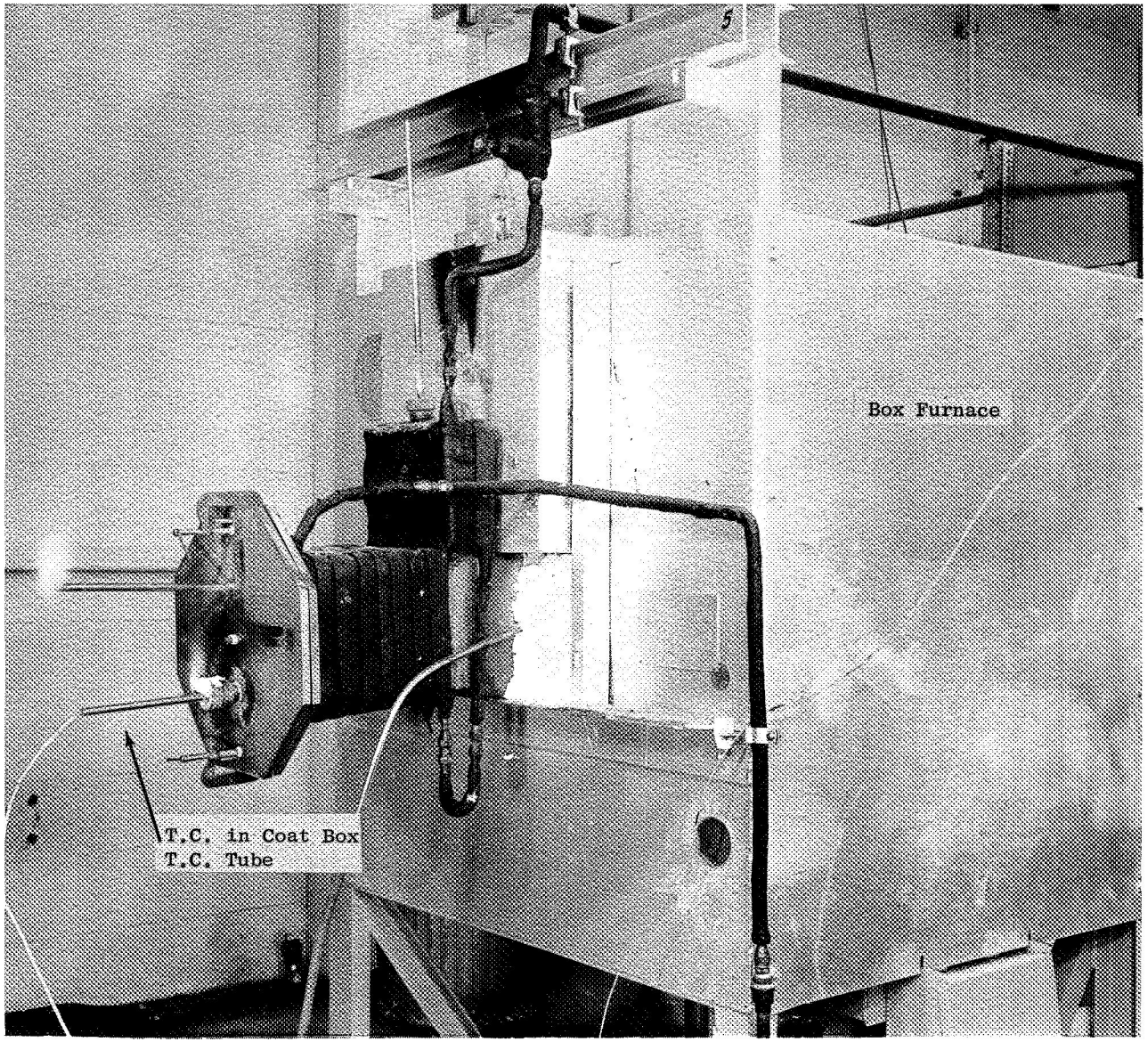

Figure A-9. Coating Process Setup With Coating Box in Place.

APPENDIX B

X-RAY DIFFRACTION ANALYSIS

Table B-I. X-Ray Diffraction Patterns for Coating System NC4-Cr.

A. As Coated				
Observed d-Spacings	Relative[1] Intensities	Indexed Phases	Remarks	Diffraction Parameters
3.48	W	Al_2O_3	Coating exhibits strong Cr intensity through particle entrapment	Radiation Cu Kα Filter - Ni Power - 40 KV, 20 MA
2.89	M	NiAl		
2.08	W	Al_2O_3, Ni_3Al		
2.04	VS	NiAl		
1.60	W	Al_2O_3		
1.44	M	NiAl; Cr		
1.18	S	NiAl; Cr		
1.02	W	NiAl; Cr		
0.91	M	Cr; NiAl		
0.832	W	Cr		
B. After EPPI Testing - 662 Hours/2000°F(1366°K)				
4.72	W	MAl_2O_4	Cr intensity much less than above MAl_2O_4 Phase could be $NiAl_2O_4$ or $FeAl_2O_4$ or both in all specimens after EPPI testing. Oxidation of iron base nozzle source for $FeAl_2O_4$	Radiation - Cu Kα Filter - Ni Power - 40 KV, 20 MA
2.90	W	NiAl; MAl_2O_4		
2.56	W	Ni_3Al		
2.47	M	MAl_2O_4		
2.08	S	Ni_3Al		
2.04	W	NiAl; MAl_2O_4		
1.79	M	Ni_3Al		
1.44	W	NiAl; Cr		
1.18	M	NiAl; Cr		
0.832	W	Cr		

(1) S = Strong
M = Medium
W = Weak
VS = Very strong

Table B-II. X-Ray Diffraction Patterns for Coating System NC11-A.

Observed d-Spacings	Relative[1] Intensities	Indexed Phases	Remarks	Diffraction Parameters
A. As Coated				
2.86	M	NiAl	High MAl intensity. No indication of embedded Al_2O_3 (Micro shows 5 - 10%)	Radiation - Cu Kα Filter - Ni Power - 40 KV, 20 MA
2.24	VW	NiAl		
2.02	VS	NiAl		
1.66	W	NiAl		
1.44	W	NiAl		
1.29	VW	NiAl		
1.18	S	NiAl		
1.02	W	NiAl		
0.91	W	NiAl		
B. After EPPI Testing - 662 Hours/2000°F(1366°K)				
2.56	M	Al_2O_3, Ni_3Al	MAl_2O_4 phase could be either $NiAl_2O_4$ or $FeAl_2O_4$ or both.	Radiation - Cu Kα Filter - Ni Power - 40 KV, 20 MA
2.045	S	MAl_2O_4		
2.08	VS	Ni_3Al, Al_2O_3		
2.03	VS	NiAl, MAl_2O_4		
1.80	M	Ni_3Al		
1.61	W	Ni_3Al, Al_2O_3		
1.56	W	MAl_2O_4		
1.43	W	NiAl, MAl_2O_4		
1.27	M	Ni_3Al, MAl_2O_4		
1.08	M	Al_2O_3, Ni_3Al		
0.823	W	MAl_2O_4		

(1) S = Strong
M = Medium
W = Weak
VW = Very weak
VS = Very strong

Table B-III. X-Ray Diffraction Patterns for Coating System NC11-A (Modified).

Observed d-Spacings	Relative[1] Intensities	Indexed Phases	Remarks	Diffraction Parameters
A. As Coated				
2.88	W	NiAl	NiAl intensity very strong. Embedment of Cr particles confirmed. Presence of Ni_2Al_3 probable; 42 w/o probe analysis suggests it may be present at surface.	Radiation - Cu Kα Filter - Ni Power - 40 KV, 20 MA
2.10	W	Ni_3Al Al_2O_3		
2.04	VS	NiAl, Ni_2Al_3, Cr		
1.66	M	NiAl		
1.44	W	NiAl, Ni_2Al_3, Cr		
1.18	VS	NiAl, Cr		
1.02	M	NiAl, Cr		
0.96	VW	NiAl		
0.91	W	NiAl, Cr		
0.83	M	Cr		
B. After EPPI Testing - 662 Hours/2000°F(1366°K)				
2.56	W	Al_2O_3, Ni_3Al	MAl_2O_4 phase could be either $NiAl_2O_4$ or $FeAl_2O_4$ or both.	Radiation - Cu Kα Filter - Ni Power - 40 KV, 20 MA
2.45	M	MAl_2O_4		
2.08	S	Ni_3Al, Al_2O_3		
2.03	VS	NiAl, MAl_2O_4		
1.80	M	Ni_3Al		
1.61	W	Ni_3Al, Al_2O_3		
1.43	M	NiAl, MAl_2O_4		
1.27	W	Ni_3Al, MAl_2O_4		
1.17	M	NiAl, Al_2O_3		
1.01	W	NiAl		

(1) S = Strong
M = Medium
W = Weak
VS = Very strong
VW = Very weak

Table B-IV. X-Ray Diffraction Patterns for Coating System NC11-C .

A. As Coated				
Observed d-Spacings	Relative[1] Intensities	Indexed Phases	Remarks	Diffraction Parameters
2.89	M	NiAl	NiAl intensity much weaker than in coatings with CODEP B - NiAl intensity weaker than in NC11-A, lower D/F No. powder used	Radiation - Cu Kα Filter - Ni Power - 40 KV, 20 MA
2.56	W	Al_2O_3, Ni_3Al		
2.04	VS	NiAl		
1.66	W	NiAl		
1.60	VW	Al_2O_3		
1.44	W	NiAl		
1.18	M	NiAl		
1.02	W	NiAl		
0.91	VW	NiAl		
B. After EPPI Testing - 175.75 Hours/2000°F(1366°K)				
2.88	W	NiAl	Moderate MAl_2O_4 intensity - NiAl intensity still strong - coating had not failed under test time of 175.75 hours	Radiation - Cu Kα Filter - Ni Power - 40 KV, 20 MA
2.56	W	Ni_3Al, Al_2O_3		
2.45	M	MAl_2O_4		
2.08	VS	Ni_3Al, Al_2O_3		
2.04	VS	NiAl		
1.80	M	Ni_3Al		
1.60	M	Al_2O_3		
1.43	W	NiAl, MAl_2O_4		
1.28	W	Al_2O_3		
1.17	M	NiAl, Al_2O_3		

(1) S = Strong
M = Medium
W = Weak
VS = Very strong
VW = Very weak

Table B-V. X-Ray Diffraction Patterns for Coating System NASA VIA/C-2.

A. As Coated				
Observed d-Spacings	Relative(1) Intensities	Indexed Phases	Remarks	Diffraction Parameters
3.48	W	Al_2O_3	NiAl intensities weaker than in Al enrichment coatings. Al_2O_3 intensity low. No TiO_2 indication, due to concentration at interface.	Radiation - Cu Kα Filter - Ni Power - 40 KV, 20 MA
2.90	M	NiAl		
2.55	W	Al_2O_3		
2.08	W	Ni_3Al, Al_2O_3		
2.04	VS	NiAl		
1.67	VW	NiAl		
1.60	VW	Al_2O_3		
1.45	W	NiAl		
1.18	M	NiAl, Al_2O_3		
1.02	VW	NiAl		
B. After EPPI Testing - 250 Hours/2000°F(1366°K)				
3.49	W	Al_2O_3	NiAl intensities much weaker than above - MAl_2O_4 intensity relatively weak due to shorter exposure.	Radiation - Cu Kα Filter - Ni Power - 40 KV, 20 MA
2.56	W	Al_2O_3, Ni_3Al		
2.44	M	MAl_2O_4		
2.08	VS	Ni_3Al, Al_2O_3		
2.04	VS	NiAl		
1.80	M	Ni_3Al		
1.60	W	Al_2O_3		
1.44	W	NiAl, MAl_2O_4		
1.27	M	Ni_3Al, Al_2O_3		
1.18	M	NiAl		
1.09	M	Al_2O_3, Ni_3Al		

(1) S = Strong
M = Medium
W = Weak
VS = Very strong
VW = Very weak

Table B-VI. X-Ray Diffraction Patterns for Coating System R'100/C-2.

A. As Coated				
Observed d-Spacings	Relative(1) Intensities	Indexed Phases	Remarks	Diffraction Parameters
3.49	M	Al_2O_3	Insoluble phases extracted through dissolving of coating included - TiO_2, TiC, $M23C_6$ and Al_2O_3 as insoluble residue measured by a separate diffraction measurement.	Radiation - Cu Kα Filter - Ni Power - 40 KV, 20 MA
2.88	VS	NiAl		
2.56	M	Al_2O_3,Ni_3Al		
2.03	VS	NiAl		
1.66	W	NiAl		
1.60	W	Al_2O_3		
1.44	S	NiAl		
1.18	VS	NiAl		
1.09	W	Al_2O_3, Ni_3Al		
0.91	W	NiAl		
B. After EPPI Testing - 321.25 Hours/2000°F(1366°K)				
2.56	W	Al_2O_3	Insoluble phases extracted through dissolving of coating included TiO_2 and Al_2O_3. Lower NiAl after exposure characteristics of CODEP C.	Radiation - Cu Kα Filter - Ni Power - 40 KV, 20 MA
2.44	M	MAl_2O_4		
2.08	VS	Ni_3Al,Al_2O_3		
2.04	M	NiAl		
1.80	M	Ni_3Al		
1.60	W	Al_2O_3		
1.27	M	Ni_3Al,Al_2O_3		
1.08	M	Ni_3Al,Al_2O_3		
0.82	---	Ni_3Al, MAl_2O_4		

(1) S = Strong
M = Medium
W = Weak
VS = Very Strong

Table B-VII. X-Ray Diffraction Patterns for Coating System NC6-T.

A. As Coated				
Observed d-Spacings	Relative(1) Intensities	Indexed Phases	Remarks	Diffraction Parameters
3.25	VS	ThO_2	ThO_2 intensity very strong - 40% particle entrapment	Radiation - Cu Kα
2.81	S	ThO_2		Filter - Ni
2.08	M	Ni_3Al		Power - 40 KV, 20 MA
2.05	VS	NiAl		
1.98	VS	ThO_2		NOTE: Insoluble phases extracted were: ThO_2 (FCC) and Laves phase A_2B (Hexagonal)
1.69	VS	NiAl, ThO_2		
1.29	M	NiAl, ThO_2		
1.18	W	NiAl		
1.14	W	ThO_2		
0.94	W	ThO_2		
B. After EPPI Testing - 158 Hrs at 2000°F(1366°K)				
3.45	W	Al_2O_3	MAl_2O_4 apparently $NiAl_2O_4$	Radiation - Cu Kα
3.21	VS	ThO_2		Filter - Ni
2.54	M	Al_2O_3		Power - 40 KV, 20 MA
2.43	M	MAl_2O_4		
2.06	VS	NiAl		
2.02	M	MAl_2O_4		NOTE: Insoluble phases extracted were: Al_2O_3 and ThO_2 (FCC)
1.79	S	Ni_3Al		
1.68	M	ThO_2		
1.60	M	Al_2O_3		
1.08	M	ThO_2, Al_2O_3		

(1) S = Strong
M = Medium
W = Weak
VS = Very Strong

Table B-VIII. X-Ray Diffraction Patterns for Coating System NC3-L.

A. As Coated				
Observed d-Spacings	Relative(1) Intensities	Indexed Phases	Remarks	Diffraction Parameters
3.68	W	LaF_3	La_2O_3 addition to the coating has been reduced by NH_4F activator	Radiation - Cu Kα
3.23	M	LaF_3		Filter - Ni
2.89	VS	NiAl		Power - 40 KV, 20 MA
2.04	VS	NiAl		
1.67	W	NiAl		
1.45	VS	NiAl		
1.18	VS	NiAl		
1.02	M	NiAl		
0.91	M	NiAl		
B. After EPPI Testing - 231.5 Hrs. at 2000°F(1366°K)				
3.58	W	Ni_3Al	La indications not apparent, may be influencing MAl_2O_4 spacings.	Radiation - Cu Kα
2.60	M	Ni_3Al		Filter - Ni
2.49	M	MAl_2O_4		Power - 40 KV, 20 MA
2.10	VS	Ni_3Al, MAl_2O_4		
2.06	W	NiAl		
1.82	M	Ni_3Al		
1.62	W	Ni_3Al		
1.56	W	MAl_2O_4		
1.44	W	NiAl		
1.09	M	Ni_3Al		

(1)
M = Medium
W = Weak
VS = Very Strong

Table B-IX. X-Ray Diffraction Patterns for Coating System NC7-L.

A. As Coated				
Observed d-Spacings	Relative(1) Intensities	Indexed Phases	Remarks	Diffraction Parameters
3.68	M	LaF_3	La_2O_3 addition in the coating has been reduced to LaF_3 by NH_4F activator; NiAl intensity weaker than in other coatings	Radiation - CuKα Filter - Ni Power - 40 KV, 20 MA
3.59	M	LaF_3		
3.23	S	LaF_3		
2.90	M	NiAl		
2.08	M	LaF_3		
2.05	S	NiAl		
1.81	W	LaF_3		
1.45	M	NiAl		
1.18	S	NiAl		
0.92	W	NiAl		
B. After EPPI Testing - 73.75 Hours at 2000°F(1366°K)				
2.69	W	$LaAlO_3$	LaF_3 occurring above is being oxidized - NiAl intensity weak. Considerable Ni_3Al formation.	Radiation - CuKα Filter - Ni Power - 40 KV, 20 MA
2.55	W	Ni_3Al; LaF_3		
2.08	S	Ni_3Al; LaF_3		
2.03	S	NiAl		
1.80	M	Ni_3Al, LaF_3		
1.74	W	Al_2O_3		
1.61	W	Ni_3Al		
1.27	W	Ni_3Al; $LaAlO_3$		
1.17	W	NiAl		

(1) S = Strong
M = Medium
W = Weak

APPENDIX C

BALLISITIC IMPACT PHOTOGRAPHS

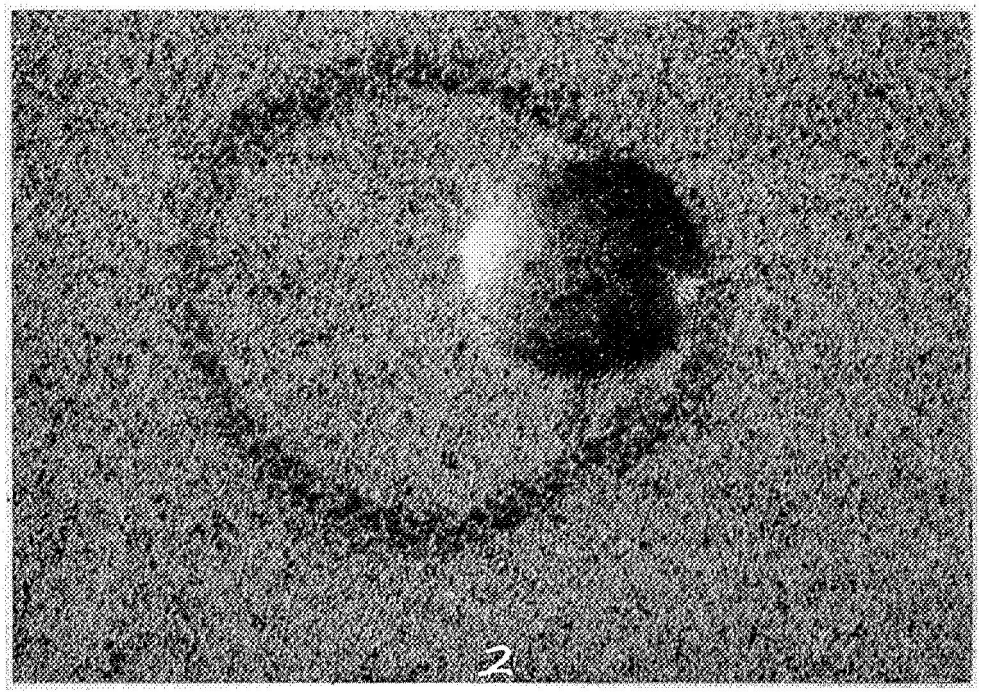

Impact Area

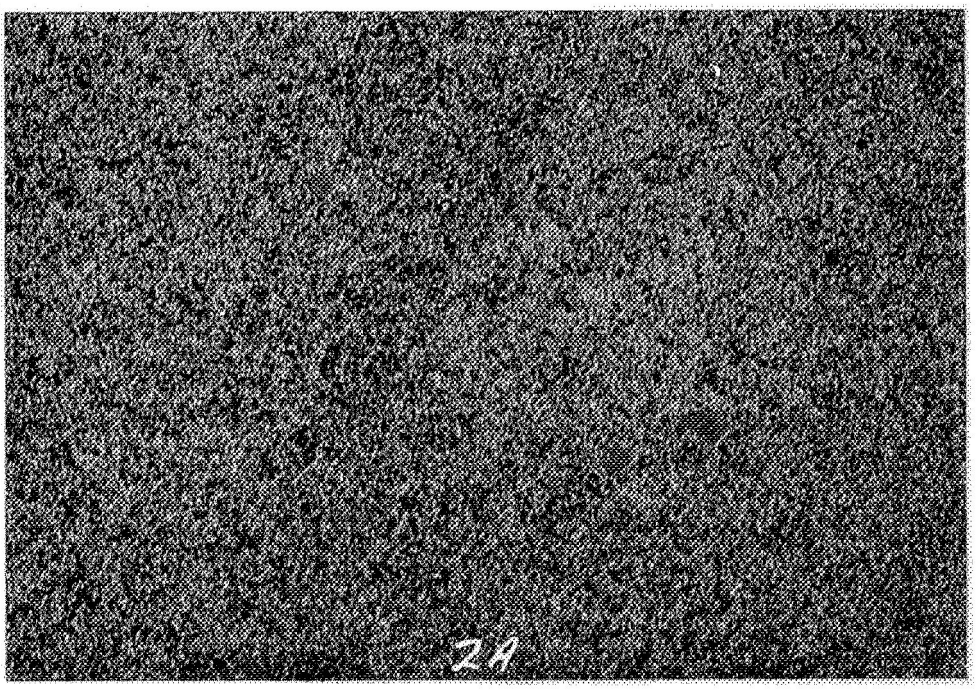

Tension Side of Impact

Figure C-1. Coating Systems NC4-Cr - Room Temperature Ballistic Impact with 1.96 Ft/Lbs Energy (15X).

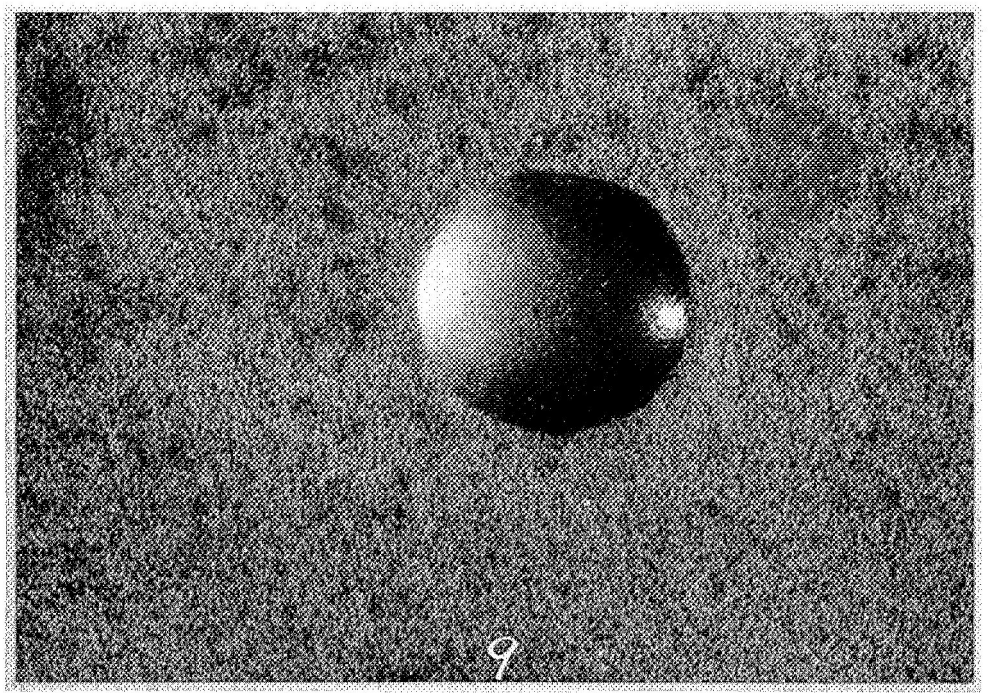

Impact Area

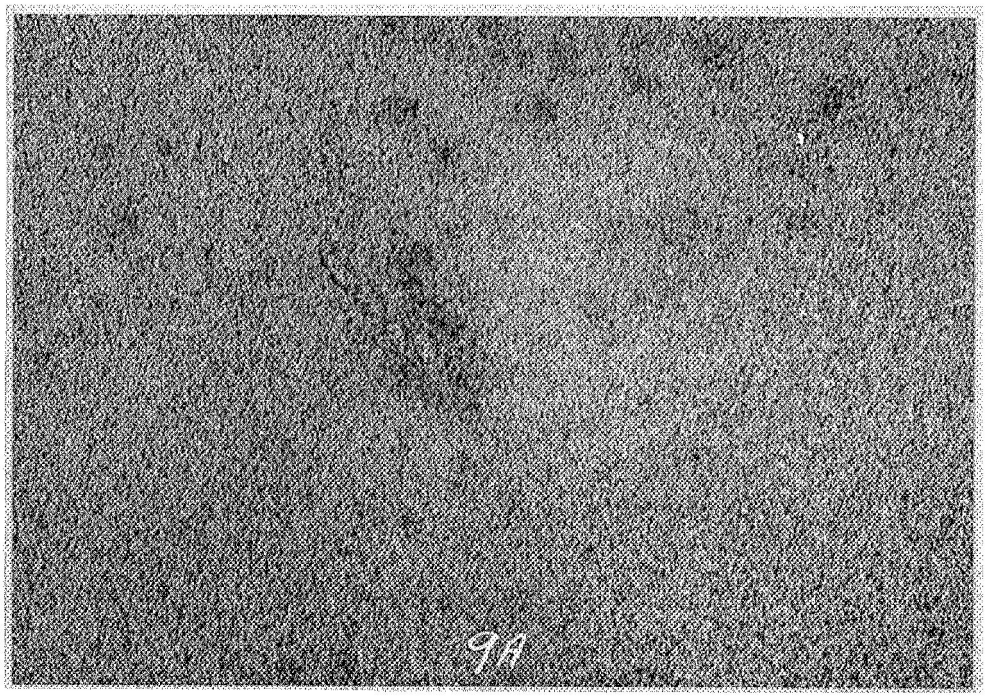

Tension Side of Impact

Figure C-2. Coating System NC4-Cr - 1800°F (1229°K) Ballistic Impact with 3.06 Ft/Lbs Energy (15X).

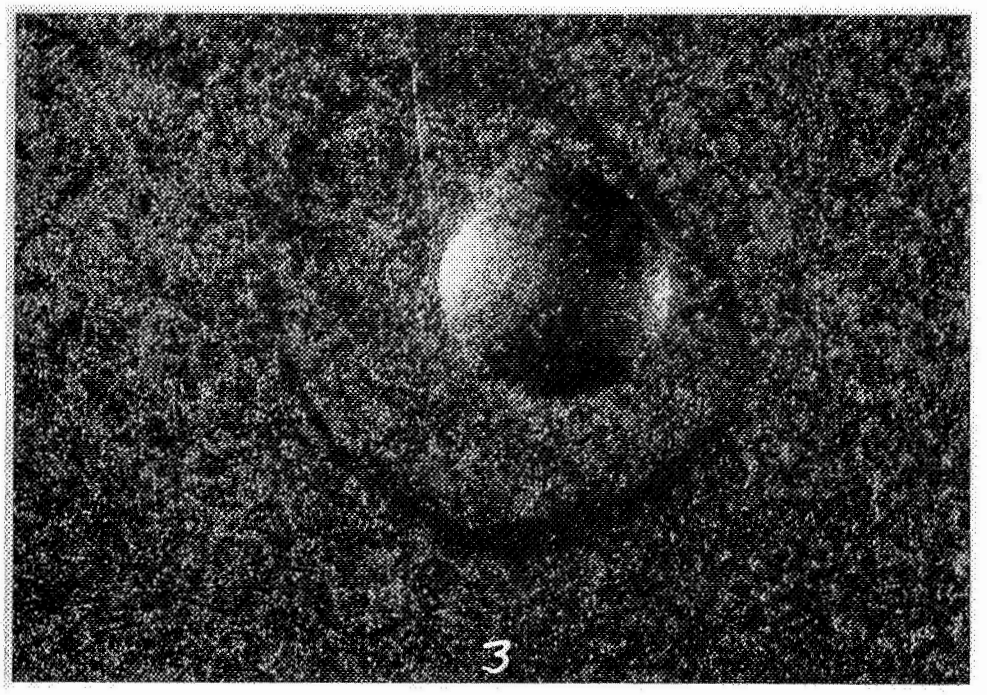

Impact Area

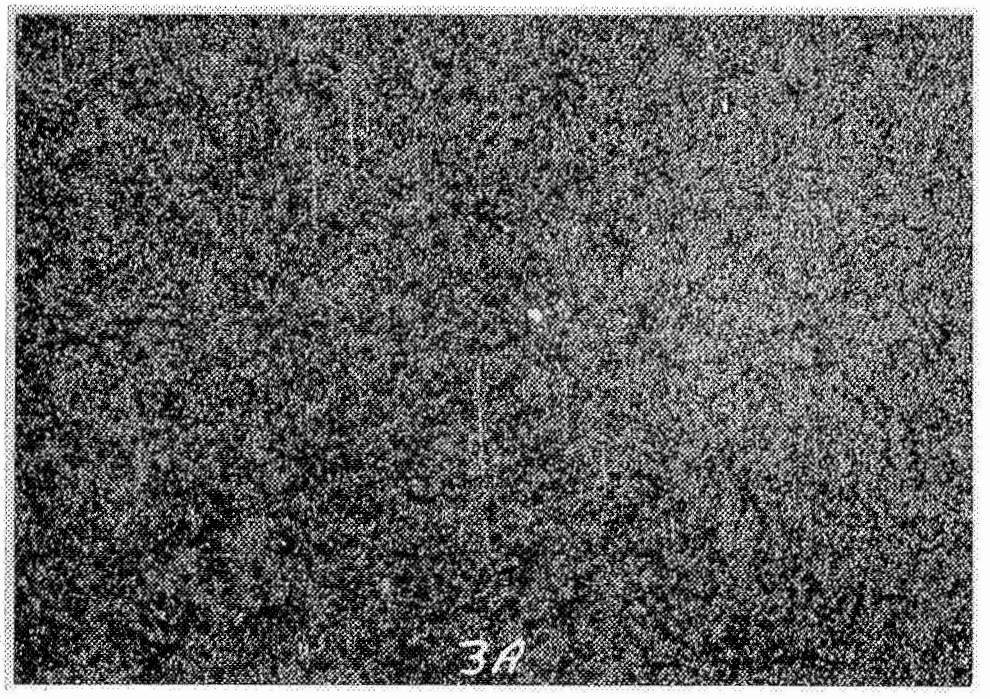

Tension Side of Impact

Figure C-3. Coating System NC11-A - Room Temperature Ballistic Impact with 1.96 Ft/Lbs Energy (15X).

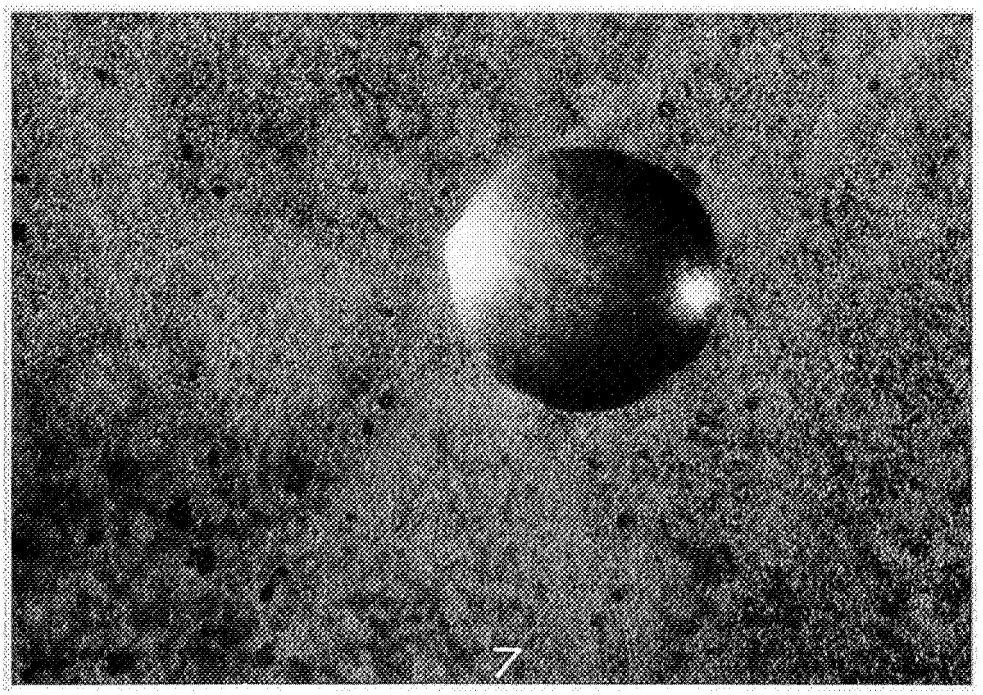

Impact Area

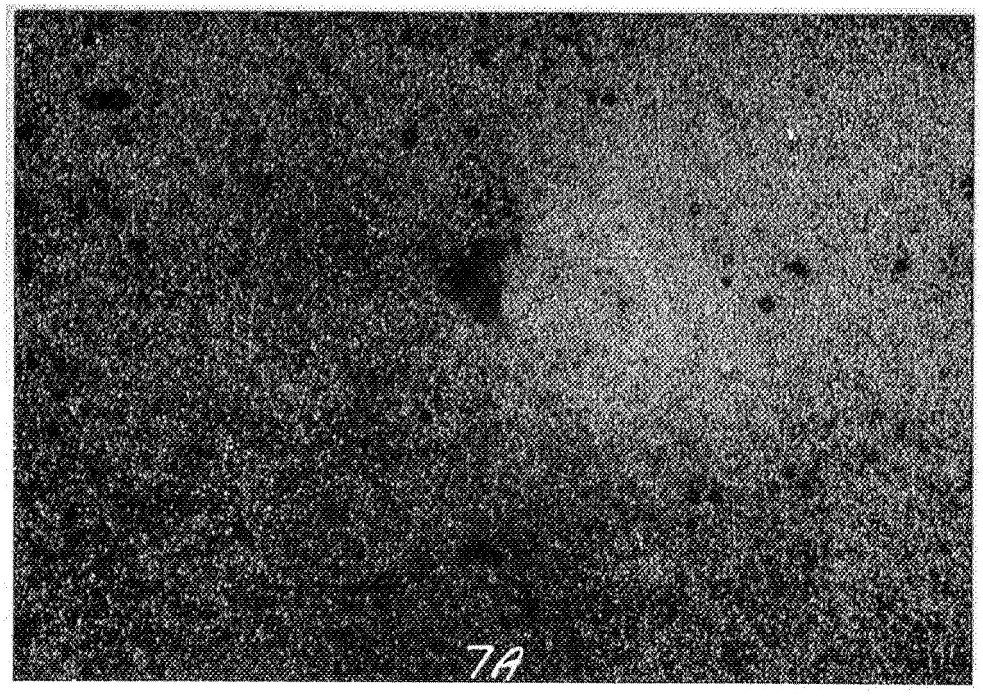

Tension Side of Impact

Figure C-4. Coating System NC11-A - 1800°F (1229°K) Ballistic Impact with 3.06 Ft/Lbs Energy (15X).

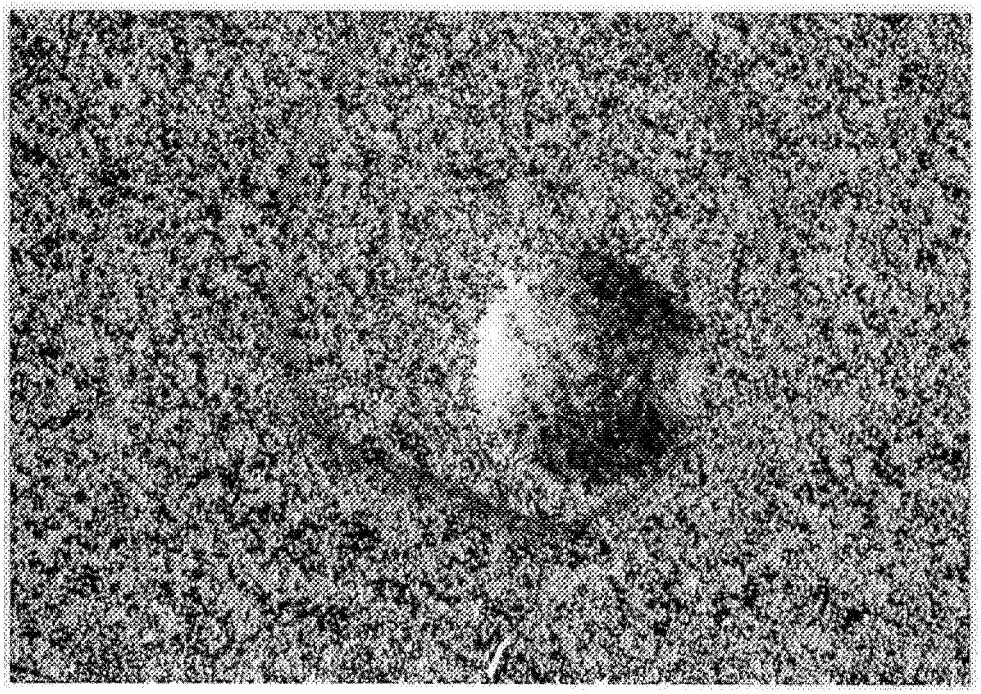

Impact Area

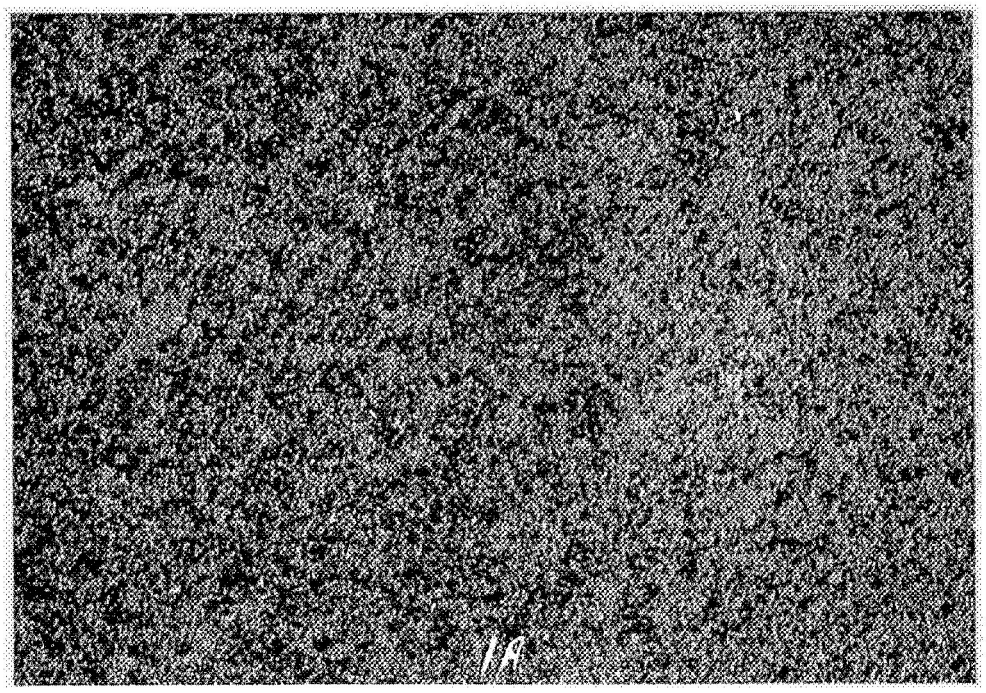

Tension Side of Impact

Figure C-5. Coating System NC11-A (Mod.) - Room Temperature Ballistic Impact with 1.96 Ft/Lbs Energy (15X).

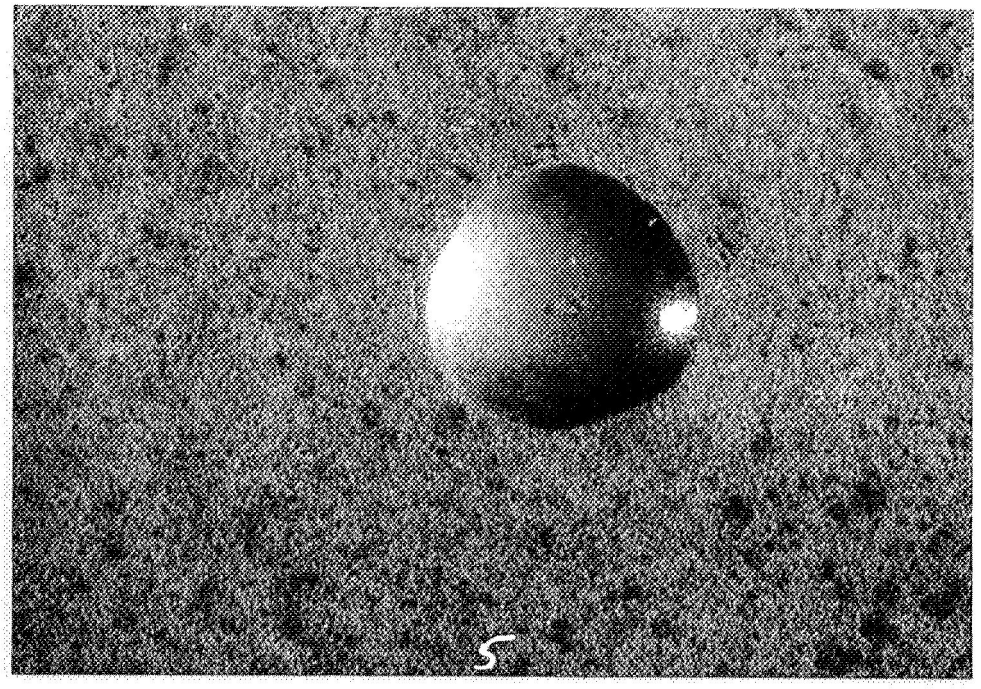

Impact Area

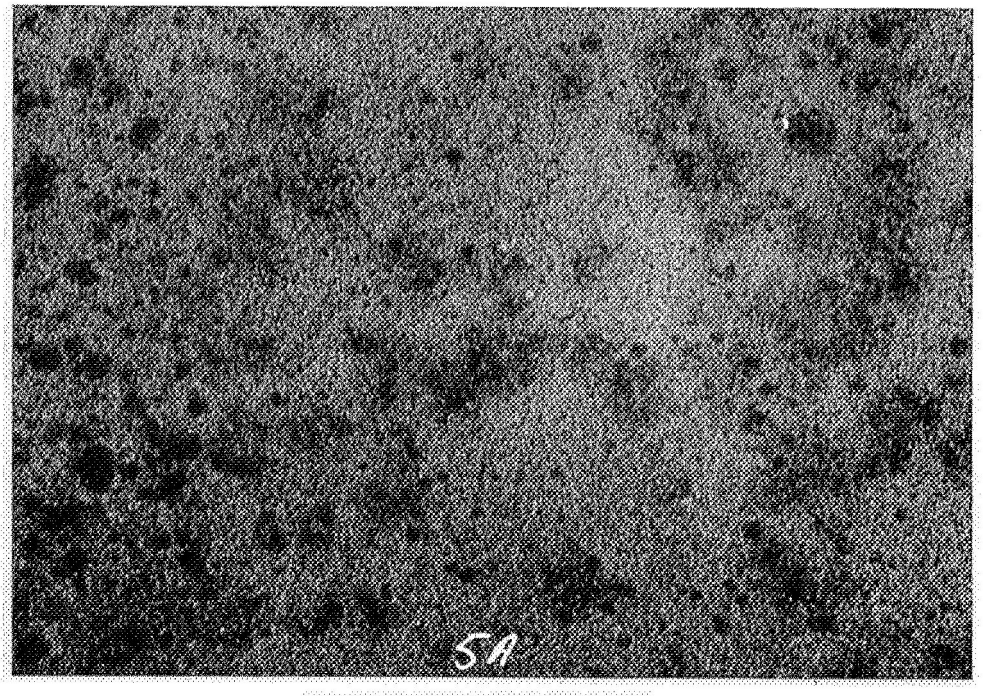

Tension Side of Impact

Figure C-6. Coating System NC11-A (Mod.) - 1800°F (1229°K) Ballistic Impact with 3.06 Ft/Lbs Energy (15X).

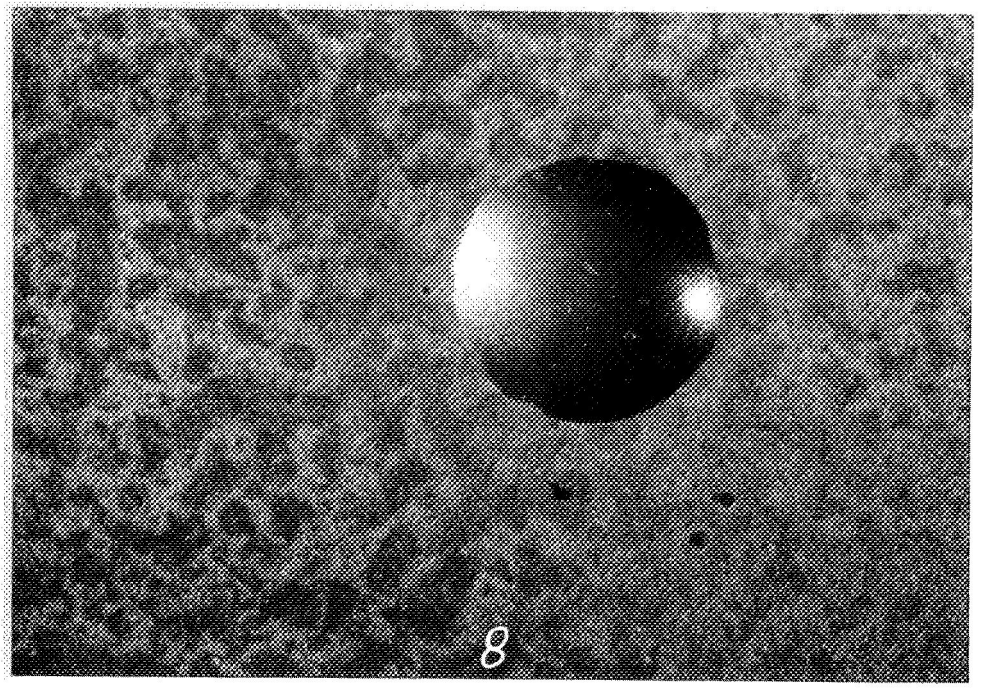

Impact Area

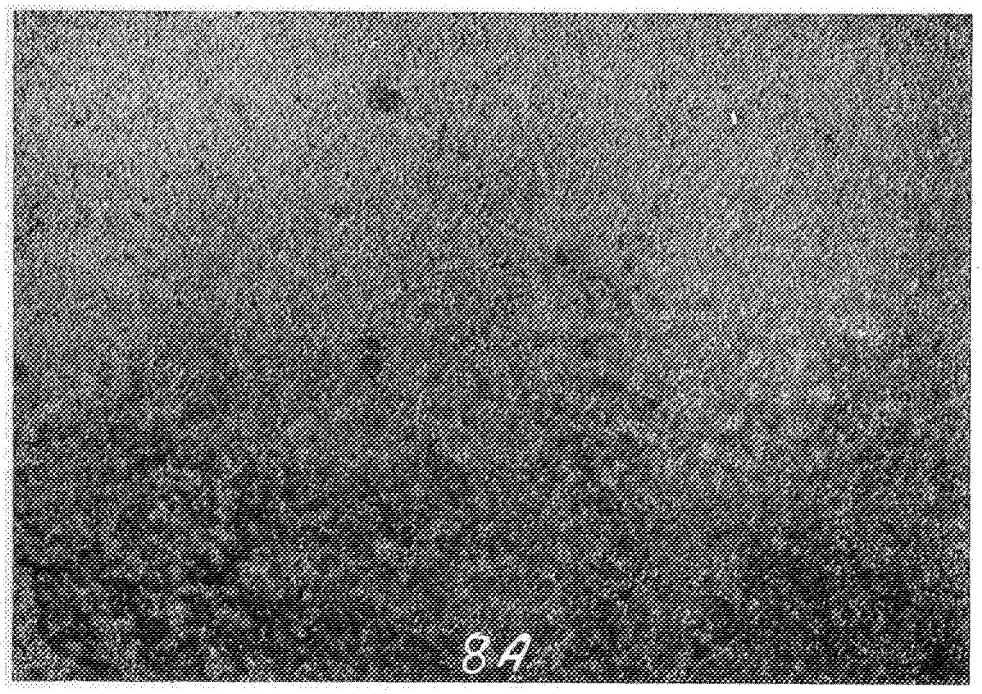

Tension Side of Impact

Figure C-7. Coating System NC3-L - 1800°F (1229°K) Ballistic Impact with 3.06 Ft/Lbs Energy (15X).

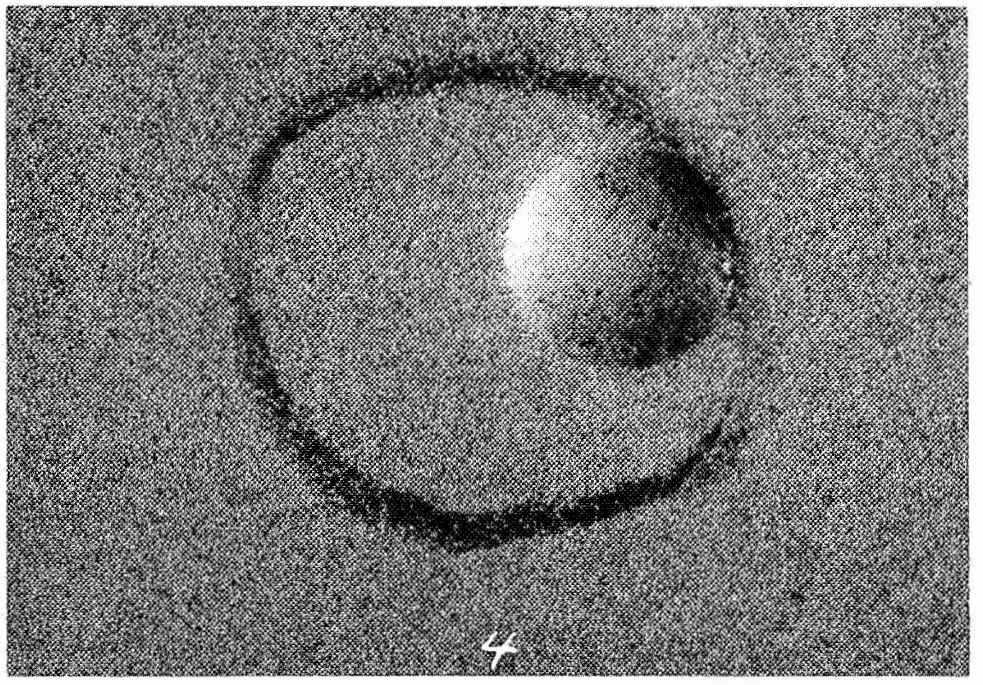

Impact Area

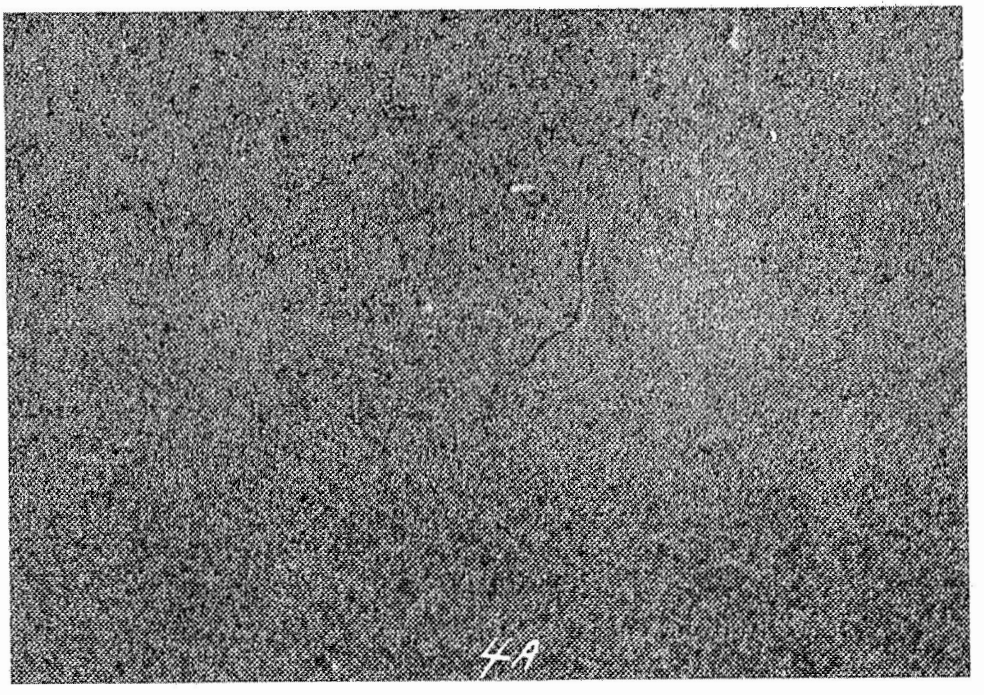

Tension Side of Impact

Figure C-8. Coating System NASA VIA/C-2 - Room Temperature Ballistic Impact with 1.96 Ft/Lbs Energy (15X).

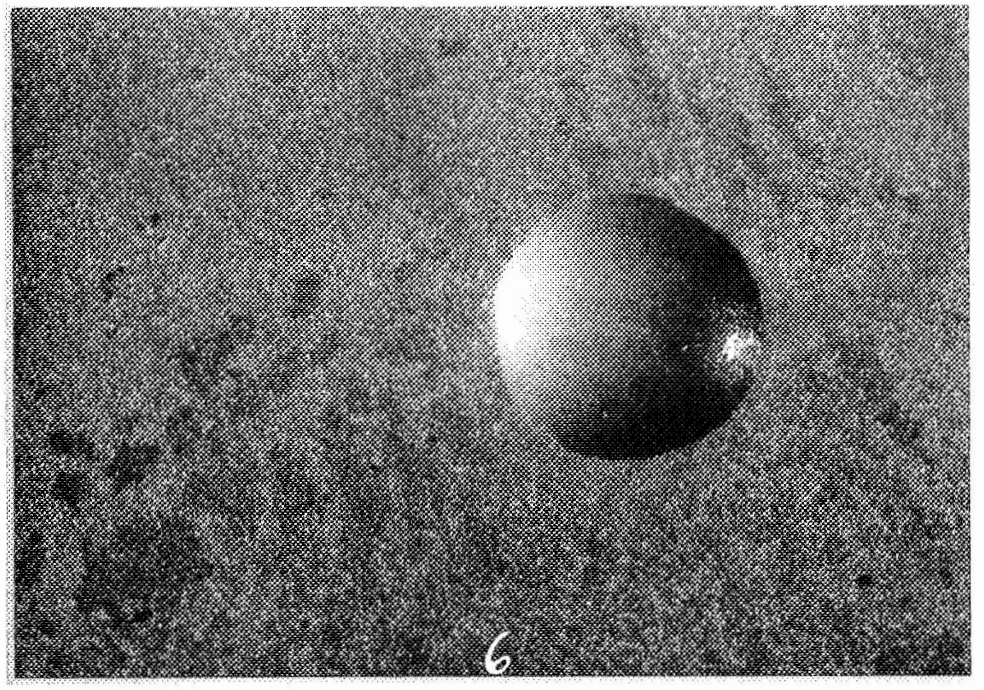

Impact Area

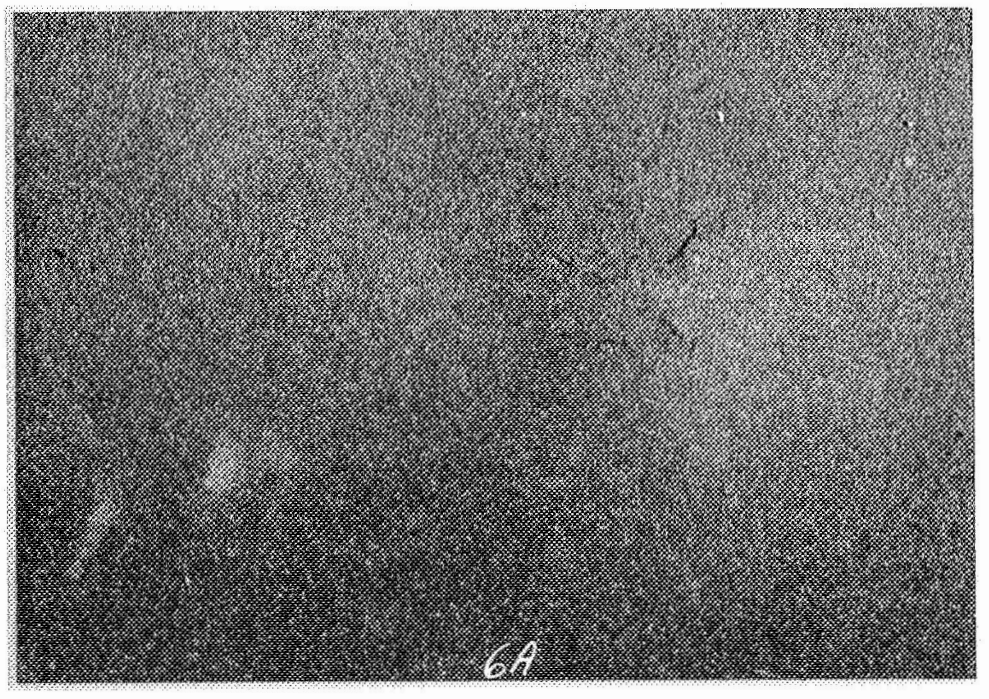

Tension Side of Impact

Figure C-9. Coating System NASA VIA/C-2 - 1800°F (1229°K) Ballistic Impact with 1.96 Ft/Lbs Energy (15X).

APPENDIX D

ELECTRON MICROPROBE ANALYSIS

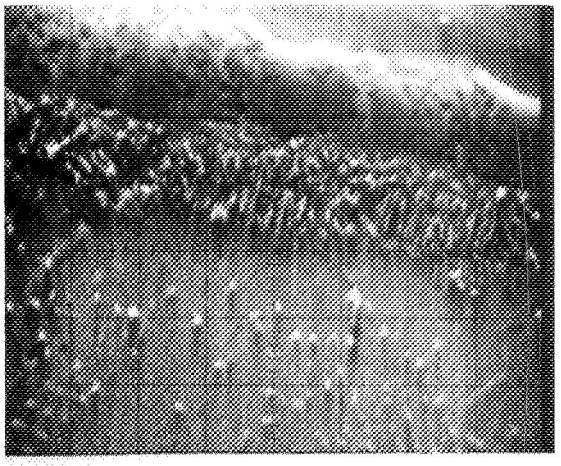

EBS

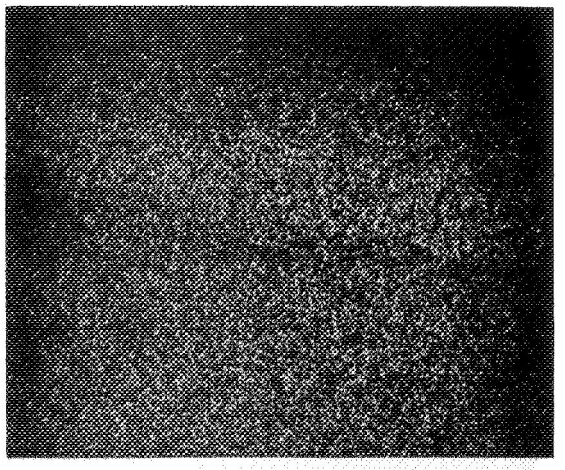

Cr

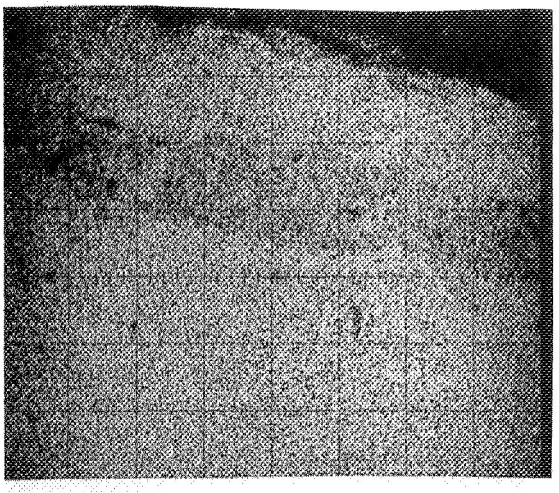

Ni

Ta

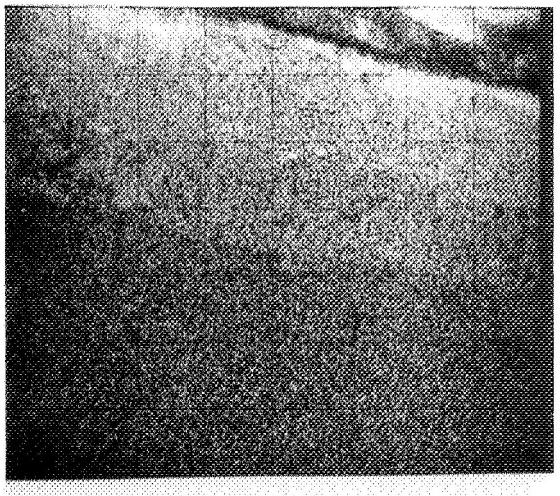

Al

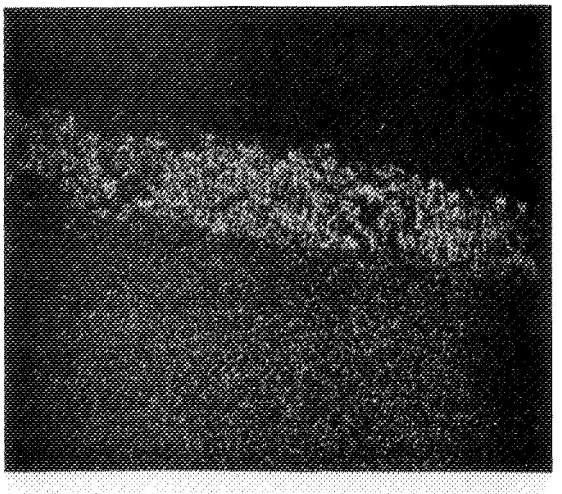

W

Figure D-1. Electron Microprobe Scan of NC11-A-S1-Coated NASA VIA Alloy for Distribution of Principal Elements in Coating and Matrix (EBS = Electron Back-Scatter Image) (360X).

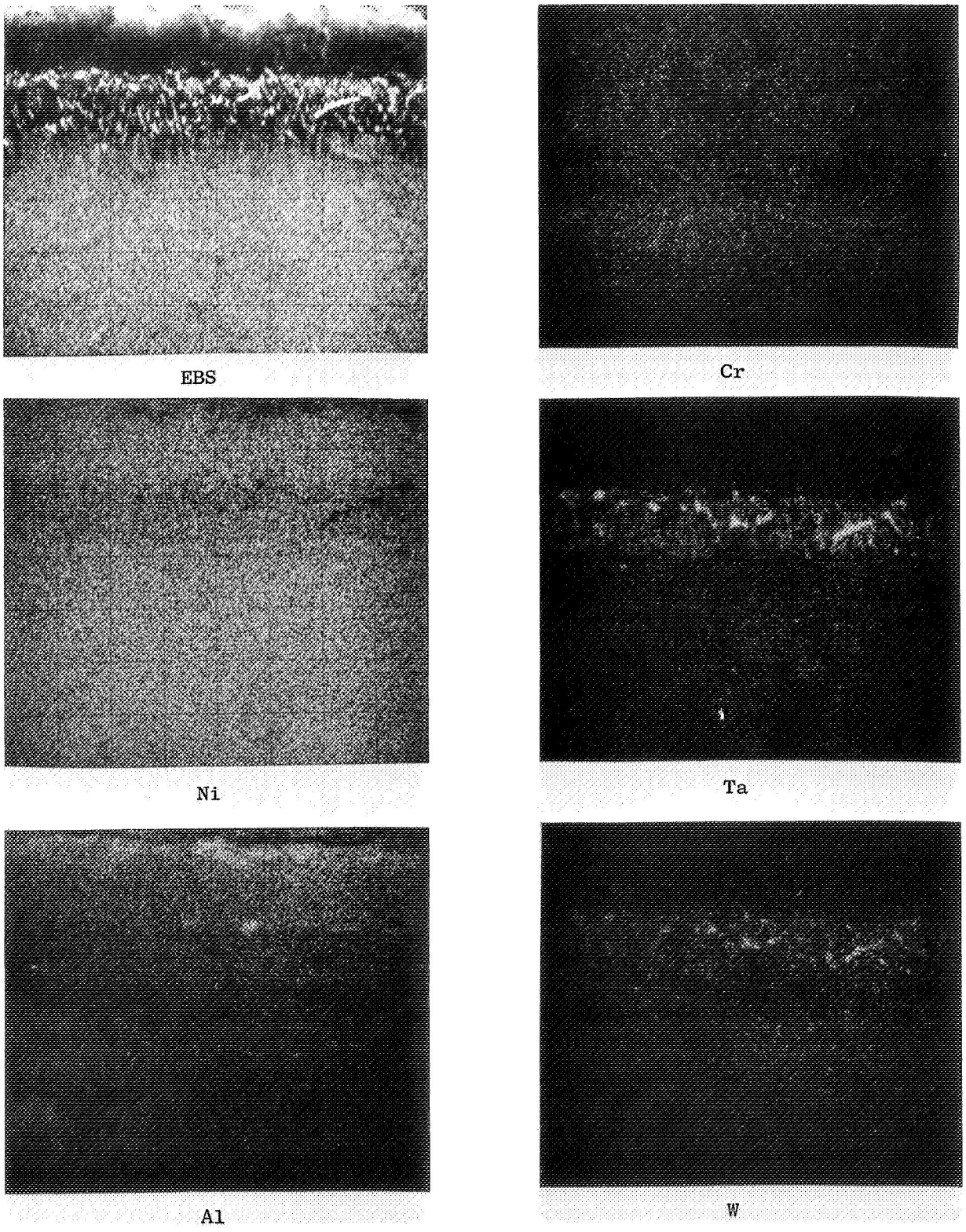

Figure D-2. Electron Microprobe Scan of NC11-A-D1-Coated NASA VIA Alloy for Distribution of Principal Elements in Coating and Matrix (360X).

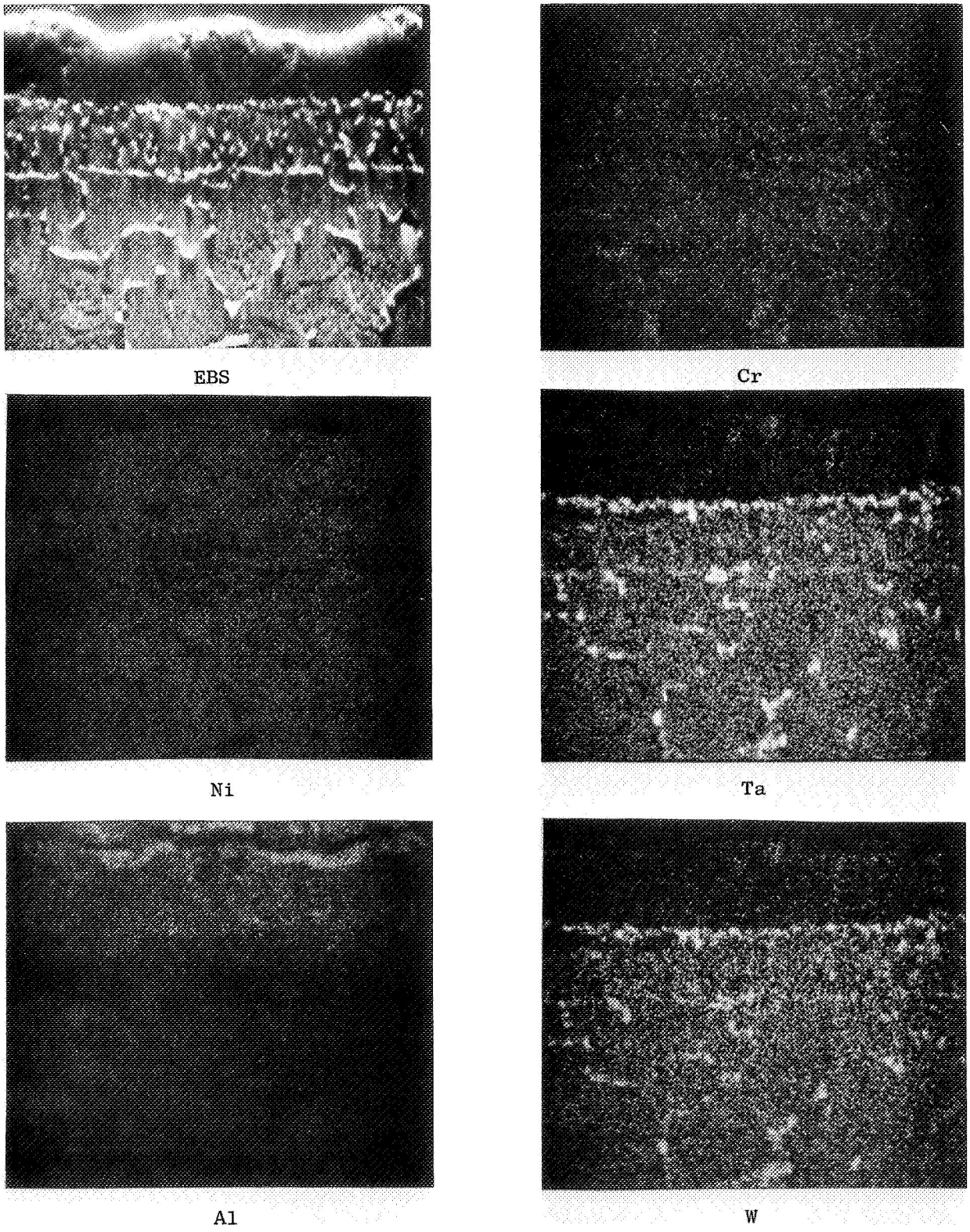

Figure D-3. Electron Microprobe Scan of NC11-A-S1-Coated NASA VIA Alloy for Distribution of Principal Elements in Coating and Matrix After 504 Hours at 2000°F (1366°K) (360X).

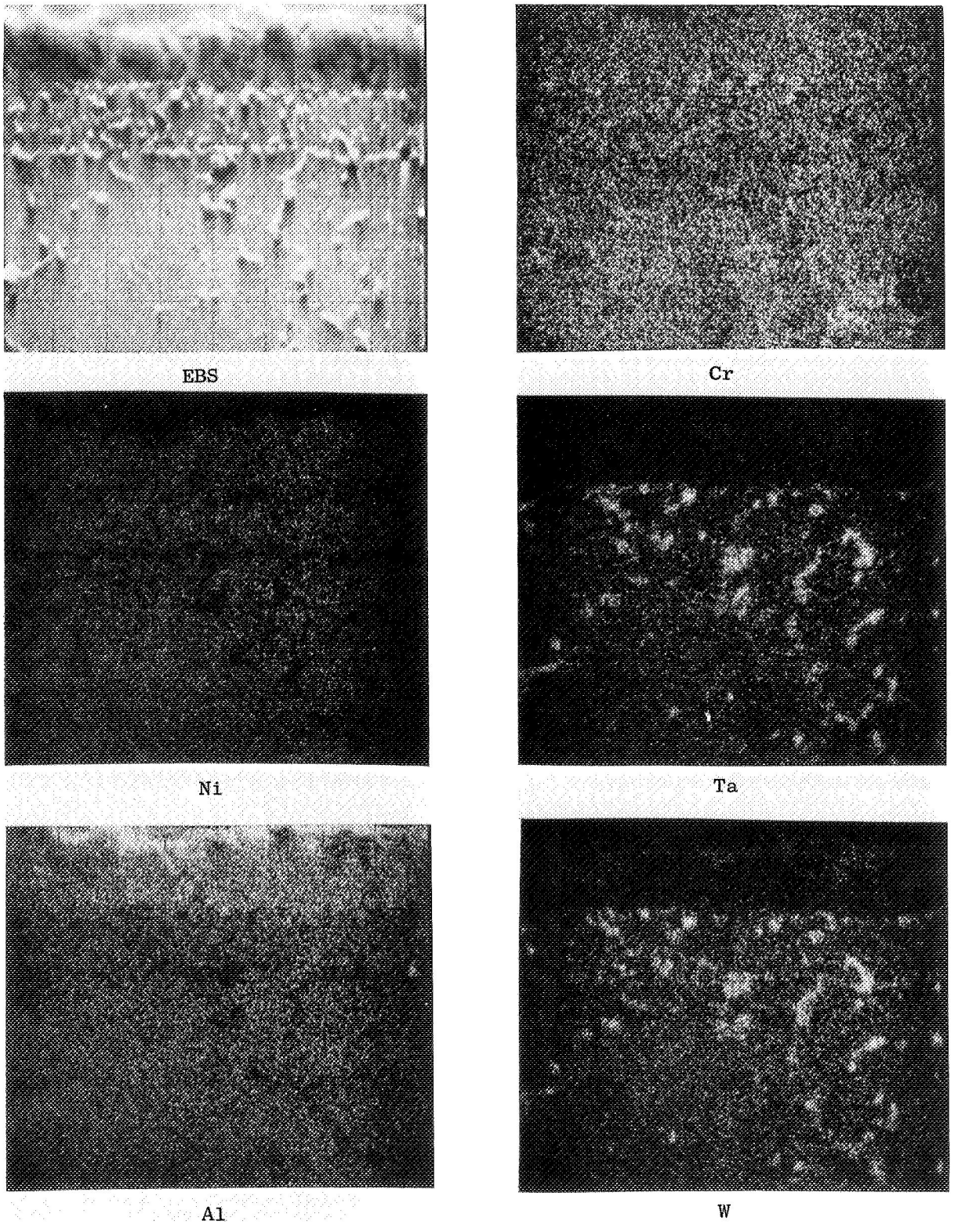

Figure D-4. Electron Microprobe Scan of NC11-A-D1-Coated NASA VIA Alloy for Distribution of Principal Elements in Coating and Matrix After 503 Hours at 2000°F (1366°K) (360X).

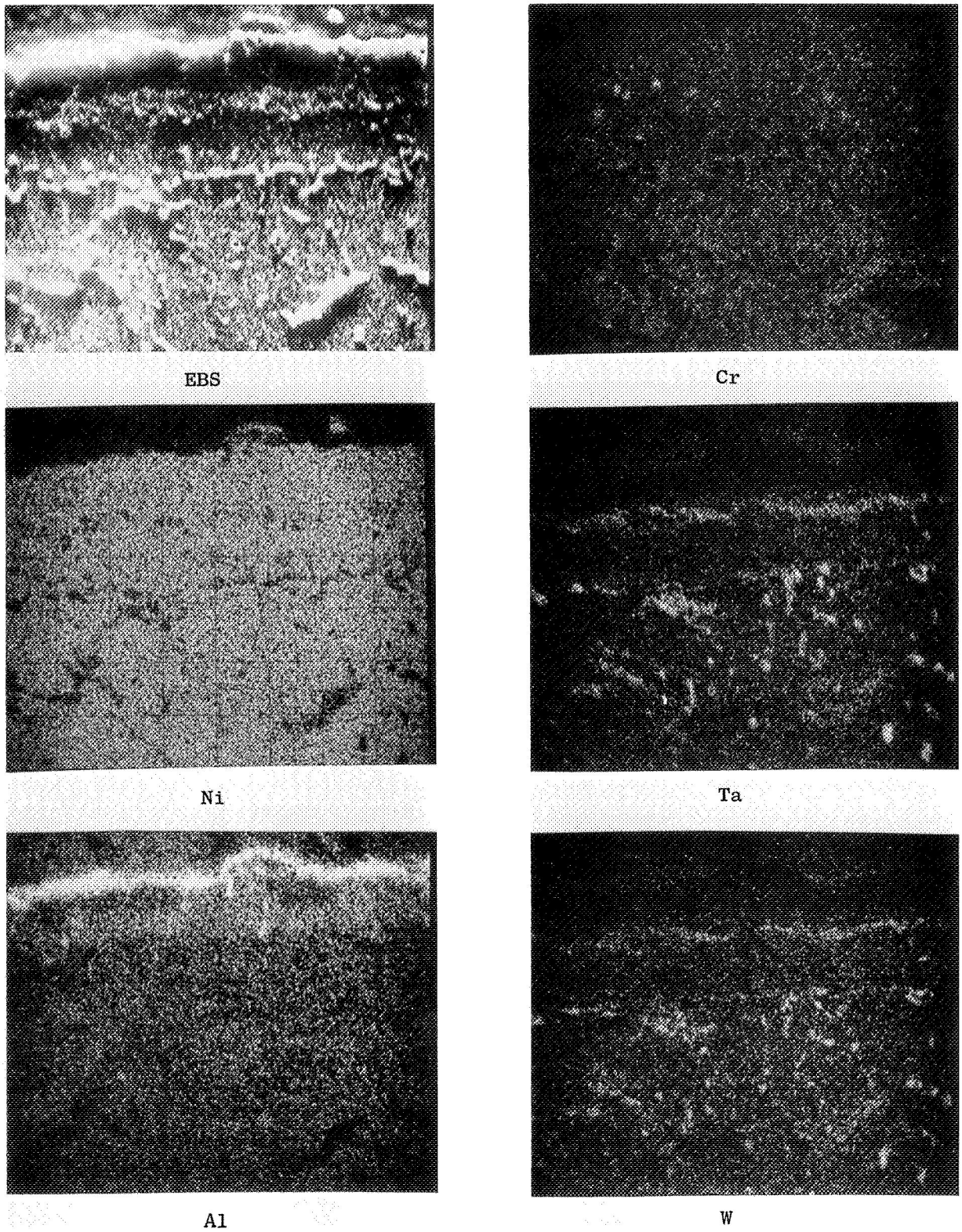

Figure D-5. Electron Microprobe Scan of NC11-A-S1-Coated NASA VIA Alloy for Distribution of Principal Elements in Coating and Matrix After 995 Hours at 2000°F (1366°K) (360X).

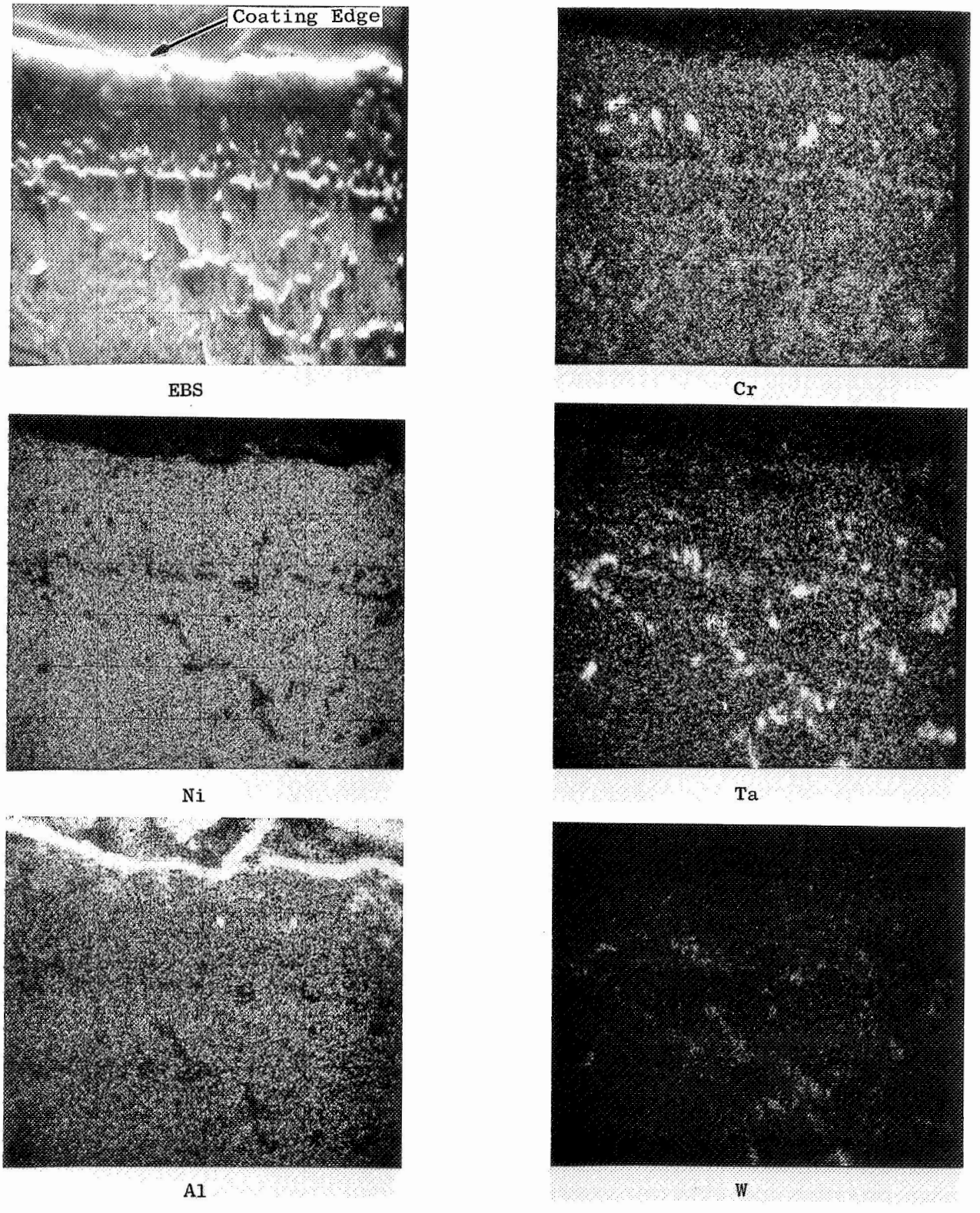

Figure D-6. Electron Microprobe Scan of NC11-A-S1- Coated NASA VIA Alloy for Distribution of Principal Elements in Coating and Matrix After 1013 Hours at 2000°F (1366°K) (360X).

EBS

Aluminum

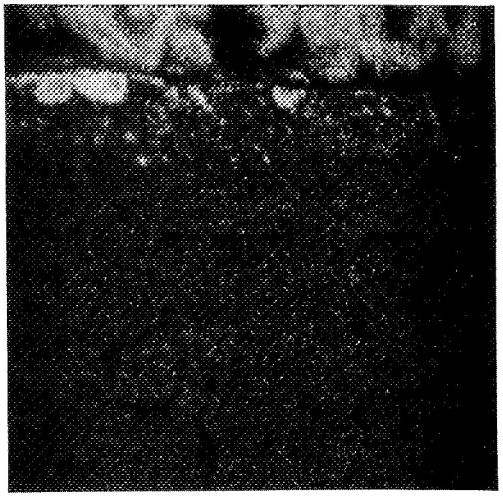

Chromium

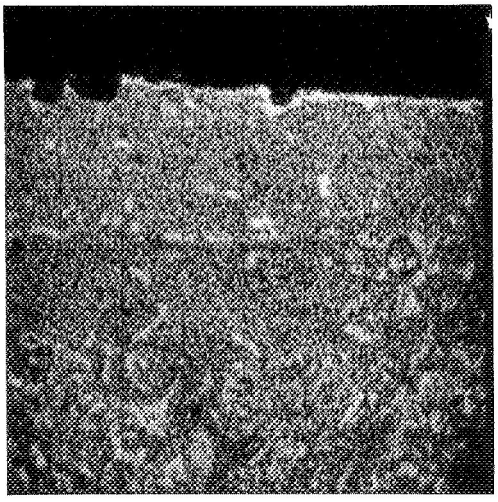

Figure D-7. Electron Microprobe Scans of NC11-A-S1 Coating After 1483 Hours at 2000°F (1366°K) for Aℓ and Cr. Top Convex Leading Edge Section (360X).

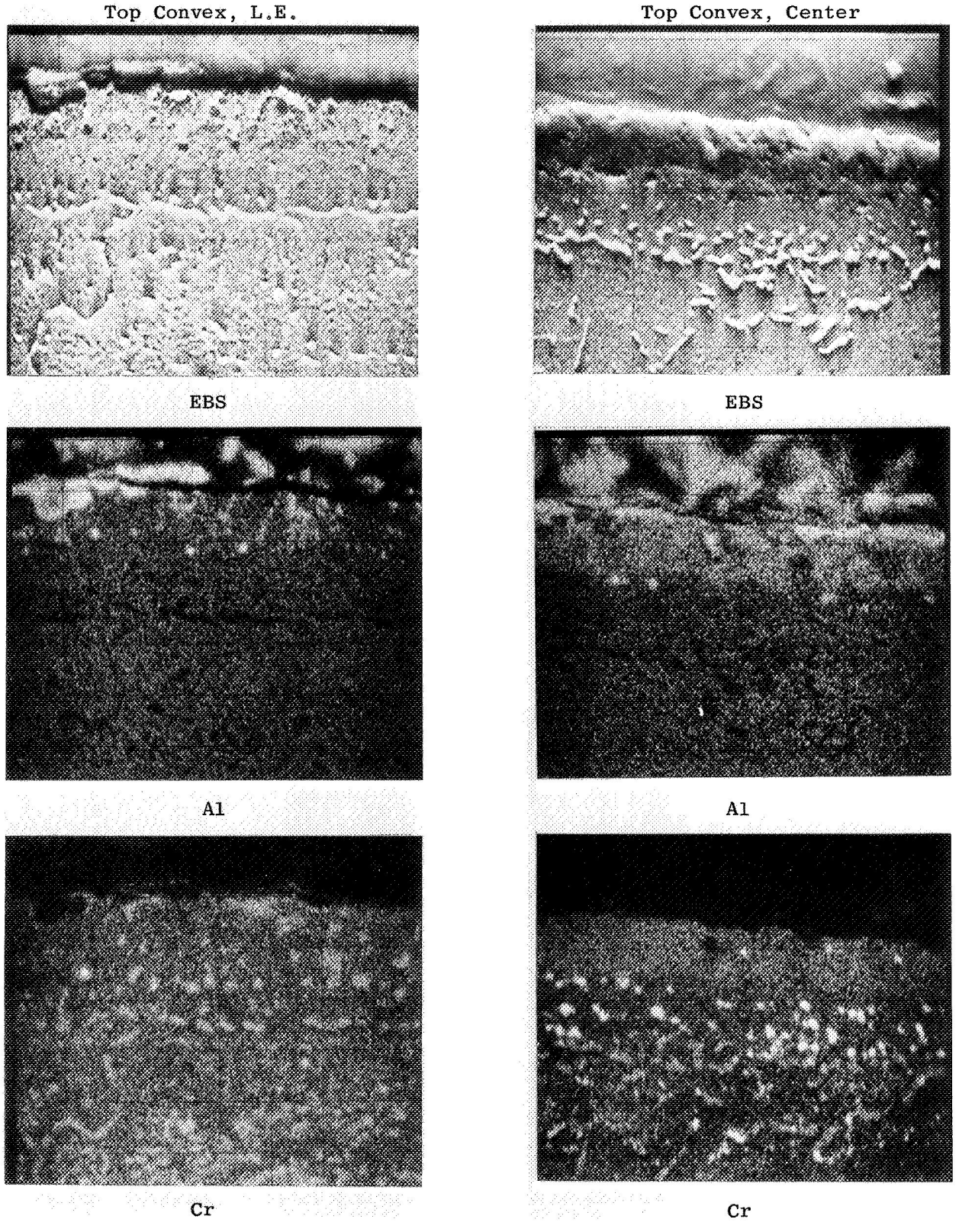

Figure D-8. Electron Microprobe Scans of NC11-A-D1 Coating After 1495 Hours at 2000°F (1366°K) for Aℓ and Cr (360X).

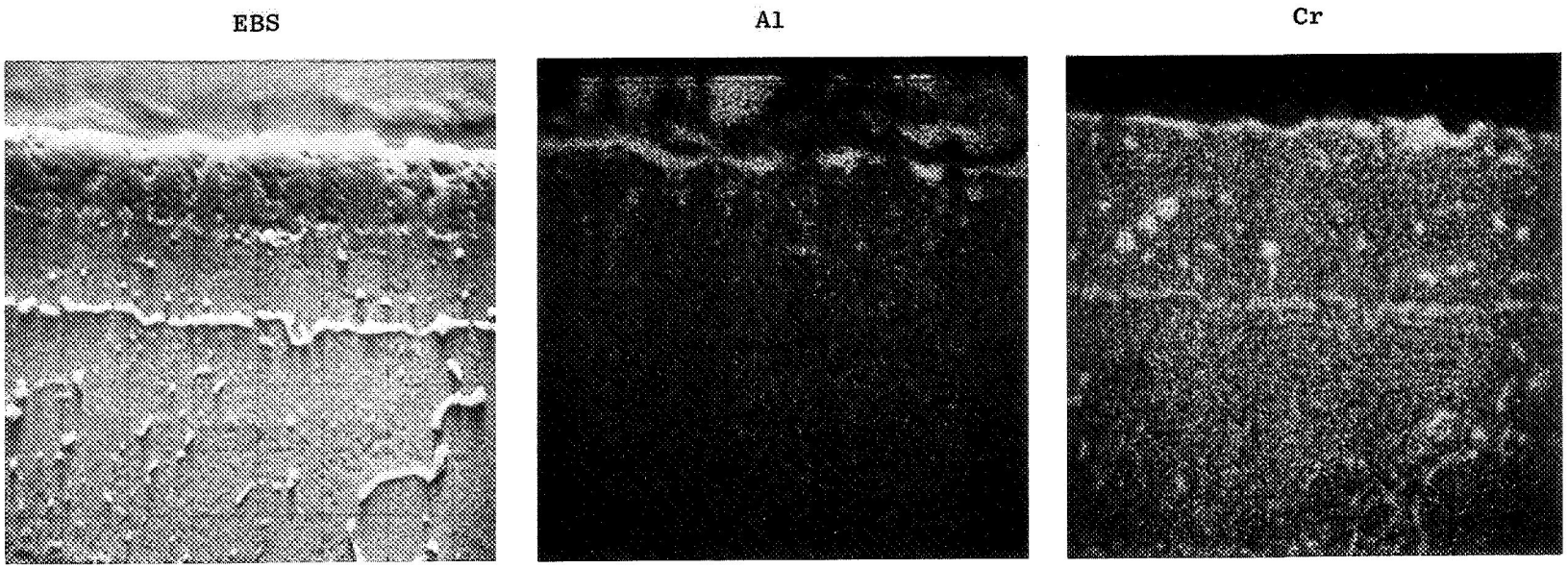

Figure D-9. Electron Microprobe Scans of NC11-A-Sl Coating After 2000 Hours at 2000°F (1366°K) for Aℓ and Cr (360X).

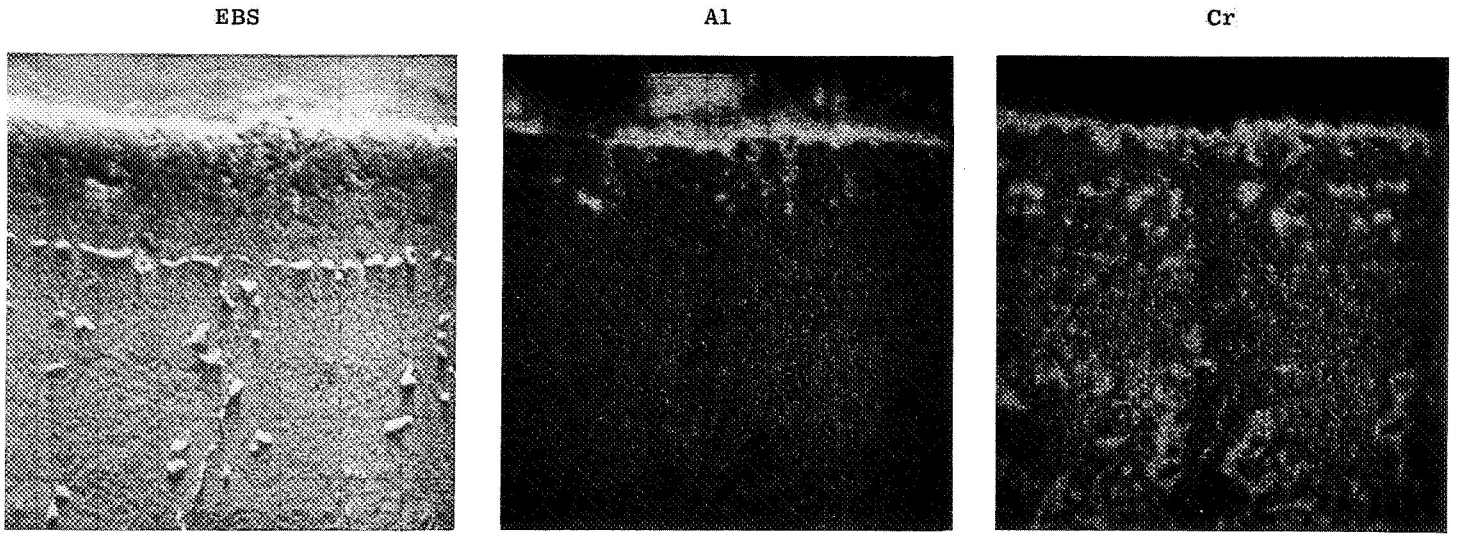

Figure D-10. Electron Microprobe Scans of NC11-A-D1 Coating After 2000 Hours at 2000°F (1366°K) for Aℓ and Cr (360X).

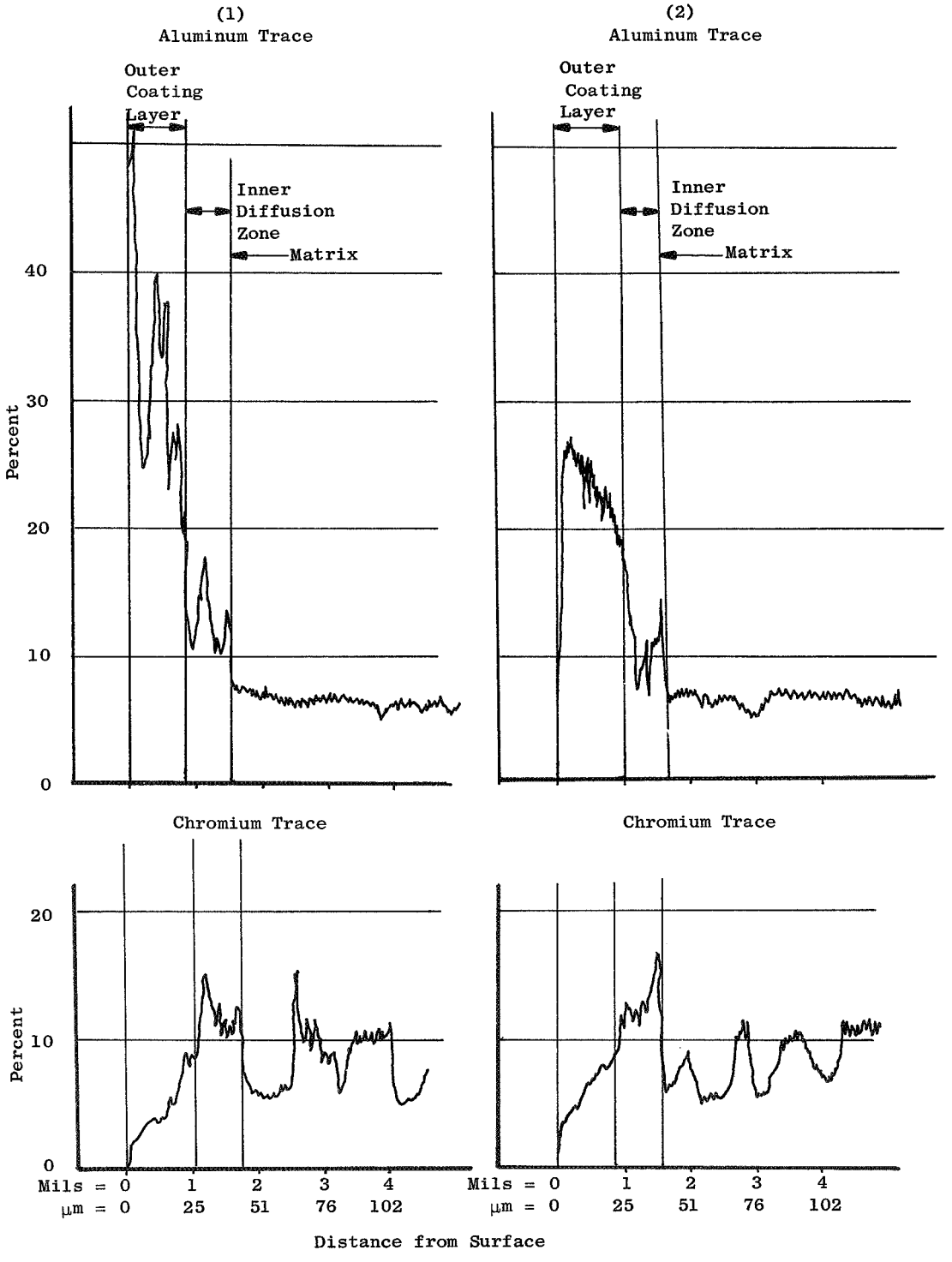

Figure D-11. Aluminum and Chromium Traces of NC11-A-S1, As Coated, Through Sections, (1) Al_2O_3 Particle Concentration and (2) No Al_2O_3 Particles.

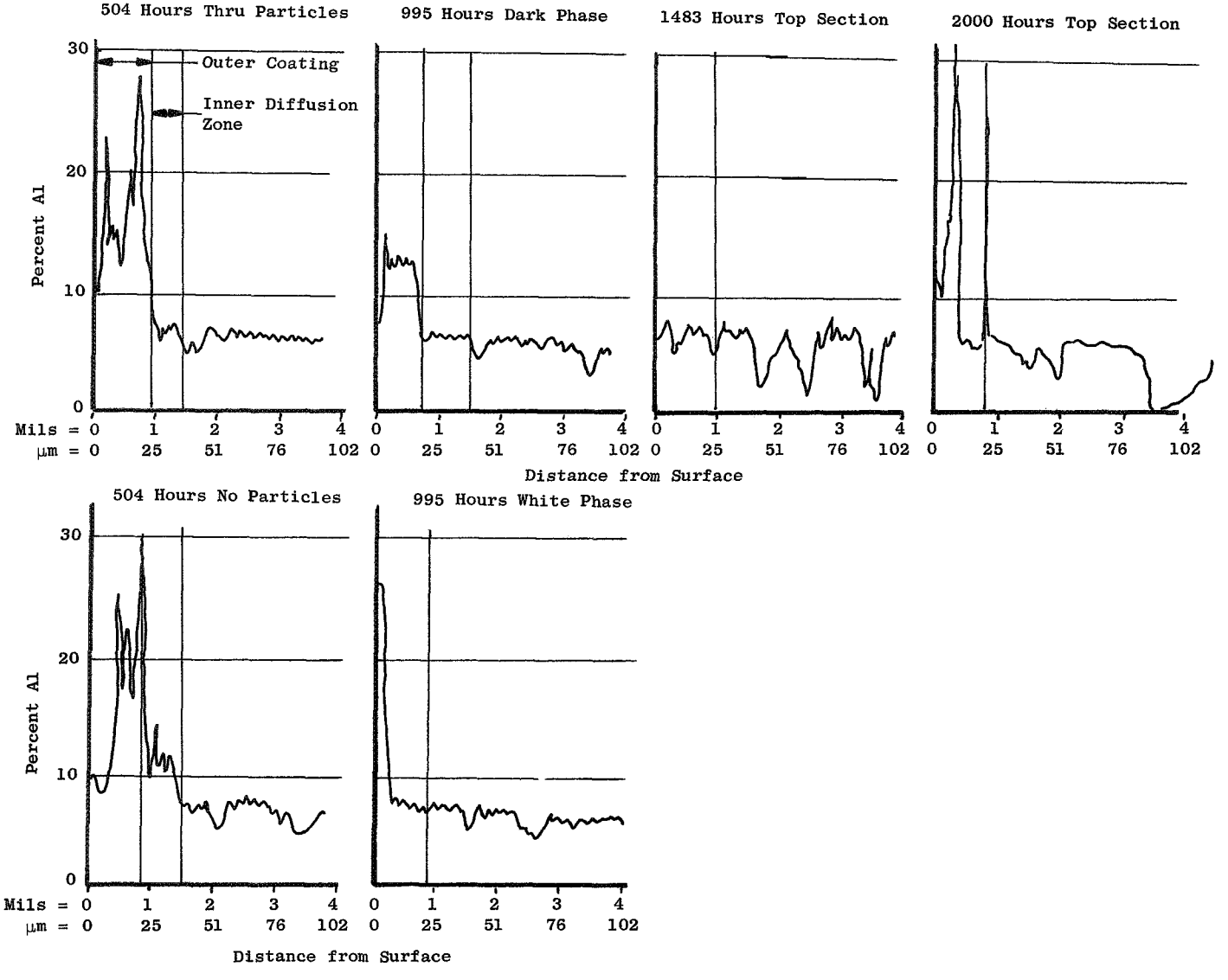

Figure D-12. Effect of 2000°F (1366°K) Burner Rig Test on Aluminum Concentration in NC11-A-S1 Coating and Matrix.

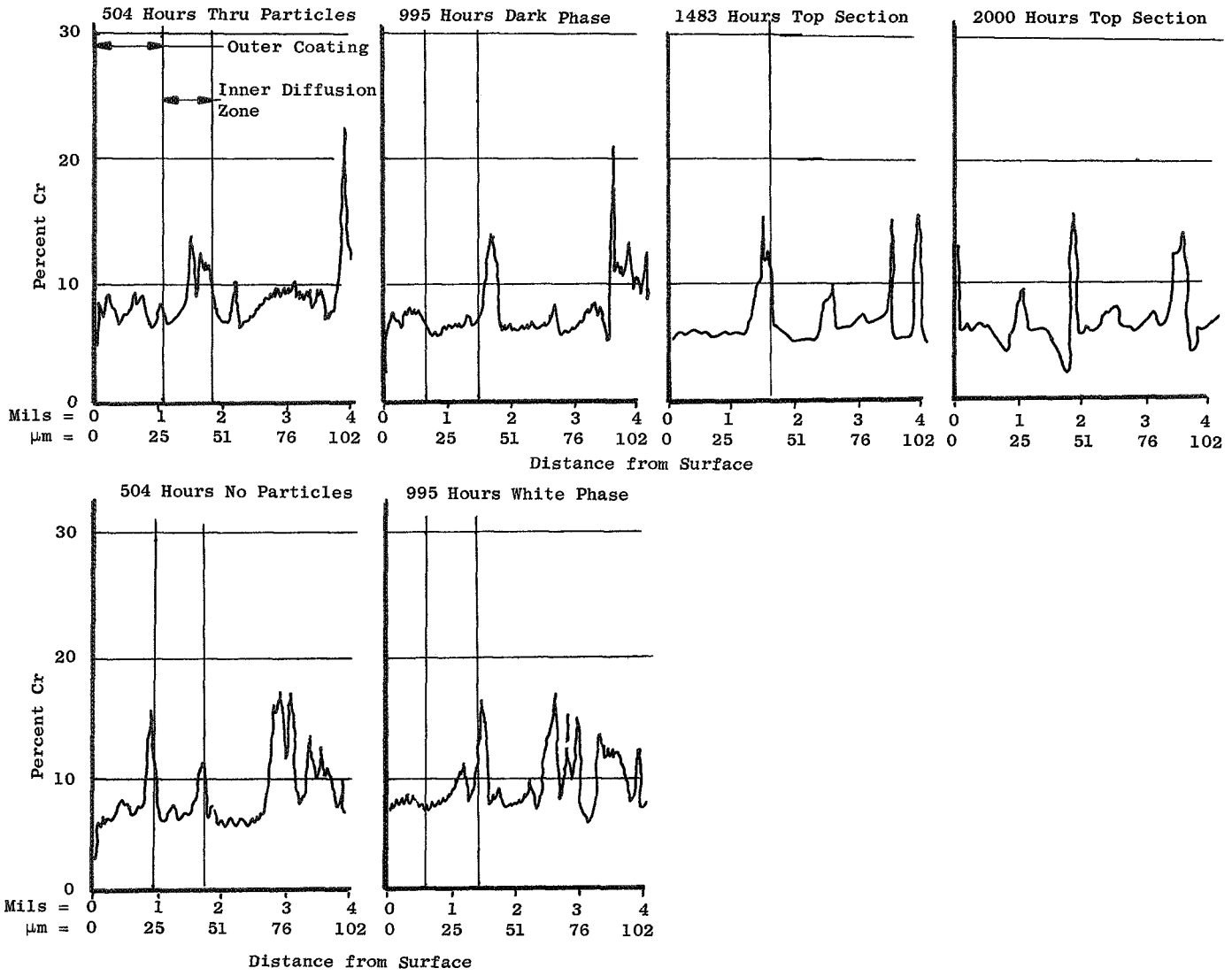

Figure D-13. Effect of 2000°F (1366°K) Burner Rig Test on Chromium Concentration in NC11-A-S1 Coating and Matrix.

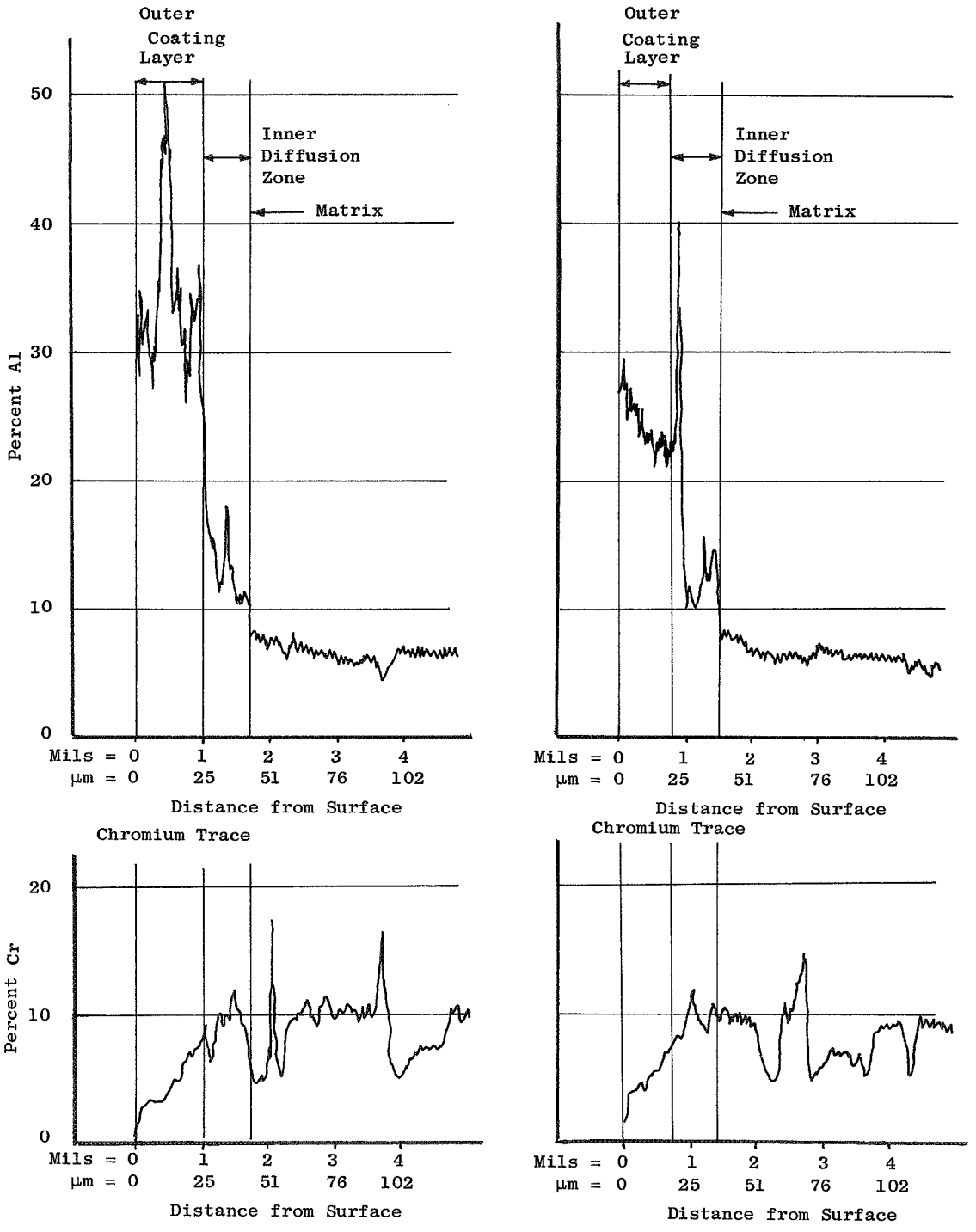

Figure D-14. Aluminum and Chromium Traces of NC11-A-D1, As Coated, Through Sections, (1) Al_2O_3 Particle Concentration and (2) No Al_2O_3 Particles.

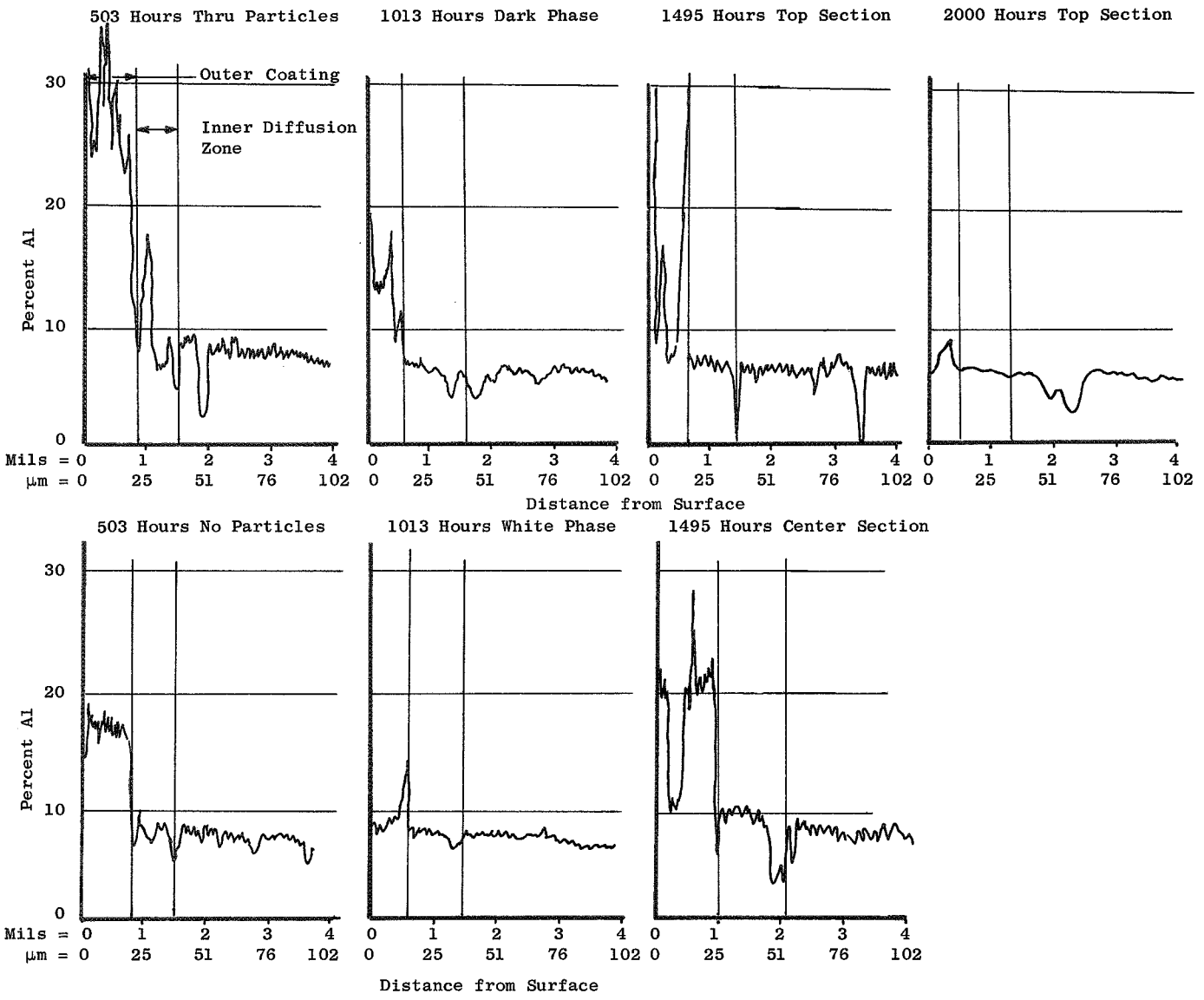

Figure D-15. Effect of 2000°F (1366°K) Burner Rig Testing on Aluminum Concentration in NC11-A-D1 Coating and Matrix.

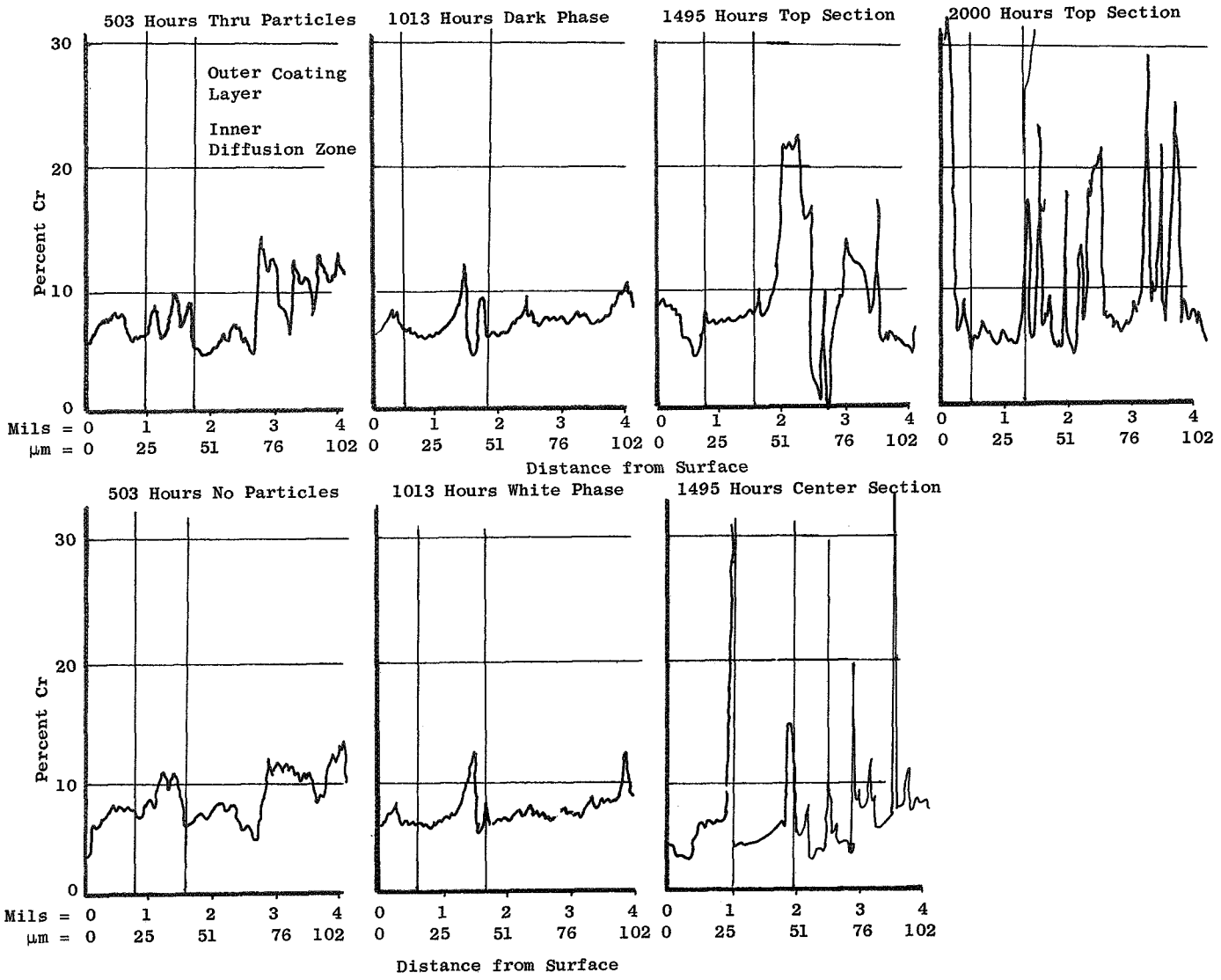

Figure D-16. Effect of 2000°F (1366°K) Burner Rig Testing on Chromium Concentration in NC11-A-D1 Coating and Matrix.